Numerical Modelling and Simulation of Fully Coupled Gas Hydrate Reservoirs and Wellbore Fluid Flow

A THESIS

BY

SABASTINE ANIBUEZE

Submitted in partial fulfilment of the requirements for the award of the degree of

Doctor of Philosophy

School of Energy and Electronics Engineering
University of Portsmouth

March, 2023

ABSTRACT

This research work explored mechanisms that control fluid flow in the natural gas hydrate reservoir and the wellbore to resolve the challenges related to the gas flow assurance and production sustainability. The study was motivated by the fact that natural gas hydrate reservoirs hold the largest deposit of natural gas whose benefit to human being, ranging from energy source to industrial products, cannot be over-emphasised. However, complex nature of the gas hydrate reservoir and factors that influence the flow dynamics in the unconventional resource have been found to correlate with the wellbore complexities to defy viable simulations of the gas hydrate system toward commercial production. Thus, current modelling approaches are limited. This thesis expatiated the transient flow problems in both the unconventional reservoir and the wellbore, incorporated the various convective and diffusive flux phenomena, non-Darcy flow effects, near-wellbore convective mixing processes, reservoir-wellbore dynamics, and developed a new kinetic hydrate reservoir simulation model and a fully implicit fully coupled reservoir-wellbore fluid flow model for natural gas hydrate application. Thus, the thesis consists of two important simulation strategies for the specific gas hydrate reservoir production simulation. First is the new reservoir model that aggregated and simultaneously incorporated the inherent defying features to the gas hydrate fluid flow including threshold pressure, diffusivity flux, Knudsen diffusion, inertia and gas slippage effects and thermal expansion and Joule-Thomson effects. The second is the fully implicit fully coupled reservoir-wellbore model for gas hydrate production optimisation. The solutions of the formulations were obtained using finite different numerical scheme and Newton-Raphson iteration method implemented in MATLAB. The models were verified and validated using CMG STARTS benchmarked with the experimental data of Li et al. (2010a) and analytical model of Selim and Sloan (1989). Simulation results showed excellent agreement with the analyses of the key variables measured, including distributions of phases saturations, pressure, temperature, production rates and cumulative productions of gas and water over time. The models have been used to perform sensitivity analysis of the important unconventional reservoir-wellbore parameters that control the flow system behaviour; and their comparative effects were evaluated using the Monte Carlo simulation technique. Furthermore, near-wellbore conditions related to the macroscopic laws of near wellbore upscaling was modelled to investigate effects of the various functions of the relative permeability and capillary pressure equations and the new optimisation technique. Results indicated that these factors can have severe cumulative negative impact of over estimation of production rate by up to 30%. It was deduced that the

gas production process at early stage is controlled by pressure depletion and sensible heat of dissociation dominated by heat advection in the hydrate zone and along the interface of the pore spaces and near wellbore. The temperature dependent model would enable long time production and the later stage gas production could had been dominated by thermal conduction-driven recovery through of the wellbore. It was identified that the thermal diffusion has a strong effect on the performance of the proposed scheme while the pressure diffusion has moderate impact beyond the threshold. The developed fully implicit fully coupled model offered a more efficient and robust flow assurance over a range of the reservoir parameterisation, including dissociation kinetics, spatial heterogeneities, intrinsic permeability and gas saturation; thus, offers a promising solution to the challenging gas hydrate reservoir production. After 1000 days of production, the cumulative gas production of decoupled model began to decrease up to 2.5 times lower than that simulated by the fully coupled approach which also has lower water production. It is concluded that application of the fully implicit fully coupled reservoir-wellbore could guarantee sustainable gas hydrate production.

DEDICATION

To God be the glory.

ACKNOWLEDGMENTS

I would like to express my profound gratitude to my first supervisor, Dr Amjad Shah for his supervision and various form of assistance. This research work would not have been possible without his intellectual contributions, mentoring, encouragement, guidance, and enthusiasm in the study. I would also like to extend my appreciation to Dr Mohammed Hasan, my second supervision, for managing me well at challenging and emotional moments. My special thanks also go to my assessors of the first year (Major Review) of the PhD programme; I benefited immensely from the philosophy of persistence and excellence of each and every one of them. My sincere thanks go to all the staff of the Graduate School, University of Portsmouth for the opportunity to attend various development courses and trainings dovetailed with the combination of skills and knowledge that made this research work possible. I thank my sponsor, Petroleum Technology Development Fund and Government of Nigeria for providing me with most of the needed financial supports. To my parents, Mr and Mrs Angus and Eucheria Anibueze Onwo, and siblings, remained blessed for always believing in me and for your continuous emotional support. Finally, I wish to thank all the staff and office of School Energy and Electronic Engineering, University of Portsmouth and all my PhD colleagues for their support and the time we shared together. Above all, I thank God Almighty without Whom every other support and effort would not have counted or amounted to the success of the research. Be glorified oh God! You made all things worked together for good and reality of this thesis.

DECLARATION

Whilst registered as a candidate for the above degree, I have not been registered for any other research award. The results and conclusions embodied in this thesis are the work of the named candidate and have not been submitted for any other academic award.

Sabastine Anibueze

March, 2023

TABLE OF CONTENTS

Contents

ABSTRACT ..... **ii**
DEDICATION ..... **iv**
ACKNOWLEDGMENTS ..... **v**
DECLARATION ..... **vi**
TABLE OF CONTENTS ..... **vii**
LIST OF TABLES ..... **x**
LIST OF FIGURES ..... **xi**
NOMENCLATURE ..... **xiv**
CHAPTER 1 ..... **1**
INTRODUCTION **1**
1.1 Background and Motivation 1
1.2 Problem Statement 3
1.3 Description of Research Gap 4
1.4 Research Questions 5
1.5 Aim and Objective 6
1.6 Scope 6
1.7 Methodology 8
1.8 Thesis Outline 9
CHAPTER 2 ..... **11**
LITERATURE REVIEW **11**
2.1 Theoretical Framework 11
2.2 Structure of Natural Gas Hydrates 14
2.3 World Hydrate Resources 15
2.4 Types of Hydrate Reservoirs 17
2.5 Classification of Gas Hydrate Reservoirs 17
2.6 Properties of Hydrates Gas Hydrate 20
2.7 Gas Hydrate Production Methods 23
2.7.1 Depressurization 24
2.7.2 Thermal Injection 24
2.7.3 Inhibitor Injection 25
2.7.4 Gas Injection 25
2.8 Reservoir Performance Prediction and Optimization 26

2.9 Pressure Drop Calculation and Multiphase Flow 29
2.9.1 Empirical Correlations 30
2.9.2 Mechanistic Models 32
2.9.3 Drift-Flux Models 32
2.9.4 Computational Fluid Dynamics (CFD) 33
2.10 Numerical Modelling and Simulation 34
2.10.1 Reservoir Modelling 36
2.10.2 Wellbore Modelling 37
2.10.3 Wellbore Hydraulics Model 39
2.10.4 Coupled Reservoir-Wellbore Modelling 41
2.12 Gas Hydrate Reservoir Performance Prediction Models 43
2.13 Inherent Defying Features in Gas Hydrate Reservoir Production 55
2.13.1 Pressure Solutions 58
2.13.2 Temperature Solutions 65
2.14 Transient Pressure and Temperature Analysis 68
2.15 Near-Wellbore Modelling and Permeability Upscaling 72
CHAPTER 3 75
NUMERICAL SIMULATION OF THE INHERENT DEFYING FEATURES IN GAS HYDRATE RESERVOIR FLUID FLOW MODELLING 75
3.1 Synopsis 75
3.2 Mathematical Formulation 76
3.2.1 Governing Equations 76
3.2.2 The Reaction kinetics: 77
3.2.3 Boundary Conditions 78
3.2.4 Accounting for Non-Darcy Effects, Knudsen Diffusion Factors, Tortuosity and Threshold Pressure 80
3.2.5 Well Flow rate (sources/sinks) 84
3.3 Solution of the multiphase flow equations 85
3.3.1 Discretisation and Linearisation 85
3.3.2 Solution algorithm 88
3.3.3 Newton Raphson method 89
3.3.4 Treatment of non-linear terms: 90
3.3.5 Final matrix equation for the gas hydrate reservoir 91
3.4 Implementation 95
3.4.1 The properties of the synthetic reservoir model 98

3.4.2 Verification and Validation of Model 100
3.5 Temperature dependent model 104
3.5.1 Heat Transfer in Porous Media (Hydrate Zone) 106
3.5.2 Governing equation 108
3.5.3 Numerical Solution 109
3.6 Validation with Experimental Data 111
3.7 Results and Discussion 115
3.7.1 Effect of Diffusive Flux 115
3.7.2 Effect of Hydrate Reservoir Heterogeneity and the dynamic Permeability 117
3.7.3 Effect of Gas Slippage Factor 119
3.7.4 Effect of Threshold Pressure Gradient (TPG). 121
3.7.5 Effect of the sensible heat of dissociation. 122
3.7.6 Effect of thermal expansion and Joule Thomson coefficient 123
3.8 Uncertainty Assessment and Conclusion 124
CHAPTER 4 128
FULLY IMPLICIT FULLY COUPLED RESERVOIR AND WELLBORE FLUID FLOW FOR NATURAL GAS HYDRATE PRODUCTION 128
4.1 Fully Coupled Wellbore Model 128
4.1.1 Mathematica Formulation 130
4.1.2 Assumptions 130
4.1.3 Mass Conservation Equation 131
4.1.4 Momentum Conservation Equation 131
4.1.5 Energy Conservation Equation 132
4.2 Treatment of Well–Reservoir Interaction and Interface Dynamics 134
4.3 Governing Equations of the Fully Coupled reservoir-wellbore Model 136
4.4 Boundary condition 137
4.5 Numerical Solutions 139
4.5.1 Discretization of the Coupled wellbore 139
4.5.2 Newton-Raphson Method 141
4.6 Implementation 143
4.7 Validation 145
4.8 Comparison with Sequential Coupled Model 148
4.9 Results and Discussions 150
4.9.1 Effect on Production rates 150

4.9.2 Gas Recovery Factors 152
4.9.3 Measurement at Wellhead 153
4.9.4 Transient Pressure and Temperature Analysis 153
4.10 Near-Wellbore Upscaling for Capillary Pressure and Relative Permeability Functions on Gas Hydrate Production. 158
4.10.1 Dynamic Permeability, Capillary Pressure and Characterization 159
4.10.2 Numerical Solutions 162
4.10.3 Effect of coarsened gridding and flow-convergence into the wellbore. 165
4.10.5 Effect on Various Relative Permeability and Capillary Pressure Equations 167
CHAPTER 5 170
CONCLUSIONS 170
5.1 Conclusion 170
5.2. Summary of Results 171
5.3 Recommendation for Future Work 172
REFERENCES 174
APPENDIX 191
A. Discretization and Linearization Procedure 191
B. Derivation of the Analytical Model for validation of the fully coupled model 195
D. Relative Permeability and Capillary Pressure Exponents Parameters 200
D. Reservoir Initialisation Code 202
E. Coupled Wellbore Initialisation Code 208

LIST OF TABLES

Table2. 1 Typical Features of Gas Hydrate Reservoirs in Different Locations. 21
Table2. 2 Literature review for gas hydrate reservoirs properties 22
Table2. 3 Gas hydrate Components properties 23
Table2. 4 Pressure Gradient Empirical Correlations Methods 31
Table2. 5 Holder et al Formulation (1982) 44
Table2. 6 Burshears et al Formulation (1986) 44
Table2. 7 Yousif et al Formulation (1991) 46
Table2. 8 Chuang et al Formulation (2001) 46
Table2. 9 EOSHYDR2 Formulation (Moridis, 2002) 47
Table2. 10 Sun et al Formulation (2002) 48
Table2. 11 Sun and Mohanty Formulation (2005) 49
Table2. 12 Gerami and Pooladi-Darvish Formulation (2006) 50
Table2. 13 STOMP-HYD Formulation (Phale and Zhu, 2006) 50
Table2. 14 TOUGH + HYDRATE Formulation (Uddin et al, 2006) 51
Table2. 15 CMG STARS Formulation (Uddin et al, 2006) 52

Table2. 16 HydrateResSim Formulation (Uddin et al, 2006) 53
Table2. 17 Flow regimes as a function of Knudsen number (Foroozesh et al. 2018). 58
Table2. 18 Basic gas slippage factors 64
Table 3. 1 Mesh and initialisation properties 98
Table 3. 2 Phases and Saturation Properties 99
Table 3. 3 Phases and Saturation Properties 99
Table 3. 4 Experimental Data and Parameters used for Simulation 112
Table3.5 Data analysis of the sensitivity parameter (Effects on gas production rate) 127
Table 4. 1 Simulation Parameters 153

LIST OF FIGURES

Figure 1.1 Schematic of the Study Methodology and Model Development 9
Figure 2:1 Phase diagram for methane hydrate formation under the (a) permafrost and (b) ocean bed (Sloan et al, 2010) 12
Figure 2:2 (a) Methane hydrate as burning ice, (b) Natural gas clathrate in marine, ... 13
Figure 2.3 Natural gas hydrate in-cage model and structural forms 15
Figure 2.4: Natural Gas Hydrate Deposits and Major Developments Locations Map 16
Figure 2.5 Schematics of Types of Hydrate Reservoirs 17
Figure 2.6 Four Classes of hydrate deposits 18
Figure 2.7 Class 1 Gas Hydrate Sediment Structural Profile (Xia *et al*, 2017) 19
Figure 2.8 Class 2 Hydrate Sediment Structural Profile (Xia *et al*, 2017) 19
Figure 2.9 Class 3 Hydrate Sediment Structural Profile (Xia *et al*, 2017) 19
Figure 2.10 Illustration of Gas Hydrate Reservoir Production Methods 23
Figure 2.11 Production System Curve 27
Figure 2.12 Illustration of Flow Regimes for Multiphase Vertical Flow 29
Figure 2.13 Illustration of gas and liquid two-phase flow regimes along a pipe 29
Figure 2.14 Flow regime map for vertical upward two-phase flow 30
Figure 2.15 Illustration of Discretised Grid Blocks 35
Figure 2.16 Schematic of typical wellbore system with completions 38
Figure 2.17 Schematic of Reservoir/Wellbore model (a) Source/Sink Model; (b) Coupled Reservoir-Wellbore 42
Figure 2.18 Schematic of the Natural Gas Pathways and Migrations 55
Figure 2.19 Various mechanisms for molecular transport in nanopore 56
Figure 2.20 Schematic of the movement of gas molecules in nanopore 57
Figure 2.21 Typical Pressure-Rate Relationship Curves with TPG 62
Figure 2.22 Schematic representation of a typical well testing operation 69
Figure 2.23 Typical Log-Log Plot of Pressure- and Pressure derivative- Rates Behaviour 70
Figure 3. 1 Illustration of Deviation from Linear Darcy 80
Figure 3. 2 Beta Factor Relationship with Permeability and Pore Pressure 81
Figure 3. 3 Tortuosity definition diagram 82
Figure 3. 4 Orthogonal Coordinates of the Two-Dimensional Reservoir Grid-blocks 92
Figure 3. 5 Reservoir modelling flow charts 97
Figure 3. 6 Illustration of the Physical model of the hydrate reservoir test domain 98

Figure 3. 7 Two-Dimensional Reservoir Model (CMG-STARS')....100
Figure 3. 8 Two-Dimensional Reservoir Model in Space (Thesis')....100
Figure 3. 9 Pressure Profile of Gas Hydrate Production....101
Figure 3. 10 Evolution of the Pressure distribution with Time....102
Figure 3. 11 Gas Saturation of Gas Hydrate Production....102
Figure 3. 12 Evolution of the Gas Saturation with time....102
Figure 3. 13 Water Saturation of Gas Hydrate Production....103
Figure 3. 14 Evolution of the Water Saturation with time....103
Figure 3. 15 Hydrate Saturation Profile of Gas Hydrate Production....103
Figure 3. 16 Evolution of the Hydrate Saturation with Time....104
Figure 3. 17 Flow Chart of algorithm for mass and heat flow in the Reservoir....111
Figure 3. 18 Production Profile – Cumulative volume of gas produced with time....113
Figure 3. 19 Production Profile – Cumulative volume of water produced with time....114
Figure 3. 20 Gas Production Rate Profile Validation....114
Figure 3. 21 Water Production Rate Profile Validation....115
Figure 3. 22 Gas production rates with and without Diffusive Flux at 350 days....116
Figure 3. 23 Gas production rates with and without Diffusive Flux at 1200 days....116
Figure 3. 24 Effect Tortuosity on Diffusive Flux....117
Figure 3. 25 Effect of Diffusion Coefficient on Diffusive Flux....117
Figure 3. 26 Effect of permeability anisotropy on cumulative production (case 1)....118
Figure 3. 27 Effect of permeability anisotropy on cumulative production (case 2)....118
Figure 3. 28 Effect of gas slippage on gas production rate....119
Figure 3. 29 Effect of gas slippage on water production rate....120
Figure 3. 30 Effect of gas slippage factor on cumulative gas production rate....120
Figure 3. 31 Effect of slippage factor on cumulative water production rate....121
Figure 3. 32 Effect threshold pressure gradients on pressure draw down....122
Figure 3. 33 The thermal expansion and Joule Thomson....123
Figure 3. 34 The thermal expansion and Joule Thomson....124
Figure 3. 35 Parameter Effects and Production Rate Probability....126
Figure 3. 36 Tornado plot of influence of variable parameters on gas production rate.127

Figure 4. 1 Schematic of Model of Physical Gas Hydrate Production System.....128
Figure 4. 2 Illustration of Discretised Fully Coupled Reservoir/Wellbore System.....129
Figure 4. 3 Schematic of delineated and discretised Wellbore.....130
Figure 4. 4 One-dimensional Discretised Wellbore.....139
Figure 4. 5 Simulation Flow Chart of the Fully Implicit fully Coupled Model....145
Figure 4. 6 Pressure Change Comparison of numerical and analytical solutions.....147
Figure 4. 7 Temperature Comparison of numerical and analytical solutions....147
Figure 4. 8 Gas Production Rate Comparison of numerical and analytical solutions.....148
Figure 4. 9 Gas production Rate of the Coupled Models....151
Figure 4. 10 Cumulative Gas Production of the Coupled Models....151
Figure 4. 11 Gas Recovery Factor with the Coupled Models....152
Figure 4. 12 Schematic of Transient Pressure and Temperature Analysis System....154
Figure 4. 13 Transient Temperature and Pressure Analysis Curve....156
Figure 4. 14 Gas recovery factor from the hydrate dynamic decomposition under different gas flow rates....156

Figure 4. 15 Effect of Wellhead Temperature on Gas Molar Fractional Flow (Aqueous CH_4 Mass Fraction) 157
Figure 4. 16 Effect of Wellhead Pressure and Temperature on Gas Molar Fractional Flow 157
Figure 4. 17 Grid Refinement and coarsened gridding model.....165
Figure 4. 18 Pressure distribution profile of fine-grids model.....166
Figure 4. 19 Pressure distribution profile of coarse-grids/upscaled model 167
Figure 4. 20 Effects of Various Relative Permeability Equations on Gas Fractional Flow from Natural Gas Hydrate.....168
Figure 4. 21 Effects of Various Capillary Pressure Equations on Gas Fractional Flow from Natural Gas Hydrate 169

NOMENCLATURE

$\bar{P}$ or ψ	*average pseudo-pressure*
ΔP	*pressure drop*
∇P	*pressure gradient*
A	*Cross-sectional*
A_s	*Hydrate dissociation surface area*
b	*non-Darcy flow coefficient*
Bg	*formation volume factor of gas*
Bw	*formation volume factor of water*
C_d	*distribution coefficient*
C_p	*specific heat capacity at constant pressure, L2/t2T*
C_t	*total compressibility*
D	*diameter.*
D	*diffusion coefficient,*
$E\infty$	*activation energy*
f	*friction factor*
g	*gravitational acceleration*
h	*formation thickness*
J	*productivity index*
J_D	*Diffusive Flux*
k	*permeability*
K_{do}	*intrinsic rate constant*
K_h	*permeability thickness product*
kr	*relative permeability*
L	*length*
M	*molecular weight/mass*
Mg	*average molecular weight of gas in mixture*
mg	*Molar mass flow rate of gas*
n	*number*
N_c	*capillary number*
N_h	*hydration number*

p	*Subscript for phase*
P_b	*bubble point pressure*
P_e	*average reservoir pressure*
P_f	*node flowing pressure*
PI	*Productive Index*
P_s	*Surface (separator) pressure*
P_{sc}	*standard pressure*
P_{sc}	*pressure at standard conditions, Pa*
P_{wf}	*average bottom-hole pressure*
P_{wh}	*wellhead pressure*
q	*flow rate*
Q	*total flow rate on the coarse cell face*
q	*well flow rate*
q_g	*gas flow rate*
q_w	*water flow rate*
r	*radius*
R	*gas-law constant,*
r_e	*external drainage radius*
RF	*Recovery Factor*
r_w	*wellbore radius*
s	*skin factor*
t	*time*
T	*absolute temperature*
t	*layer thickness*
T_{sc}	*standard temperature*
Tsc	*temperature at standard conditions, K*
T_{sf}	*Sandface temperature*
T_{wh}	*wellhead temperature*
u	*Darcy velocity*
v	*velocity,*
V	*volume,*
Vp	*pore volume*

V_{sc}	*volume at standard conditions*
WI	*well index*
Z	*elevation*
z	*compressibility factor (gas-deviation factor)*
z_{sc}	*compressibility factor at standard conditions*
α	*void fraction*
β	*conversion factor or beta factor*
γ_g	*specific gravity for gas*
ΔP	*pressure drop*
Δx	*grid-block dimensions in the x directions*
Δy	*grid-block dimensions in the y directions*
ε	*pipe roughness*
μ	*viscosity*
ρ	*fluid density*
σ	*Surface tension*
τ	*Hydraulic tortuosity*
ϕ	*porosity*
D	*depth of the coarse block*
P_c	*capillary pressure*
P_{wb}	*well bottom-hole pressure*
S_{rw}	*Residual water saturation*
Sg	*gas saturation*
S_w	*water saturation*
S_{wc}	*connate water saturation*
T^m	*Transmissibility*
V	*Volume*
f_g	*gas fractional flow*
f_w	*water fractional flow*
k	*absolute reservoir permeability*
$k*$	*pseudo relative permeability of phase p*
k_{rg}	*gas relative permeability*
k_{rw}	*water relative permeability*

$\tilde{m}$	*well (source/sink) term*
Δz	*Grid-block thickness*
γ	*gas specific gravity*

Subscripts Indices:

g	*gas*
h	*hydrate*
p	*phase*
w	*water*

CHAPTER 1

INTRODUCTION

1.1 Background and Motivation

Natural gas huge abundancy and the cleaner energy attributes have put it in the position of becoming the major fossil fuel energy source for the world, especially as the world transitions to a lower carbon energy system. The annual demand of natural gas is already trendily increasing more than the other major energy sources, oil and coal (International Energy Outlook, 2021; BP Energy Outlook, 2021). To meet up with the growing demand and to ensure energy security, exploitation of natural gas is moving from conventional to unconventional sources. Thus, a motivation of this research. Conventional reservoirs are rocks having interconnected pore spaces of porosity and permeability for easy fluid flow. They include sandstone, carbonate and limestone reservoirs. Unconventional reservoirs, on the other hand, produce from low permeability, low porosity, tight to ultra-tight formations in typically challenging depositional environments. These create predicament of unlikelihood of extracting the natural resources trapped in the reservoir using traditional production methods (Donev et al., 2021). Examples of unconventional reservoirs are Tight Gas Sands, Coal Bed Methane, Shale Gas, and Natural Gas Hydrate Reservoirs (Chong, 2016). This thesis focuses on gas production from the natural gas hydrate reservoirs, simply known as natural gas hydrates or gas (methane) hydrates.

Natural gas hydrate reserves existence and potential was acknowledged since 1965 by Petroleum Company operating in Siberia, Russia and north region of Alaska. By 1980's and 1990's, marine expeditions and laboratory analyses offered evidences of natural gas hydrate's energy potentiality and existence in large amount in many continental shelves and beneath permafrost (Sloan and Koh, 2008). The Reservoir viability depends on the rock type or sediment bearing the hydrate. Coarser-grained sediments have the most viable deposit. They have lower capillary pressures which permit preferential accumulation of hydrates in the sediment with abundant hydrates concentration disseminated in the pores and/or fractures (Collett, 2013). Studies have demonstrated that $1m^3$ of natural gas hydrate contains about 164 m^3 of methane at standard temperature and pressure, and the world potential reserve of natural

gas hydrates stands at about 0.15 x 10^{15} m^3 to 3.05 x 10^{18} m^3. This is twice as large as the other fossil fuel resources combined together (Aregba, 2017; Dillon, 1992). Thus, the interest of this research in the gas hydrate resource – methane hydrates represent an exciting and untapped resource that would help meet our expanding energy needs well into the future. Though investigations on the gas production have been confronted with defying features to possible commercial production, researches have proved that four conventional methods are effective for feasible production of the natural gas hydrates deposits. The methods include depressurization, thermal stimulation, inhibitor injection and gas replacement techniques; with depressurization method deemed the best approach (Zhao *et al*, 2016; Lee *et al*, 2015; Hope and Schaefer, 2015; Birkedal *et al*, 2015; ; Schoderbek *et al*., 2012; Moridis *et al*., 2011; Cranganu, 2009; Rochelle *et al*, 2009; Anderson, 2014; Pooladi-Darvish, 2004; Ohgaki, 1997). It has also been evaluated that combining pressurisation and thermal stimulation methods would optimize the recovery (Pooladi-Darvish, 2004; Kawamura et al., 2006; 2008; Feng et al, 2015). Experiments and numerical simulations studies by different researchers have expatiated that hydrate dissociation mechanism herald the production and the gas flow within certain thermodynamic conditions under the various approaches. For instance, Sloan (2008) explained that when arriving at critical radius, hydrate dissociation and formation will occur at random, with the hydrate growth commonly accumulating at the interface where gas and water are readily available at favourable condition for hydrate regeneration. Available production performance and optimization prediction models have not provided adequate analyses of the kinetics of the hydrate flow behaviour and phase transition to overcome the production drawbacks; hence no commercial gas production from hydrate hitherto (Vedachalam, et al, 2016; Kurihara et al, 2011). Understanding the range of uncertainty in the gas transport in the hydrate reservoir and the wellbore would help to shape the optimisation strategy, increasing the resilience of the recovery.

This research would review the existing gas hydrate performance simulation models, evaluate the modelling approaches of the fluid flow in the reservoir and wellbore. The thesis acknowledged that models that coupled reservoir and wellbore flow models offer more accurate performance prediction than the non-coupled models; and fully implicitly coupled models are being advised (Livescu et al., 2010; Ozkan *et al*, 1999; Penmatcha and Azizi, 1998; Sung *et al*. 2000, 2015; Li *et al*, 2018; Khoriakov et al, 2012; Jiang et al, 2016; Hagdu *et al*.1995; Murray and Gunn, 1993; Hasan *et al*, 2009; Pruess *et al*, 1999; Baht *et al*, 2005; Gudmundsdottir, 2012). However, there is less research focus on fully implicitly coupled

reservoir-wellbore model for gas hydrate application. This left a gap in the development of integrated gas hydrate production simulation model that better capture the reservoir-wellbore interactions, near-wellbore convective mixing processes, wellbore hydraulics, thermal effects, etc obtainable by coupling the fluid flow equations in the reservoir and well via appropriate interface treatments that yield simultaneous solutions both systems. Thus, this thesis would develop a new numerical simulation model that account for the non-Darcy flow factors, the advective and diffusive fluxes in gas hydrate reservoir for improved gas hydrate recovery. Based on the model, a fully implicitly coupled reservoir-wellbore model for gas hydrate application would be developed and a new interpretation framework for pressure and temperature transient analyses would be generated. Also, the thesis would evaluate the capillary pressure functions and relative permeability equations for the production optimisation.

1.2 Problem Statement

Natural gas hydrate reservoirs are unconventional reservoirs with gas stored primarily as caged methane in crystalline solid and the production involves the uniquely hydrate dissociation process. Fluid flows could be characterised by non-Darcy flow effects, non-linearity viscous and diffusive flow rigours such as molecular, pressure and thermal diffusions (Javadpour et al, 2009). Moreover, a typical feature of the multiphase flow in gas wells is the near-wellbore complexities encompassing complex flow phenomena, near-wellbore convective mixing processes and thermal wellbore effects leading to quick cessation of gas hydrate production noted in various researches in literature (Chong *et al.*, 2017; Oyama *et al.*, 2009; Song *et al.*, 2015; Zhao *et al.*, 2015; Moridis *et al.*, 2011; Moridis *et al.*, 2004; Collette, 1993; Yamamoto, 2014; Li *et al.*, 2010a, 2010b; Konno *et al.*, 2010; Mutalik, 1989; Li *et al*, 2007; Davie and Buffett, 2003; Yakushev and Istomin, 1992; Bai *et al.*, 2015; Kuhs *et al.*, 2004; Stern *et al.*, 2001; Komai *et al.*, 2004; Ohno, Narita and Nagao, 2011; Sun *et al.*, 2011; Bai *et al.*, 2015). Flow regime changes with different phases distributions influenced by pressure differentials and velocity changes can be correlated to capillary pressure gradients and relative permeability functions (Jansen and Currie, 2004). Phases separate and travel with different velocity; the highly compressible gas phase expands with increasing in-situ volumetric flow rate; phases have different pressures; and gas slippage, liquid hold-up, near-wellbore complexities are

prominent. More so, the gas hydrate system is known to be characterised by exclusive features, such as hydrate dissociation, reformation, and transient temperature effects. Thus, solving the transient flow problems and the flow assurance challenges could require incorporation of the multiphase and multicomponent parameters and processes affecting the delivery of inflow and intake profiles in the gas hydrate reservoir expanse and the wellbore into the modelling approach for the more accurate performance predictions; and models that provide for coupled the reservoir and wellbore fluid flow as a single continuum are being advised (Yin et al, 2016; Miller,1980; Stone et al, 1989, 2002; Pourafshary et al., 2009, Souza et al, 2014; Pan, 2014; Ertekin, 2001; Mazumba, 2016; Halliburton, 2017; Song et al, 2015; Tatar et al., 2014; Pan and Oldenburg, 2014; Naderi et al, 2015; Li et al, 2018). Continued use of the decoupled approach for the gas hydrate system evaluations might be attributed to the difficulty in solving simultaneously the integrated systems of equations which fully implicitly coupled the reservoir and well. Considering the vast differences in length and time scales for both systems, combining the challenges of the strongly coupled processes in the reservoir and wellbore with the potential for complex flow patterns in gas hydrate wells is a daunting task requiring a lot of computational time. However, the issuing results obtained using the integrated approach motivated the modelling concept. Numerical simulation of the fully coupled model had been demonstrated to give improved accuracy in the well deliverability analyses and thus have become very attractive. This thesis would incorporate and integrate the defying features of the fluid flow in the unconventional gas hydrate system and develop a fully implicit fully coupled reservoir-wellbore fluid flow model for gas hydrate application.

1.3 Description of Research Gap

There is no known existing gas hydrate numerical simulation model in literature that has simultaneously incorporated the inherent defying features to gas hydrate fluid flow such as impact of gravity, threshold pressure, diffusivity flux, Joule-Thomson effect, inertia and gas slippage effects in the analyses of the gas hydrate production. This thesis would develop a simulation model of natural gas hydrate production that accounts for the unconventional fluid dynamics, non-Darcy flow factors and the various convection and diffusion fluxes that correlate with the complex nature of the gas hydrate reservoir to impede the fluid flow assurance. More so, there is no model in literature that focused much on fully implicit, fully

coupled gas hydrate reservoir and wellbore fluid flow for the production optimisation. The available gas hydrate reservoir simulators and well models in literature (including HydrateResSim, CMG STARS and TOUGH+HYDRATE) do not offer the fully integrated solutions. Besides, their algorithms are not necessarily available for modification to obtain the seamlessly fully implicit fully coupled model. Moreover, relevant open source simulators cannot be used in this research work because their algorithms are also not readily available for accurate required numerical tuning. Furthermore, for heterogeneous reservoirs like gas hydrate reservoir with complex thermodynamics and fluid flow processes, application of fully coupled models created for other specific reservoirs studies is disadvantageous because of the unique unconventionalities of the gas hydrate reservoir including hydrate dissociation kinetics. This research would incorporate and solve simultaneously the phase transitions and transient flow phenomena associated with the gas hydrate reservoir and wellbore fluid flow, as an apparent system that exhibits convective fluxes, advective and diffusive mass and heat fluxes, to develop a fully implicit coupled reservoir-wellbore fluid flow model for gas hydrate application. Furthermore, the thesis would leverage on the model to handle simultaneous heat and mass transfer processes for the pressure and temperature transient analyses application; and investigate the relative permeability and capillary pressure equations using near-wellbore upscaling.

1.4 Research Questions

The relevant questions below would guide the research objectives, the methodology used and results obtained:

- What factors and/or mechanisms affect the unconventional fluid flow and the convective mixing processes in gas hydrate reservoir production.
- Does fluid flow in the well has influence on pressure responses from the reservoir.
- How best can the dynamic interactions and hydraulic communications between the wellbore and the reservoir be captured.
- Can commercial production be deemed feasible within the modeling approach.
- What pressure and temperature values would result in gas flow assurance and production optimisation.

- How do different capillary pressure and relative permeability equations affect gas hydrate fluid flow analyses and the well deliverability; and what is the impact of hydrate saturation.

1.5 Aim and Objective

The aim of this research is to identify the microscopic and macroscopic flow parameters and processes defying gas hydrate production, aggregate them into the modelling approach, and develop a fully implicit coupled reservoir-wellbore model for gas hydrate application.
The objectives are to:

- Incorporate the various unconventional multiphase parameters that affect fluid flow in the hydrate reservoir and well deliverability.
- Couple the advective and diffusive mass fluxes and conservely formulate the continuity equations focusing on depressurisation-induced gas hydrate production.
- Develop the transient flow numerical simulation model for the more accurate gas hydrate reservoir performance predictions.
- Incorporate wellbore hydraulics, near-wellbore convective mixing processes/crossflow parameters, and fully implicitly couple the reservoir and wellbore to optimise production.
- Develop pressure and temperature transients' interpretation workflow (numerical solutions) based on the analytical model.
- Evaluate the parameters for capillary pressure and relative permeability functions and analyse the effects of the different equations on gas hydrate production.

1.6 Scope

The thesis would leverage on computational fluid dynamics techniques that describe gas hydrates flow fluid behaviour in the reservoir and well to create new kinetic formulations for the reservoir performance evaluations. It would expound the unique characteristics of the gas hydrate reservoirs and the wellbore, review the fluid flow modelling approaches and large pools of widely used fluid flow models, provide fundamental understanding of the parameters governing the fluid flow equations, develop and use new simulation models to analyse the effects of various factors on the way gas and water flow in a hydrate reservoir including the rates of production through of the wellbore to the surface facility. Specifically, the research

would be directed at developing a fully coupled reservoir-wellbore numerical simulation model that allows for the more integrated modelling of gas hydrate fluid flow behaviour. The reservoir was described by a two-dimensional cross-sectional discretised grids model and the well one-dimensional; and simulation is tended to proceed in vertical conformance. The work derived the gas hydrate reservoir fluid flow equations by assuming non-Darcy flow, no flow boundaries conditions, and isothermal wellbore effect in the depressurisation-induced gas hydrate production. More so, since gas hydrate dissociation is an endothermic reaction, the system would be further treated as a non-isothermal system. Other assumptions are:

- Sediment is not compressible.
- Three discrete phases are present – hydrate, water and gas
- Conservations law is phase-wise, not component-wise.
- Gas dissolution in water phase, water vapor formation and Ice formation are neglected.
- No precipitation of dissolved salt in the process and no chemical reactions.
- Reservoir is infinitely acting.
- Reservoir is heterogeneous, anisotropic
- For Isothermal case, the system is assumed to gain or loss heat from the surrounding under adiabatic expansion and Joule–Thomson process.
- For non-isothermal case, thermal wellbore/external heat source is considered
- Fluid Flows under slip and inertial forces, viscous and Knudsen diffusions mechanisms
- Advective mass flux and the diffusive mass flux terms were at play.
- Hydraulic communication between reservoir and wellbore is prominent.

The limitations to this work include approximation of some parameters whose field values could not be obtained from validated literature sources. More so, the research could not go into the importance mechanisms such as poro-elasticity and geomechanics which are known to affect the fluid flow dynamics and features related to deformation of gas hydrate sediments. Besides, coupling of the full thermal wellbore effects could include accounting for the heat transfers linked with the complete well completions, tubing, annulus, insulation, casing and cementing, which are necessary following that gas hydrate is a strong candidate of thermal production method. The techno-economics of the hydrate system and model have not been provided for analyses.

1.7 Methodology

This thesis leveraged on the physics and quantitative analysis of fluid flow and coupling processes in gas hydrate reservoir and the wellbore system. This thesis utilised the conservation laws of mass, momentum and energy to develop a scalable reservoir and wellbore mathematical models that better define and describe the fluid flow in the gas hydrate production. Considering that flow dynamics in gas hydrate reservoirs is characterized by very low-permeability, heterogeneity, reaction kinetics (dissociation reaction) and high-to-low flow rates effects, assumptions of non-Darcy flow sufficed. Complex factors, which are conventionally neglected, that affect fluid flow in the gas hydrate reservoir such as threshold pressure, inertial and gas-slippage effects, advective and diffusive fluxes are incorporated in the formulation of a new flow model in this thesis. More so, a fully coupled reservoir-wellbore model is developed by seamlessly linking the reservoir model to the well model by incorporating the near-wellbore convective mixing processes, the reservoir-wellbore interactions, wellbore hydraulics. The fully coupled method involves simultaneously solving the wellbore and reservoir flow equations using a numerical scheme that is forward in space and time. The equations for flow in both the reservoir and wellbore are derived for each occurring phase and discretised across the reservoir grids and well segments of the hydrate production system. These would result in stiff coupled partial differential equations. The numerical solutions are obtained by discretization of the equations in time and space using finite difference scheme. Time discretisation is by first-order up-winding finite difference and space discretisation by first and second order central finite difference scheme. The solutions of the discretised equations are obtained by fully implicit approach using Newton-Raphson method implemented in MATLAB. MATLAB is a programming language, efficient in solving numerical problems related to fluid dynamics. Additionally, macroscopic laws of near wellbore upscaling associated with capillary pressure and relative permeability is implemented and effects of the different equations are evaluated to optimise flow and quantify production. Schematic of the model development is presented in Figure 1.1 below:

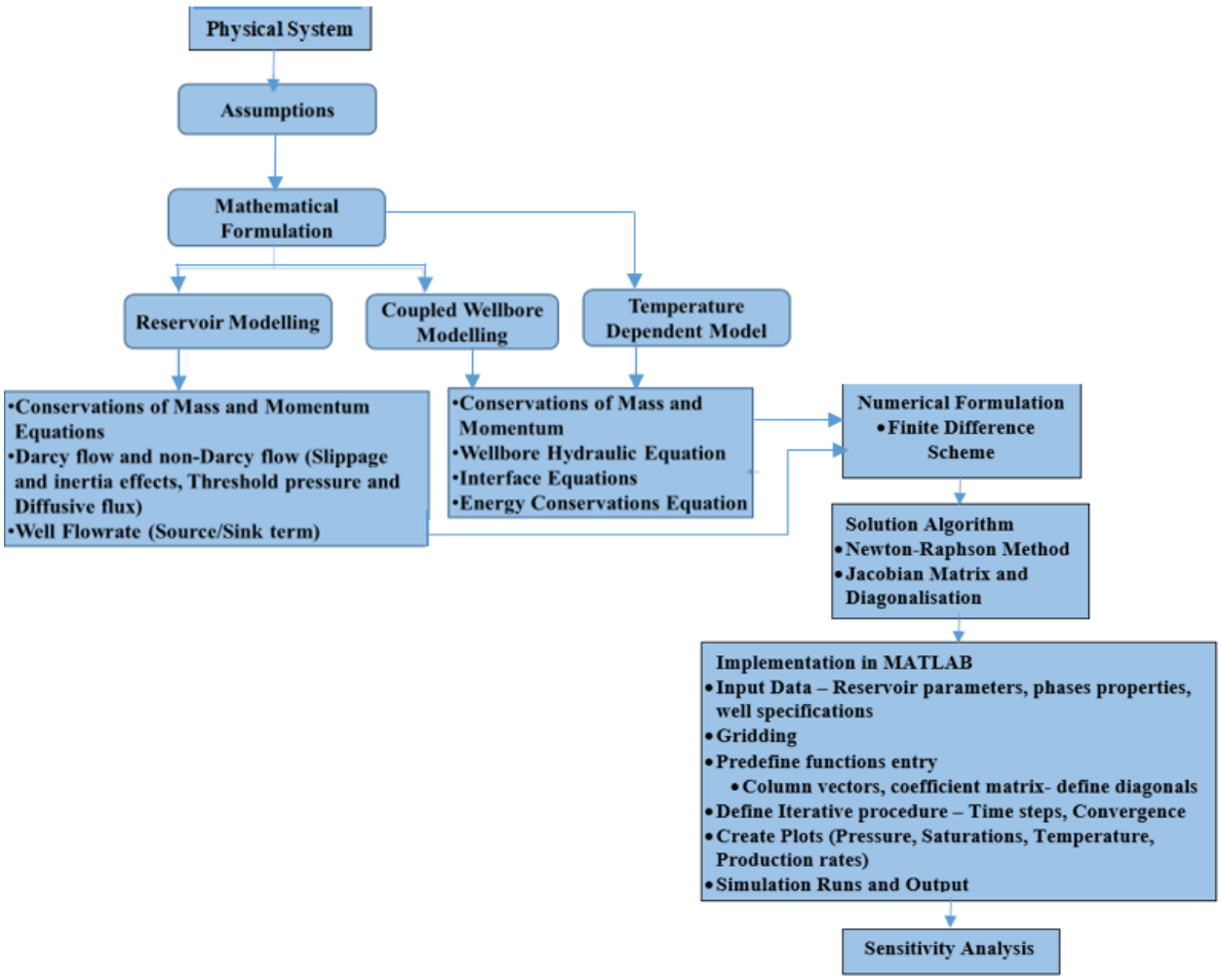

Figure1.1 Schematic of the Study Methodology and Model Development

1.8 Thesis Outline

This sequence of the thesis is as follows:

Chapter 1 introduced and contextualised the research. It presents the background, motivation, research gap, aim and objectives of the study, addressing the scope, methodology and outline of the thesis.

Chapter 2 contains the literature review of the critical aspect of the gas hydrate resources, the reservoir production, performance prediction and optimisation schemes. The chapter dovetailed into identifying and substantiating the conceptual and theoretical

frameworks upon which the research problems, gap(s) and solutions methodologies are built.

Chapter 3 covers the modelling techniques and incorporations of the inherent defying features of gas hydrate reservoir fluid flow. In this chapter, the modified governing equations of the reservoir fluid are formulated and solved using the prescribed numerical scheme and modelling approach, finite difference approximation and Newton-Raphson implicit numerical scheme, that resolve the reservoir flow dynamics in space and time. Specifically, this chapter presents a new two-dimensional reservoir flow model for natural gas hydrates application and the results and discussions of some sensitivity parameters, and use of Monte Carlos simulation method implemented in MATLAB for the uncertainty analyses.

Chapter 4 described the fully implicit fully coupled reservoir and wellbore fluid flow modelling approach for gas hydrate application. Here, the detail wellbore mass and heat transport and the coupling gas hydrate reservoir conservations equation are presented and solved. The algorithm for the coupled reservoir-wellbore model are also developed and presented. This chapter presented the validation and comparison of the fully implicit fully coupled model with an analytical solution of one-dimensional transient pressure and temperature wellbore model. The scheme is used to evaluate some parametric effects. Pressure and temperature transient analyses are carried out using the developed model. The chapter further extend the model to near-wellbore upscaling and analyses of the effects of the various capillary pressure and relative permeability functions on gas hydrate production.

Chapter 5 concludes the thesis and finding of the research, making recommendations for the future work.

CHAPTER 2

LITERATURE REVIEW

2.1 Theoretical Framework

Hydrates are crystalline solid mixture of light gaseous molecules (methane, ethane, propane, carbon dioxide, nitrogen etc) and water molecules. They are formed when gaseous molecules (acting as guest) got entrapped in the water molecule lattice (the host) under thermodynamic conditions of low temperature, above or below the freezing point of water, and high pressure as in Eq.1 (Sloan and Koh, 2008). Methane hydrates, normally called gas hydrate or natural gas hydrates, are ice-like clathrates of methane and water (Licence, 2008). They naturally occur as solid deposits confined in reservoir rocks found in two kinds of geological depositional environment: under permafrost and beneath ocean floor of continental shelves. Figure1.1a and Figure1.1b showed the generic phase diagrams for methane hydrate formation under permafrost and ocean bed respectively. The yellow sections in the diagrams indicate the gas hydrate stability zones (GHSZ) which are regions in the permafrost and oceanic sediments where the methane hydrate formations and depositions are favourable. The methane hydrates would form because of existence of appropriate pressure and temperature for the hydrate stability. In the figure 1.1, the stable region is situated between depths of 200m and 1,100m for the permafrost and from about 1200m to 1500m for the sediments of oceanic or continental margins. The oceanic deposits thickness is said to be around 300 – 500m thick in the sediments. Though the stability zone can be lengthened to above the sea floor, the concentration of methane is usually elusive above the sea floor to create viable hydrates, methane being gaseous (Dickens,1997).

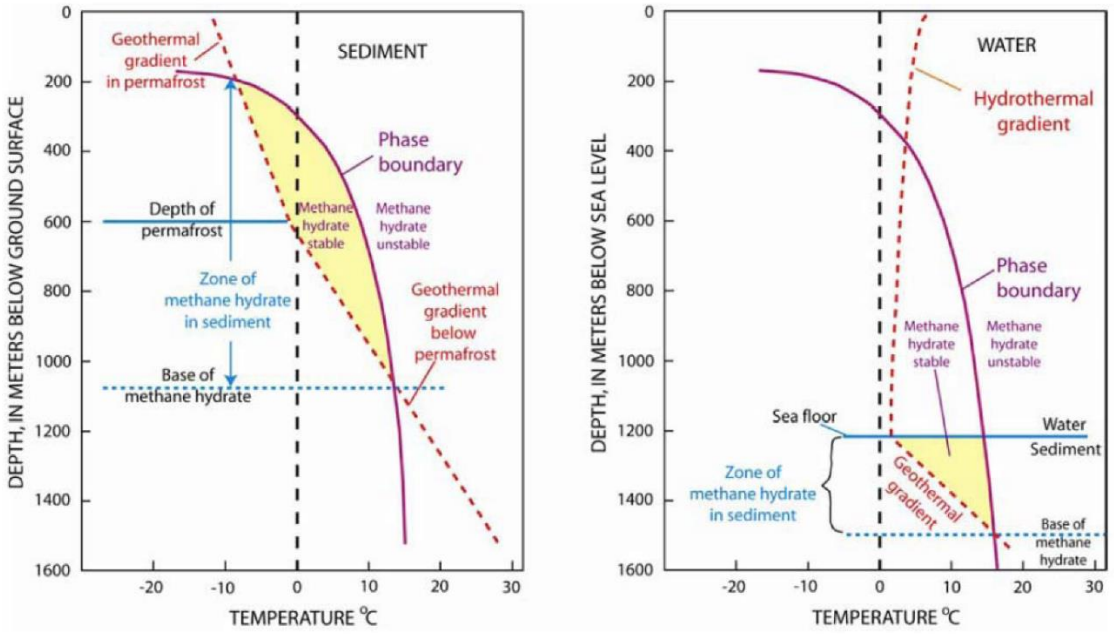

Figure 2:1 Phase diagram for methane hydrate formation under the (a) permafrost and (b) ocean bed (Sloan et al, 2010)

Aman and Koh, (2016) noted that the accumulation of the methane hydrate is a function of the mass and heat transfer rates, influenced by the gas consumption with time at a constant pressure and temperature to achieve the hydrate formation and stability (Aman and Koh, 2016). Generally, molar reaction of gas (G) hydrate is expressed as follows:

$$G + N_h H_2 0 \rightleftarrows G.N_h H_2 O \quad (2.1)$$

Typically, the stoichiometry for natural gas hydrate can be represented as

$$CH_4 + N_h H_2 O \leftrightarrow CH_4.N_h H_2 O \quad (2.2)$$

Silva and Dawe, (2011) described Natural gas hydrate as a deep-freezing version of liquefied natural gas (LNG) and an enticing source of methane gas. This is because the crystalline lattice or cage of the hydrate is firmly packed with the methane molecules inside it with large energy density. Compared to ice, hydrogen bonds found in hydrate is about 1% more than in ice; hydrates are more impervious to crush compared to ice (higher yield strength); hydrates depict more thermal expansion and lower dielectric constant. When the methane hydrates are exposed to conditions that are not favourable to keep it stable, especially change in pressure and temperature, it would begin to undergo dissociation process – the solid lattice turning into water with the trapped gas escaping. The gas ignites when the dissociating hydrate is lit – reason why

the hydrate being called burning ice (Beaudoin, 2014). The hydrate pressure – temperature phase diagram, figure 2.2, is used to describe the thermodynamic phenomena (Sloan, 1998). All these make natural hydrate an exploitable and viable energy source. Figures 2.2a – 2.2c below present different physical appearance of methane hydrate in natural form.

(a): Methane hydrate as burning ice (Bump, 2012).

(b) Natural gas clathrate in marine environment (Wusel007, 2002)

(C). Natural Gas hydrate core sample (Beaudoin, 2014).

Figure 2:2 (a) Methane hydrate as burning ice, (b) Natural gas clathrate in marine, (c) Natural Gas hydrate core sample

This thesis does not intend to underscore the mechanisms of natural gas hydrate formation as it is not within the scope of the thesis; however, the understanding of the nature of hydrate formation, appearance and occurrence are necessary in analysing the hydrate phase behaviour, fluid dynamics, production and viability.

2.2 Structure of Natural Gas Hydrates

Hydrates are categorised into three structures based on the geometries of the structural orientation of the constituent water and gas. We have Structure 1 (SI), Structure 2 (SII) and Structure H (SH). The differences between the structures arose from thermodynamics stability of the host and occupying guest molecules (Xia et al., 2017). Structures I and II are cubic while structure H is hexagonal. The guest molecules have size ranging from 0.40 - 0.90 nm in diameter and are entrapped in cavities of different sizes. The molar gas (guest) to water (host) ratio is 1:5.57 at standard temperature and pressure (STP), corresponding to 168.27m^3 (Methane):1m^3(Water) by volume optimal occupancy. Sloan (2008) noted most experiments are based 90% occupancy in conversely realistic. the gas to water ratio is 1:6.39 (corresponding to 155 m^3 methane occupation) at STP (Sloan, 2008). The calculation is made as below:

$$\left(\frac{16\text{gm/mole}}{16\text{gm/mole}+6.39\ \text{Xx}\ 18\text{gm/mole}}\right)\left(\frac{900\text{kg}}{0.717\text{kg/m}^3}\right) = 155\text{m}^3 \qquad (2.3)$$

SI hydrates are found to be the most prevalent of the three structures and are common with deep waters. SI make up greater than 99% of every hydrate found in oceanic environments (Jemai, 2014). The crystalline cages are wide and centrally organised such that the water molecules (host) can always re-shape (Sloan and Koh, 2008). The methane hydrate model is shown in Figure 2.6 below. Silva and Dawe (2011) described that the guest molecules are small, of diameter 0.40 - 0.55 nm, as such that a unit cell of a SI hydrate has 46 molecules contained in a shape of two small dodecahedral cages (12 pentagon faces each, 5^{12}) and six large tetra-decahedral cages (12 pentagon 2 hexagon faces each, $5^{12}\,6^2$). It was further pointed that the SII and SH hydrates can accommodate higher molecular weight molecules; however, they are not widespread in nature; SH is the least found in nature. SII typically encases propane or iso-butane while SH encases cycloheptane or combinations of methane gas and nexohexane. SII types can consists of eight 512 64 cages, sixteen 512 and 136 molecules of water while Structure H can contain two 435663 cages, three 512 cages and one 512 68 cages with 34 molecules of water.

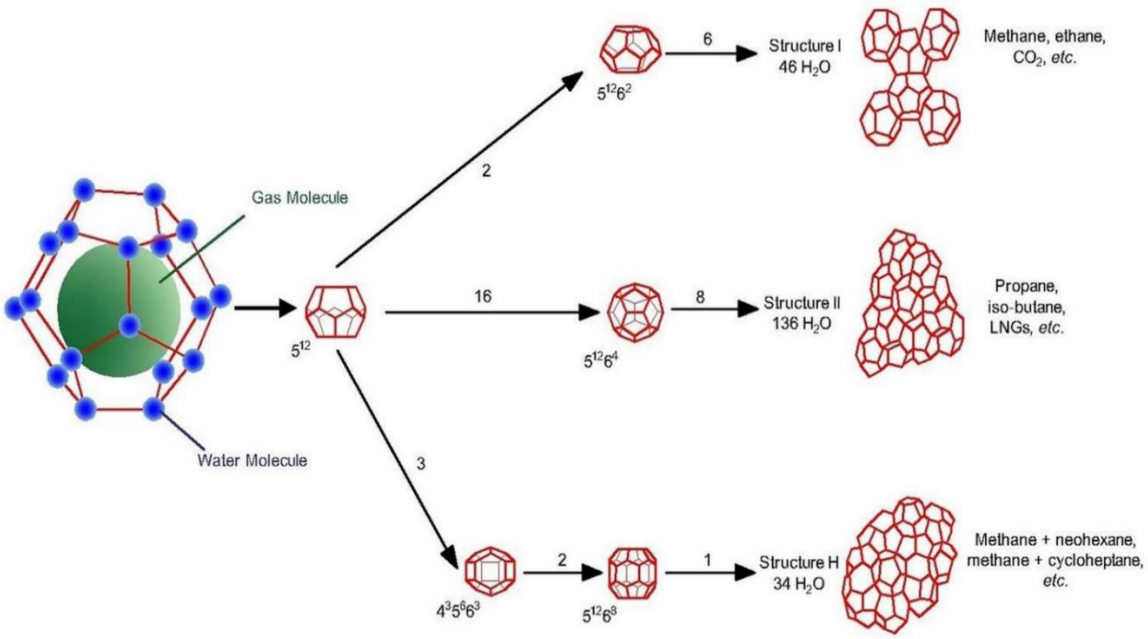

Figure 2.3 Natural gas hydrate in-cage model and structural forms (Sholihah and Sean, 2021)

2.3 World Hydrate Resources

Natural gas hydrates are found under the permafrost and beneath seabed along most continental margins, at depths ranging from 130m to 2000m (Huneker, 2010). The reservoirs are tagged hydrate bearing sediments (HBS). Moridis et al, (2008) and Dawe et al, (2007) estimated that the world potential reserve of gas hydrates stands at about 0.15 x 10^{15} m^3 to 3.05 x 10^{18} m^3 at STP, with 97% located offshore and 3% on land (Permafrost). Saxena, (2012) noted that the total world natural hydrate resources are twice as large as the combined fossil fuel resource and that 1m^3 of methane hydrate contains about 164 m^3 of methane at standard temperature and pressure. Lu, (2015) evaluated that the energy needed for the hydrate dissociation is 85% less the energy value of the produced methane, underscoring high production efficiency. Research and development of gas hydrate are therefore being advanced. The first world gas hydrate field production test was in 2007 at the Malilik site, Mackenzie River Delta, Canada and the latest and first offshore production pilot test was in 2013 at Nankia Trough, Japan. Vedachalam (2016) noted that there are about two hundred and thirty (230) Natural Gas Hydrate deposits locations worldwide and those with experimental drilling data are:

- Mallik site, Mackenzie river delta in Canada
- Nankai Trough in Japan,

- Mouth Elbert, North Slope Alaska, Gulf of Mexico, USA
- Krishina basin in India
- Messoyakha Field, Russia
- Pearl mouth basin, South China sea, China
- Shenhu basin, South China sea, China
- Ulleng basin in Korea.

The wide spread of the methane rich hydrate reservoirs around the world and the restriction to shallow lithosphere (that is < 2000m) all constitute in the high interest in the resources. It is worth noting that a country like Japan that rely import to meet her natural gas needs are recorded to have huge hydrate deposits that can make them self-reliant. Thus, when hydrate production become commercially feasible, it might become the game changer in the world energy market. Figure 1 shows the worldwide distribution and locations of potential hydrate deposits.

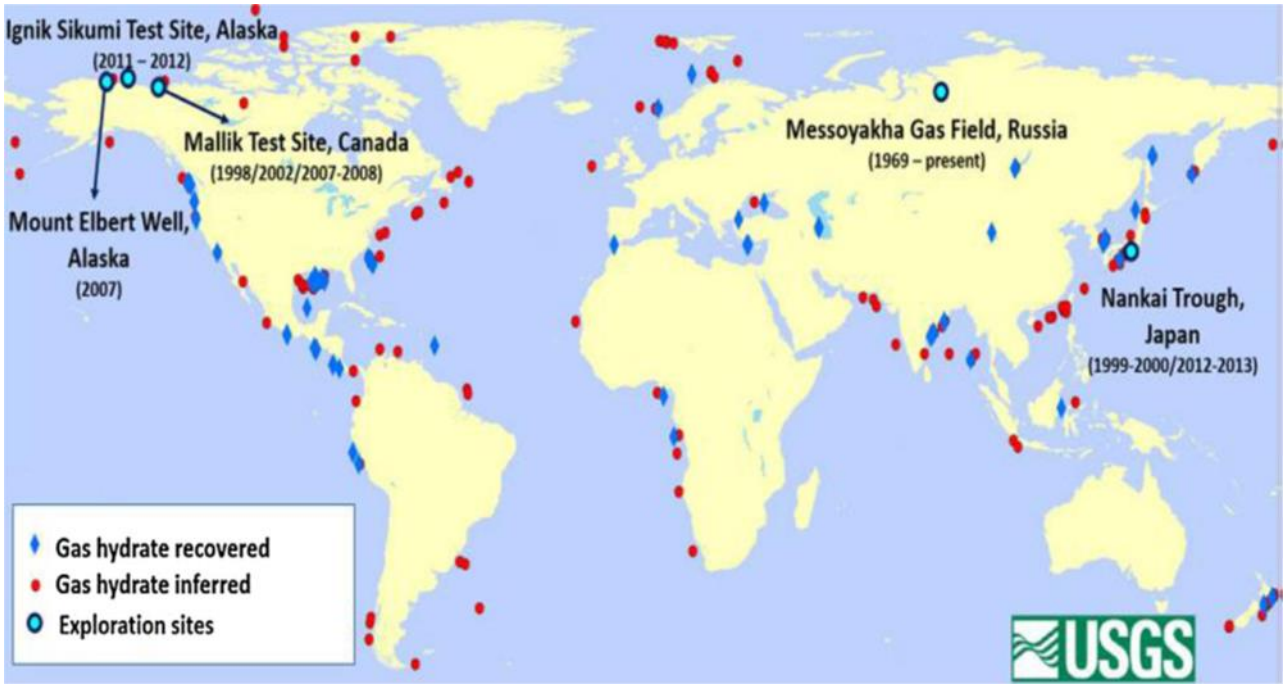

Figure 2.4: Natural Gas Hydrate Deposits and Major Developments Locations Map (Vedachalam et al, 2016).

2.4 Types of Hydrate Reservoirs

There are three types of natural gas hydrate reservoirs based on their depositional environment, the hydrate distribution and saturation characteristics (Kurihara and Ouchi, 2011). Figure 2.6 presents the hydrate forms; they include:

i. **Pore filling type methane hydrate reservoir:** Sand-rich reservoir rock with pore spaces and/or fractures, typical of conventional reservoirs, filled with hydrates. These hydrate reservoirs are found in the Eastern Nankai Trough, Japan, Mallik site and Mt. Elbert, Canada.

ii. **Naturally fractured type methane hydrate reservoir:** Hydrates found in natural fractures of formations of impermeable layers like shale. Example are those of offshore India and Korea.

iii. **Massive/nodule methane hydrate deposit:** Methane hydrates existing in lumps and accumulation in fine-grained mud at sea floor. The deposits are found offshore Gulf of Mexico and Sea of Japan.

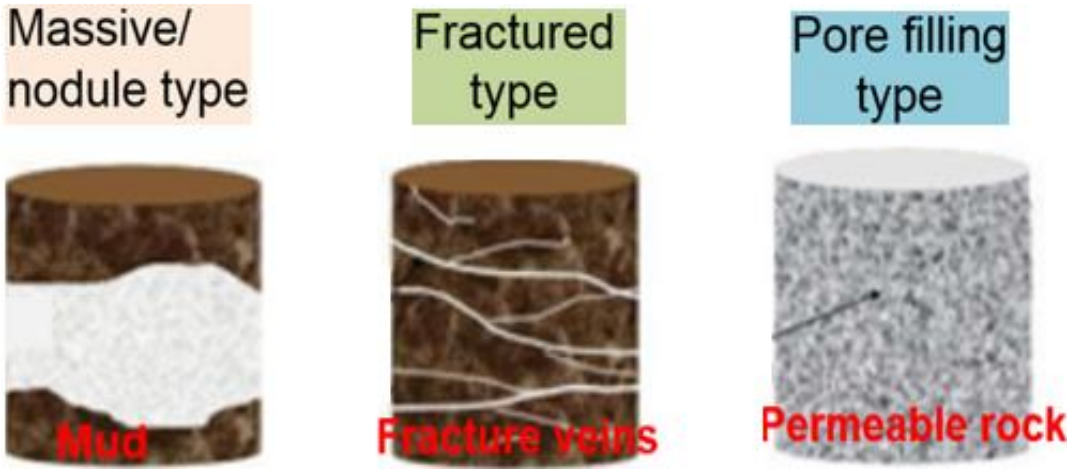

Figure 2.5 Schematics of Types of Hydrate Reservoirs
(Kurihara and Ouchi, 2011)

2.5 Classification of Gas Hydrate Reservoirs

Gas hydrate bearing sediments have also been classified in line with the structural layering and profile of the position of the hydrate deposit in the arrays of the surrounding with respect to the bottom of the hydrate stability zone (BHSZ) (Xia *et al*, 2017 and Vedachalam *et al*, 2016). The

Classifications include three distinct classes and a fourth class that is yet to be well grasped. The diagrammatic representations are as in figure 2.6 below.

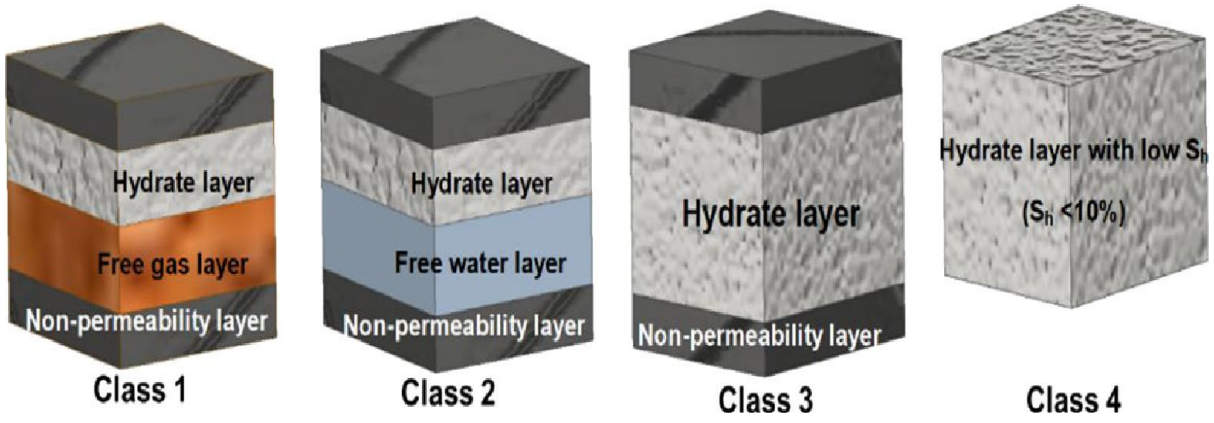

Figure 2.6 Four Classes of hydrate deposits (Lee et al., 2011)

These are explained as follows:

- *Class 1 (Reservoir underlain by free gas*): The reservoir consists of two layers of hydrate interval (a pore space layer containing large hydrate saturation and an underlying layer containing aqueous phase with free gas) crammed between impermeable under-burden and over- burden layers. Class 1 Accumulation is shown in figure 2.9.1. Messoyakha Field in Russia and Sagavanirktok Formation in Alaska are typical examples of this type of reservoir.
- *Class 2 (Reservoir underlain by water zone):* The hydrate bearing sediment is underlain by water bearing sediment (such as an aquifer) with no free gas. Figure 2.9.2 illustrates the class 2 hydrate accumulation. A part of Eastern Nankai Trough Japan and the Mallik site in Canada are examples of Class 2 methane hydrate reservoirs.
- *Class 3 (Confined reservoir).* These are single zone hydrate bearing sediments with no underlying fluid sediment layer, Figure 2.9.3. The hydrate sediment is rather directly crammed between impermeable layers like shale wherein the pore spaces might be filled with hydrates with small amount of water and no gas contact. Most MH reservoirs discovered in the Eastern Nankai Trough, Mallik site and Mt. Elbert 9 are categorised as Class 3.
- *Class 4 (Mud layer with sparsely deposited hydrate reservoir).* Moridis et al (2008) noted that the Class4 MH reservoir is poorly understood and appears to have no

potential for production. Xia *et al*, (2017) expressed that class 4, unlike others, has no intrinsic permeability.

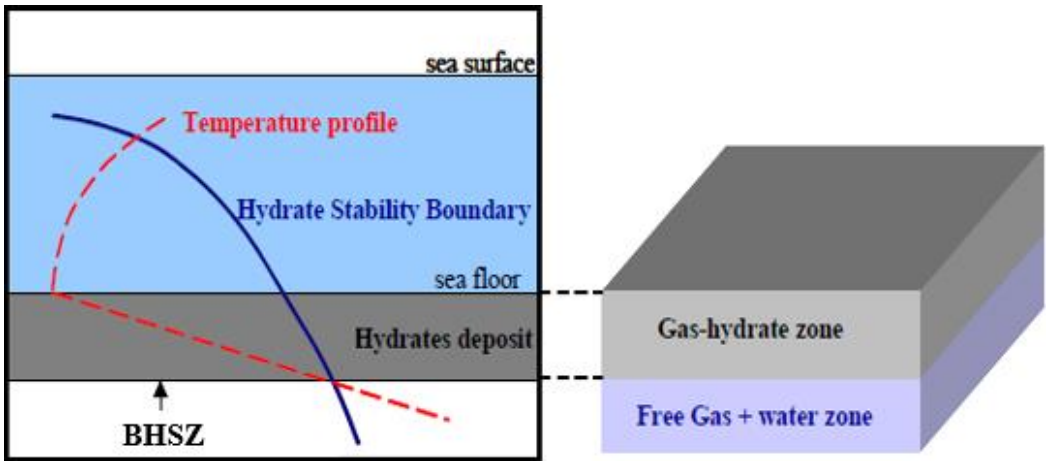

Figure 2.7 Class 1 Gas Hydrate Sediment Structural Profile (Xia *et al*, 2017)

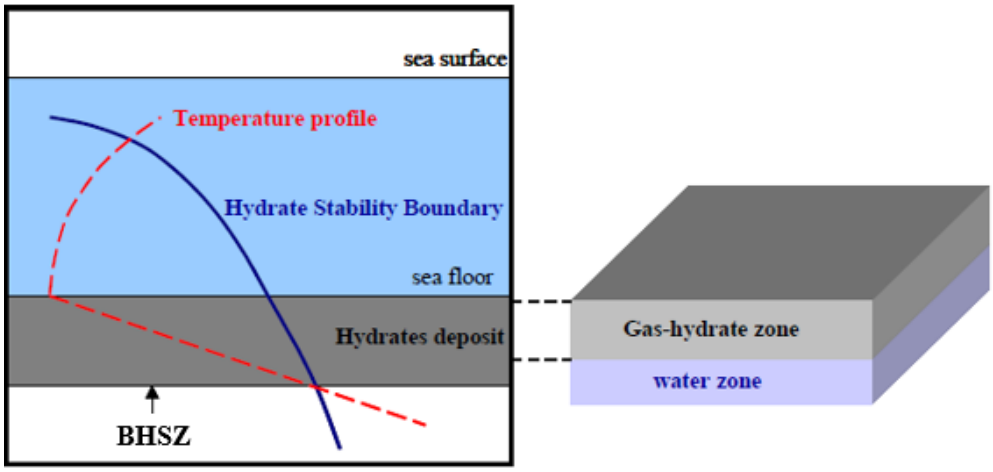

Figure 2.8 Class 2 Hydrate Sediment Structural Profile (Xia *et al*, 2017)

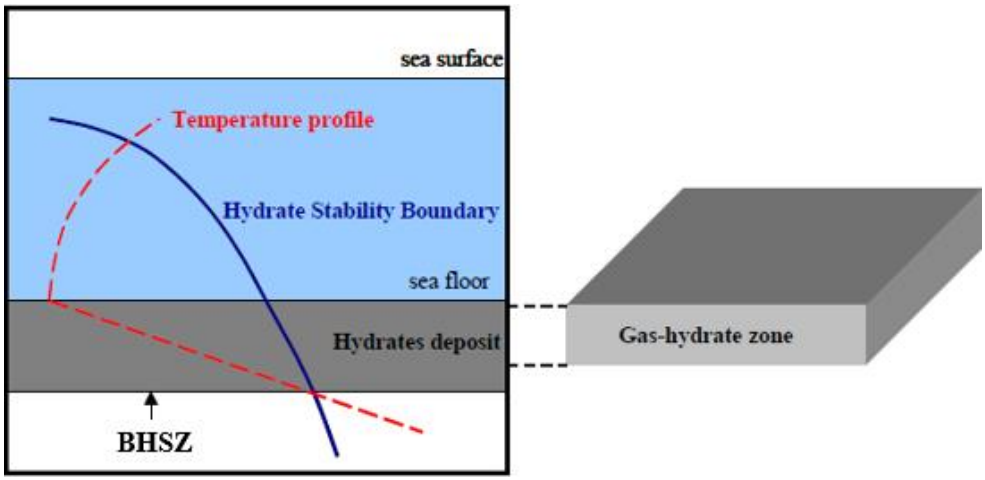

Figure 2.9 Class 3 Hydrate Sediment Structural Profile (Xia *et al*, 2017)

Conventionally the hydrate intervals are crammed between impermeable underburden and overburden layers, lending themselves to economical exploitation. Moridis and Collett (2003) explained that the hydrate phase becomes unstable below the BHSZ because pressure and temperature increase with depth under sea floor. Thus, perturbation within the hydrate stability zone can cause changes in pressure and temperature due to geothermal gradient, induce dissociation and production process.

2.6 Properties of Hydrates Gas Hydrate

Understanding of the parameters and characteristic of the methane hydrate reservoir is necessary to model the behaviour and performance of the reservoir under different condition and develop appropriate production process. Field and experimental studies have been carried many researchers to examined and validated the reservoir parameters and components properties. The properties and behaviour of hydrate sediments result from complex Thermo-physico-chemical and mechanical interactions between the reservoir pore grains and the fluids. The parameters contributing to the interactions are expressed as sediment index properties, and are used to conceptualise, characterise and model the reservoir, engineering design, and production. The properties have been shown to be of variable values and are affected by the natural gas hydrates reservoir type, form, location and depositional environment as demonstrated in table 1 (Waite et al., 2009). Table 2 and 3 present the literature data of different values of some of physical properties gas hydrate and the components characteristics respectively. Representative experimental data would be selected from the literature and used to create a base case simulation model and subsequently carry out sensitivity analysis of the impacts of the value limits on the gas recovery.

Table2. 1 Typical Features of Gas Hydrate Reservoirs in Different Locations.

Reservoir Type	Sediment Type	Dominant Gas Hydrate Type	Hydrate Saturation, Max (%)	Locations		LL (PI)	Reference
Coarse grained	Sand, gravel	Pore filling	80	Mackenzie Delta (Permafrost), Canada,		-	Delimore et al. (1999); Uchida and Takashi (2004); Winters et al. (1999)
Fine grained	Clay, silt	Finely disseminated, nodules, layers	≈10	Nankia Trough, Japan		-	Uchida and Takashi (2004)
				Blake Ridge, Canada		0.68 - 0.99 (0.44–0.64)	Paull and Matsumoto (2000); Trehu et al. (2004); Winters (2000); Winters et al. (2007).
				Hydrate Ridge, Oregon-USA		0.64 - 0.87 (0.25 - 0.45)	Tan et al. (2006).
				Gulf of Mexico		0.51- 1.02 (0.28 - 0.57)	Francisc et al. (2005)
				India Continental shelf, offshore India		0.73 - 0.75 (0.34 - 0.36)	Yun et al. (2009)
Fractured	Clay, silt	Complex vertical vein	≈100	India Continental shelf, offshore India		-	Collett et al. (2008); Winters et al. (2008)

Table2. 2 Literature review for gas hydrate reservoirs properties

Parameter	Chen et al. (2010)	Myshakin et al (2009)	Liu et al. (2009)	Uddin et al. (2008)	Waite et al. (2009)	Kurihara et al. (2011)	White et al. (2003)	Hamed Tabatabaie & Pooladi-Darvish (2010)	Howe et al. (2009)	Sung et al. (2002)
Porosity	0.5	0.35	0.2	0.28	0.3	0.35	0.3	0.3	0.36	0.2
Permeability (mD)	0.1	1,000	4.2	20	140	1,000	1,000	-	300	10–100
Thickness (m)	-	60	-	10	-	12.5	30	16	15	15
Radius (m)	-	900	100	200	-	450	567	100	-	-
Initial pressure (MPa)	20.37	10.9	-	6.91	-	6.8	10.67	8.54	-	5.51
Initial temperature (°C)	3.1	12.45	12-16	10	-	2.8	13.5	12	11	4.75
BHP (MPa)	-	-	3-4	4.3	2	-	4	-	2.07	3.45
Initial Saturation, Gas	-	-	-	0.1	-	0	-	0	0.1	0.4
Initial Saturation, Water	-	-	-	0.3	-	0.35	-	0.25	0.2	0.3
Initial Saturation, Hydrate	-	0.4	0.19	0.6	-	0.65	-	0.75	0.7	-
Heat capacity, Rock (J/kg·K)	-	-	2,200	1,600.5	2,031	1,300	-	1,600	1,350	-
Thermal conductivity, Rock (W/m·K)	1	0.5	2.73–5.57	1.5–8	2.7	2	0.5	1.5	1.7	-
Heat of Reaction, Rock (KJ/mol)	-	-	54.7	51.9	-	-	-	-	-	-

Table2. 3 Gas hydrate Components properties

Parameter	Methane-Hydrate	H_2O	CH_4	Data Source
Density (kg/m3)	919.7	1000	27.6	Hong et al. (2010)
Molecular weight (kg/kmol)	119.5	18	16	Uddin et al. (2008)
Heat capacity (J/kg·K)	2200	b*	b*	Liu et al. (2009)
Thermal conductivity, Rock (W/m·K)	0.5	0.6	0.04	Gabitto et al. (2010)

2.7 Gas Hydrate Production Methods

Physical experiments and numerical simulations have been conducted by many researchers to investigate the production performance and the optimization mechanisms under various approaches. Presented production methods that have also been efficiently explored include – Depressurization method, thermal injection method, Inhibitor injection and Gas Injection techniques. Challenges identified to have hindered commercial production to date include, among others, inadequate understanding of the mechanisms that control the dissociation and the gas flow (Pooladi-Darvish, 2004; Moridis et al., 2005; Schoderbek et al., 2012).

The methods, demonstrated to have technical viability include: depressurization, thermal stimulation, inhibitor injection and CO_2 replacement (Moridis *et al*., 2011).

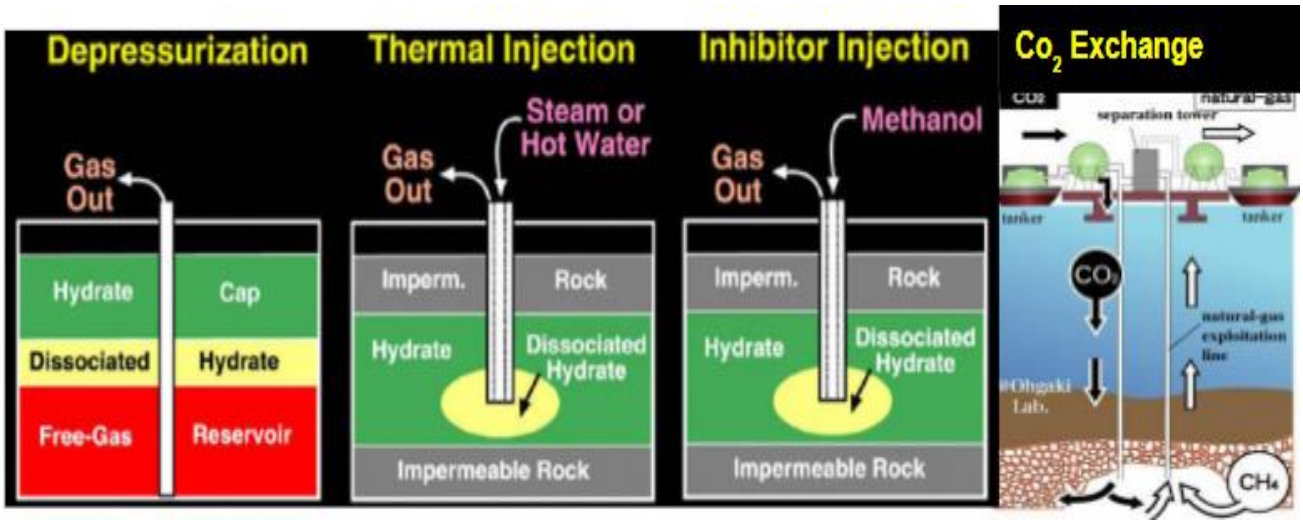

Figure 2.10 Illustration of Gas Hydrate Reservoir Production Methods (Graue, 2010).

2.7.1 Depressurization

In the depressurization process, a pump is installed in the downhole to induce the dissociation of the methane hydrate by depleting the reservoir pressure. The pump is operated to reduce the pressure below the equilibrium pressure of the methane hydrate formation. The dissociation process is an endothermic process and in the depressurization method, the necessary heat flow comes only naturally from the surroundings. The method is effective in producing gas from reservoirs consisting of alternative layers of sand and mud (Nagao, 2012; Holder, 1982). Though many researchers have quoted depressurization as the most viable method for gas recovery, the shortfalls of this method include (Makogon Y.F. 1997; Pooladi-Darvish M. 2004):

- Subsidence and submarine landslides
- Hydrate reformation due to endothermic process
- Excess water production

2.7.2 Thermal Injection

Gas recovery from methane hydrate via thermal injection or stimulation has been investigated by many researchers ((Tang *et al.*, 2005; TSYPKIN, 2000; Moridis, 2003, 2004; Moridis et al., 2004; Pooladi-Darvish, 2004; Zhu, 2007). The thermal method entails increasing the reservoir temperature to promote methane hydrate dissociation by adding heat either through circulating hot fluids downhole or through electric and sonic means. The system temperature increases until it reaches the hydrate dissociation temperature or where all heat that is added is spent on hydrate dissociation (Phale, 2006). Tang et al. (2005) documented that thermal stimulation methods include thermal flooding technology using heat sources such as hot brine injection, steam injection, cyclic steam injection, fire flooding; electrical heating technology such as electromagnetic heating and microwave heating. The major limitation to thermal flooding techniques is that result to high heat losses and wet produced gas. For instance, by products from fire flooding can dilute the natural gas produced; hot brine injection the dissolved salt lowers the gas hydrate dissociation temperature (Zhu, 2007). Problems associated with this method are

- Slow production rate
- High heat losses
- Cost

2.7.3 Inhibitor Injection

Inhibitors lower the hydrate formation temperature and can result in hydrate dissociation when injected into a gas hydrate bearing formation (Sung et al., 2002). The is based on thermodynamic principle as the inhibitors shift the 3-phase equilibrium conditions to high pressure and low temperature side and hence move the reservoir conditions to the methane hydrate dissociation region reducing the temperature at which hydrates form (Zhu, 2007). Known thermodynamic inhibitors include alcohols such as methanol, glycols such as ethylene glycol, Ionic salts such as NaCl, NaBr, and KCl. Problems associated with this method are

- Cost (inhibitors are expensive)
- Quantity required and dispersion in low permeability porous medium
- Thermal adjustment
- Environmental issue

2.7.4 Gas Injection

Ohgaki et al. (1994; 1996) first advanced the concept of exchanging CO_2 with methane, through experiments that showed CO_2 to be preferentially clathrated over methane in the hydrate phase and demonstrated the possibility of producing methane gas by injecting CO_2 gas (Zhu, 2007; Seo et al. 2001; Zhu, 2007). Lee et al (2003) estimated that approximately 64% of methane could be released via exchange with CO_2 (Zhu, 2007). Smith et al., (2001) added some contributions saying the heat of CO_2 hydrate formation (- 57.9KJ/mole) is greater than the heat of dissociation of methane hydrate (54.5KJ/mole), which is favorable for natural exchange of CO_2 with methane hydrate because the exchange process is exothermic. Fluorine is another gas being used to displace methane in hydrate production and is being explored as a new horizon. Preliminary studies of the Fluorine exchange process in sediments showed higher methane production at Pressure-Temperature conditions near the methane hydrate stability and pressure values near saturation levels where CO_2 injection are hampered (Jadhawar et al., 2005). Challenges of gas injection methods include

- Flow impairment in gas hydrate reservoirs with low permeability
- Environmental issues and climate change
- Cost
- Slow production rate

2.8 Reservoir Performance Prediction and Optimization

Reservoir recovery calculations and predictions ranges from classical methods to numerical simulation approach requiring use of digital computers. Classical techniques include material balance calculations and analytical method such as Buckley-Leverett approach, which consist of development of simple mathematical models to describe the physics of reservoir depletion and fluid flow (Ertekin et al 2001). The general form of the material balance equation was first presented by Schilthuis in 1941. The equation is derived as a volume balance which equates the cumulative observed production, expressed as underground withdrawal, to the expansion of fluids in the reservoir resulting from finite pressure drop. Simple classical models are inadequate and cannot provide the required solutions to reservoir deliverability problems. Dake (2001) noted that in a natural water drive reservoir, for instance, the classical material balance can be used to predict the volume of water influx, but it can never predict where the water will preferentially move in the reservoir and such knowledge may be required to determine the location of additional production or injection wells. Furthermore, not all reservoir problems can be formulated in terms of linear differential equations for which standard solutions can be sought. Buckley and Leverett made a major in-road into the subject of immiscible, incompressible displacement in a reservoir and their work formed the basis for the generation of relative permeability as a function of the thickness average water saturation. However, the Buckley-Leverett theory is limited as it is only applicable to one dimensional flow. Classical methods are also not sensitive to accuracies in measured reservoir pressure. They fail when there is no extensive depletion in reservoir pressure (Ertekin, 2001).

Brill and Mukherjee (1999) presented many of the concepts normally used to analyse reservoir fluid production and presented that the production system is made up of inflow performances from the reservoir and vertical lift performance in the well. For each component, the flow rate, q, is related functionally to the pressure differential, ΔP, across the component {i.e. $q = f(\Delta P)$}. Inflow performance is a measure of reservoir deliverability defined as the fluid flow rate achievable from a reservoir at a given bottom-hole pressure (Guo *et al.*, 2007). The difference between reservoir pressure and bottom-hole pressure (pressure drawdown) is the driving force for inflow into the wellbore (Wiggins *et al*., 1992). The vertical lift performance relays on the motion of fluids in the production string as related to the pressure drops along the well completion (Bradley *et al*., 1987). The mathematically relationship between the flowing

bottom-hole pressure and the pressure losses in the well starting from fixed wellhead or separator pressure is given as:

$$P_{wf} = P_{sep} + \Delta P_h + \left(\Delta P_{fl} + \Delta P_t + \Delta P_{ch}\right)_f + \Delta P_{acc} \quad (2.4)$$

Where,

P_{wf} = bottom-hole flowing pressure, P_{sep} = separator pressure, ΔP_h = hydrostatic pressure loss, $\left(\Delta P_{fl} + \Delta P_t + \Delta P_{ch}\right)_f$ = friction pressure losses through the flowline, tubing, choke or restrictions, and ΔP_{acc} = pressure loss because of acceleration.

The system analysis for determination of fluid production rate and pressure at a specified node is called Nodal Analysis (Beggs, 1991). It is based on the principle of continuity of pressure (i.e. there is only one unique pressure value at a given node regardless of whether the pressure is evaluated from upstream or downstream location). A node is any point in the production system where the pressure can be calculated as a function of flow rates. Plotting the total pressure drop against production rates in reservoir and well would result in an inflow performance curve and tubing performance curve respectively. The point of intersection of the system graphs represents the operating condition or solution point that gives the actual flow rate and bottom-hole pressure as below:

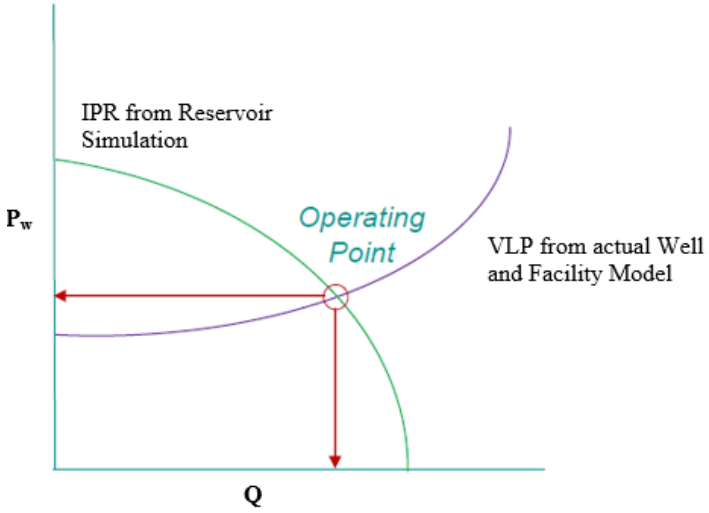

Figure 2.11 Production System Curve

The nodal system analysis is a simplified analytical description and rate calculation procedure generally (Brill and Mukherjee, 1999). The Inflow performance relationship (IPR) is the production rate q from a reservoir in relation to the flowing bottom-hole pressure (pressure in the near wellbore area). It is a measure of reservoir deliverability, defined as the oil or gas flow rate achievable from reservoir at a given bottom-hole pressure (Guo et al, 2007). The difference between the reservoir pressure and the bottom-hole pressure, BHP of a well is the driving force for inflow into the wellbore,

called pressure drawdown. Although this relationship is often complex, for a reservoir producing above its bubble point pressure, the IPR might be constant (an almost-linear relationship). Against this backdrop, it is called the productivity index (PI or J), defined as below –

$$PI = \frac{q}{(P_e - P_{wf})} \tag{2.5}$$

$$q = \frac{2\pi kh(P_e - P_{wf})}{B\mu \ ln\left(\frac{r_e}{r_w}\right) + S} \tag{2.6}$$

$$p_{wf} = p_{wh} + \int_0^L \frac{dP}{dz} dz \tag{2.7}$$

$$\frac{dp}{dz} = \rho_m v_m \frac{dv_m}{dL} + \frac{f_m \rho_m v^2 m}{2d} + \rho_m g \sin\theta \tag{2.8}$$

(The generic wellbore multiphase flow – Pressure Gradient)

The solutions of the system of equations can be semi-analytically expressed with the default well model representation in a numerical simulator. The conventional numerical simulator computes the flowing bottom-hole pressure from the analytical expression as follows:

$$P_{wf} = P_e - C\mu Bq \frac{ln\left(\frac{r_e}{r_w}\right) + S}{kh} \tag{2.9}$$

Uncertainty in the accuracy of the semi-analytical methods becomes a concern when dealing with complex reservoir and multiphase flow. Engineers are therefore often called upon to predict the deliverability of a reservoir through of the wellbore and to evaluate the different operating possibilities to ascertain the optimum production scheme. This would require application of the knowledge of the pressure-rate behaviour of the reservoir and numerical simulation techniques combining flows in both the reservoir and well to accommodate information from well grids that traverse the completions, near-well flow restrictions and well effects (Fung et al, 2005; Ahmed, 2007; Dogru, 2010). The numerical modelling entails using responsive variables to describe a network of ten's to hundreds of nodes with proper correlation and model validity of fluid flow in both the reservoir and well production system. Of interest are the pressure drops along the length of the production string, the wellbore hydraulics, which must be accounted for to obtain the accurate optimum flow rate for the well. This needs to be coupled with the reservoir inflow performance relationship to create an integrated system that ensures parallelism and scalability for accurate determination of the surface production rate as an integrated system (Bendakhlia and Azizi, 1989; Pan, 2015). The numerical coupled simulations present better reservoir performance evaluation, accuracy, and improved overall economy of the field (Allen and Robert, 1993; Lyons and Plisga, 2005; Guo *et al*, 2007). Brief literature review on reservoir modelling, wellbore modelling, multiphase flow modelling and

numerical simulation research efforts that would dovetail into gas hydrate production and optimization would be presented in this thesis.

2.9 Pressure Drop Calculation and Multiphase Flow

Multiphase flow is a common phenomenon in many petroleum production systems. That is, materials being processed often occur as complex combinations of two or more phases (gas, liquid or solid). Gas-liquid flows are commonest in oil and gas industry and present most complex cases. The presence of a compressible phase presents a deformable interface, such that for a given flow-rate, a gas-liquid interface would arrange itself into different forms. As a result, many old schools of thought concluded that, although theoretically possible with Navier–Stokes equations, it is difficult to solve the two-phase flow problem without first determining the flow distribution patterns. This has led to classification of the gas – liquid flow into several different phenomenological patterns or flow regimes for both horizontal and vertical wells (Jansen and Currie, 2004). Namely – bubble, slug/plug, churn, and annular flow. For example, for vertical well, the flow regimes are as shown in figure 2.12 and 2.13 below:

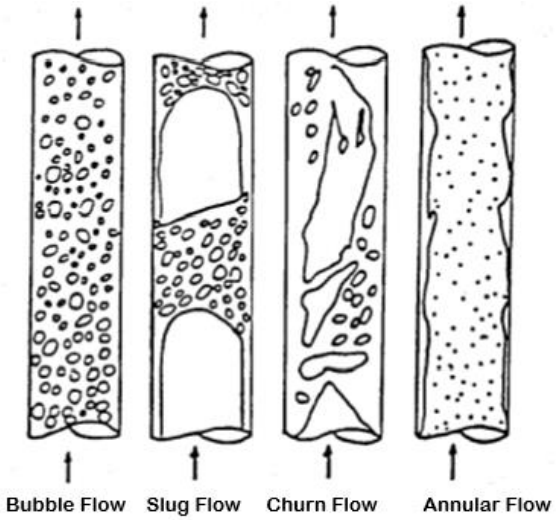

Figure 2.12 Illustration of Flow Regimes for Multiphase Vertical Flow (Jansen and Currie, 2004).

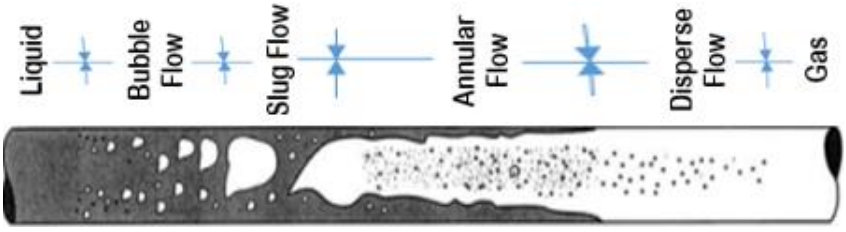

Figure 2.13 Illustration of gas and liquid two-phase flow regimes along a pipe (modified from Jansen and Currie, 2004).

These flow regimes occur as a progression with increasing gas flow rate for a given liquid flow rate. In bubble flow, gas phase is dispersed in the form of small bubbles in a continuous liquid phase. In slug flow, gas bubbles coalesce into larger bubbles that eventually fill the entire pipe cross-section as bullet-shaped slugs that remain more or less centred in the wellbore. Between the large bubbles are slugs of liquid that contain smaller bubbles of entrained gas. In churn flow, the larger gas bubbles become unstable and collapse, resulting in a highly turbulent flow pattern with both phases dispersed. In annular flow, gas becomes the continuous phase, with liquid flowing in an annulus, coating the surface of the pipe and with droplets entrained in the gas phase. Essentially, three approaches exist for flow regimes predictions – The flow regime transition maps, empirical correlations and analytical models.

The flow regime map, figure 2.14, are sometimes utilised to analyse and predict the flow regime distributions. They are, however, not widely used as they are associated with significant error functions which compared to other techniques, may reach up to 80% (Besagni *et al,* 2018). They are derived from visual observation and experimental mapping of phases superficial velocities (*u*) against the transition boundaries coordinates (Zhang *et al*, 1997).

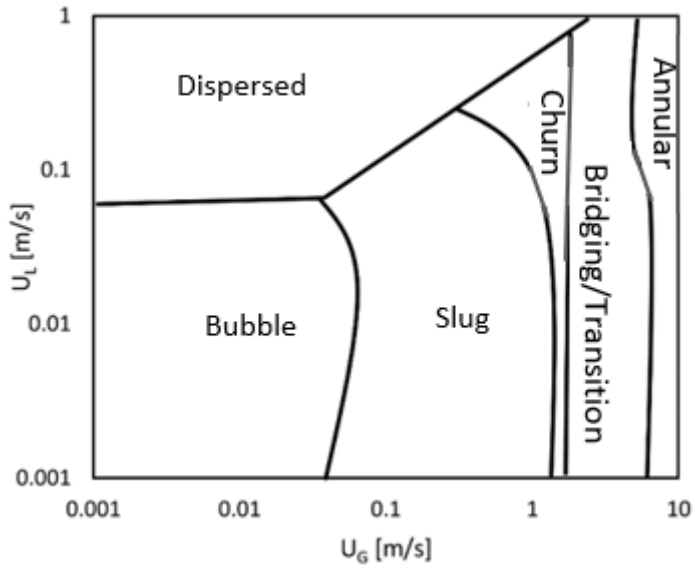

Figure 2.14 Flow regime map for vertical upward two-phase flow (Zhang *et al*, 1997)

2.9.1 Empirical Correlations

The empirical correlation involves curve fittings of the experimental or field data. Their applicability is therefore limited within the experiments conditions and assumptions been explored (Shi et al., 2005). The advantage of empirical correlations is mainly the simplicity

and close representation of field conditions (being a curve fit to laboratory and field data). However, there are uncertainty when extrapolations of the flow correlations beyond the experimental conditions are required (Moniem, 2015). The different empirical correlation methods have been developed to predict the multiphase flowing pressure – gradients; the techniques mainly differ in the manner used to calculate the friction factors for the different flow regimes (Mukherjee and Brill, 1987). The empirical correlations were placed into three categories:

Category 'a' (No slip, no flow pattern consideration). Mixture density is calculated based on the two–phase friction factor from gas/liquid ratio input. The gas and liquid are assumed to travel at the same velocity and distinction is made from different flow patterns.

Category 'b' **(**Slip considered, flow pattern not considered). The liquid and gas are considered to travel at different velocities. The method required prediction of the portion of the pipe occupied by a phase at any given point or location. Thus, a correlation is required for both the liquid holdup and friction factor for all the flow patterns.

Category 'c' **(**Slip considered, flow pattern considered). Here, the method used to calculate the pressure gradient depends on the flow pattern. The correlations to predict liquid holdup and friction factor are determined based on the established flow pattern.

Some of the recognised empirical correlations models and the categories in which they belong are listed in table 2.1 below (Mukherjee and Brill, 1999)

Table2. 4 Pressure Gradient Empirical Correlations Methods

Method	***Category***
Poettmann and Carpenter (1952)	*a*
Baxendell and Thomas (1961)	*a*
Fancher and Brown (1963)	*a*
Hagedorn and Brown (1965)	*b*
Asheim (1967)	*b*
Duns and Ros (1986)	*c*
Orkiszewski (1963)	*c*
Azia et al (1967)	*c*
Chierici et al (1972)	*c*
Beggs and Brill (1991)	*c*
Mukherjee and Brill (1999)	*c*

2.9.2 Mechanistic Models

Mechanistic models, are based on fundamental physics and principles of fluid flow such as conservations of mass, momentum and energy (Posluszny et al., 2010). Mechanistic models can predict pressure drop and fluid flow properties in situations where experimental data are not reliably available and empirical correlations cannot be easily modelled. Also, available empirical models are inadequate for some type of fluids and conditions encountered in oil and gas fields due to their limitation with respect to the range of data on which they were created. Moreover, such models exhibit large discontinuities when used for the simultaneous simulation of reservoirs and wellbore (Petalas, N. and Aziz, K., 2010). These give mechastic models advange over empirical correlations. The many mechanistic models in literature have been employed in calcution and prediction of pressure gradient and fluid flow properties in wellbore with good accuracy and they include Ansari et al., Hasan and Kabir, LedaFlow , OLGA and TACITE (Xiao et al., 1990; Hasan, et al., 2007; Ahmed, 2006). However, mechanistic models are often more complex, and though the approach is based on mass and momentum conservation equations, it does not capture the informations about the local gradients at interfaces and the reservoir - wellbore interfacial transfers. Most are flow regime dependent, requirig closure relationship that would incorparate the empirical correlations. As such, you would first determine the flow regime and variables and then use a separate model to predict the hydrodynamics (Gomez et al., 1999). Hasan, et al., (2007) therefore attempted and made a great advancement in the basic homogenous wellbore modelling that led to the so development of the so called drift-flux models.

2.9.3 Drift-Flux Models

A drift-flux model is a wellbore multiphase flow model in which fluid properties are represented by mixture properties and treated as continuous but differentiable flow mechanism with velocity flux of each phase and slip between the phases accounted for. The homogeneous models do not consider slip between the phases and all phases share the same in-situ flow velocity. The general form of the drift-flux model can be written as

$$V_g = C_0 V_m + V_d$$

Where

V_g= gas phase velocity

C_0= distribution parameter

V_m = volumetric flux of the fluid mixture (weighted velocity)

$V_{\square}$ = weighted mean drift velocity of the gas (buoyancy effect of the gas phase; a function of saturation and density).

$$C_0 = 1.2 - 0.2\sqrt{\frac{\rho_g}{\rho_l}}$$

$$V_{\square} = 2^{\frac{1}{2}}\left(\frac{\Delta\rho g\sigma}{\rho_l^2}\right)^{1/4}\left(1 - S_g\right)^{1\frac{3}{4}} \text{ for bubbly flow or } V_{\square} = 0.35\left(\frac{\Delta\rho g\sigma}{\rho_l}\right)^{1/2} \text{ for slug flow}$$

$$V_{\square} = S_g V_g + (1 - S_g)V_w$$

$$V_{\square} = \frac{(1 - S_{\square}C_0)V_m}{1 - S_g} - \frac{S_g V_d}{1 - S_g}$$

The drift-flux model is easier to be implemented than mechanistic models in reservoir simulation and are well suited for incorporation and wellbore coupling in reservoir simulation. They continuous and differentiable, and reduces the non-convergence risk in the coupling simulation (Shi et al., 2005). The drift-flux model performance has been considered good that many simulation models like Eclipse Multi segment Well has deployed it (Shi et al., 2005; Hasan, et al., 2007; Ahmed, 2006). Drift-flux models can offer correlation of the liquid holdup and the empirical relation on the gas velocity. Drift-flux models can eliminate the need to model the interactions at the interface, such as the momentum transfer or the effects due to the interfacial pressure. One major disadvantage of the drift-flux model is that closure equation is given by a slip law which assumed a steady-state flow. Thus, it is an approximation formulation. It is not well characterized for flow regimes with high slip velocities and as such might still require implementation of an empirical correlation for the slip velocities (Holmes *et a*l. 1998; Hasan & Kabir, 1998; Shi *et al*., 2005; Aarsnes *et al*, 2014, 2016). A more rigorous approach is given by the Computational Fluid Dynamics method where the velocities and/or the pressures of each phase can be treated distinctly.

2.9.4 Computational Fluid Dynamics (CFD)

The CFD models are formulated by a set of conservation equations governing the balance of mass, momentum and energy of each phase. The transport processes of each phase are expressed by their own balance equation. Thus, the model can predict more interface and detailed changes and interactions than the drift-flux model. It can resolve conservation equations combined with other flow equations, such as Darcy and Navier-Stokes equations, to estimate flow parameters especially when considering complex flow geometry and stress related flow (Linga et al. 2017, Parsi et al. 2014). Examples include the Eulerian Model and Mixed Models which involve solving of a set of continuity and momentum equations for each phase and coupling the equations through pressure and interphase exchange coefficients. The phases are considered to be interpenetrating

continua and the mixture momentum equation are solved with or without the phases' relative velocities. CFD is a form Eulerian transformation. It assumes that fluid flow involves two separate but inter-mixed continua for a two-phase flow. Track on the individual phase may not be kept but the volume averaged description of the domain would be represented. The local averaged quantities for each phase are defined at each point in space and the relative inter-phase velocity is accounted for. The treatment allows for evaluation of two distinct velocities and perhaps different phase pressures. The formulation is categorised into: pressure-free models/ global momentum equation (no pressure in the equations; single-pressure models (the two phases pressures are assumed to be equal) and two-pressure models (the two phases pressures are assumed to be different) (Pauchon and Banerjee, 1989; Ransom and Hicks, 1984; Saurel and Abgrail, 1999; Watson, 1990) The pressure difference arising from the dynamic and interfacial effects (interfacial force terms, wall shear force, interfacial pressure, phase pressures and pressure correction term) may need to be accounted or some information would lost in the equations. Thus, constitutive equations, called closure relations, are therefore normally introduced to the set of equations (Romate, 2000). In this thesis, CFD principles would be applied to develop the numerical simulation model that couples the gas hydrate reservoir fluid flow processes and wellbore hydraulics equations to optimise the well performance prediction. The main concern is to incorporate the transient phenomena and the multiphase flow problems in the gas hydrate production system and create a numerical simulation model that implicitly fully coupled the fluid flow in both the reservoir and well.

2.10 Numerical Modelling and Simulation

Reservoir modelling starts first from building a geological model, which usually consist of tens to hundreds of millions grid blocks, to describe the physical reservoir pore-network and heterogeneity. Although, the geological model grids are can be said to be fine cells, they are still much larger than the small-scale heterogeneity of the natural reservoir. Therefore, it becomes necessary to average the small-scale reservoir properties in order to make them suitable for use in the geological model. A numerical simulator is a computer program which permits the user to divide the reservoir or/and wellbore into discrete grid blocks, as shown in figure 2.15, which may have same or different properties. The flow of fluid from block to block is governed by the principle of conservation and continuity of the flow equations. In all, numerical simulation involves reducing the problem to logical sequences represented by mathematical equations which are then applied to a control volume/discrete prototypes of the whole model. This produces a set of partial differential equations (PDE) that predict over time

and space, the behavior of the modeled variables (Michael, 2011). The solutions of the differential equations are generally formulated through numerical discretisation. It involves approximation of the fluid flow equation to finite analogues using numerical techniques such as finite difference, finite volume and finite element methods.

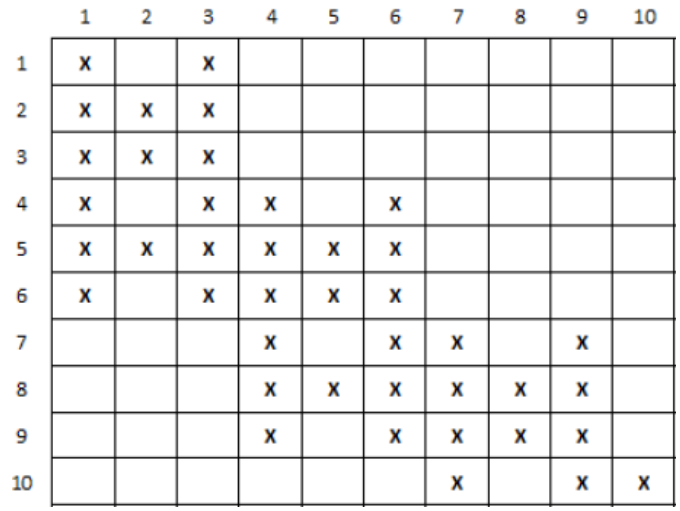

Figure 2.15 Illustration of Discretised Grid Blocks

Finite difference scheme is found to be appropriate for the solutions of the coupled gas hydrate reservoir and wellbore fluid flow considered in this thesis. This is because the method offers resolutions to stiff coupled non-linear partial differential equation requiring weighted averaging of the parameters of the continuity equation and approximations of the total conservations in the continuous system where time and space discretization is required. More so, it is attributed with small error function that does not propagate with time, ensuring the stability of the solution of the equations. The different numerical methods of the finite difference scheme exist. These include Implicit Pressure-Explicit Saturation (IMPES) method, Implicit method and Fully Implicit techniques. According to IMPES method the pressures of the phases are solved at new time step using saturations at former time step, and the solution obtained at the new time is used to solve for saturation at the new time level. In the fully implicit scheme, the flow coefficients are updated in an iterative process and the primary variables are calculated with respect to the unknown at the new time level (Fanchi, 2018). This thesis leveraged the fully implicit finite difference scheme to generate optimization algorithms for gas hydrate fluid flow from the reservoir to the wellhead and vis-à-vis develop the fit-for-purpose fully coupled reservoir and wellbore hydraulics model. The coupling of the continuity and momentum conservation equations in both the reservoir and wellbore would result in stiff partial differential equations requiring large computation time. The fully implicit schemes have

been proven to guarantee stability and fast convergence during iterations (Ertekin, 2001; Mazumba, 2016). The solutions of the equation are usually solved using Newton-Raphson method or the Successive over relaxation/substitutions method. The system of partial differential equations to be solved is normally defined which method to be used. The Newton-Raphson converges to solution in implicit approach to nonlinear approximations while the successive substitution method is at best super linear and tends to converge to the trivial solution when the system exhibits stiff partial equations. The mathematical equations are obtained from the mass, momentum and energy conservations of the individual phases and equations of state with respect to the system being modeled.

2.10.1 Reservoir Modelling

Mathematical formulae that relate pressure drawdown to flow rate to predict the Inflow performance relationship formed the basis of numerical simulation of reservoir fluid flow. Typically, reservoir models integrate geophysics, geology, petro-physics, engineering, computer science and economics (Guo *et al*, 2007; Bendakhlia and Azizi, 1989). Dake (2001) opined that the empirical equations for modelling reservoirs dynamics have developed from the time of Henry Darcy (1856) and are continually advanced. Darcy's law was the first to establish the relationship that the rate of fluid flow through a porous media is proportional to the magnitude of the pressure drawdown (gradient in hydraulic head and the hydraulic conductivity) as follows:

$$Q = \frac{kA}{\mu L}\Delta P \qquad \text{or} \qquad q = -\frac{k}{\mu}\nabla P$$

The significance of Darcy's law is that it introduced flow rates, and invariably, time scale into reservoir modelling and the fluid(s) recovery calculations. For single phase reservoirs and incompressible fluid flow in steady-state, the proportionality is considered to be constant (a linear relationship) and is called productivity index, *PI or J* (Itodo, *et al*, 2010).

Chen (2018) explained that, for multiphase flow and gas reservoirs, a single *J* value cannot be assigned, as it would rather vary for each phase. To describe the behaviour of the multiphase variables, it is considered that each phase flow and production rate would be conserved in relation with the rock and fluid properties changes as a function of the various phase saturation and the relative permeability. Thus, the systems of equations that described the reservoir fluids flow are the mass transport of the individual phases as a function of the pressure rate propagation (for isothermal case) and temperature propagation (for non-isothermal case). In all, the dynamic reservoir model in the substantial region of the multiphase flow regime is a

combination of conservations of mass, momentum and energy of the individual phases (Chukwudozie, 2013). The conservation equations are usually derived from the material balance of the flow parameters and equation of state based on the mass density or other convertible quantities and dependent variables that are normally calculated in the industry.

The continuity equations are generally expressed as a system of non-linear partial differential as below.

$$\sum_{p=phase}\left(\frac{\partial M}{\partial t}\right)_p = \sum \nabla.(\rho v)_p + \sum q_p \qquad (2.10)$$

The well flow rate is a source or sink term represented by the sum of internal inflow of any phase and all phases as a function of their respective relative permeabilities, mobility/transmissibility and well index (Wolfsteiner et al., 2001). If a well is constrained to operate at a given flow-rate, the sum of the fluid inflow rates from each phase through the complete grid-cells must equal the target total fluid flow rate (Holmes, 2001). The conventional well rate relationship is given by:

$$q_{psci} = \sum WI\, \lambda_p\, \rho_p \left(P_i - P_{wfi}\right) \qquad (2.11)$$

There are lots of high – fidelity reservoir simulators such as ECLIPSE, IMEX, CMG STARS, GEM, TOUGH etc and numerous other personalised and industry in-house simulators in use for reservoir performance evaluation. There are also successful wellbore softwares such as PIPESIM and IPM to evaluate accurately the pressure profile necessary for production at the surface facilities (DeBaun et al., 2005; Guyaguler and Ghorayeb, 2006; Holmes et al., 2010). An integrated model that connect the reservoir and well simulations and account for the effects of the near wellbore accumulations and the near well convective processes is being advised in this thesis.

2.10.2 Wellbore Modelling

Standard wellbore model presents well as a source or sink term to a reservoir model. The well is treated as a boundary condition such that the detailed fluid dynamics in the full length are ignored. In the petroleum industry, the well is the only channel that connects the subsurface reservoirs to the surface facilities and it is needed all through the life of the reservoir development. Reservoir recovery and production performance are functions of factors and parameters related to wells such as the well trajectory, geometry and performance. In a typical production well, fluids (oil, gas and water) flow into the wellbore by the driven force arising

from the pressure, temperature and volume differences between the formation and the well. This differential can be induced sometimes by the aided of a pump or injection schemes allied to the well. The complete well system comprises the formation, wellbore, casing, cementing, annulus, insulation and the tubing (as shown in Figure 2.16). Full understanding of the working dynamics of this system remains a challenge in the petroleum industry, and the accurate modelling of the coupled flow system is becoming more essential as more energy resources are sought from unconventional sources. Conventional reservoir modelling represents the well deliverability as a source/sink term. That is, wells are considered to be internal boundaries (wellbore) of the reservoir system; there is no hydraulic communication (Ertekin, 2001; Halliburton; 2017). However, modelling the complete well system will require accounting for the fluid and heat flows in both the reservoir and wellbore. The detailed wellbore modelling and its coupling with reservoirs are increasingly gaining research interest (Economides *et al*., 1994; Uddim, 2010; Pan, 2015).

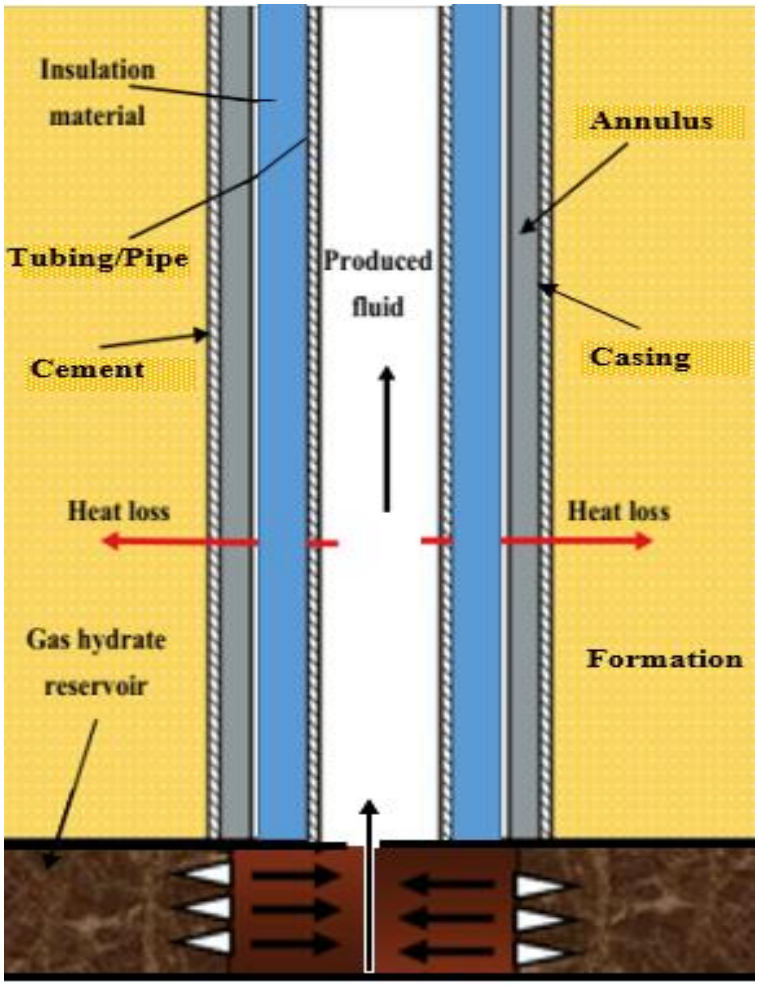

Figure 2.16 Schematic of typical wellbore system with completions

The research interests in modelling and simulation of sophisticated well systems are being directed at incorporating the full wellbore hydraulics into the reservoir model. Correspondingly, they are aimed at resolving the complexity associated with increasing need for advance wells for unconventional recovery and assisted well performance. Ramey (1962) was first to model a comprehensive wellbore analytical formulation, used to calculate temperature profiles along the wellbore. Although Ramey's is a highly simplified model, the work formed the basis for all advances in wellbore modelling and simulation. Several researchers including Willhite (1967), Ali (1981), Fontanilla and Aziz (1989), and Hasan and Kabir (2002) proposed various analytical models based on Ramey's. The modern advances have led to development of wellbore case-sensitivity technologies such as Cyclic steam stimulation (CSS), Steam assisted gravity drainage (SAGD), Hybrid SAGD, Fast-SAGD, multiple-tubing wellbore, Wedge well technology and coupled reservoir-wellbore models (Coşkuner, 2009; Ghanbari et al., 2012; Hasan and Kabir, 2002; Li et al., 2010b; Xu et al., 2014; Jeong et al., 2013; Sarapardeh et al., 2013; Manchuk and Deutsch, 2013).

2.10.3 Wellbore Hydraulics Model

Fluid flow modelling in wellbore is similar to those in reservoir and requires the three governing equations (mass, momentum and energy). Bradley *et al* (1987) defined Wellbore Hydraulics as the branch of production engineering that deals with the motion of fluids in the production string. Consideration is given to the relationship among fluid properties, fluid motion, and well system. However, it is specifically intended to solve the problems associated with the determination the pressure. Application of these principles permits the calculation of pressure drops along the completion length. Novy (1992) presented that the basis for virtually all computation involving fluid flow in pipes is conservation of mass, momentum and energy. For steady state flow, the resultant equation can be expressed:

$$\frac{dP}{dL} = -\rho_m v_m \frac{dv_m}{dL} - \frac{f_m \rho_m v^2 m}{2d} - \rho_m g \sin\theta \qquad (2.12)$$

Where

$\rho_m v_m \frac{dv_m}{dL}$ = Acceleration or kinetic energy component

$\frac{f_m \rho_m v^2 m}{2d}$ = Friction component

$\rho_m g \sin\theta$ = Elevation or hydrostatic component

The components of the pressure drop equation are described as follows (Jansen and Currie, 2004):

The friction component is the frictional loss that results from friction or shear stress at the pipe wall. It is caused by the dissipation of energy by viscous forces in the fluid. This term depends strongly on the fluid properties, the flow regime (laminar or turbulent) and the fluid velocity. It is usually the most important component in pipelines and represents 5 – 20% of the total pressure drops in wells.

The Elevation or hydrostatic component is the static change in pressure caused by elevation or potential energy change. It is measured as head loss. The pressure between surface and bottom-hole changes basically due to the weight of the column of fluid in the well, even if it is not flowing. The hydrostatic pressure loss is normally the predominant term in well and contributes from 80 – 95% of the pressure gradient. However, in horizontal pipelines this component might not be significant (Ohaegbulam et al, 2017).

The acceleration component is loss associated with change in momentum (velocity) when the fluid is accelerated in the well due to expansion. This term is usually considered as negligible, but it can become of significance at high velocity and flow rate, and where a compressible phase exists at relatively low pressure, such as gas wellbores near the surface (Osiadacz, 1987).

However, in the substantial region of the wellbore, the flow dynamic is a transient model with conservations of mass, energy and momentum in time and space (Osiadacz and Chaczykowski, 2001). Thus, while the wellbore mass and energy conservations would be derived from similar formulation to that of the reservoir, momentum conservation is derived from pressure drop equation as a function of time to account for the velocity vector. The change is normally represented by the transient form of the momentum equation below.

$$\frac{\partial \rho_p v}{\partial t} + \frac{\partial (\rho v^2)}{\partial z} = \frac{\partial P}{\partial z} - \frac{f_m \rho_m v^2{}_m}{2d} - \rho_m g \sin\theta \qquad (2.13)$$

Applications of the wellbore hydraulics simulation model abound. Popular among them are simulators such as OLGA (Bendiksen et al., 1991), FlowManager^{TM} Dynamic (Holmas and Lovli, 2011) and LedaFlow (Danielson et al., 2011). Though these models are ranked as high degree predictive models, they are complex and are mainly used for archetypal pipelines flow simulation or general-purpose reservoir-well transient flow simulations (Shi *et al*., 2003, Aarsnes *et al*., 2014, 2016; Ambrus *et al*., 2016). From a reservoir engineering perspective, the simulators do not provide for fully coupling of the well and the reservoir system. They would

suffer from discontinuities difficulties and convergence problems when used within coupled reservoir simulation (Shi *et al*., 2003, Aarsnes *et al*., 2014, 2016; Ambrus *et al*., 2016). As a result, many simplified models are being developed in the industry including the earlier popular drift-flux model which also served as baseline for many others (Kaasa et al., 2012; Reitsma and Couturier, 2012; Godhavn, 2010; Chaczykowski, 2009). To account properly for the time derivatives of the accumulation terms and capture the full transient behaviour of both mass transport and pressure rate propagation, models that fully coupled the reservoir and wellbore fluid flow are advised (Pourafshary, 2009; Pan, 2014; Souza, 2014; Ertekin, 2001; Mazumba, 2016; Halliburton, 2017). Of research interest therefore is the development of a transient flow numerical simulation model of a fully implicit coupled reservoir-wellbore for natural gas hydrate application.

2.10.4 Coupled Reservoir-Wellbore Modelling

Coupling wellbore and reservoir models can be by sequential/segregated procedure (decoupled model) or by fully implicit scheme (fully coupled model). In decoupled models, the reservoir and wellbore are independently modelled and then coupled as blocks in multi interaction continua gridding without hydraulic communication. This implies separate modelling of the wellbore hydraulics base bottom-hole constraint(s) to account for the well completion and the flow performance of the production string. As such, the wellbore is can still be discretised into segments but the model equations would be applied to each block starting from the surface and solving till the bottom-hole value is obtained. On the other hand, fully implicit coupling entails treating the reservoir and well system as one seamless continuum with appropriate interface treatment that capture the interface interactions between the reservoir and the wellbore (Pan and Oldenburg, 2014; Ertekin, 2001; Mazumba, 2016; Peng et al, 2022; Halliburton, 2017). The coupling is executed via an interface scheme which account for the transient problems, such as phase segregation and counter-current phase flow, associated with reservoir-wellbore dynamics in the near-well. Relevant variables and equations that affect fluid flow in the reservoir and wellbore are integrated and solved simultaneously to provide solutions of the systems of equations. Illustration of the wellbore model are as shown in figure 2.17 (Designed using CMG STARS).

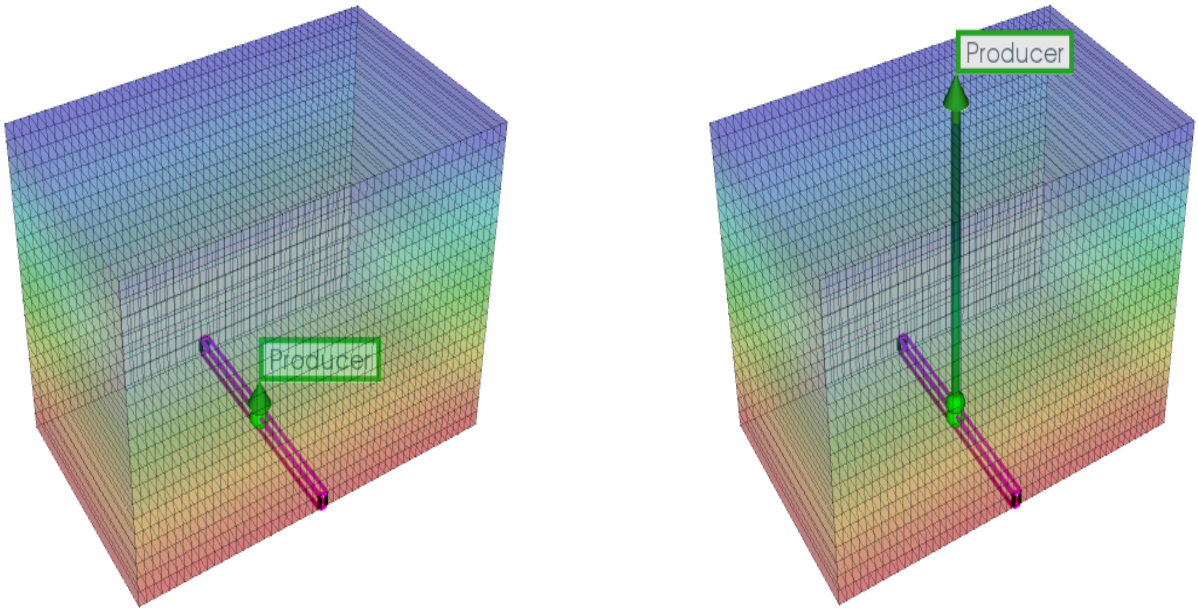

(a) (b)

Figure 2.17 Schematic of Reservoir/Wellbore model (a) Source/Sink Model; (b) Coupled Reservoir-Wellbore

One of the earliest reservoir-wellbore coupled models was by Miller (1980) who deployed the model in a well test to investigate the transient phase behaviour through of a geothermal reservoir. Hagdu et al. (1995) developed an explicit coupled reservoir – wellbore model by coupling two independent simulators, a reservoir model – TOUGH and a wellbore mode – WFSA, to optimised production. Murray and Gunn (1993) coupled a reservoir simulator TETRAD and a wellbore simulator WELLSIM by implicit method to generate tables of wellbore pressure for a range of enthalpies and mass flow rates to establish requisite wellhead pressure. Hasan et al. (2009) proposed an effective reservoir-wellbore coupling via drift-flux model to optimise a two-phase flow in geothermal wells. Pruess et al. (1999) explained that the reservoir fluid flow simulator, TOUGH2 has interface for wellbore model coupling. Baht et al. (2005) coupled TOUGH2 and a well model (HOLA) using an explicit numerical approach to evaluate enthalpies and flow rates. TOUGH2+HOLA was used to predict wells deliverability at constant wellhead pressure and bottom-hole pressure (Rivera Ayala, 2010). (Gudmundsdottir, 2012) created a wellbore model, FLOWELL coupled with reservoir simulator, TOUGH2, for geothermal reservoirs production optimisation. CMG FlexWell is another coupled wellbore hydraulic model but it is tailored for steam assisted gravity drainage (CMG STARS, 2016). COMSOL Multiphysics is another simulation software that offers fully coupled modelling capabilities and simulation applications. However, it is a general-purpose

simulation software used in all fields of engineering and the algorithm might not be readily available for tuning for the gas hydrate's fit-for-purpose application. Other coupled reservoir-wellbore models are general-purpose formulation by Stone et al., 1989, 2002; Pourafshary et al., 2009; Souza et al., 2014; and T2Well by Pan and Oldenburg, 2014. Others are – semi-analytical coupled model by Li et al. (2018), Livescu et al. (2010) model, Ozkan et al. (1999) model, point source model (PSM) by Khoriakov et al. (2012), and distributed-volumetric source (DVS) model by Jiang et al., (2016). A review of coupled dynamic well-reservoir simulation can also be found in da Silva and Jansen (2015). Most of the coupled well-reservoir simulation model do not account for the reservoir-wellbore interface coupling properties (Penmatcha and Azizi, 1998; Sung et al. 2000).

Rutqvist and Moridis (2017) explained that gas hydrate reservoirs exhibit geological variations which may be influenced by the weight of well structure altering the pressure profile and the hydrate compositions. Consequently, there can be a reduction in permeability due to formation damage, invasion of undesirable flow into the well, and susceptible interaction at the reservoir/wellbore interface when rate of gas inflow increases or decreases due to mass, momentum and energy exchange between the wellbore and the reservoir (Minghao *et al*, 2016, Pourafshary, 2009). Conversely, to more accurately evaluate the reservoir deliverability and the gas throughput, the reservoir and wellbore hydraulics models are coupled as one integrated system. More so, for heterogeneous reservoir like gas hydrate sediments, limitation of some of applications to horizontal wells is also disadvantageous because of challenges of hydrate reformation. Uneven distribution of inflow profile can easily occur along the wellbore with horizontal well due to pressure drop (Li et al., 2018; Naderi et al., 2015; Song et al., 2015; Tatar et al., 2014). In this thesis, a fully coupled reservoir-wellbore model with vertical conformance has been proposed for the gas hydrate application to more accurately simulate the fluid flow behaviour in the reservoir and well for production optimization.

2.12 Gas Hydrate Reservoir Performance Prediction Models

Amid the growing interest in gas hydrate production performance, extensive research efforts encompassing kinetics of hydrates dissociation, thermodynamic and fluid flow analyses as well as reservoir performance prediction have been conducted by means of mathematical models of different predictive powers. Lawrence Berkeley National Laboratory created the first publicly available simulation model, TOUGH+HYDRATE, exclusively for simulation of gas hydrate

reservoir production evaluation (Moridis, 2014; Reagan et al, 2014). National Energy Laboratory USA designed the precursor code called HydrateResSim which is still in use (Moridis et al., 1998). Zheng, (2018) used the simulator, HydrateResSim to appraise the sensitivities of dissociation front velocity of natural gas hydrate under given pressure and temperature conditions. Parameters evaluated included initial hydrate saturation, intrinsic reaction rate of hydrate, overall heat conductivity, thermal boundary conditions, intrinsic permeability, wellbore heating temperature and bottom-hole pressure. Other relatively mature Hydrate Reservoir Simulators include MH21-HYDRES by the National Institute of Advanced Industrial Science and Technology, Japan Oil Engineering Co. Ltd & University of Tokyo (Kurihara et al., 2011); STOMP-HYD by the Pacific Northwest National Laboratory and the Petroleum Engineering Department at the University of Alaska (Phale et al., 2006, White and Ostrom, 2006; White, 2012); the commercially available simulator, CMG-STARS by Computer Modelling Group Calgary Canada (Uddin et al., 2006; Myshakin et al., 2016; Nandanwar et al., 2016). There is also TOUGH + HYDRATE + FLAC3D, a geo-mechanic model for coupling geomechanics in hydrate bearing sediment and the flow model. Various simulation models have been developed and used in an attempt to meet the various challenges of simulating more correctly the gas hydration system (Rutqvist and Moridis, 2008; Kim et al., 2012; Liu and Flemings, 2007). Some of these models are as follows:

Table2. 5 Holder et al Formulation (1982)

Pressure distribution	$\nabla\left(\frac{K(\nabla P)}{\mu B}\right)+Q=\frac{d\left(\frac{\emptyset}{b}\right)}{dt}$
Temperature distribution	$\nabla^2 T=\frac{1}{\alpha}\frac{\partial T}{\partial t}$
Hydrates dissociation	$\frac{q}{2}=k\frac{\partial T}{\partial z}=\frac{\nabla H_D}{2}=\left(\frac{\dot{m_H}}{A}\right)$

Table2. 6 Burshears et al Formulation (1986)

Pressure distribution	$\nabla\left(\frac{Kk_{rw}}{\mu_w B_w}(\nabla P_w - P_w g z)\right)+Q_w=\frac{d\left(\emptyset\frac{S_w}{B_w}\right)}{dt}$

Saturation relationship	$\nabla\left(\frac{Kk_{rg}}{\mu_g B_g}\left(\nabla P_g - P_g g\nabla z\right)\right) + Q_g = \frac{d\left(\emptyset\frac{S_g}{B_g}\right)}{dt}$
Capillary pressure Relationship	$S_w + S_g = 1$
Temperature Distribution	$P_w + P_c = P_g$
Dissociation pressure	$\nabla^2 T = \frac{1}{\alpha}\frac{\partial T}{\partial t}$
	$P_{e=} exp\left[a + \frac{b}{T}\right]$ (*pure* gas)
Dissociation enthalpy	$ln\left(\frac{P_e}{P_o}\right) = \sum\left(A_j x_i + B_i x_i^2\right)$ (*mixed* gas)
	$H_D = c + dT$ (*pure* gas)
	$ln\left(\frac{H_e}{H_{Do}}\right) = \sum\left(A_j x_i + B_i x_i^2\right)$ (*mixed* gas)

Table2. 7 Yousif et al Formulation (1991)

Pressure distribution	$\frac{\partial}{\partial x}\left(\frac{P_w K k_{rw}}{\mu_w}\frac{\partial P_w}{\partial x}\right) + m_w = \frac{\partial}{\partial t}\left(\emptyset \frac{p_w}{S_w}\right)$ (water) $\frac{\partial}{\partial x}\left(\frac{P_g K k_{rg}}{\mu_g}\frac{\partial P_g}{\partial x}\right) + m_g = \frac{\partial}{\partial t}\left(\emptyset \frac{p_g}{S_g}\right) \quad -m_H = \frac{\partial}{\partial t}\left(\emptyset \frac{p_H}{S_H}\right)$ (gas)
Saturation relationship	$S_w + S_g + S_H = 1$
Capillary pressure Relationship	$P_w(S_w) += P_g - P_w$
Temperature Distribution	$\nabla^2 T = \frac{1}{\alpha}\frac{\partial T}{\partial t}$
Dissociation pressure	$P_{e=} exp\left[a + \frac{b}{T}\right]$ (*pure* gas) $In\left(\frac{P_e}{P_o}\right) = \sum\left(A_j x_i + B_i x_i^2\right)$ (*mixed* gas)
Dissociation enthalpy	$H_D = c + dT$ (*pure* gas) $In\left(\frac{H_e}{H_{Do}}\right) = \sum\left(A_j x_i + B_i x_i^2\right)$ (*mixed* gas)

Table2. 8 Chuang et al Formulation (2001)

Pressure distribution	$\frac{2\Phi_n \mu}{k_n}\frac{\partial P_n}{\partial t} = \frac{\partial^2 P_n^2}{\partial x^2}$
Hydrate phase equilibrium	$\log_{10} P_D = a(T_D - T_0) + a(T_D - T_0)^2 + c$
Conductive-convective Heat transfer	$a_n \frac{\partial^2 T_n}{\partial x^2} = \frac{\partial T_n}{\partial t} - \frac{c_v k_n}{c_v \mu}\frac{\partial T_n}{\partial x}\left(\frac{\partial T_n}{\partial x} - \delta \frac{\partial P_n}{\partial x}\right) - n\frac{\Phi_n c_v}{c_n}\frac{\partial P_n}{\partial t}$
Production rate equation	$Q = \frac{k_1}{\mu}\frac{\partial P_1(0,t)}{\partial x} = \frac{k_1}{\mu}\frac{P_D^2 - P_G^2}{P_G}\frac{1}{erf(\alpha_1)}\frac{1}{2\sqrt{\pi x_1 t}}$

Table2. 9 EOSHYDR2 Formulation (Moridis, 2002)

	$\frac{d}{dt}\int_{V_n} P^k\, dV = \int_{r_n} F^k . n d\Gamma + \int_{V_n} q^k\, d\mathrm{V}$
Flow equations	$M^k = \sum_{\beta=A,G,I}(\phi S_\beta \rho_\beta X_\beta^w) + M_H^w$; $M^{m,v} = \sum_{\beta=A,G,I}(\phi S_\beta \rho_\beta X_\beta^{w,v}) + M_H^{w,v}$
Hydrate Dissociation	$q^k = X_k W_k A_k k_k exp\left(\frac{\Delta E^k}{RT}\right)(f_{ek}(T) - f_k);\quad k = m, v$ $q^k = X_k W_k A_k k_k exp\left(\frac{\Delta E^k}{RT}\right)(f_{ek}(T) - f_k);$
Dissociation Pressure	$P_e(kP_a) = exp\left(e_1 - \frac{e_1}{T(K)}\right)$
Dissociation Rate (Optional)	$\dot{m}_g = K_d M_g A_{dec}(f_c - f)$
Heat of Dissociation	$\Delta H^0 = zRT^2 \frac{d(\ln P)}{T(K)}$
Heat Flux	$F^\theta = -[(1-\varphi)K_R + \phi(S_H K_H + S_A K_A + S_G K_G + S_I K_I)]\nabla T + f_\sigma \sigma_0 \nabla T^4 + \sum_{\beta=A,G} h_\beta F_\beta$

Table2. 10 Sun et al Formulation (2002)

Flow equations	$\frac{\partial}{\partial t}(\emptyset P_{\mathrm{g}} S_{\mathrm{g}}) + \frac{\partial}{\partial x}(P_{\mathrm{g}} v_{\mathrm{g}}) = \dot{m}_{\mathrm{g}}$ $\frac{\partial}{\partial t}(\emptyset P_w S_w) + \frac{\partial}{\partial x}(P_w v_w) = \dot{m}_w$ $\frac{\partial}{\partial x}(\emptyset P_h S_h) = \dot{m}_h$
Dissociation Rate	$\dot{m}_h = k_d A_s (P_e - P)$
Dissociation Pressure	$P_e = 1.15 exp\left(49.3185 - \frac{9459}{T}\right)$
Relative Permeability	$k_{rw} = \left(\frac{\frac{s_w}{(s_w + s_{\mathrm{g}})} - S_{wirr}}{1 - S_{wirr} - S_{\mathrm{gr}}}\right)^{n_w}$ $k_{r\mathrm{g}} = \left(\frac{\frac{s_{\mathrm{g}}}{(s_w + s_{\mathrm{g}})} - S_{wirr}}{1 - S_{wirr} - S_{\mathrm{gr}}}\right)^{n_{\mathrm{g}}}$
Capillary Pressure	$\frac{P_c}{P_c^e} = h_c(s_w) = \left(\frac{\frac{s_w}{(s_w + s_{\mathrm{g}})} - S_{wirr}}{1 - S_{wirr}}\right)^{-n_c}$
Gas Viscosity	$\mu_{\mathrm{g}} = 2.4504x10^{-3} + 2.8764x10^{-5}T + 3.279x10^{-9}T^2$ $-3.7838x10^{12}T^3 + 2.0891x10^{-5}P_{\mathrm{g}} + 2.5127x10^{-7}P_{\mathrm{g}}^2$ $-5.822x10^{-10}P_{\mathrm{g}}^3 + 1.838x10^{-13}P_{\mathrm{g}}^4$
Energy Balance	$\frac{\partial}{\partial t}\left[\emptyset\left(P_{\mathrm{g}} S_{\mathrm{g}} H_{\mathrm{g}} + P_{\mathrm{w}} S_{\mathrm{w}} H_{\mathrm{w}} + P_{\mathrm{h}} S_{\mathrm{h}} H_{\mathrm{h}}\right) + (1 - \emptyset) P_{\mathrm{s}} H_{\mathrm{s}}\right]$ $+ \frac{\partial}{\partial x}\left(P_{\mathrm{g}} V_{\mathrm{g}} H_{\mathrm{g}} + P_{\mathrm{w}} V_{\mathrm{w}} H_{\mathrm{w}}\right) = \frac{\partial}{\partial x}\left(\lambda \frac{\partial T}{\partial x}\right) + q$

Table2. 11 Sun and Mohanty Formulation (2005)

Mass Transfer Flux	$\bar{F}^i = P_G \bar{V}_G w_G + P_A \bar{V}_A w_A + \bar{J}_G^i + \bar{J}_A^i$
Heat Flux	$\bar{F}^E = P_G \bar{V}_G H_G + P_A \bar{V}_A H_A - \lambda \nabla T$
Mass balance	$\frac{\partial}{\partial t}\left[\emptyset \sum_{j=H,G,A,I} P_j S_j W_j^m\right] + \nabla \cdot \bar{F}^m = q^m$ (*methane*)
	$\frac{\partial}{\partial t}\left[\emptyset \sum_{j=H,G,A,I} P_j S_j W_j^m\right] + \nabla \cdot \bar{F}^w = q^w$ $(water$
Energy Balance	$\frac{\partial}{\partial t}\left[\emptyset \sum_{j=H,G,A,I} P_j S_j \ U_j \ + (\emptyset + 1) P_R U_R\right] + \nabla \cdot \bar{F}^E = q^E$
Capillary Pressure	$P_c = P_{ce}(S_A^{e*})^{-n_c} \ where \ P_{ce} = P_{ce0}\sqrt{\frac{\emptyset^e k_o}{\emptyset_0 k}}$
Local Absolute Permeability	$\frac{k}{k_0} = \frac{\emptyset^e}{\emptyset_0}\left(\frac{\emptyset^e(1-\emptyset_0)}{\emptyset_0(1-\emptyset^e)}\right)^{2\beta} \ where \ \emptyset^e = \emptyset\left(S_g + S_a\right)$
Relative Permeability	$k_{rG} = k_{rG}^0 (S_G^{e*})^{n_G}$ $k_{rA} = k_{rA}^0 (S_A^{e*})^{n_A}$

Table2. 12 Gerami and Pooladi-Darvish Formulation (2006)

Material balance	$\frac{\overline{P(t)}}{z(t)} = \frac{P_i}{z_i}\left(1 - \frac{G_p(t) - G_g(t)}{G_f}\right)$
Energy balance	$\frac{dT}{dz}\Big\|_{z=0} = \left(1 - \frac{\nabla H \cdot P_H}{k_{cr} \cdot A \cdot E_H}\right)\frac{dG_g}{dt} + \left(\frac{P \cdot c_p \cdot V_b}{k_{cr} \cdot A}\right)\frac{dT_{se}}{dt}$
Dissociation	$P_e = exp\left(\lambda - \frac{\beta}{T_{se}}\right)$
Temperature gradient At hydrate interface	$\frac{dT}{dz}\Big\|_{z=0} = 2 \cdot b(t)\sqrt{\frac{t}{\pi\alpha_r}}$
Gas dissociation rate	$q_g(t) = \frac{E_H AHP^{c_p}}{P_H \Delta H} b(t)\left(\frac{4P_r c_{pr\sqrt{\alpha_r}}}{3Pc_p H\sqrt{\pi}}\sqrt{t+1}\right)$
Hydrate recovery	$R_h(t) = \frac{Pc_p}{\emptyset S_H P_H \Delta H} b(t)\left(\frac{8P_r c_{pr\sqrt{\alpha_r}}}{3Pc_p H\sqrt{\pi}}\sqrt{t+1}\right)\cdot t$
Temperature parameter	$b(t) = q_w\left(\frac{1 - \frac{(p_{oe}Z_i)}{(p_i Z_{oe})}}{T_i - T_{oe}} G_f + \frac{E_H AHP^{c_p}}{P_H \Delta H}\left(\frac{8}{3Pc_p H\sqrt{\pi}}\sqrt{k_{cr}c_{pr}P_r t + 1}\right)\right)$
Initial free gas-in-place	$G_f = \frac{(T_i - T_i)\left[\frac{q_w}{b_{match}} - \frac{E_H A}{P_H \Delta H}\left(\frac{8\sqrt{t_{avg}}}{3\sqrt{\pi}}\sqrt{k_{cr}P_r c_{pr} + HPC_p}\right)\right]}{1 - \frac{(P_{oe}Z_i)}{(P_i Z_{oe})}}$
Hydrate cap thickness	$H = \frac{1}{PC_p}\left[\left(\frac{q_w}{b_{match}} - \frac{1 - \frac{(p_{oe}Z_i)}{(p_i Z_{oe})}}{T_i - T_{oe}} G_f\right)\frac{E_H A}{P_H \Delta H} - \frac{8\sqrt{t_{avg}}}{3\sqrt{\pi}}\sqrt{k_{cr}P_r c_{pr} + HPC_p}\right]$

Table2. 13 STOMP-HYD Formulation (Phale and Zhu, 2006)

Energy conservation	$\frac{\partial}{\partial t}\sum_{\gamma=l,\mathrm{g},n,h,i,p}[(\phi P_\gamma S_\gamma u_\gamma)+(1-\phi)P_s u_s] = -\sum_{\gamma=l,\mathrm{g},\mathrm{n}}[\nabla(h_\gamma F_\gamma)] - \sum_{\zeta=w,\mathrm{a},\mathrm{o}}[\nabla(h_{\mathrm{g}}^{\zeta} J_{\mathrm{g}}^{\zeta}) - \nabla(k_e \nabla T) + \sum_{\gamma=l,\mathrm{g},\mathrm{n}}(h_\gamma \dot{m}_\gamma)] + \dot{q}$
Mass conservation	$\frac{\partial}{\partial t}\sum_{\gamma=l,g}(\emptyset P_\gamma S_\gamma \omega_\gamma^{\zeta}) = \sum_{\gamma=l,\mathrm{g},}\nabla(\omega_\gamma^{\zeta} F_\gamma) - \sum_{\gamma=l,\mathrm{g},}\nabla(J_\gamma^{\zeta}) + \sum_{\gamma=l,g}(\omega_\gamma^{\zeta}\dot{m}_\gamma)$ $where \zeta = w,a,o,s$
Diffusion-dispersive Flux and advective	$F_\gamma = -\frac{P_\gamma k_{r\gamma} k_i}{\mu_\gamma}(\nabla P_\gamma + P_\gamma \mathrm{g} z_{\mathrm{g}})$ $where\ \gamma = l,\mathrm{g},\mathrm{n}$
Diffusive mass flux	$J_\gamma^{\zeta} = -\phi t_\gamma P_\gamma S_\gamma \frac{M^{\zeta}}{M^{\gamma}} D_\gamma^{\zeta}(\nabla x_\gamma^{\zeta})\ for\ \gamma = l\ and\ \zeta = w,a,o,s$ $for\ \gamma = \mathrm{g}\ \mathrm{and}\ \zeta = \mathrm{w},\mathrm{a},\mathrm{o}$

Table2. 14 TOUGH + HYDRATE Formulation (Uddin et al, 2006)

Mass conservations	$\frac{d}{dt}\int_{V_n} M^k\, dV = \int_{r_n} F^k . n d\Gamma + \int_{V_n} q^k\, d\mathrm{V}$ $\sum_{\beta=A,G,}\phi S_\beta \rho_\beta X_\beta^k = \sum_{\beta=A,G}\left[-\frac{k_{r\beta}\rho_\beta}{\mu_\beta} X_\beta^k(\nabla P_\beta - \rho_w g) + J_\beta^k\right] + \sum_{\beta=A,G}(X_\beta^k q_\beta + Q^k);\ k = w,i,g$
Energy conservation	$(1-\phi)\rho_\beta C_\beta T + \sum_{\beta=A,G,H,I}\phi S_\beta \rho_\beta X_\beta^k = \sum_{\beta=A,G}\left[-\frac{k_{r\beta}\rho_\beta}{\mu_\beta} X_\beta^k(\nabla P_\beta - \rho_w g) + J_\beta^k\right] + \sum_{\beta=A,G}(X_\beta^k q_\beta + Q^k)$

Table2. 15 CMG STARS Formulation (Uddin et al, 2006)

Mass Balance for Methane(CH_4)	$-\frac{1}{r}\frac{\partial(r\rho_g v_{gr})}{\partial r}-\frac{\partial(r\rho_g v_{gz})}{\partial z}+\acute{g}_g=\frac{\partial(\phi\rho_g S_g)}{\partial t}$
Mass Balance for Water(H_2O)	$-\frac{1}{r}\frac{\partial(r\rho_w v_{wr})}{\partial r}-\frac{\partial(r\rho_w v_{wz})}{\partial z}+\acute{g}_w=\frac{\partial(\phi\rho_w S_w)}{\partial t}$
Mass Balance for Methane Hydrate(CH_4-Hyd)	$\acute{g}_H=\frac{\partial(\phi\rho_w S_w)}{\partial t}$
Energy Balance	$-\frac{1}{r}\frac{\partial}{\partial r}\left(rk\frac{\partial T}{\partial r}\right)+\frac{\partial}{\partial z}\left(k\frac{\partial T}{\partial z}\right)-\frac{1}{r}\frac{\partial}{\partial r}(r\rho_g \square_{\square\square} h_g+r\rho_w \square_{\square\square} h_w)$ $-\frac{\partial}{\partial z}\left(\rho_g v_{gr}h_g+\rho_w v_{wr}h_w\right)+\bar{Q}_H+\bar{Q}_{in}$ $=\frac{\partial}{\partial t}\left[(1-\phi)\rho_g u_g+\phi S_H\rho_H u_H+\phi S_g\rho_g u_g+\phi S_w\rho_w u_w\right]$ Where: $\bar{Q}_H=\frac{\acute{g}_g}{M_H}\Delta H_g$ $\acute{g}_g=K_d M_g A_{dec}(f_c-f)$ $\acute{g}_w=5.75\acute{g}_g\frac{M_w}{M_g}$ $\acute{g}_w=-\acute{g}_g\frac{M_H}{M_g}$ $-\frac{1}{V}\frac{dn_{CH4HYD}}{dt}=K_d^0\,exp\left(\frac{-E}{RT}\right)(\phi_f S_H A_{SH})(\phi_f S_w)(P_c-P_{CH4})$

Table2. 16 HydrateResSim Formulation (Uddin et al, 2006)

Mass conservation	$M^k = \quad F^k \quad + \quad q^k$
Accumulation Term	$M^k = \frac{d}{dt}\left(\sum_{\beta=A,G,I} \phi S_\beta \rho_\beta K_\beta^k\right); \quad k: w, m, i$
Flux Term:	$F^k = \left(\sum_{\beta=A,G,I} F_\beta^k\right); \quad k: w, m, i$
For aqueous phase	$F^k = F_A = -\mathrm{k}\frac{k_{rA}\rho_A}{\mu_A}(\nabla P_A - \rho_A g)$
For gas phase	$F^k = F_G^k = -k_0\left(1+\frac{b}{P_G}\right)\frac{k_{rG}\rho_G}{\mu_G} X_G^k(\nabla P_G - \rho_G g) + J_G^k;\ k: w, m$
Production rate	$q^k = \sum_{k=A,G} X_\beta^k q_\beta\ ;\ k: w, m$
Gas rate from dissociation	$\acute{g}_g = K_d M_g A_{dec}(f_c - f)$
Energy conservation	$(1-\varphi)\rho_R C_R T + \sum_{\beta=A,G,H,I} \phi S_\beta \rho_\beta U_\beta + \mathrm{Q}_{diss} = -\nabla\left[(1-\varphi)K_R + \phi\sum(S_\beta K_\beta)\right]\nabla T + f_\sigma \sigma_0 \nabla T^4 + \sum h_\beta F_\beta$

The various gas hydrate simulation models above were created by the researchers using differing approaches and assumptions according to their objectives (Liu, X., and Flemings, 2007; Liu et al, 2015; Wilder *et al.*, 2008; National Energy Technology Laboratory, 2017; Yin *et al.*, 2016). Holder and Angert (1982) investigated gas production from a hydrate bearing sediment with respect to well placement. The study established that hydrate dissociation produced an advancing split of two parts - a dissociated zone and a dissociating/hydrate zone – and with stronger dissociation front near the wellbore. The study opined that the dissociation generated hydrate-aqueous interface at a uniform depth over the reservoir radial extent (Cui, et al. 2018). Burshears *et al*. (1986) used a 3D-simulator to investigate hydrate production using depressurization method. Water produced in the hydrate dissociation was said not to impair gas flow and there was no undesirable increased water-gas ratio. It was also assumed that the dissociation generated hydrate-gas interface at equilibrium temperature and pressure without

external heat source. In contrast, later studies opined that dissociation fronts occur where temperature and pressure become greater than and less than equilibrium values respectively (Sun, et al., 2005; Ji, et al., 2003; Sakamoto, et al; 2007). Yousif et al., (1991) developed a 1D numerical simulation model that incorporated hydrate phase rate into hydrate reservoir flow equation to simulate gas production from hydrate by depressurization. Chuang, et al., (2001) evaluated that dissociation of hydrate reservoir does not occur in the entire volume, and is rather is constrained to a narrow region where pressure and temperature favour formation of dissociation fronts – a near-well zone with natural gas and water only and adjacent zone further from well having hydrate and free natural gas. However, effects of temperature could not have been properly accounted with the model assumption of no heat conduction in the entire reservoir (Moridis, 2002). EOSHYDR2 was presented as gas hydrate simulator developed by modifying the general-purpose simulator for multicomponent, TOUGH2. This was applied to simulate non-isothermal gas flow and phase behaviour under equilibrium conditions of gas hydrate deposits (Catak, 2006). Sun et al. (2004, 2005) incorporated a function called dissociation-flow/time-scale ratio, developed 1-D model and identified two non-equilibrium flow regimes: dissociation-controlled regime and flow-controlled regime.

While the numerous numerical simulation packages can model reservoir performance accurately, wellbore hydraulic effects are not fully incorporated. Besides, they are not necessarily equipped for critical modification to fully couple the reservoir-wellbore interaction and near-well convective mixing effects, thus new formulations are advised (Pan, 2015; Yin, 2016; Adesina et al., 2016; Mazumba, 2016). More so, further studies on measurement of temperature and pressure on flow for efficient gas recovery and economic development of hydrate reservoirs have been suggested (Ahmadi et al. 2010).

2.13 Inherent Defying Features in Gas Hydrate Reservoir Production

Historically, non-Darcy flow in petroleum engineering was basically attributed to and had been treated as consequence of skin factor acting in the vicinity of the near wellbore. Non-Darcy flow implies deviations from the linearity of flow and the Darcy's empirical model. Darcy flow is represented by a simple linear relationship between flow rate and pressure drop. At high gas velocity or increased flow rate, gas flow through the porous media tends to deviate from Darcy's law. Use of Darcy's law for flow in gas hydrate reservoir would lead to misleading results and over predicting of the productivity (Nguyen, 1986). More so, advance in research on unconventional reservoirs has shown that non-Darcy effects are eminent in heterogeneous reservoirs with increasing velocity/flowrate, and can be functions of complex reservoir geometry, anisotropy and convective mixing flow processes (Miskimins, 2005). It has been evaluated that as the depth of hydrate sediment increases, the gas concentration also increases, and change in the reservoir thickness can result to the gas concentration decrease. The non-Darcy flow mechanism has been predicated on the time dependent permeability and Knudsen diffusion. Non-Darcy flow occurs when the intrinsic parameters that incorporate the geometry relation and timescale flow including inertia forces and viscous forces are at play (Hagoort, 2004; Javadpour, 2009; Sun et al., 2018). Figure 2.18 demonstrates the porous medium flow process and the system geometry pathway.

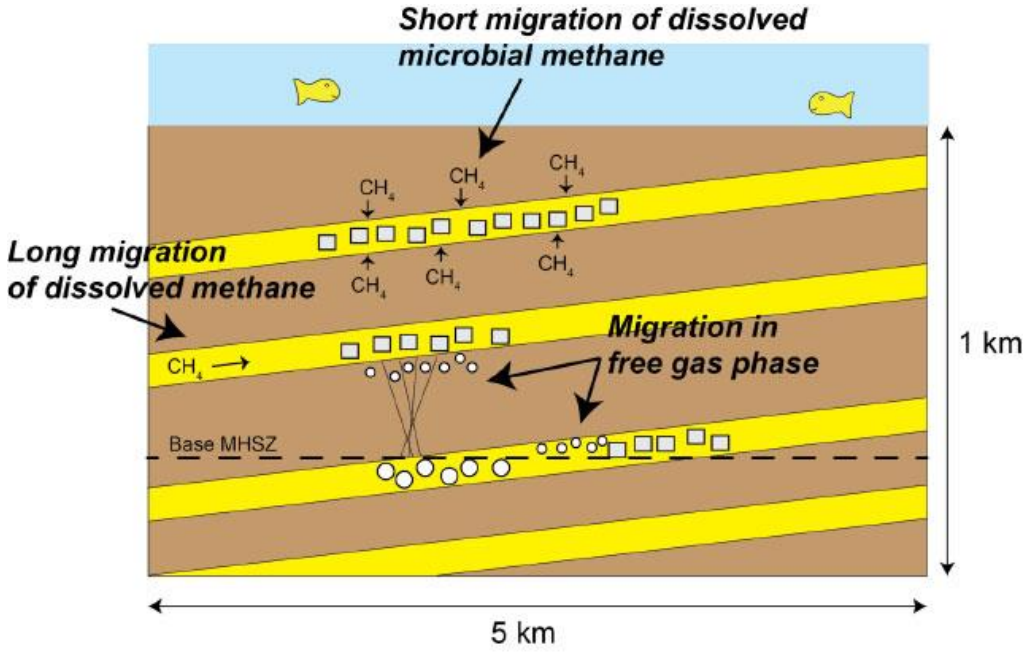

Figure 2.18 Schematic of the Natural Gas Pathways and Migrations (Beaudoin, 2014).

The in the gas hydrate reservoirs would be related to the unconventional reservoir fluid dynamics and diffussion flow effects such as the Knudsen diffussion. Pores diameters of unconventional gas reservoirs are usually between 0.1 and 100 nm and the flow in the pore network might be characterised Knudsen diffussion in addition to the real gas effect, viscous–slip flow (Song, et al. 2017; Cussler, 2009). The various mechanisms for the molecular transport and the typical gas movement in nanopore can be depicted as shown in figures 2.19 and 2.20 respectively. The pore-networks are flow conduits akin to molecular gas mean free paths where the collision between the gas molecules and the wall surfaces (molecules-walls attractions) become more prominent to the intermolecular collisions (Karniadakis, et al. 2005). Knudsen diffusion underscored the transient flow in the low permeability reservoir of small pore diameter with the mean free path of the gas close to the pore diameter (Mao and Zeidouni, 2017c). The ratio of the mean free path to the pore diameter is defined as Knudsen number (Lee and Kim, 2016; Sakhaee-Pour and Bryant, 2012; Kast and Hohenthanner, 2000).

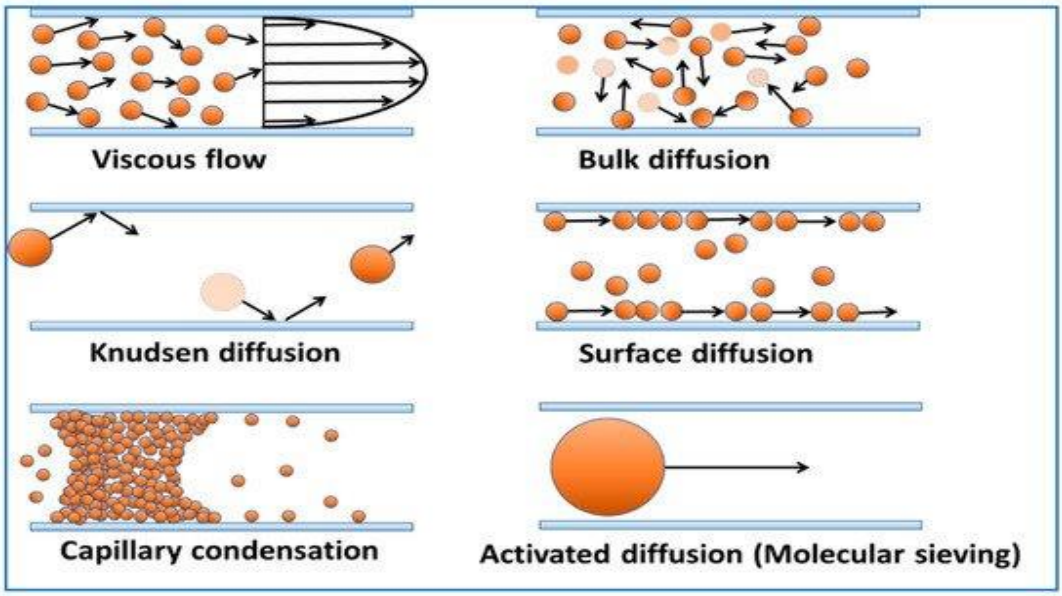

Figure 2.19 Various mechanisms for molecular transport in nanopore (Ratnakar and Dindoruk, 2022).

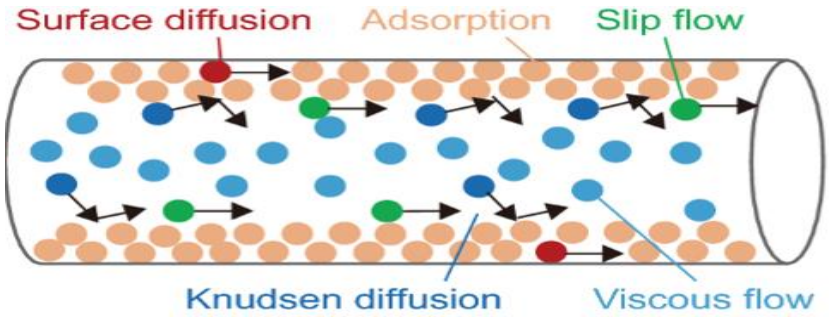

Figure 2.20 Schematic of the movement of gas molecules in nanopore (Zhang, 2020).

Knudsen number (Kn) can be indicative of the different flow regimes such as viscous flow, slip flow, transient flow and free-molecular flow in multiphase flow model (Javadpour et al. 2007; Florence et al. 2007; Javadpour 2009; Freeman et al. 2011; Deng et al. 2014; Song et al. 2015). When the Knudsen number is less than one, flow is normally described as viscous flow that is that the mean free path of the gas is smaller compared to the pore diameter. The viscous flow caused by pressure gradient can be described by Darcy's law. Knudsen diffusion is more likely to occur when the pore diameter is small enough so that the mean free path of the gas is close to the pore diameter, that is, that the Knudsen number will be greater than 1. In such circumstances, the collision between the gas molecules and the wall surfaces dominates (Kast and Hohenthanner, 2000). Table 5.2 describes the different flow regimes categorized as functions of Knudsen numbers.

The formulation of the Knudsen number (Kn) is given as follows (Foroozesh et al., 2018).

$$K_n = \frac{\lambda}{d_p}$$

Where λ = mean free path of the gas; d_p = pore diameter. The mean free path can be estimated from equations of Heidemann et al. (1984) in Foroozesh, et al. (2018). For real gas

$$\lambda = \frac{K_B T}{\sqrt{2}\pi\delta^2 d_p}$$

$$\lambda = \sqrt{\frac{\pi ZRT}{2M}}\,\frac{\mu}{P}$$

where K_B = Boltzmann constant (1.3805 E-23 J/K), T = temperature, P = pressure, μ= viscosity, δ = collision diameter of the gas molecule,

Table2. 17 Flow regimes as a function of Knudsen number (Foroozesh et al. 2018).

Knudsen Number (*Kn*)	Flow regime
$0 - 10^{-3}$	Continuum flow (No slip/Darcy flow)
$10^{-3} - 10^{-1}$	Slip Flow
$10^{-1} - 10$	Transition flow
$10 - \infty$	Free – molecular flow

With increasing interest in gas hydrate reservoirs development, it has become pertinent to extend research into the comprehensive gas hydrate reservoir simulation modelling that implicitly coupled the non-Darcy effects, and transport mechanism including permeability anisotropy, viscous and Knudsen diffusion factors that affect unconventional tight gas reservoirs. The Knudsen equation or Klingenberg permeability effect can be incorporated in the diffusivity equation to account for the slip flow process in low permeability formations and under low-pressure conditions (Gao et al, 2021; Sakhaee-Pour and Bryant, 2012). This thesis, therefore, would take into consideration the pressure and temperature factors that might affecting the diffussive flux and convective flux processes.

2.13.1 Pressure Solutions

Pressure solutions for flow in porous media are usually derived from the diffusivity equation and the energy balance equations and there exist convectional formulations to derive transient pressure solutions. However, considering the nonlinearity and the pressure dependence of flow in reservoir of highly compressible fluid, the derivation of the pressure solution of the diffusivity equation for gas becomes critical and application of analytical solution may become limited. With non-Darcy flow effects, the usual definition of skin factor would be expanded to include slippage and inertia effects (Raghavan, 1989). Some of the existing analytical solution methods for pressure solutions derivation are as follows:

i. **Pressure approximation method**:

It assumed that gravitational effects and capillary pressure are negligible, and variations in saturation and pressure graduate can be ignored; the pressure solutions were based on total mobility value (Chaudhry, 2003; Belyadi, et al, 2019). Thus, it can be termed the total

mobility method. This is applicable where relative permeability data cannot be gotten. The pressure equation is written as:

$$\frac{1}{r}\frac{\partial}{\partial r}\left(r\frac{\partial P}{\partial r}\right) = \frac{\phi C_t}{\lambda_t}\frac{\partial P}{\partial t} \tag{2.13}$$

ii. **Pressure-squared method**:

In pressure-squared method, ideal gas behaviour is assumed and gas viscosity and pressure gradient are assumed to be independent of pressure and very small respectively. The flow equation for multiphase flow is expressed as

$$\frac{1}{r}\frac{\partial}{\partial r}\left(r\frac{\partial P^2}{\partial r}\right) = \frac{\phi C_t}{\lambda_t}\frac{\partial P^2}{\partial t} \tag{2.14}$$

As

$\left(\frac{\partial P}{\partial r}\right)^2 \rightarrow 0$, Equation 12.14 can written

$$\nabla^2 P^2 = \frac{\phi C_t}{\lambda_t}\frac{\partial P^2}{\partial t} \tag{2.15}$$

To account for fluid compressibility, the differential equation would be substituted into the gas-law equation. This gives an approximation of the differential equations that approaches the linear form of the classical solutions of the diffusion equation used for gas-well drawdown and buildup tests (Eq.2.16).

$$P_i^2(\Delta t) - P_{wf}^2(t) = m\left[\lg t + \lg\left(\frac{\lambda_t}{\phi C_t r_w^2}\right) + 0.9077 + 0.8686S\right] \tag{2.16}$$

For pressure draw down, the skin factor, *S*, can be gotten according to Equation (2.17):

$$S = 1.1513 \text{ x } \left[\frac{P_i^2 - P^2(\Delta t=1)}{|m|} - \lg\left(\frac{\lambda_t}{\phi C_t r_w^2}\right) - 0.9077\right] \tag{2.17}$$

For pressure build up, the following formula can be derived for the skin factor:

$$S = 1.1513 \text{ x } \left[\frac{P_{lh}^2 - P_{wf}^2(\Delta t=0)}{|m|} - \lg\left(\frac{\lambda_t}{\phi C_t r_w^2}\right) - 0.9077\right] \tag{2.18}$$

The solutions for the equation are obtained by plotting the pressure square against the log of the derivative of the time function.

$$P_{ws}^2(\Delta t) = P_i^2(t) + m\lg\frac{\Delta t}{t+\Delta t} \quad (2.19)$$

The slope, m, is substituted in the gas phase relative permeability equation to obtain the gas permeability

$$k_{\mathrm{g}} = 4.242 \text{ x } 10^{-3} \text{ x } \frac{q_{\mathrm{g}}\mu_{\mathrm{g0}}Z_0TP_{sc}}{mhT_{sc}q_{sc}} \quad (2.20)$$

Then the water phase permeability can be derived according to the surface water gas ratio:

$$k_{\mathrm{w}} = R_{\mathrm{wg}} \text{ x } \frac{\mu_w B_w}{\mu_{\mathrm{g}} B_{\mathrm{g}}} k_{\mathrm{g}} \quad (2.21)$$

iii. Pseudo-pressure method: Pseudo-pressure is typically the normalizing pressure for gas viscosity and compressibility as they vary at different pressures. It is a mathematical function established by Al-Hussainy et al. (1966) to account for the properties variations and is defined as follows (Ahmed, 2010):

$$\psi(P) = 2\int_{P_1}^{P} \frac{P}{\mu Z} dP \quad (2.22)$$

For liquid flow in reservoirs, constant properties assumptions are made (compressibility, density, viscosity, total porosity, fluid saturation are assumed constant), and the liquid flow equations can be solved by the analytical method used for liquid well test analysis which is based on pressure approximation to the constant and log of time.

Pressure ≈ Constant * log(time)

For unconventional reservoirs such as gas reservoirs and gas hydrate reservoirs, the constant properties assumptions would be invalid. This is because the variation of gas compressibility, density and viscosity with pressure can be significantly; and this become very apparent in reservoirs like natural gas hydrate where sediment permeability changes with pressure. The real gas pseudo-pressure is applied to linearise the gas diffusion equation and aggregate the analysis of the ranges of the variable pressure. The variation of permeability with pressure is incorporated into the pseudo-pressure term to modify the gas flow equation as follows:

$$\psi(P) = 2\int_0^P \frac{P.k_m(p)}{\mu Z} dP \quad (2.23)$$

Where $k_m(p)$ is the permeability multiplier and can be expressed as effective permeability, the changing permeability, over the initial pressure as follows:

$$k_m(p) = \frac{k_{eff}(p)}{k} \quad (2.24)$$

Thus, the pseudo-pressure method linearized the diffusivity equation by equating the pressure dependent terms (viscosity and gas compressibility) to a pseudo-pressure term. As such, when assumptions are made that the parameters changes are small, the gas flow equation can be written in the form of the liquid flow equation used for gas well test analysis.

Though the pseudo-pressure method has been adjudged the best of the established gas well testing methods, it has some limitations. For instance, the pseudo-pressure approach cannot provide for all the complex flow factors and the nonlinearity effects associated with gas wells where the non-isothermal and relative permeability data are difficult to get (Firoozabadi, 1979). Without the accurate data, the methods would be based on the total mobility value interpretation with truncation error. The effects and the impact on gas hydrate production are very important because of the difficulty in getting accurate relative permeability data and using the well testing formulations would culminate to neglecting a considerable amount of additional pressure drop in the gas well. While there are controversies over the formulation used to estimate the magnitude of the associated pressure drop, there are many empirical relations that have been developed to describe the phenomenon, including Forchheimer's equation (Wang and Economides, 2009). The Forchheimer equation modeled the non-Darcy behaviour experienced in high rate in a way similar the Darcy's equation but with an extra pressure drop parameter which is the quadratic velocity function. This equation and the correlations for estimating the Forchheimer parameter is given by

$$-\nabla P = \frac{\mu}{kh} v + \beta \rho v^2 \qquad (2.25)$$

For gas hydrate reservoir fluid flow, incorporating various parameters related to dual flow nature, viscous flow and diffusion fluxes, and mixing processes, including threshold pressure, inertia and slippage effects, are necessary in developing comprehensive fully implicit coupled model that would provide a more accurate reservoir performance. Exploring some of these challenges was the motivation of this thesis, with the objective function to improve the well performance analyses.

The threshold pressure gradient (TPG) is defined as the minimum pressure gradient that enables the gas to start flowing against viscous forces between solid and gas. The threshold pressure phenomena in porous media were firstly studied in the early 1970s. TPG are found to affect development of tight gas reservoirs and fluid flow at low velocity. Huang (2018) found that TPG has a significant impact on production and as it increases, permeability decreases, and production continues to drop. Song et al. (2015) believed that inaccurate assessment of well productivity may result if the impact of the TPG in tight gas reservoirs is not considered, and that the stable production time would be shortens in spite that the initial production rate goes up with increased permeability TPG increases as the permeability decreases or water saturation

increases. Both production rate and cumulative production are always less when the TPG is considered because of the sharp decrease of pressure. The study showed that in presence of larger TPG, more pressure drop is needed to maintain a constant-rate production. Generally, TPG is experimentally obtained, and derived from plot of flow rate against pressure gradient as shown in the typical flow curve, Figure 2.19. The intercept of the of the extension line of linear part of the curve to horizontal axis gives the pseudo threshold pressure gradient (PTPG). Pseudo-threshold pressure gradient is used to describe the initial nonlinear stage (Zhang et al., 2015; Zeng and Zhao, 2008; Wang et al., 2020).

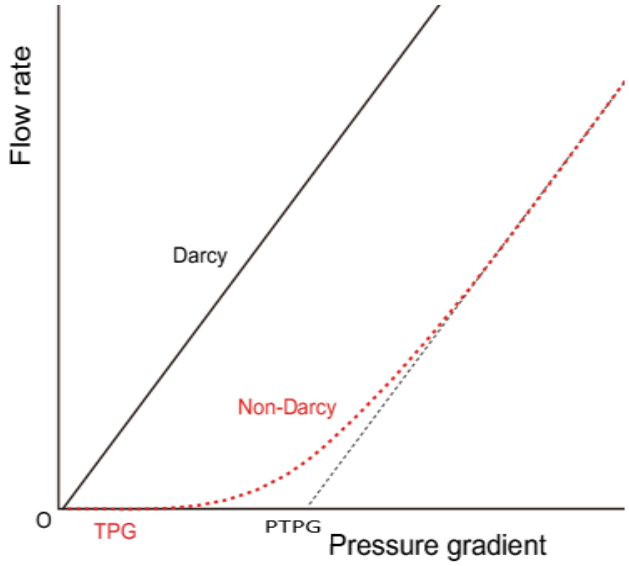

Figure 2.21 Typical Pressure-Rate Relationship Curves with TPG (Luo et al., 2019).

It has been argued that the effect of TPG in reservoir performance prediction is negligible and hence should not be ignored. However, researchers have established the existence of effective threshold pressure gradient in tight gas reservoirs, like natural gas hydrate reservoirs where boundary layer is formed (Wang and Dou, 2002; Thomas, et al., 1968; Wu, et al., 2001). In gas hydrates reservoirs, the interaction between the solid sediments and the fluid results in boundary effect. Fluid flow is consequent upon viscous flow and Knudsen diffusion with occurring dissociation front and boundary layer. Moreover, as the movable fluid saturation flow to the near-wellbore, flow rate is lowered and boundary layer is formed. TPG increases as the mainstream throats get smaller and the movable fluid saturation gets greater towards the wellbore. This thesis looked at the non-linear variation derived from TPG in production of the

nano-porous gas hydrate reservoirs with further fluid flow friction and mixing processes around the wellbore.

Mathematical models that characterised the nonlinear flow and TPG effect abound. (Pascal, 2001) used the permeability tensor and yield relationship equation (Eq. 2.14a) to investigate the TPG effect in non-steady flow of oil. The integral numerical method is used obtain analytical solutions of the effects of the threshold pressure gradient on gas well of hydraulically fractured tight gas formation. Zeng (2013) investigated TPG using the non-linear flow model, power law, to predict the influence of TPG on the permeability of different fluids and deformation in low permeability reservoir was analysed and related. Civan, (2017) and Wang, (2012) published rigorous TPG correlations of flow through tight sandstones and shale-gas reservoirs with TPG effect. Yang et al (2017) leveraged on gas bubble and differential pressure flow methods to investigate TPG and seepage characteristics of tight sandstone gas under the influence of water saturation and develop the equations of threshold pressure gradient for multiphase flow of gas and water phase (Eq.2.141e).

$$\lambda_p = \frac{\beta\tau_0}{\sqrt{k_a}} \tag{2.26a}$$

$$\lambda_p = a_l k_a^{-b_l} \tag{2.26b}$$

Where $k_a = k_{ri}\left(\frac{\sigma_e}{\sigma_{ei}}\right)^{-S_p}$

$$\lambda_p = a_l \left(\frac{k_a}{\mu}\right)^{b_l} \tag{2.26c}$$

$$\lambda_p = a_l S_w^{b_l} (k_a)^{jS_w^{b_l}} \tag{2.26d}$$

where λ is the TPG; β is the dimensionless constant determined by experiment; τ is the yield stress; σ is the stress sensitivity value; a, b, j and l are fitting coefficients; k_a is the absolute permeability; μ is the viscosity; S_w is the water saturation.

On the other hand, Gas slippage is a phenomenon associated with Knudsen diffusion and gas flow effects in very low permeability porous media. Knudsen diffusion underscored the flow in the low permeability formations and the collision between the gas molecules and the wall surfaces (Kast and Hohenthanner, 2000). It explained that gas slippage is obtained where pore diameter is so small that the mean free path of the gas is close to the pore diameter (Mao and

Zeidouni, 2017c). The ratio of the mean free path to pore diameter is denoted by Knudsen number, *Kn* and it is indicative of prevailing flow regimes in the porous (Lee and Kim, 2016; Mousavi & Bryant, 2012). The non-laminar flow and the non-linearity effect have been represented by Knudsen equation or by introducing Klingenberg permeability effect in diffusivity equation.

The effective permeability proposed by Klinkenberg (1941) is expressed as

$$k_{eff} = k\left(1 + \frac{b}{P}\right) \tag{2.27}$$

$$k_{rg}(S_w, p_m) = k_{rg\infty}(S_w)\left(1 + \frac{bS_w}{P_m}\right) \tag{2.29}$$

where

$$b = \frac{16\mu}{3r\gamma}\left(\frac{8RT}{\pi M}\right)^{0.5} + \left(\frac{8\pi RT}{M}\right)\frac{\mu}{r}\left(\frac{2}{\alpha} - 1\right) \tag{2.28}$$

Where b_m is the gas slippage factor.

The gas slippage factor in low permeability reservoirs has also been evaluated and expressed as a function of the gas permeability by various researchers (Ertekin, et al., 1986; Estes and Fulton, 1956; Jones, 1987; Sampath and William, 1982; Rushing, et al., 2004).

Table2. 18 Basic gas slippage factors

Basic gas slippage factor	$b = 0.86k_{\infty}^{-0.33}$
Sampath and William, 1982	$b = 0.0955\left(\frac{k_{\infty g}}{\phi}\right)^{-0.53}$
Rushing et al., 2004	$b = 38\left(\frac{k_K}{\phi_g}\right)^{-0.45}$

2.13.2 Temperature Solutions

In pressure solution scheme for reservoir fluid flow, it is assumed that the reservoir is isothermal, or that the change in temperature is quite small and the effects on the fluid properties and pressure responses are negligible. Though accurate results of high practical value are often obtained with this conventional assumption, it is however not true because temperature changes considerably during production in most unconventional reservoir, especially in near the wellbore (Duru & Horne 2008). Thus, various temperature dependent models have been developed and used in the analyses of fluid flow behavior in the porous media (Sui and Zhu, 2008; Muradov et al. 2017). It is important to note that pressure solutions would be gotten first before temperature solutions since the changes in temperature are directly dependent on the pressure changes and the fluid flow. As discussed earlier on hydrate reservoir models, gas hydrate production involves an endothermic process, and it is a strong candidate of thermal stimulation scheme, and would require a robust transient temperature analysis model. Generally, many hydrate models are non-isothermal models which considered the temperature change in the porous media and less focus on wellbore heat effect. More so, most of the models are based on liquid flow equations normally solved to obtain a sequential varying temperature solution in the reservoir (usually at the sandface), and most of the well test solutions are based on transient pressure analysis (PTA). The PTA is typically used to quantify near wellbore damage (Skin) and it gives the skin as a lump indicating amount of production decline due to damage or additional pressure drop; PTA does not give information on the depth and probability of the damage region, which is necessary to design a proper well stimulation program (Sui and Zhu, 2008; Muradov et al. 2017, Chekalyuk 1965). Transient temperature analyses have been prescribed to further characterise formations, investigate near wellbore conditions, depth of damage zone, fluid breakthrough and well performance (Sui et al., 2008; Malakooti, 2015; Muradov et al., 2017; Ramazanov et al., 2010; Onur, 2016; Yoshioka et al., 2006) in unconventional reservoirs. This model has been employed to evaluate the properties of a reservoir or the produced fluids through of a wellbore of known sandface temperature (Muradov, et al., 2017; Ramazanov, et al., 2010; Davie and Buffett, 2003; Sui, et al. 2008). The model can be expressed as:

$$\phi \frac{d}{dt} \int_{\Omega} e dx + \phi \int_{\partial\Omega} q_{adv}.nds + \phi \int_{\partial\Omega} q_{cond}.nds = \int_{\Omega} Q_T dx \qquad (2.30)$$

Solving the surface integral and rearranging over the whole reservoir, the above equation is usually expressed as

$$\phi \frac{de}{dt} + \nabla . e + \phi \nabla . q_{cond} + \phi \nabla . q_{adv} = \nabla . Q_H \quad (2.31)$$

where

e = the internal energy density; $= \rho_p c_p \Delta T$

$q_{cond} = -k_T \nabla T$

$q_{adv} = eu$

u = total volume flux and is related to intrinsic velocity, v as follows

$u = v\phi$

nds = unit flux vector over cross-sectional area, s, that

$\nabla . Q_H$ = energy production term

k_T = thermal conductivity

c_p = specific heat capacity of a phase, p

ρ_p = density of a phase, p

By substituting for e, v, Q, and neglecting the internal energy conservation, the final heat transfer equation is given as:

$$\rho_p c_p \frac{\partial T}{\partial t} + \nabla . (-K_T \nabla T) + \rho_p c_p v_p . \nabla T = Q_{source/sink} \pm Q_{loss/gain} = o \quad (2.32)$$

(Onur and Cinar, 2016; Wang, 2016) explained that the conductive term can be neglected without significantly affecting the accuracy of the solution since heat conduction had been investigated to has little effect on transient temperature especially at early times. However, gas hydrate production is an endothermic process. The reservoir temperature would increase at early stage of production since pressure changes in the formation are coupled to the temperature derivatives from begging of production, and fluid flow solutions are functions of diffusion and viscous flow. App and Yoshioka (2011) showed that when the Peclet number (a dimensionless number that represents the ratio of the convection/advective rate to the diffusion/conduction rate driven by a transport gradient – like heat transfer – in a continuum) is low, approaching zero, it signified that conduction flow is significant; and this evidence in tight formations with

very low permeability like gas hydrate reservoirs. For production from gas hydrate reservoirs thermal conduction effects will be considered.

This thesis will dovetail into developing a transient temperature analysis (TTA) model for gas hydrate application. The development of accurate TTA system for gas hydrate production would imply having a forward model that incorporates unique properties of gas and most of the thermal flow effects – convection, conduction, Joule-Thomson effect and expansion – in both the reservoir and wellbore. The unique features of the temperature dependent model as relates to gas hydrate reservoir in this thesis are the Joule-Thomson effects and thermal wellbore effects (wellbore heat loss) whose contribution to the temperature changes still remain a research challenge. Joule-Thomson effect can be expressed as the change in temperature that accompanies expansion of a gas without production of work or transfer of heat (Perry and Green, 1984; Edmister and Lee, 1984; De Waele, 2017). At standard temperatures and pressures, all real gases except hydrogen and helium cool upon such Joule-Thomson or adiabatic expansion. It is a measure of the rate of change of temperature with pressure at constant enthalpy. The Joule-Thomson effect and thermal expansion processes are expressed in terms of the heat capacity at constant pressure, as function of Joule–Thomson (Kelvin) coefficient and thermal expansion coefficient respectively as follows (Nield and Bejan, 2013):

$$\mu_{JT} = \left(\frac{\partial T}{\partial P}\right)_H = \frac{V(\beta_T \nabla T - 1)}{C_p} = \frac{(\beta_T T - 1)}{\rho_g C_p} \tag{2.33}$$

$$\alpha_L = \frac{1}{V}\left(\frac{\partial V}{\partial T}\right)_P = \frac{(\beta_T \nabla T)V}{C_p} = \frac{\beta_T T}{\rho_g C_p} \tag{2.33}$$

Thermal wellbore effects describe the wellbore heat loss which affects the fluid properties around the wellbore and inside the tubing and they present transient temperature phenomena. Wellbore temperature solution based on sand-face temperature values, normally measured by installed gauge at or near the mid-perforation point, cannot be relied on for accurate transient temperature analysis because transient sand-face temperature effects should be measured at some distance away from these subsurface locations but it is rarely done due to practical limitations. Furthermore, the conventional thermal wellbore modelling is based on pressure signal created from the average reservoir properties and the temperature change through of the wellbore is based on the average value of the whole production or injection interval, making it difficult to discriminate zones. Thermal wellbore effects that provide for reservoir – wellbore temperature dynamics is required in order to model the accurate transient temperature analysis for comprehensive well performance prediction. Modelling of heat transfer challenges

associated with gas hydrate reservoir - wellbore fluid flow with respect to transient temperature analyses has been of little research focus, leaving a knowledge gap which this thesis would address.

According to Weibo, et al. (2008), the analytical formulation for wellhead temperature calculation was first considered Ramey, 1982. That is the first detailed wellbore heat transmission and transient temperature solution. The Ramey model was based on back-calculating sand face temperature using the temperature value measured by the subsurface gauge and a given wellhead temperature. Following Ramey model, various other models have been developed (Hagoort 2004; Hasan et al., 2005; Duru and Horne, 2010). The especially pertinent among the studies with emphasis on transient temperature analysis are Duru and Horne (2010) and Hagoort (2004) as they investigated the effect of changing bottom-hole flowing temperature in their models, while the others are based on a constant bottom-hole temperature. Though, the available literatures are not rich in the terms of gas hydrate reservoir-wellbore heat loss modelling, schemes for thermal gas well modelling and methods that capture the impact of thermal wellbore-reservoir interactions are available (Muradov, 20l7; Sui and Zhu, 2008)) and would be leverage on to present a more accurate transient temperature solution for gas hydrate application.

2.14 Transient Pressure and Temperature Analysis

There are several methods in the petroleum industry to acquire information about the reservoir and the near-wellbore. Methods that have been used for the data acquisition include well logging, side coring, mud logging, and well testing. The well logging is a local measurement carried out along or in the wellbore, in space and/or time, to determine some physical parameters. Sidewall coring involves taking larger pieces of rocks from the side(s) of the wellbore down the depth and evaluating for information about the rock and wellbore. In mud logging, information is obtained from drilled cuttings gathered at the well surface. Sidewall coring and mud logging data may not be of high accuracy as because of drilling mud or local fluids contamination, and changes due to variations in pressure and temperature of the samples at the surface in relation to the subsurface. Well testing, unlike the other method described above, can give global information about the reservoir and the near-wellbore. Thus, well testing provides more reliable input data for the reservoir simulators. In a typical well testing job, a well testing tool is run inside the wellbore and kept near and across the perforations. The

formation section is isolated by packers from the wellbore, as shown in figure 2.19, and the reservoir is then made to produce at controlled rates for certain amount of time while changes of pressure with time are recorded. After that, the formation is shut-in and the transient pressure is measured until the pressure stabilises. The transient pressures data are then analysed with a mathematical model or well testing software to obtain the desired information.

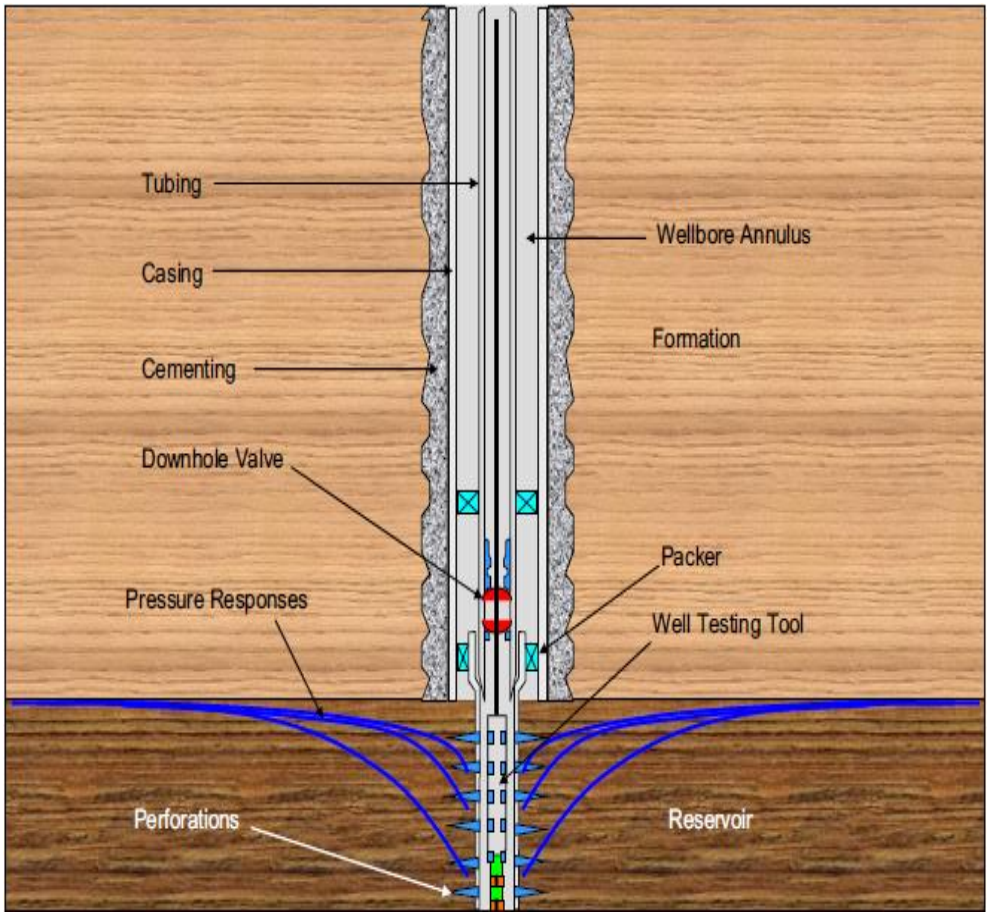

Figure 2.22 Schematic representation of a typical well testing operation

The cost of well testing is high and particularly extremely for unconventional and gas reservoirs. The conservative estimates for the annual cost of conventional well testing across the world are over two billion dollars (Hawkes et al. 2001). In addition to the costs, running the well testing tools in such reservoirs like gas hydrates is very difficult and failure of the tools is common. In this case, instead of running the well testing tool down the wellbore, a permanent pressure gauge is installed at the bottom-hole and the well is shut-in at the wellhead. Then the recorded transient pressure is analysed. Most well testing models are based on analytical schemes with simplifying assumptions such as isothermal behaviour, and not accounting for wellbore-reservoir dynamic interaction. The analytical methods

tend to give asymptotic or approximate solutions and the interpretation and results obtained can be sometimes misleading in comparison with practical values of the well production performance (Fan 1998; Ramazanov, et al., 2010; Davie and Buffett, 2003; Dada, et al., 2017; Onur and Çinar, 2016; Mao and Zeidouni 2017b).

Well testing is typically called pressure transient analysis (PTA) because involves a measure of temporary change in production rate as a function of pressure responses (Bourdet, 2002). It has been used for decades for reservoir and fluid flow characterization, and near-wellbore analysis. It provides key information on the reservoir and the well, including effective permeability, reservoir heterogeneities, reservoir boundaries, wellbore storage, skin, pressure, well production potential and well geometry. The depth of investigation of well testing tool depends on the duration of the test period and can range up to a diameter of few tens of meters around the well. During a well test, a transient pressure response is created by a temporary change in production rate (Bourdet, 2002). Reservoir parameters, such as effective permeability can be estimated from the pressure derivatives plots typical of figure 2.20 and other specialized plots obtained through the well testing methods which include pressure drawdown and build-up schemes.

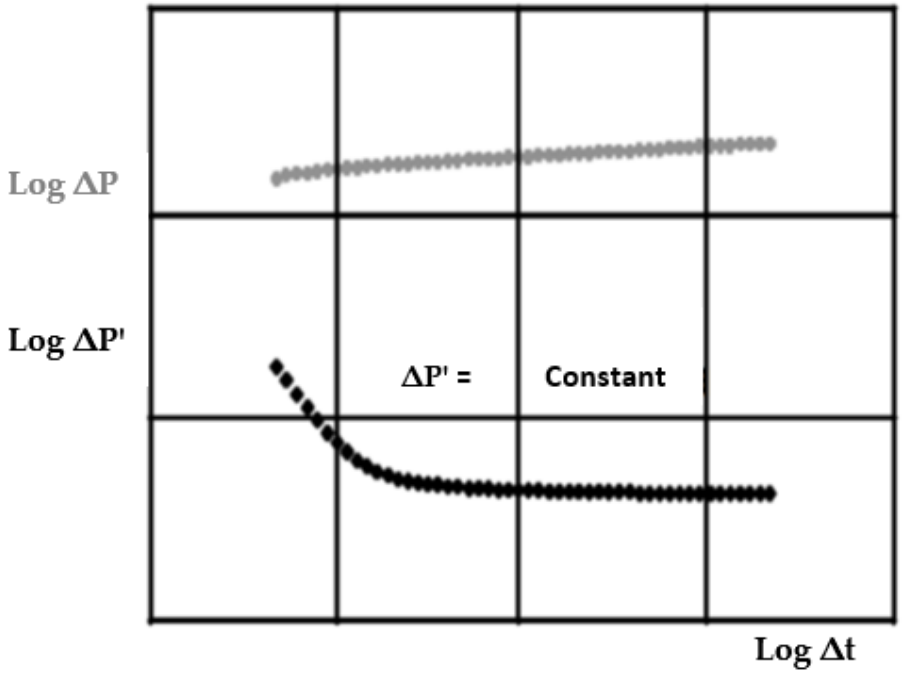

Figure 2.23 Typical Log-Log Plot of Pressure- and Pressure derivative- Rates Behaviour (Bourdet, 2002).

Although reservoirs are different from each other in terms of physical and thermodynamics description, their dynamic behaviours during well testing are circumscribed (Gringarten, 2008). The dynamic behaviours are divided into three main stages that dominate at different times of the well test (Gringarten, 2008). They include Early Time Region (ETR), Middle Time Region (MTR), and Late Time Region (LTR). The ETR represents the near-wellbore effects at early times resulting from the well completion or high contrast in permeability distribution due to the near-wellbore geology. The MTR is representative of the dynamic behaviour of the reservoir in the middle times of the well test and is usually the same for all the wells in a given reservoir. The LTR is representative of the boundary effects at late times and may differ from well to well in a given reservoir depending on the nature of the reservoir boundaries and the distance of the well from the boundaries. Extensive description of well test principles, interpretation techniques, analysis and applications have existed for long and can be found in various literatures (Agarwal 1980; Ramey, 1992; Bourdet, 2002; Gringarten, 2008).

In gas hydrate reservoir production, the hydrate undergoes dissociation, an endothermic reaction process, for the water and gas generation under thermodynamic influence of pressure and temperature changes even without external heat source (Slaon, 1998). To evaluate the accurately the gas hydrate reservoir performance, there is need for temperature transient analysis (TTA), of which have neglected and analyses which effects hydrate dissociation and fluid flow through the wellbore with minimised tendency for hydrate reformation. While pressure transient analyses (PTA) are often used to predict the pressure solutions, temperature transient analyses (TTA) are still developing. Temperature values are normally obtained by downhole temperature measurements using applicable subsurface sensors such as Distributed Temperature Sensing cable (DTS), and Resistance Temperature Detector (RTD) – a point/location temperature sensor (Kanno et al., 2014). TTA is simply an analysis technique that makes use of the measured temperature data from the well monitoring and testing just similarly like PTA though the applications are different. Monitoring involves continuous assessment (measuring, transmitting and analysing) of the conditions of the wellbore or the formation, while testing is a snapshots analysis at a given interval of time and space. Research has shown that temperature transient analysis could provide information that pressure transient analysis may be unable to provide, thus complementing it. Temperature signal can travel quite slower and deeper than pressure signal making it advantageous to be used for more detailed analysis of the reservoir/wellbore, zonal monitoring, multiphase metering transient. Application of TTA can minimise frequent production logging. It can be applied to any well

with installed subsurface temperature sensor (temporary or permanent). It is however more relevant to wells with installed permanent down-hole gauges (advanced wells. While ddifferent types of sensors or transducers exist, the underlying physics are the same. They typically provide measurement of the applicable physical parameters, convert and transmit them (usually in form electrical, acoustic or optical signal) to a logging device where they are stored or analysed directly. When the monitoring and control capabilities are integrated into the well, it is called a smart or intelligent well (Bellarby, 2009). The control part involves capability of changing the behaviour of a well in response to the actionable information obtained from the monitoring process and it allows for remote action to control the reservoir, well and/or production processes. This research focuses on the development of analysis methods for gas hydrate production that incorporate the features that impact transient pressure and temperature behaviours such as threshold pressure gradient, slippage and inertial effects, Joule-Thomson effect and thermal wellbore effects.

2.15 Near-Wellbore Modelling and Permeability Upscaling

Considering the complex nature of the hydrate-bearing sediments and the complex flow processes, better prediction of gas and water production rates would require proper determination of the parameters which values changes with changing flow path near the wellbore. Relative Permeability and capillary pressure are considered the most important parameters that controls the pressure-rate behaviour in the reservoir as flow transient to the wellbore and thus governs the reservoir production (Johnson et al., 2011; Gupta, 2008; Mingawaga et al., 2005; Kleinberg et al., 2005). Many relative permeability and the capillary pressure models used to predict the gas production performance of hydrate-bearing sediments are based on soil-water characteristic curve such as Corey 1954, Brooks and Corey1964, Stone, 1970 and van Genuchten, 1980; and are analytical expressions that captured relative permeability and the capillary pressure as functions of average water saturations (Myshakin et al., 2012, Anderson et al., 2014; Myshakin et al., 2011; Moridis et al., 2009; Kurihara et al., 2011; Moridis and Regan, 2007a; Moridis and Regan, 2007b; Moridis et al., 2005). The parameters for the relative permeability equations and capillary pressure functions are normally determined by laboratory experiments. However, modelling and simulating fluid flow in hydrate reservoirs is much more complicated than in conventional reservoirs due to the solid hydrate phase which can effect the intrinsic permeability and the capillary pressure functions. Some investigations have argued that the relative permeability should be a function of initial hydrate saturation but there have been no

experimental or numerical data to guide the simulations (Lucia 1999; Nordahl 2004; Akbar et al. 2001). Ringrose et al. (2008) explained that capillary pressure and permeability are difficult to constrain in heterogeneous reservoirs like gas hydrate because some subsurface processes such as drainage and imbibition that are controlled by the geological phenomena. When gas hydrate dissociates, gas is generated inside the sediment from many of the reservoirs pores instead of being compel from outside, and may result and in errors in the calculation of the relative permeabilities due to uncertainty of the wetting phase. In this research, near wellbore modelling and upscaling scheme would be explored to evaluate the representativeness of the relative permeability and capillary pressure functions in the reservoir model. Selection of the reliable fitting parameters by averaging and re-scaling of the geological data has been employed to answer questions about the multi-scale geological-petrophysical heterogeneities in reservoirs where direct measurement of permeability in the subsurface might not be reliably deterministic and the precision of the measurements cannot capture the pore scale complexity and flow pattern (Nordahl, 2004, Brandsæter et al. 2001; Corre et al. 2000). Routine averaging methods such as analytical/simple averaging and geostatistical methods would be ineffective in gas hydrate cases because permeability is highly scale-dependent and hydrate reservoirs are more or less anisotropic with high multi-scale heterogeneities (Bea,r 1972; Elfenbein et al., 2005; Nordahl et al., 2005). These conventional methods are based on the idea of pressure averaging and that average petrophysical properties of a reservoir can be defined for representative elementary volume (Deutsch, 2010).

However, averaging the properties within the geological models can still be with complications and are might not be feasible for best simulations runs. There can be high computation time, cost and possible rise of convergence problems, especially when it is required to run multiple fine-scale simulations in order to assess various geological and development scenarios. Therefore, building more coarse and practical models (usually referred to as upscaled models) becomes important. In the simulation model, the number of fine grid cells is reduced by merging the fine cells into larger. Afterwards, the reservoir properties are averaged within the coarse domain. The process of coarsening the fine grid is usually referred to as up-gridding, while averaging reservoir properties within the coarse cells is referred to as upscaling. Near-wellbore upscaling method can be employed to address the parameters characterisation and optimisation needed to provide more accurate estimates of the reservoir performance. Of importance are the changes in the relative permeability and capillary pressure functions in the near-wellbore that affect integrate the coupled reservoir – wellbore interface convective mixing

processes as applicable to hydrate dissociation and gas production (Wen et al., 1998; Nordahl, 2004; Ringrose, 2005; Ringrose et al. 2008). The procedure does not aim to speed up reservoir simulations at the cost of simulation results. The target of upscaling is to replace the very fine and detailed models with coarse models that preserve the most important flow characteristics of fine models and capture the sub-grid heterogeneity with less data. The novel aspect of using the near wellbore upscaling in this thesis is that the workflow enables the implicit representation of the relative permeability and capillary pressure function based on hydrate saturation. This thesis will attempt to explore the various equations and account for the effects of the relative permeability and capillary pressure factors.

CHAPTER 3

NUMERICAL SIMULATION OF THE INHERENT DEFYING FEATURES IN GAS HYDRATE RESERVOIR FLUID FLOW MODELLING

3.1 Synopsis

Gas productions from low permeability hydrate reservoirs are subjects to unconventional and coupled flow processes, including strong rock/fluid interaction, heterogeneity, dissociation kinectics, complex flow geometry, strong interactions between fluid (gas and water) molecules, solid constituents transport in the pores network, pressure and time dependent permeability (Li and Horne, 2004). To describe the flow of gas in the unconventional reservoir, pore network flow dynamics are evaluated for a gas hydrate reservoir with small pore throat and mean free path for gas close to the pore diameter. Dual-mechanism transport characterised inertia and viscous forces with slippage and non-Darcy effects is envisaged for the non-linear multiphase flow in the reservoir. Molecular diffusion is experienced in the gas hydrate pore network and with gas flow to and across the hydrate dissociation front and towards the wellbore (Guo et al., 2015; Kast and Hohenthanner, 2000). It is integral to consider the free gas flow in the pore space in addition to the gas from the hydrate dissociation under the convective and Knudsen diffusion mechanisms, and to account for the threshold pressure (the minimum pressure which the gas phase needed to overcome to displace the water and flow out of the disssociation front). Wu et al. (2014) expressed that effective permeability and capillary pressure of unconventional reservoirs correlate and change with changing mean pressure of the reservoir which relates to the sediment overburden, changing net pressure stress on the rock and the effective porosity. Understanding of how dual permeability evolves with emerging wettability variation of the pore network and changes in flow regimes over pressure depletion are among the major challenges to applicability of the available numerical simulators for adequate prediction of gas hydrate production performance. Accounting for the slippage and inertia effects would be necessary for accurate calculation of the relative permeability which vary with the test pressures; otherwise the permeability may be calcuated to be less than the actual permeability or greater than one at some water saturations (Mao and Zeidouni, 2017). More so, hydrate dissociation and dissociation rate are highly temperature depedent. This chapter will however consider the temperature effects under the natural thermal convection wherein the sediment's surroundings is the heat source. Therefore, in building up the advanced mathematical model for fluid flow in the hydrate production, considerations are given to the coupling of the hydrate

dissociation kinetics and other tangible influencing factors in the low permeability reservoirs, such as non-Darcy flow factors, gas slippage, threshold pressure, thermal gradient effects. Although, some of these features have been investigated, there is limited understanding of how the combined processes influence gas hydrate flow assurance and there is no model that have coupled the simultaneous effects on the ultimate gas recovery. This thesis presents an integrated mathematical model that incorporate the known flow mechanisms and the defying features of two-phase gas - water flow in gas hydrate sediment and processes that relate to the strong rock/fluid interaction, the convective mixing processes, flow regimes and dynamic (time dependent) permeability that affect the gas hydrate production. Specifically, non-Darcy flow effects, Knudsen diffusion factors, inertial, and gas-slippage effects, threshold pressure effects, gas expansion and Joule–Thomson thermal effects are incorporated in the formulation of a new flow model in this thesis.

3.2 Mathematical Formulation

Generally mathematical formulations fluid flow in porous media are derived from conservation laws of mass, momentum and energy. The rate of flow of mass of each fluid component/phase in the fluid per unit cross-sectional area is known as flux. Assumptions of non-Darcy flow for a gas hydrate reservoir with no flow boundaries conditions have been made in this thesis. A three-phase flow model that considered solid (hydrate) phase, water phase and gas phase is considered in this study. The solid phase (hydrate) is conserved as it undergoes dissociation phenomenon. It is assumed that the hydrate would either be completely dissociated or partially dissociated and the dissociating zone remained within the solid rock or behind a dissociation front and no solid hydrate or ice flow to the wellbore. More so, since hydrate dissociation is an endothermic reaction, the energy conservation equation would be solved to evaluate the temperature dependent model.

3.2.1 Governing Equations

Therefore, the multiphase-flow model presented and treated as two-phase gas – water flow model on the precinct of black-oil model (i.e. each component is assumed to be existing only in the associated phase). The continuity equations for the hydrate, gas and water flow through the porous medium can be written as

$$\frac{\partial}{\partial t}\left(\phi\rho_g S_g\right) + \frac{\partial}{\partial x}\left(\rho_g v_g\right) = q_g + \dot{m}_g \quad (3.1)$$

$$\frac{\partial}{\partial t}\left(\phi\rho_w S_w\right) + \frac{\partial}{\partial x}\left(\rho_w v_w\right) = q_w + \dot{m}_w \quad (3.2)$$

$$\frac{\partial}{\partial t}\left(\phi\rho_h S_h\right) = -\dot{m}_h \quad (3.3)$$

ρ_g, ρ_w and ρ_h are densities of the gas, water and hydrate respectively; S_g, S_w and S_h are the saturations of gas, water, and hydrate, respectively; $\dot{m}_g$, $\dot{m}_w$, and $\dot{m}_h$ are the mass rates of gas, water, and hydrate generated from dissociation; q_g and q_w are the flow rates of gas and water respectively across the boundary.

Dissociation Formulation

$$\dot{m}_h = K_{d,0} e^{-\left(\frac{\Delta E_\infty}{RT}\right)} \sqrt{\frac{\phi^3(1-S_H)^3}{2k}}\left(P_{eq} - P_g\right) = -\frac{N_h(M_w+M_g)}{M_g}\dot{m}_g \quad (3.4)$$

$$\dot{m}_g = K_d A_s M_g\left(P_{eq} - P_g\right) \quad (3.5)$$

$$\dot{m}_w = \frac{N_h M_w}{M_g}\dot{m}_g \quad (3.6)$$

The constitutive equations:

$$P_g = P_w + P_{cgw} \quad (3.7)$$

$$S_g + S_w + S_H = 1 \quad (3.8)$$

3.2.2 The Reaction kinetics:

The stoichiometry of the dissociation of the natural gas hydrate for gas production is given as:

$$1CH_4.5.75H_2O \leftrightarrow 1CH_4 + 5.75H_20 \quad (3.9)$$

The gas generation rate, $\dot{m}_g$, follows Kim-Bishnoi model and is related to hydrate dissociation rate, $\dot{m}_h$, and the local mass rate of water produced, $\dot{m}_w$, as follows (Kim et al., 1987; Yousif et al., 1991):

$$\dot{m}_g = K_d A_s\left(f_e - f_g\right) = K_d A_s\left(P_e - P_g\right) \quad (3.10)$$

$$\dot{m}_h = -\frac{1}{V}\frac{\partial(N_{CH_4HYD})}{\partial t} = -\frac{N_h M_w + M_g}{M_g}\dot{m}_g \quad (3.11)$$

$$\dot{m}_w = \frac{N_h M_w}{M_g}\dot{m}_g \quad (3.12)$$

Where, the kinetic rate or reaction constant, K_d , and the parameters have been experimentally evaluated as follows (Clarke and Bishnoi, 2001; Vlasov, 2013)

$$K_d = K_{d0} e^{\left(-\frac{\Delta E_\infty}{RT}\right)} \quad (3.14)$$

K_{do} = 3.6 x 10^4 mol.m^{2}Pa.S.

E_∞/R = 9752.73K.

K_{do} = intrinsic decomposition/reaction rate constant, E = activation energy.

A_s is reaction surface area available for hydrate decomposition (i.e. the interface area between hydrate and fluid phases), and is given as

$$A_s = \sqrt{\frac{\phi^3 (1-S_H)^3}{2k}} \quad (3.15)$$

The methane-water-hydrate equilibrium pressure, P_e , is calculated from Thermodynamic equilibrium relationship given by Jia et al. (2018).

$$P_e = 8\ X\ 10^{-13} e^{\ 0.1052T} \quad (3.16)$$

The real gas equation of state is used to relate density and pressure at standard conditions

$$\rho = \frac{PM}{ZRT} \quad (3.17)$$

The absolute permeability and relative permeability of gas and water phase is calculated using Corey expression (Naridoust and Ahmadi, 2007; Masuda *et al*., 1999)

$$k = k_0 (1 - S_H - S_I)^N \quad (3.18)$$

$$S_n = \frac{S_w - S_{wc}}{1 - S_{wc} - S_{gr}} \quad (3.19)$$

$$k_{rw} = S_n^2 \quad (3.20)$$

$$k_{rg} = (1 - S_n)^2 \quad (3.21)$$

3.2.3 Boundary Conditions

Simulation of flow in the reservoir requires proper definition of the boundary conditions that delineate the reservoir with operating conditions that allowed for discrete determination of the solutions of the continuous system.

- **Initial conditions**

The initial condition from which the solution of the pressure and saturation equations propagates is as simple as specifying a single value of pressure and saturation throughout of the grid blocks of the reservoir, such that

$$P_g(x, y, 0) = P_g^0(x, y, 0) \quad (3.22)$$

$$S_g(x, y, 0) = S_g^0(x, y, 0) \quad (3.23)$$

- **Inner Boundary condition**

The internal boundary conditions are constraints considered at the wellbore. They can be a pressure or rate constraint, depending on if the bottom –hole pressure is specified or the flow rate is specified respectively. In the case of the hydrate reservoir in this thesis, the molar flux of the gas across the symmetrically located well would equate the absolute value of the rate of gas generation through the interface. We obtain the inner boundary condition:

$$J_p^k = |\dot{m}_g|, \ t > 0 \quad (3.24)$$

More so considering the well as infinite conductivity, it can be assumed that the well-bore pressure and the pressure along the open portion of the reservoir are uniform and the integral of the flux over the perforated interval is equal to the constant specified rate. The flow rate can be gas production rate, water production rate or total production rate. This can be written:

$$q_{psc} = -\int_{P_{ref}}^{P_{sc}} \frac{2\pi hkk_{rw\infty}}{\mu_p B_p} r \left.\frac{dP}{dr}\right|_{r=r_w} \quad (3.25)$$

$$\left.\frac{d\,(P-\lambda_{bw}r)}{dr}\right|_{r=r_w} = q_{gsc}\frac{\mu_g}{2\pi rhk_g}\frac{zTP_{sc}}{T_{sc}P} + \beta\rho_g\left(\frac{q_{gsc}}{2\pi \mathrm{rh}}\frac{zTP_{sc}}{T_{sc}P}\right)^2 \quad (3.26)$$

- **Outer Boundary condition**

The reservoir is subjected to a no – flow boundary condition and constant outer boundary pressure. This is equivalent to the reservoir system bounded on all sides by impermeable media such that fluid flow rate into the boundary cells is zero. This is achieved mathematically by specifying a value of zero for the phase transmissibility on the interfaces of the boundary grid blocks.

$$q_{p_{sc,bb}}^n = 0 \quad (3.27)$$

$$\left.\frac{\partial P_{fg}}{\partial x}\right|_{x=0}^{x=L,W,H} = 0 \quad (3.28)$$

3.2.4 Accounting for Non-Darcy Effects, Knudsen Diffusion Factors, Tortuosity and Threshold Pressure

Understanding and incorporation of the complex fluxes associated with the phase changes, non-Darcy and unsteady state transient flow in the hydrate production is critical to the reservoir management. Modelling of the intricate phase distributions and the fluid flow processes from the hydrate reservoir to wellbore has become the research interest of this thesis as there is no comprehensive model that have uniquely modelled all the variables and processes that characterizes the flow scenarios. The tangential influencing factors in the low permeability hydrate reservoirs, such non-Darcy flow, gas slippage and threshold pressure gradient effects would be incorporated into the diffusivity equation. Thus, in addition to the viscous flow and the dissociation kinetics, the Knudsen and convective diffusion mechanism are modelled. The non-Darcy behaviour is illustrated in figure 3.1 below

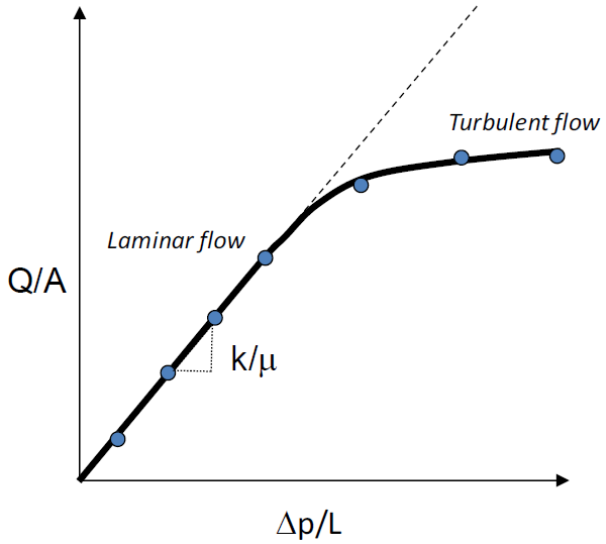

Figure 3. 1 Illustration of Deviation from Linear Darcy (Yao et al., 2020)

The non-Darcy permeability is accounted for by introducing Klinkenberg effect in the diffusivity equation for gas (Kast and Hohenthanner, 2000). The formulation, Eq. 3.24, modified the absolute permeability for the gas flow by introducing a beta factor in the pressure function relationship. It modified the relationship between changes in the hydraulic properties, permeability and mean pressure in the system as shown in figure 3.2 (Ozkan, et al. 2010; Sakhaee-Pour and Bryant, 2012; Lee and Kim, 2016).

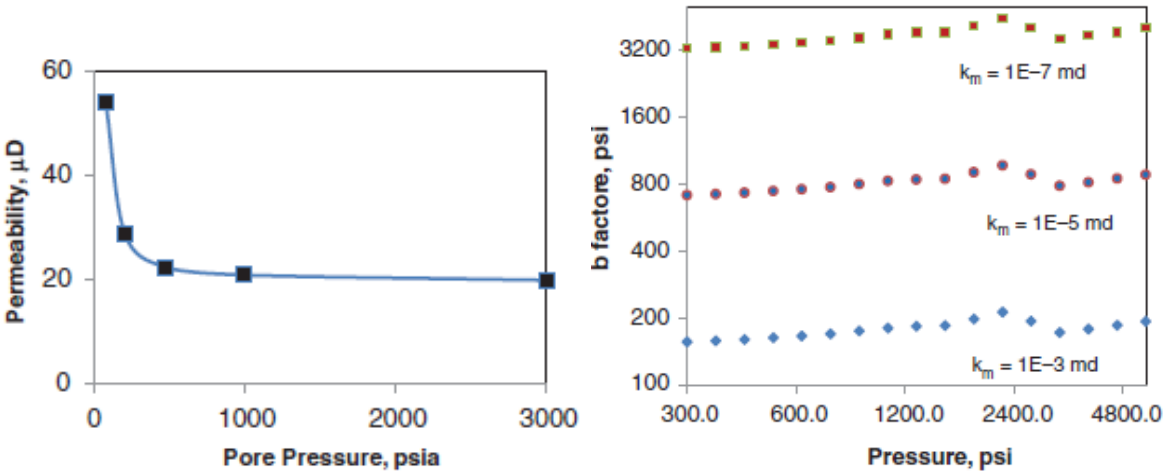

Figure 3. 2 Beta Factor Relationship with Permeability and Pore Pressure (Wu et al. 2014**).**

$$k_{eff} = kk_{rg}\left(1 + \frac{b}{P_g}\right) \tag{3.24}$$

$$b = \beta_1\left(\frac{kk_r(S_g)}{\phi}\right)^{-\beta_2} \tag{3.25}$$

$b = 0.86k^{-0.33}$ (for permeabilities ranges of 0.0001 to 10 md). (3.26)

Where b = Klinkenberg effect, beta factor or slip correction coefficient (when accounting for slippage); β =inertia coefficient.

The vector term of the diffusivity equation for non-Darcy flow is then expressed as

$$\overrightarrow{v_g} = \left(-k\left(1 + \frac{b}{P_g}\right)\frac{k_{rg}}{\mu_g}\left[\nabla P_g - \rho_g \mathrm{gH}\right]\right) \tag{3.27}$$

The beta factor is estimated from the correlation, or it would be established by laboratory experiment. Various models of the correlations exist (Evans and Civan, 1994; Sampath and William, 1982; Ertekin et al, 1986; Rushing et al, 2004; Jones, 1987). The beta factor can also be modelled as a dynamic slippage factor by considering it from the molecular and macroscopic flows of the gas under concentration gradient and pressure field respectively (Ertekin et al. 1986; Jones and Bird, 1985). The expression is presented as follows

$$b = P\left(\frac{c_g D_g \mu}{k_g}\right) \tag{3.28}$$

Where, c_g= gas compressibility; D_g= diffusivity coefficient of gas

Fick's law of diffusion can be employed to account for the gas concentration and velocity field necessary for the fluid permeation and diffusion in the internal flow path of the gas hydrate reservoirs (Civan, 2011; Brogioli and Vailati, 2001). Fick's law states that the magnitude of the diffusive flux, J_D, is proportional to the gas concentration gradient.

$$J_p^k = -D_a \frac{dC_a}{dx} \tag{3.29}$$

Thus, we incorporate the diffusive flux by equating the molar flux of the gas through the hydrate surface to the rate of change in the gas concentration on the surface. Based on the kinetic theory of gas, the Fick's law can be expressed as:

$$\overrightarrow{v_g}^F = \frac{dC_a}{Mdt} - \frac{MD_a}{\rho_g} \nabla(C_a) \tag{3.30}$$

$$M = \frac{\rho_g zT}{P} \tag{3.31}$$

$$C_a = -\frac{\rho_g}{M} S_g$$

$$D_a = D_c \tau \tag{3.32}$$

D_c is the binary diffusion coefficient for gas (methane) – water system; C_a is the gas conentration, expressed as a function of density and saturation; τ is the tortuosity, defined as ratio of actual flow path length to the straight-line distance between those points (it relates fluid's diffusion coefficient when it is not confined by a porous medium to its effective diffusion coefficient when confined in a porous medium). Various formulations exist for tortuosity calculations (Lanfrey et al., 2010; Matyka et al., 2008; Tjaden et al., 2018; Ghanbarian et al., 2013). It can be expressed diagrammatically as below:

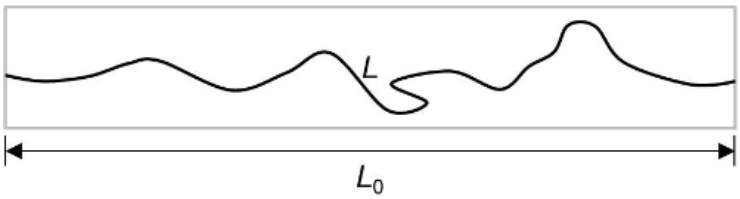

Figure 3. 3 Tortuosity definition diagram

$$\tau = \frac{L}{L_0} = \phi^n \tag{3.33}$$

where, $1 \leq n \leq 3$

For real gas, at standard condition, the gas density and formation volume facor can be expressed as

$$\rho_g = \frac{MP_g}{zRT} \tag{3.34}$$

$$B_g = \frac{zT}{P}\left(\frac{P_{sc}}{T_{sc}}\right) \tag{3.35}$$

Therefore, Eq. 3.10a can be written as

$$J_p^k \frac{\partial(\rho_g v_g)}{\partial x} = D_c \tau\left(\rho_g \nabla S_g\right) \tag{3.36}$$

$$\overrightarrow{v_g^F} = -D_a \nabla\left(\frac{S_g}{B_g}\right) \tag{3.37}$$

To develop the model that combined transports due to ordinary diffusion, Knudsen diffusion, porous medium effects, the convective and advectives fluxes are summed up. The threshold pressure effect would be incorporated by defining the threshold pressure gradient for gas and water phases. Based on the unconventional reservoir studies of Tian et al (2018), the values can be expressed as:

$$\lambda_{tpg} = \left(\frac{\alpha_1}{kk_r} + \alpha_2\right) \tag{3.38}$$

$$\lambda_{tpw} = \left(\frac{\alpha_3 \mu_w}{kk_r}\right)^{\alpha_4} \tag{3.39}$$

The total flux term for the gas and water are therefore a kinematic system of equations obtained as the sum of the convective flow vector and the diffusive fluxes through the hydrate sediment as follows:

$$v_g = -\frac{kk_r}{\mu_g}\left(1 + \frac{b}{P_g}\right)\left(\nabla P_g - \gamma_p \nabla z - \lambda_{tpg}\right) - D_F \nabla S_g \tag{3.40a}$$

$$v_w = = -\frac{kk_{rw}}{\mu_w}\left(\nabla P_w - \gamma_w \nabla z - \lambda_{tpw}\right) \tag{3.40b}$$

Note that the water phase velocity is not impacted by Knudsen diffusion effect.

Combining the above with the conservation of mass of the individual phases, and applying the concept of pressure dependence of density and formation volume facor for real gas at standard condition, the governing equations obtained for flow in the natural gas hydtare system are:

$$\frac{\partial}{\partial t}\left(\frac{\phi S_g}{B_g}\right) = -\nabla.\frac{kk_{rg}}{\mu_g B_g}\left(1 + \frac{b}{P_g}\right)\left(\nabla P_g - \gamma_p \nabla z - \lambda_{tpg}\right) - D_F \nabla\left(\frac{S_g}{B_g}\right) + \dot{m}_g + \frac{q_{gsc}}{B_g} \tag{3. 41}$$

$$\frac{\partial}{\partial t}\left(\frac{\phi S_w}{B_w}\right) = -\nabla.\frac{kk_{rw}}{\mu_w B_w}\left(\nabla P_g - \gamma_p \nabla z - \lambda_{tpw}\right) + \dot{m}_w + \frac{q_{wsc}}{B_w} \tag{3. 42}$$

$$\frac{\partial(\phi\rho_h S_h)}{\partial t} = -\dot{m}_h \quad (3.43)$$

The partial derivative, ∇, is generalised to obtain flux vector terms in two dimensions (two-dimensional) or more.

3.2.5 Well Flow rate (sources/sinks)

The source/sink terms are considered and treated for individual phase. They are flow rates for the gas and water phases related through their respective relative permeabilities that are functions of the water saturation. Source terms (e.g., injector) take positive signs while sink (e.g., producer) are negative. The source/sink terms can be expressed using the conventional Peaceman's wellbore model defined by

$$q_{psci} = \pm\frac{G_{w_i}}{B_p\mu_p}k_{rp}\left(P_i - P_{wfi}\right) \quad (3.44)$$

$$G_{wi} = \frac{2\pi k\Delta z}{\ln\left(\frac{r_{eq}}{r_w}\right)+S} \quad (3.45)$$

To accounts for the non-Darcy flow effect in the hydrate wellbore, interpretation of the well-block pressure (P_n) is extended to incorporate the anisotropic permeability (case of the principal axes of the permeability tensor not being equal, i.e. $\Delta x \neq \Delta y$). To this end, Houpeurt pressure square analytical deliverability equation for gas flow is applied (Kazeem, A.L., 2007, Craft et al,1991). Accordingly, the flowing bottom-hole pressure of the fictitious well, P_{wf} , is related to the pressure of the block containing the well, P_n, as follows:

$$q_{psci} = \pm\frac{2\pi\beta_c k_{eq}\Delta z}{B_p\mu_p \ln\left(\frac{r_{eq}}{r_w}+S\right)}k_{rp}\left((P')^2 - \left(P_{wf}\right)^2\right) \quad (3.46)$$

$$P'(fP) = P_n - P_{t_\lambda}^m$$

Where k_{eq} is the equivalent permeability of an isotropic media derived from the anisotropic permeabilities of the grid block; r_{eq} is the equivalent wellblock radius, and they are given by:

$$k_{eq} = \sqrt{k_x k_y} \quad (3.47)$$

$$r_{eq} = 0.28\frac{\left[\left(k_y/k_x\right)^{0.5}(\Delta x)^2 + \left(k_x/k_y\right)^{0.5}(\Delta y)^2\right]^{0.5}}{\left[\left(k_y/k_x\right)^{0.25} + \left(k_y/k_y\right)^{0.25}\right]} \quad (3.48)$$

S is the skin factor, expressed as

$$S = ln\left(\frac{x}{2r_w}\right) \quad (3.49)$$

Combining the threshold pressure gradient and gas slippage effect accordingly, the gas and water flow rate through a fictitious well of a cross-sectional area of the gas hydrate reservoir can be expressed as:

$$q_{gsc} = \frac{2\pi h\beta_c k_{eq}}{In\left(\frac{r_{eq}}{r_w}+S\right)B_g\mu_g}\left[\left(P_g - \lambda_{tp}{}^{m}_{gl,n} r_{eq}\right)^2 - \left(P_{wf} - \lambda_{tp}{}^{m}_{gl,n} r_{eq}\right)^2\right] \quad (3.50)$$

$$q_{wsc} = \frac{2\pi h\beta_c k_{eq}}{In\left(\frac{r_{eq}}{r_w}+S\right)B_w\mu_w}\left[\left(P_w - \lambda_{tpw}{}^{m}_{l,n} r_w\right) - \left(P_{wf} - \lambda_{tp}{}^{m}_{wl,n} r_{eq}\right)\right] \quad (3.51)$$

3.3 Solution of the multiphase flow equations

The numerical solutions would be obtained by discretization of the continuity equations using a scheme that is forward in time and space and solving the system of the non-linear equations by fully implicit approach using Newton-Raphson method. The discretisation steps convert the continuous non-linear equations into difference equations (partial differential equations with defined discrete functions/values at each point in space and time). Linearisation scheme is then used to convert the resultant solution equations into linear algebraic functions. The solutions of the systems of the equations are then combined together at the level of the Jacobian matrix and computationally implemented.

3.3.1 Discretisation and Linearisation

Our systems of equations are solved by use of the fully implicit finite difference scheme, with time discretised by first order backward difference method (Eq. 3.52), and the spatial discretization by first and second order central difference method (Eqs. 3.53a and 3.53b).

$$\frac{\partial f}{\partial t} = \frac{f_i^{n+1} - f_i^n}{\Delta t} \quad (3.52)$$

$$\frac{\partial f}{\partial x} = \frac{f_{i+1} - f_{i-1}}{2\Delta x} = \frac{f_{i+1.j} - f_{i,j}}{\Delta x_{i+\frac{1}{2}j}} + \frac{f_{i.j} - f_{i-1,j}}{\Delta x_{i-\frac{1}{2}j}} \quad (3.53a)$$

$$\frac{\partial^2 f}{\partial x^2} = \frac{f_{i+1} - 2f_i + f_{i-1}}{\Delta x^2} \quad (3.53b).$$

3.3.1.1 Flow Vector Term

The flow vectors are discretisation in space of the flux component of the continuity equation. For a two-dimensional system, the finite difference discretisation would generate a five-point stencil as follows:

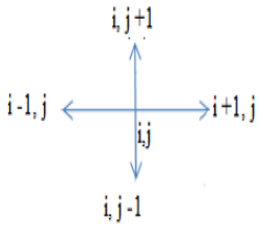

The two-dimensional geometry is considered to ensures that the spatial coupling between the different block components are correctly resolved such that there would be no spurious spatial effects in the flow process simulation, especially as dissociation kinetics are involved. The The finite difference discretisation of the flux term of the governing diffusivity equation for any phase, *p*, in two-dimensional, can be expressed as follows:

$$\overrightarrow{F_p^v} = \Delta_1 T_p^m \left(P_{p,l}^m - P_{p,n}^m\right) \tag{3.54}$$

$$\Delta_1 T_p^m = \left(T^m_{pi-\frac{1}{2},j}\Delta x_{i-\frac{1}{2},j} - T^m_{pi+\frac{1}{2},j}\Delta x_{i+\frac{1}{2},j} + T^m_{pi,j-\frac{1}{2}}\Delta y_{i,j-\frac{1}{2}} - T^m_{pi,j+\frac{1}{2}}\Delta y_{i,j+\frac{1}{2}}\right) \tag{3.55}$$

$T_p^m = \left[G\left(\frac{k_{rp}}{\mu_p B_p}\right)\right]_{l,n}$ is the transmissibility of phase *p* between grid blocks, *l* and *n*.

G is the geometric factor defined as $G = \frac{k_h A_h}{\Delta h}$, where *h = x or y dimension of the reservoir.*

Hence, using the finite difference discretisation scheme, the gas hydrate continuity equations are discretised in next time step, n+1, into the following expression:

For gas:

$$\frac{V_b}{\Delta t}\left[\left(\frac{\phi(1-S_w)}{B_g}\right)^{n+1} - \left(\frac{\phi(1-S_w)}{B_g}\right)^{n}\right]_n = \sum_{l\in\psi_n} T_{gl,n}^{n+1}\left[\left(P_{fg_l}^{n+1} - P_{fg_n}^{n+1}\right) + \lambda_{tp_g}\right] + \sum_{l\in\psi_n} T_{Dgl,n}^{n+1}\left[\left(\frac{1-S_w}{B_g}\right)_l^{n+1} - \left(\frac{1-S_w}{B_g}\right)_n^{n+1}\right] + \sum_{l\in\xi_n} \acute{m}_{gsc_n}^{n+1} + q_{gscl,n}^{n+1} \tag{3.56}$$

For water:

$$\frac{V_b}{\Delta t}\left[\left(\frac{\phi S_w}{B_w}\right)^{n+1} - \left(\frac{\phi S_w}{B_w}\right)^{n}\right]_n = \sum_{l\in\psi_n} T_{wl,n}^{n+1}\left[\left(P_{fgl}^{n+1} - P_{fg_n}^{n+1}\right) - \left(P_{cgw_l}^{n+1} - P_{cgw_n}^{n+1}\right) + \lambda_{tp_w}\right] + \sum_{l\in\xi_n} \acute{m}_{wn}^{n+1} + q_{wsc_{l,n}}^{n+1} \tag{3.57}$$

For hydrate:

$$\frac{V_b}{\Delta t}\left[(\phi\rho_h S_h)^{n+1} - (\phi\rho_h S_h)^n\right]_n = 0 \tag{3. 58}$$

Where

$$P_{fg} = P_g - \gamma_g H \quad (3.59)$$

$$P_{fw} = P_{fg} - P_{cgw} \quad (3.60)$$

$$S_g = 1 - S_w \quad (3.61)$$

3.3.1.2 Expansion of Accumulation Term

By considering the analytical expressions of pressure dependence of compressibility, porosity, formation volume factors and viscosity as follows:

$$B_p = \frac{B_{pb}}{\left(1 + c_p(P - P_{ref})\right)} \quad (3.62)$$

$$\phi = \phi_{ref}\left[1 + c_\phi\left[P - P_{ref}\right]\right] \quad (3.63)$$

$$\mu_g = \frac{\mu_{g,ref}}{\left(1 - c_{\mu,g}(P - P_{ref})\right)} \quad (3.64)$$

$$\acute{\phi}_n = \phi_{n,ref}\, c_\phi \quad (3.65)$$

The accumulation terms (left hand sides) of the governing continuity equations, were expanded into terms containing the primary unknowns by taking the partial differential with time using the steps developed by Erteki et al (2001) as follows:

$$\frac{V_b}{\Delta t}\left[\left(\frac{\phi(1-S_w)}{B_g}\right)^{n+1} - \left(\frac{\phi(1-S_w)}{B_g}\right)^{n}\right]_n = C_{gpn}\left(P_{fg_n}^{n+1} - P_{fg_n}^{n}\right) + C_{gsn}\left(S_{w_n}^{n+1} - S_{w_n}^{n}\right) \quad (3.66a)$$

$$\frac{V_b}{\Delta t}\left[\left(\frac{\phi S_w}{B_w}\right)^{n+1} - \left(\frac{\phi S_w}{B_w}\right)^{n}\right]_n = C_{wpn}\left(P_{fg_n}^{n+1} - P_{fg_n}^{n}\right) + C_{wsn}\left(S_{w_n}^{n+1} - S_{w_n}^{n}\right) \quad (3.66b)$$

$$\frac{V_b}{\Delta t}\left[(\phi\rho_h S_h)^{n+1} - (\phi\rho_h S_h)^{n}\right]_n = C_{hpn}\left(P_{fg_n}^{n+1} - P_{fg_n}^{n}\right) + C_{hsn}\left(S_{w_n}^{n+1} - S_{w_n}^{n}\right) \quad (3.66c)$$

Where,

$$C_{gpn} = \frac{V_b}{\Delta t}\left(1 - S_{w_n}^{n}\right)\left[\phi_n^{n+1}\left(\frac{1}{\acute{B}_{g_n}}\right) + \frac{1}{B_{gn}^{n}}\acute{\phi}_n\right] = \frac{V_b}{\Delta t}\left(1 - S_{w_n}^{n}\right)\left[\frac{\phi_n^{n+1} c_g}{B_{bg_n}} + \frac{\phi_{n,ref} c_\phi}{B_{gn}^{n}}\right] \quad (3.67)$$

$$C_{gsn} = -\frac{V_b}{\Delta t}\left(\frac{\phi}{B_g}\right)_n^{n+1} \quad (3.68)$$

$$C_{wpn} = \frac{V_b}{\Delta t} S_{w_n}^{n}\left[\phi_n^{n+1}\left(\frac{1}{\acute{B}_{w_n}}\right) + \frac{1}{B_{w_n}^{n}}\acute{\phi}_n\right] = \frac{V_b}{\Delta t}\left(S_{w_n}^{n}\right)\left[\frac{\phi_n^{n+1} c_w}{B_{bw_n}} + \frac{\phi_{n,ref} c_\phi}{B_{w_n}^{n}}\right] \quad (3.69)$$

$$C_{wsn} = \frac{V_b}{\Delta t}\left(\frac{\phi}{B_w}\right)_n^{n+1} \quad (3.70)$$

$$C_{hpn} = -\frac{V_b}{\Delta t}\left(\acute{m}_{h,l,n}^{n+1}\right) = -\left[\frac{1}{V}\frac{\partial(N_{CH_4HYD})}{\partial t}\right]_{l,n}^{n+1} = \frac{(N_h M_w + M_g)}{M_g}\acute{m}_{fg}^{(n+1)^v} \quad (3.71)$$

$$C_{hsn} = S_h A_{sh} \frac{V_b}{\Delta t} \left(\frac{\phi}{B_w}\right)_n^{n+1} \quad (3.72)$$

$$\acute{m}_{fg}^{(n+1)^v} = K_{d_o}^n e^{-\left(\frac{E_\infty}{RT}\right)} A_{d_{ec}}^n \left(-1 + \frac{\partial P_e}{\partial P_{fg}}\right) + \left(1 - e^{-\left(\frac{E_\infty}{RT}\right)}\right) \frac{V_b}{\Delta t} \left(\frac{\phi_n^{n+1} c_g}{B_{bg_n}} + \frac{\phi_{n,ref} c_\phi}{B_{g_n}^n}\right) \partial P_{fg} \quad (3.74)$$

Eq. (3.67) through to Eq. (3.74) are substituted into eqns. (3.66a – c) accordingly to obtain the final discretised systems of equations for the gas hydrate reservoir as follows:

For gas phase:

$$C_{gpn}\left(P_{fg_n}^{n+1} - P_{fg_n}^n\right) + C_{gsn}\left(S_{w_n}^{n+1} - S_{w_n}^n\right) = \sum_{l \in \psi_n} T_{gl,n}^{n+1} \left[\left(P_{fg_l}^{n+1} - P_{fg_n}^{n+1}\right) + \lambda_{tp_{gl,n}}\right] + \sum_{l \in \psi_n} T_{Dgl,n}^{n+1} \left[\left(\frac{1 - S_w}{B_g}\right)_l^{n+1} - \left(\frac{1 - S_w}{B_g}\right)_n^{n+1}\right] + \sum_{l \in \xi_n} \acute{m}_{gsc_n}^{n+1} + q_{gscl,n}^{n+1} \quad (3.75)$$

For water phase:

$$C_{wpn}\left(P_{fgn}^{n+1} - P_{fg_n}^n\right) + C_{wsn}\left(S_{w_n}^{n+1} - S_{w_n}^n\right) = \sum_{l \in \psi_n} T_{wl,n}^{n+1} \left[\left(P_{fgl}^{n+1} - P_{fg_n}^{n+1}\right) - \left(P_{cgw_l}^{n+1} - P_{cgw_n}^{n+1}\right) + \lambda_{tp_{wl,n}}\right] + \sum_{l \in \xi_n} \acute{m}_{wn}^{n+1} + q_{wsc_{l,n}}^{n+1} \quad (3.76)$$

For hydrate

$$C_{hpn}\left(P_{fg_n}^{n+1} - P_{fg_n}^n\right) + C_{hsn}\left(S_{w_n}^{n+1} - S_{w_n}^n\right) = 0 \quad (3.77)$$

3.3.2 Solution algorithm

The discretized equations described the flow of the individual phases across each and all the grid blocks in the reservoir system when driven by an applied potential. Examination of the equations showed that the coefficients of the equations are functions of pressure, P_{fg}, and saturation, S_w, the unknown which are the desired solutions of the equations. In solving the systems of equations, Newton Raphson method of simple iteration of all non-linear coefficients is used. The coefficients of all the unknown would be made functions of the unknown. Thus, to obtain the implicit solutions, the discretized continuity equations would be arranged in a sequence of δP_{fg} and δS_w and then scaled up by updating transmissibility and flow rate terms in the next time step (transmissibility is is a function of pressure and saturation through the formation volume factor, B_p and relative permeability, k_{rp}).

3.3.3 Newton Raphson method

According to the Newton Raphson method, the desired solutions of the systems of equations would expanse, simultaneously, to zeroes of the '*k'* continuously differentiable functions (Aziz and Settari,1979). This is equivalent to finding the zeroes of a vector-valued function for a change in a variable (*X*) from *(k)* to *(k+1)* in an iterative process from time (t^n) to (t^{n+1}). The expression can be written as follows;

$$X^{k+1} - X^n = X^k + \delta\vec{X} - X^n = \delta X$$

$$\delta X^v = X^v - X^{(v-1)}$$

$$\left(\delta\vec{X}\right)^{n+1^{v+1}} = \vec{X}^{n+1^{v+1}} - \vec{X}^{n+1^v}$$

Where v = 1,2,3….. is number of iterations, $\vec{X}$ is the unknown vector, and $\left(\delta\vec{X}\right)$ is the incremental or correction vector of the unknown. For implicit scheme, calculation is made in next time step (stepping from time level, *n,* to new time level, *n+1*), while it iterates from (*v*) to (*v+1*). All coefficients for the first Newton iterations are calculated by the values at time level, *n+1,* and is used as the initial values for next iteration.

To increase numerical stability, the implicit Newton method provided that multiplying the differential vector-valued function with the Jacobian matrix of the function would result to the residual, $R \to 0$. That is, the iteration would converge when both δ and *R* approaches zero. The expression is given as:

$$J[f(X^n)]\delta\vec{X} = -R[f(X^n)] \qquad (3.\ 78)$$

Where

$[J[f(X^n)]$= the Jacobean matrix (matrix of the first-order partial derivatives of the coefficients of the unknown variables of in the solutions of the systems of equations).

R = the residual of the equations or vector component.

Hence, based on the Newtons method, for a system of multidimensional function, $[f]^{(n)}$, with *N* unknowns, the solution of the nonlinear equations, $[\Delta\phi]^n$, can be transformed into linear matrix form,

$$Ax = b$$

Which, in turn, is a Taylor series written in matrix form as follows:

$$\begin{bmatrix} \frac{\partial f_1}{\partial \phi_1}|(0) & \frac{\partial f_1}{\partial \phi_2}|(0) & \dots & \frac{\partial f_1}{\partial \phi_N}|(0) \\ \frac{\partial f_2}{\partial \phi_1}|(0) & \frac{\partial f_2}{\partial \phi_2}|(0) & \dots & \frac{\partial f_2}{\partial \phi_N}|(0) \\ \vdots & & & \\ \frac{\partial f_N}{\partial \phi_1}|(0) & \frac{\partial f_N}{\partial \phi_2}|(0) & \dots & \frac{\partial f_N}{\partial \phi_N}|(0) \end{bmatrix} \begin{bmatrix} \delta\phi_1 \\ \delta\phi_2 \\ . \\ . \\ . \\ \delta\phi_N \end{bmatrix} = \begin{bmatrix} -f_1(\phi_1, \phi_n, \dots \phi_N) \\ -f_1(\phi_1, \phi_n, \dots \phi_N) \\ . \\ . \\ . \\ -f_1(\phi_1, \phi_n, \dots \phi_N) \end{bmatrix} \quad (3.79)$$

Hence the solutions of the equations (Eqs. 3.75 - 3. 77) of our gas hydrate system are scaled up by multiplication with their respective formation volume factors and then combined. The final expression obtained is expressed as:

$$h_n^{n+1^v} = \sum_{l\epsilon\psi_n}\left[\left(B_{g,n}^{n+1^v}\Delta_1 T_{fgl,n}^{n+1^v} + B_{w,n}^{n+1^v}\Delta_1 T_{wl,n}^{n+1^v}\right) - \left(B_{g,n}^{n+1^v} C_{gsn}^{n+1^v} + B_{w,n}^{n+1^v} C_{wsn}^{n+1^v}\right)\right]\left(\delta P_{fg} + \delta S_w\right) + \sum_{l\epsilon\psi_n}\left[\left(B_{g,n}^{n+1^v}\Delta_1 T_{fgln}^{n+1^v} + B_{w,n}^{n+1^v}\Delta_1 T_{fwl,n}^{n+1^v}\right) - \left(B_{g,n}^{n+1^v} C_{gpn}^{n+1^v} + B_{w,n}^{n+1^v} C_{wpn}^{n+1^v}\right)\right]\left(\delta P_{fg} + \delta S_w\right) + \sum_{l\epsilon\psi_n}\left[B_{w,n}^{n+1^v}\Delta_1 T_{wl,n}^{n+1^v}\left(P_{cgw,l}^{n+1^v} - P_{cgw,n}^{n+1^v}\right)\left(P_{fg}^n + S_w^n\right) - \left(B_{g,n}^{n+1^v} C_{gpn}^{n+1^v} + B_{w,n}^{n+1^v} C_{wpn}^{n+1^v}\right) - \left(B_{g,n}^{n+1^v} C_{gsn}^{n+1^v} + B_{w,n}^{n+1^v} C_{wsn}^{n+1^v}\right)\right]\left(\delta P_{fg} + \delta S_w\right) + \sum_{l\epsilon\psi_n}\left[\left(B_{g,n}^{n+1^v} T_{fgl,n}^{n+1^v}\Delta_1\lambda_{tpg} + B_{w,n}^{n+1^v} T_{wl.n}^{n+1^v}\Delta_1\lambda_{tpw}\right) - \left(B_{g,n}^{n+1^v} C_{gpn}^{n+1^v} + B_{w,n}^{n+1^v} C_{wpn}^{n+1^v}\right)P_{fg}^n - \left(B_{g,n}^{n+1^v} C_{gsn}^{n+1^v} + B_{w,n}^{n+1^v} C_{wsn}^{n+1^v}\right)\right]\left(\delta P_{fg} + \delta S_w\right) + \sum_{l\epsilon\psi_n}\left[\left(B_{g,n}^{n+1^v}\Delta_1 T_{Dgln}^{n+1^v}\right)\left(B_{g,n}^{n+1^v} C_{gpn}^{n+1^v} + B_{g,n}^{n+1^v} C_{gsn}^{n+1^v}\right)\right]\left(\delta P_{fg} + \delta S_w\right) - \sum_{l\epsilon\psi_n}\left[\left(B_{w,n}^{n+1^v} C_{hpn}^{n+1^v} + B_{w,n}^{n+1^v} C_{hsn}^{n+1^v}\right) - \left(B_{g,n}^{n+1^v} C_{gpn}^{n+1^v} + B_{w,n}^{n+1^v} C_{wpn}^{n+1^v}\right)P_{fg}^n - \left(B_{g,n}^{n+1^v} C_{gsn}^{n+1^v} + B_{w,n}^{n+1^v} C_{wsn}^{n+1^v}\right)S_w^n\right]\left(\delta P_{fg} + \delta S_w\right) + \sum_{l\epsilon\psi_n}\left[\left(B_{g,n}^{n+1^v} + B_{w,n}^{n+1^v}\right)\left(q_{gsc,n}^{n+1^v} q_{wsc,n}^{n+1^v} - \acute{m}_{g,l,n}^{n+1^v} - \acute{m}_{w,l,n}^{n+1^v} - \acute{m}_{h,l,n}^{n+1^v}\right)\right] = 0 \quad (3.80)$$

3.3.4 Treatment of non-linear terms:

The finite difference operator can be express in line with Newton method as follows:

$$\Delta_1 T_p = \delta T_{p_{i-\frac{1}{2}.j}}\Delta x_{i-\frac{1}{2}.j} - \delta T_{p_{i+\frac{1}{2}.j}}\Delta x_{i+\frac{1}{2}.j} + \delta T_{p_{i,j-\frac{1}{2}.}}\Delta y_{i,j-\frac{1}{2}} - \delta T_{p_{i,j+\frac{1}{2}}}\Delta y_{i,j+\frac{1}{2}.}$$

Where *p = gas, water or hydrate phase*

$$\left[f\left(P_{fg}^{n+1} + S_w^{n+1}\right)\right] = \frac{\partial T_p}{\partial P}\delta P + \frac{\partial T_p}{\partial S_w}\delta S_w$$

$$\Delta T_p^{n+1^v} = \Delta T_p^k$$

$$\Delta T_p^{n+1^{v+1}} = \Delta T_p^{k+1}\left[f\left(P_{fg}^{n+1} + S_w^{n+1}\right)\right] = T_p^k + \frac{\partial T_p^{n+1}}{\partial P}\delta P + \frac{\partial T_p^{n+1}}{\partial S_w}\delta S_w$$

$$\Delta T_g^{k+1}\Delta(P)^{n+1} = T_g^k(P)^k + T_g^k\delta P + \left(\frac{\partial T_g}{\partial P}\delta P + \frac{\partial T_g}{\partial S_w}\delta S_w\right)P^k$$

$$\Delta T_w^{k+1}\Delta\left(P - P_{cgw}\right)^{n+1} = T_w^k P^k + T_w^k\delta P + \frac{\partial T_w}{\partial P}P^k\delta P + \frac{\partial T_w}{\partial S_w}P^k\delta S_w - T_w^k\frac{\partial P_{cgw}}{\partial S_w}\delta S_w$$

$$\Delta T_{Dg}^{k+1}\Delta\left(\frac{1-S_w}{B_g}\right)^{k+1} = T_{Dg}^{k}\left(\frac{1-S_w}{B_g}\right)^{k} - T_{Dg}^{k}\left(\frac{1}{B_g}\right)\delta S_w + T_{Dg}^{k}\left(c_g\frac{1-S_w}{B_g}\right)\delta P$$

$$\partial T_g = \left(c_g T_g\right)\delta P + \left(\frac{T_g}{k_{rg}}\right)^{k}\frac{\partial k_{rg}}{\partial S_w}\delta S_w$$

$$\partial T_w = \left(\frac{T_g}{k_{rw}}\right)^{k}\frac{\partial k_{rw}}{\partial S_w}\delta S_w$$

$$T_g = \left[\frac{kk_{rg}}{\mu_g B_g}\left(1+\frac{b}{P_g}\right)\right];\;\; T_w = \left[\frac{kk_{rg}}{\mu_g B_g \Delta x}\right]$$

$$C_{gpn} = \frac{V_b}{\Delta t}\left(1-S_{w_n}^{n}\right)\left[\frac{\phi_n^{n+1}c_g}{B_{bg_n}} + \frac{\phi_{n,ref}c_\phi}{B_{gn}^{n}}\right];\quad C_{gsn} = -\frac{V_b}{\Delta t}\left(\frac{\phi}{B_g}\right)_n^{n+1}$$

$$C_{wpn} = \frac{V_b}{\Delta t}\left(S_{w_n}^{n}\right)\left[\frac{\phi_n^{n+1}c_w}{B_{bwn}} + \frac{\phi_{n,ref}c_\phi}{B_{wn}^{n}}\right];\; C_{wsn} = \frac{V_b}{\Delta t}\left(\frac{\phi}{B_w}\right)_n^{n+1}$$

$$B_{p,n}^{n+1^{v}}C_{pn}^{k+1} = \left(1-S_{w_n}^{k}\right)\left[\left(\frac{c_g}{B_{gb_n}}\right) + \frac{\phi_{ref}c_\phi}{\phi_n^{n+1}B_{gn}^{n+1}}\right]\left[\left(P_{g_n}^{k+1} - P_{gn}^{k}\right) - \frac{1}{B_{gn}^{n+1}}\left(S_{w_n}^{k+1} - S_{w_n}^{k}\right)\right]$$

$$\left(1-S_{w,n}^{n+1^{v}}\right)\left[\left(P_{g_n}^{k+1} - P_{gn}^{k}\right) - \frac{1}{B_{gn}^{n+1}}\left(S_{w_n}^{k+1} - S_{w_n}^{k}\right)\right] = S_{w,n}^{n} +$$

$$\frac{1}{C_{wwn}^{n+1^{v}}}\left\{\sum_{l\epsilon\psi_n} T_{wl,n}^{n+1^{v}}\left[\left(P_{fg,l}^{n+1^{v+1}} - P_{fg,n}^{n+1^{v+1}}\right) - \left(P_{cgw,l}^{n+1^{v+1}} - P_{cgw,n}^{n+1^{v+1}}\right)\right] + q_{wsc,n}^{n+1} -\right.$$

$$\left. C_{wpn}^{n+1^{v}}\left(P_{fg,n}^{n+1^{v+1}} - P_{fg,n}^{n}\right)\right\}$$

$$P_{t\lambda_p}r_e = B_{g,n}^{n+1^{v}}T_{gl,n}^{n+1^{v}}\Delta_1\lambda_{tp_{gl,n}}$$

3.3.5 Final matrix equation for the gas hydrate reservoir

According to the control volume finite difference method, a grid block, *n*, in a two-dimensional plane has four (4) block neighbours in the East, West, North and South directions as shown in the figure 3.4 below.

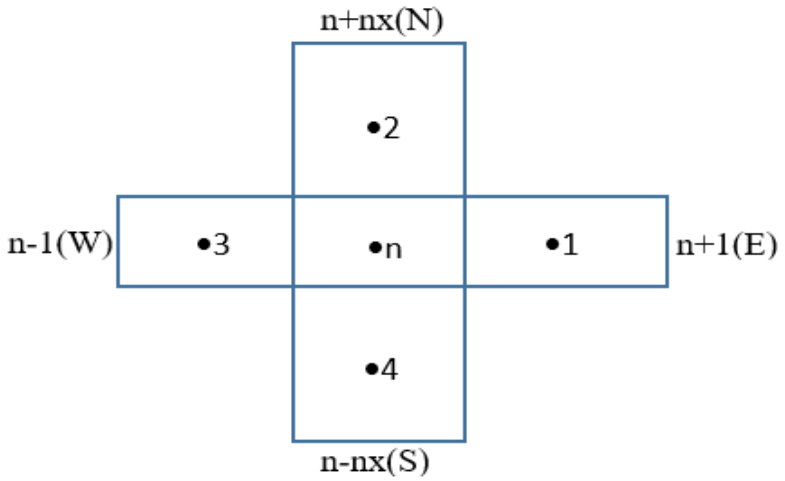

Figure 3. 4 Orthogonal Coordinates of the Two-Dimensional Reservoir Grid-blocks

Each set contains four (4) elements for interior grid blocks, three (3) elements for grids that fall on one reservoir boundary or two (2) elements for grids that are on two reservoir boundaries. Neumann boundary condition was applied to describe the summation terms of the continuity equation.

ψ_n = set whose elements are the existing neighboring blocks to block '*n*' in the reservoir.

ξ_n = set whose elements are the reservoir boundaries (b_S,c_W,e_E, f_N). Thus, ξ_n is either an empty set for interior blocks or a set that contains one element for boundary blocks that fall on one reservoir boundary and two elements for boundary blocks that fall on two reservoir boundaries,

From the description of the sets $\psi_{\square}$ and $\xi_{\square}$ their sums must be equal to the four for the two-dimensional system. i.e.

$$\psi_{\square} + \xi_n = 4$$

If ξ_n is empty, it implies that the block does not fall on a reservoir boundary and as such, its fictitious flow rate term for any of the phases is zero.

$$\sum_{l\in\xi_n} q_{gscl,n}^{n+1} = \sum_{l\in\xi_n} q_{wscl,n}^{n+1} = 0 \qquad (3.81)$$

For the source /sink inflow, a fluid flow rate is specified and the flow rate of the other phase is calculated using

$$q_{psci} = \left(\frac{k_{rp}}{B_p\mu_p}\right)_i q_{spp} / \left(\frac{k_{rpp}}{B_{pp}\mu_{pp}}\right)_i \qquad (3.82)$$

$\left(\frac{k_{rpp}}{B_{pp}\mu_{pp}}\right)$, $\left(\frac{k_{rp}}{B_p\mu_p}\right)$ are the fluid properties of the fluid whose flow rate is specified and the fluid whose flow rate is to be determined respectively while q_{spp} is the liquid flow rate for the

specified phase. In addition, where a total fluid production rate is specified, the rate is prorated between the phases, and for any phase, its rate is given by;

$$q_{psci} = \left(\frac{k_{rp}}{B_p\mu_p}\right)_i \frac{q_{Tsp}}{\left[\left(\frac{k_{rg}}{B_g\mu_g}\right)_i + \left(\frac{k_{rw}}{B_w\mu_w}\right)_i\right]} \quad (3.83)$$

$\left(\frac{k_{rp}}{B_p\mu_p}\right)_i$ = the property of the phase whose flow rate q_{psci}, is being calculated; q_{Tsp} = the total specified production rate.

For the discretized gas and water equations, $T_{p_{l,n}}$ is defined as

$T_{p_{l,n}} = G_{l,n}\left(\frac{k_{rp}}{B_p\mu_p}\right)_{l,n}$, $G_{l,n}$ is a geometric factor between blocks *n* and *l*.

Thus, expanding the summation terms of the difference equations for the fluid flow, we obtain:

For gas phase:

$$C_{gpn}\left(P_{fg_n}^{n+1^v} - P_{fg_n}^n\right)P_{fg} + C_{gsn}\left(S_{w_n}^{n+1^v} - S_{w_n}^n\right)\delta S_w$$
$$= \Delta T_g^k \Delta\delta P_{fg} + \Delta P_{fg}^k \Delta\left(\frac{\partial T_g}{\partial P}\delta P_{fg} + \frac{\partial T_g}{\partial S_w}\delta S_w\right) + P_{t\lambda g}\left(\Delta\frac{\partial T_g}{\partial P}\delta P_{fg} + \frac{\partial T_g}{\partial S_w}\delta S_w\right) + \Delta T_{Dg}^k \Delta\left(1 - S_{w_n}^n\right)\left[\left(\frac{c_g}{B_{gb_n}}\right) + \frac{\phi_{ref}c_\phi}{\phi_n^{n+1}B_{gn}^{n+1}}\right]\left(P_{g_n}^{n+1} - P_{gn}^n\right) - \frac{1}{B_{gn}^{n+1}}\left(S_{w_n}^{n+1} - S_{w_n}^n\right)\delta P_{fg} - \Delta T_{Dg}^k \Delta S_{w,n}^n +$$
$$\frac{1}{C_{wwn}^{n+1^v}}\sum_{l\epsilon\psi_n} T_{wl,n}^{n+1^v}\left[\left(P_{fg,l}^{n+1^{v+1}} - P_{fg,n}^{n+1^{v+1}}\right) - \left(P_{cgw,l}^{n+1^{v+1}} - P_{cgw,n}^{n+1^{v+1}}\right)\right] + q_{wsc,n}^{n+1} - C_{wpn}^{n+1^v}\left(P_{fg,n}^{n+1^{v+1}} - P_{fg,n}^n\right)\delta S_w - \acute{m}_{g,l,n}^{n+1} + q_{gscn}^{n+1}$$

$$= \Delta T_g^{n+1^v}\delta P_{fg} + \Delta T_{fg}^{n+1^v}\left(\frac{\partial T_g}{\partial P}\delta P_{fg} + \frac{\partial T_g}{\partial S_w}\delta S_w\right) + P_{t\lambda g}\left(\Delta\frac{\partial T_g}{\partial P}\delta P_{fg} + \frac{\partial T_g}{\partial S_w}\delta S_w\right) + \Delta T_{Dg}^{n+1^v}\Delta\left[\left(\frac{c_g}{B_{gb_n}}\right)\delta S_w + \left(\frac{\phi_{ref}c_\phi}{\phi_n^{n+1}B_{gn}^{n+1}}\right)\delta P_{fg}\right] + \left[\Delta T_{Dg}^{n+1^v}\left(\frac{\phi_n^{n+1}c_g}{B_{bgn}} + \frac{\phi_{n,ref}c_\phi}{B_{gn}^n}\right)\delta P_{fg} - \frac{\phi}{B_{gn}^{n+1}}\delta S_w\right] + \frac{1}{C_{wwn}^{n+1^v}}\sum_{l\epsilon\psi_n} T_{wl,n}^{n+1^v}\left[\frac{\partial T_g}{\partial P}\delta P_{fg} - T_w^{n+1^v}\Delta\frac{\partial P_{cgw}}{\partial S_w}\delta S_w\right] - q_{wsc,n}^{n+1^v} - \acute{m}_{g,l,n}^{n+1^v} + q_{gscn}^{n+1^v} \quad (3.84a)$$

For Water phase:

$$C_{wpn}\left(P_{fgn}^{n+1^v} - P_{fg_n}^n\right)\delta P_{fg} + C_{wsn}\left(S_{w_n}^{n+1^v} - S_{w_n}^n\right)\delta S_w$$
$$= \Delta T_w^{n+1^v}\delta P_{fg} + \Delta T_w^{n+1^v}\left(\frac{\partial T_w}{\partial P}\delta P_{fg} + \frac{\partial T_w}{\partial S_w}\delta S_w\right) + T_w^{n+1^v}\Delta\frac{\partial P_{cgw}}{\partial S_w}\delta S_w + P_{t\lambda w}\left(\Delta\frac{\partial T_g}{\partial P}\delta P_{fg} + \frac{\partial T_g}{\partial S_w}\delta S_w\right) + \left[\frac{\phi_n^{n+1}c_w}{B_{bw_n}} + \frac{\phi_{n,ref}c_\phi}{B_{wn}^n}\right]\delta P_{fg} + \left(\frac{\phi}{B_w}\right)_n^{n+1^v}\delta S_w - \acute{m}_{w,l,n}^{n+1^v} + q_{wscn}^{n+1^v} \quad (3.84b)$$

Applying the equations to any grid block would give a penta-diagonal matrix as follows

$$b_n^{n+1^{v+1}}\left(\delta P_{fg}+\delta S_w\right)_{n-nx} + \; c_n^{n+1^{v+1}}\left(\delta P_{fg}+\delta S_w\right)_{n-1} + \; d_n^{n+1^{v+1}}\left(\delta P_{fg}+\delta S_w\right)_n + e_n^{n+1^{v+1}}\left(\delta P_{fg}+\delta S_w\right)_{n+1} + \; f_n^{n+1^{v+1}}\left(\delta P_{fg}+\delta S_w\right)_{n+nx} = \; h_n^{n+1^{v+1}} \quad (3.84)$$

The solution of the systems of equations for the gas and water (multiphase) flow can be expressed in matrix form as follows-

$$\begin{bmatrix} b_{n_g}^1 & b_{n_g}^2 \\ b_{n_w}^1 & b_{n_w}^2 \end{bmatrix}\begin{bmatrix} \delta P_{fg_{i,j-1}} \\ \delta s_{w_{i,j-1}} \end{bmatrix}+\begin{bmatrix} c_{n_g}^1 & c_{n_g}^2 \\ c_{n_w}^1 & c_{n_w}^2 \end{bmatrix}\begin{bmatrix} \delta P_{fg_{i-1,j}} \\ \delta s_{w_{i-1,j}} \end{bmatrix}+\begin{bmatrix} d_{n_g}^1 & d_{n_g}^2 \\ d_{n_w}^1 & d_{n_w}^2 \end{bmatrix}\begin{bmatrix} \delta P_{fg_{i,j}} \\ \delta s_{w_{i,j}} \end{bmatrix}$$

$$+\begin{bmatrix} e_{n_g}^1 & e_{n_g}^2 \\ e_{n_w}^1 & e_{n_w}^2 \end{bmatrix}\begin{bmatrix} \delta P_{fg_{i+1,j}} \\ \delta s_{w_{i+1,j}} \end{bmatrix}+\begin{bmatrix} f_{n_g}^1 & f_{n_g}^2 \\ f_{n_w}^1 & f_{n_w}^2 \end{bmatrix}\begin{bmatrix} \delta P_{fg_{i,j+1}} \\ \delta s_{w_{i,j+1}} \end{bmatrix} = \begin{bmatrix} h_{n,fg}^{n+1^{v+1}} \\ h_{n,w}^{n+1^{v+1}} \end{bmatrix} \quad (3.85)$$

Where,

Superscripts 1 and 2 denote the coefficient of P_{fg} and S_W respectively in the difference equations of both gas and water phase flow. $b_n, c_n, e_n \; and \; f_n$ are the coefficients of the diagonal elements of the matrix in the East, West, North and South directions respectively. The diagonal element of the summed matrix is d_n while h_n is the right-hand vector.

$$b_n^{n+1^{v+1}} = B_{g,n}^{n+1^v}T_{g,S}^{n+1^v} + B_{w,n}^{n+1^v}T_{w,S}^{n+1^v} + P_{t\lambda_g}r_e + P_{t\lambda_w}r_e + T_{Dg,S}^{n+1^v}(B_{g,n}^{n+1^v}C_{gpn}^{n+1^v} + B_{g,n}^{n+1^v}C_{gsn}^{n+1^v}) \quad (3.86)$$

$$c_n^{n+1^{v+1}} = B_{g,n}^{n+1^v}T_{g,W}^{n+1^v} + B_{w,n}^{n+1^v}T_{w,W}^{n+1^v} + P_{t\lambda_g}r_e + P_{t\lambda_w}r_e + T_{Dg,W}^{n+1^v}(B_{g,n}^{n+1^v}C_{gpn}^{n+1^v} + B_{g,n}^{n+1^v}C_{gsn}^{n+1^v}) \quad (3.87)$$

$$e_n^{n+1^{v+1}} = B_{g,n}^{n+1^v}T_{g,E}^{n+1^v} + B_{w,n}^{n+1^v}T_{w,E}^{n+1^v} + P_{t\lambda_g}r_e + P_{t\lambda_w}r_e + T_{Dg,E}^{n+1^v}(B_{g,n}^{n+1^v}C_{gpn}^{n+1^v} + B_{g,n}^{n+1^v}C_{gsn}^{n+1^v}) \quad (3.88)$$

$$f_n^{n+1^{v+1}} = B_{g,n}^{n+1^v}T_{g,N}^{n+1^v} + B_{w,n}^{n+1^v}T_{w,N}^{n+1^v} + P_{t\lambda_g}r_e + P_{t\lambda_w}r_e + T_{Dg,N}^{n+1^v}(B_{g,n}^{n+1^v}C_{gpn}^{n+1^v} + B_{g,n}^{n+1^v}C_{gsn}^{n+1^v}) \quad (3.89)$$

$$d_n^{n+1^{v+1}} = B_{g,n}^{n+1^v}T_{g,S}^{n+1^v} + B_{w,n}^{n+1^v}T_{w,S}^{n+1^v} + B_{g,n}^{n+1^v}T_{g,W}^{n+1^v} + B_{w,n}^{n+1^v}T_{w,W}^{n+1^v} + B_{g,n}^{n+1^v}T_{g,E}^{n+1^v} + B_{w,n}^{n+1^v}T_{w,E}^{n+1^v} + B_{g,n}^{n+1^v}T_{g,N}^{n+1^v} + B_{w,n}^{n+1^v}T_{w,N}^{n+1^v} + 2\left(P_{t\lambda_g}r_e + P_{t\lambda_w}r_e\right) + 4T_{Dg,l,n}^{n+1^v}(B_{g,n}^{n+1^v}C_{gpn}^{n+1^v} + B_{w,n}^{n+1^v}C_{gsn}^{n+1^v}) + (B_{g,n}^{n+1^v}C_{gpn}^{n+1^v} + B_{g,n}^{n+1^v}C_{gsn}^{n+1^v}) + \left(B_{w,n}^{n+1^v}C_{wpn}^{n+1^v} + B_{w,n}^{n+1^v}C_{wsn}^{n+1^v}\right) + (B_{g,n}^{n+1^v}C_{hpn}^{n+1^v} + B_{w,n}^{n+1^v}C_{h,sn}^{n+1^v}) \quad (3.90)$$

$$h_{n,fg}^{n+1^{v+1}} = \Delta_1\left(B_{g,n}^{n+1^{v+1}}T_{fgl,n}^{n+1^{v+1}} + B_{w,n}^{n+1^{v+1}}T_{wl,n}^{n+1^{v+1}} + P_{t\lambda g}r_e + T_{Dgln}^{n+1^{v+1}}B_{g,n}^{n+1^v}C_{gpn}^{n+1^{v+1}}\right) - \left(B_{g,n}^{n+1^{v+1}}C_{gpn}^{n+1^{v+1}} + B_{w,n}^{n+1^{v+1}}C_{wpn}^{n+1^{v+1}} + B_{g,n}^{n+1^{v+1}}C_{hpn}^{n+1^{v+1}}\right) - \acute{m}_{h,l,n}^{n+1^{v+1}} - \acute{m}_{g,l,n}^{n+1^{v+1}} + B_{g,n}^{n+1^{v+1}}q_{gsc,n}^{n+1^{v+1}} = 0 \quad (3.91)$$

$$h_{n,w}^{n+1^{v+1}} = \Delta_1 T_{wl,n}^{n+1^{v+1}} \left[\left(P_{cgw,l}^{n+1^{v+1}} - P_{cgw,n}^{n+1^{v+1}} \right) + P_{t\lambda w} r_e \right] + \left(B_{g,n}^{n+1^{v+1}} C_{gsn}^{n+1^{v+1}} + B_{w,n}^{n+1^{v+1}} C_{wsn}^{n+1^{v+1}} + \right.$$
$$\left. + B_{w,n}^{n+1^{v+1}} C_{hsn}^{n+1^{v}+1} \right) \left(P_{fg}^{n+1} + S_w^{n+1} \right) - \acute{m}_{w,l,n}^{n+1^{v}} - \acute{m}_{h,l,n}^{n+1^{v+1}} + B_{w,n}^{n+1^{v+1}} q_{wsc,n}^{n+1^{v+1}} = 0 \quad (3.92)$$

The reservoir flowing pressure, phases saturations and inflow performance relationship are computed as follows:

$$P_{\square\square\square}^{n+1^{v+1}} = P_{fgn}^{n+1^{v}} + \delta P_{fgn}^{n+1^{v}} \quad (3.93)$$

$$S_{\square\square}^{n+1^{v+1}} = S_{wn}^{n+1^{v}} + \delta S_{wn}^{n+1^{v}} \quad (3.94)$$

$$P_{\square\square\square}^{n+1^{v+1}} = P_{fgn}^{n+1^{v}} - P_{cgw}^{n+1^{v}} \quad (3.95)$$

$$S_{\square\square}^{n+1^{v+1}} = 1 - S_{wn}^{n+1^{v}} - \Delta_1 S_h \quad (3.96)$$

$$q_{gsc} = \frac{2\pi h k_{eq}}{In\left(\frac{r_{eq}}{r_w}+S\right) B_g \mu_g} \left[\left(P_{fg} - P_{t\lambda_g} r_e \right)^2 - \left(P_{wf} - P_{t\lambda_g} r_w \right)^2 \right] \quad (3.97)$$

$$q_{wsc} = \frac{2\pi h k_{eq}}{In\left(\frac{r_{eq}}{r_w}+S\right) B_w \mu_w} \left[\left(P_{fw} - P_{t\lambda_w} r_w \right) - \left(P_{wf} - P_{t\lambda_w} r_{eq} \right) \right] \quad (3.98)$$

The hydrate saturation profile is obtained from the expression of the dissociation equation -

$$\Delta_1 S_h = 1 - \phi \left[\sqrt[3]{\frac{2\dot{k}_{m,g}^2}{\left(K_{d,0} e^{-\frac{\Delta E_\infty}{RT}} \right)^2 \left(P_{eq} - P_{fgn}^{n+1^{v+1}} \right)^2}} \right] \quad (3.99)$$

3.4 Implementation

The Newton iteration of the numerical solution of the discretised systems of equations were implemented in MATLAB. First, a synthetic cartesian two-dimensional model of the hydrate reservoir was built. A 1000m x 100m reservoir is considered and synthesised into a grid system vertical and horizontal layers measuring of 20m x 20m and uniformly spaced. The reservoir was initialized with pressure and temperature gradients that yield saturated conditions (hydrate phase) in first 10 layers and unsaturated aqueous condition in other 10 layers. The matrix of the numerical solution of the discretised reservoir systems of equations were executed in the MATLAB using matrix block-diagonal minimization and Newton Raphson iterative methods. The model computations were applied to each block by initiating a drive potential (reducing the reservoir pressure from initial condition of 3.5MPa to 2.25MPa). The solution algorithm proceeded as follows: Starting from the initial condition, at each time step, the equations were

iterated until the solution obtained converges with a predefined tolerance level. During the iteration step, the coefficients were updated with the pressure and saturation calculated for the next time step. The program continued to compute for δP_{fg} and δS_w in v+1 iteration until the values were small enough, with tolerance,

$$\left|\delta P_{fgn}^{n+1^{v+1}} \leq P_{fgn}^{n+1^{v+1}} - P_{fgn}^{n+1^{v}}\right| = /tol \leq \varepsilon_1 / \leq 10^{-6}. \quad (3.100)$$

$$\left|\delta S_{wn}^{n+1^{v+1}} \leq S_{wn}^{n+1^{v+1}} - S_{wn}^{n+1^{v}}\right| = /tol \leq \varepsilon_2 / \leq 10^{-6} \quad (3.101)$$

To check the time dependency of the numerical scheme, the time-step size is successively decrease for different test-runs. Iterative Gauss-Seidel scheme was used to apply and couple the solutions for each section of the reservoir grid blocks; this formed the outer the outer loop. Once convergence is achieved, the solutions obtained for the current and the next time steps were used to update the coefficients of the systems of equations and then the algorithm proceeds to end. The corresponding average reservoir pressure, phases saturations, flow rates and production rates were collected as the simulation output. The simulation flow chart is represented by figure 3.4 below.

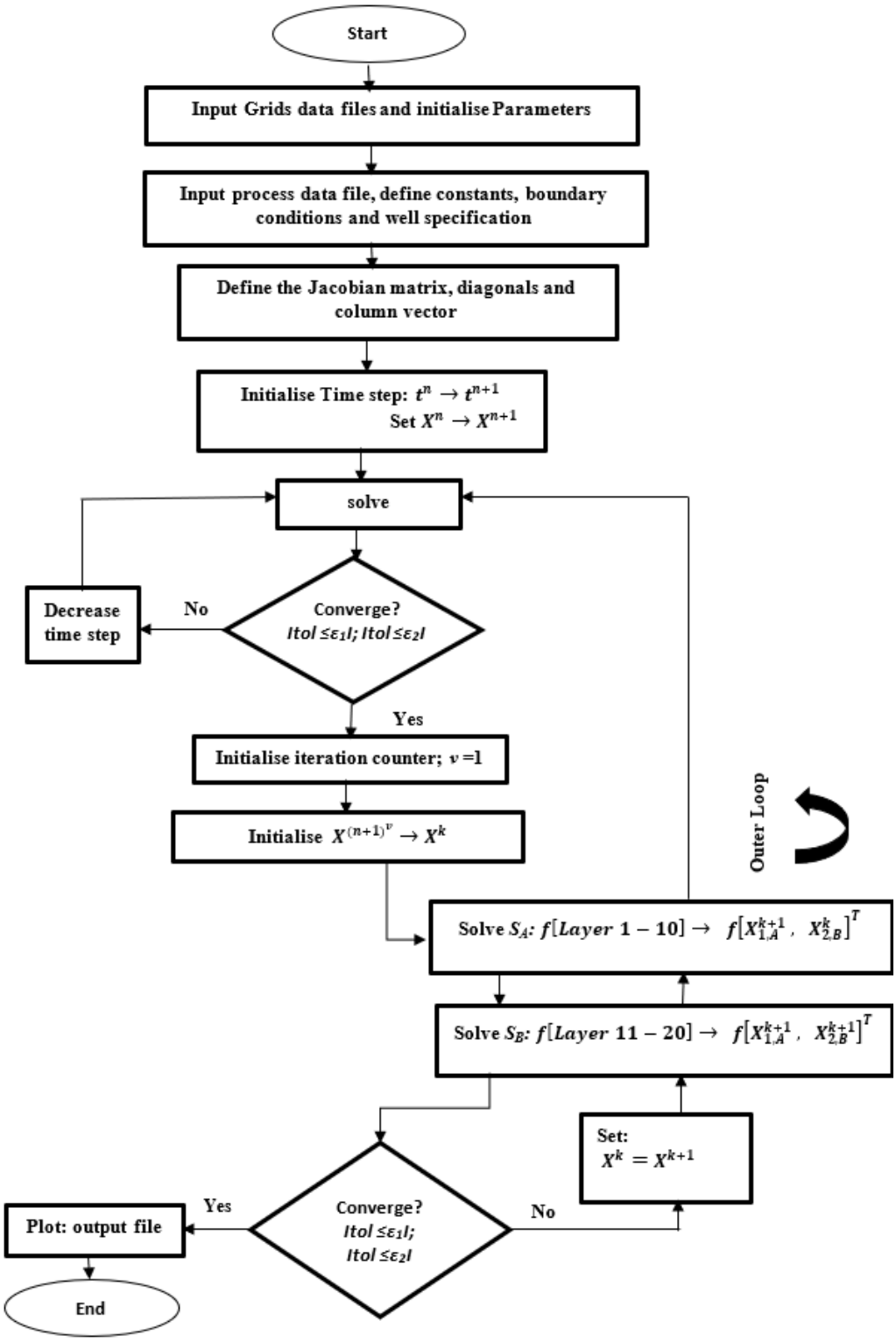

Figure 3. 5 Reservoir modelling flow charts

3.4.1 The properties of the synthetic reservoir model

A schematic of the physical test domain is shown in Figure 3. 4. The synthetic reservoir models are presented in Fig. 3.2 and Fig 3.5. The initialisation data is in table 3.1. Data selection was processes from multiple literature sources, benchmarked with Boswell et al. (2017).

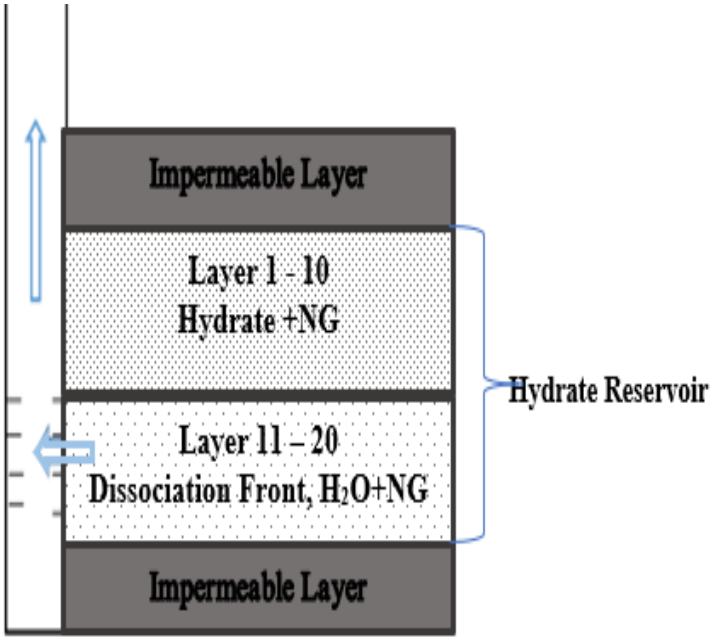

Figure 3. 6 Illustration of the Physical model of the hydrate reservoir test domain

Table 3. 1 Mesh and initialisation properties

Reservoir properties		**Fluid properties**	
Lx (ft)	5500	B_{gb} *(RB/STB)*	1.3
Ly (ft)	4500	B_{wb} *(RB/STB)*	1.0142
nx	11	C_w *(psi-1)*	$3.00x10^{-06}$
ny	9	C_g *(psi-1)*	$5.00Ex10^{-05}$
nz	1	*Cμ,g (psi-1)*	$4.00x10^{-06}$
Reservoir Thickness*(ft)*	100		
Permeability (*md*)	20	P_{ref} *(psi)*	14.7
Porosity	0.3	$P_{\mu,ref}$ *(psi)*	14.7
Pressure (*psi*)	3200	*BHP(psi)*	1000
Temperature (℃)	-8.25°*C*		
Well conditions			
Producer		**Wellbore Radius *(ft)***	
Gas rate = 1000SCF/day		0.25	

Table 3. 2 Phases and Saturation Properties

Properties	Values	Properties	Values
Gas saturation (Layer 1-10)	0.3	Molecular weight of Water (H_2O)	$18.015x10^{-3}$ *kg /gmole*
Water Saturation (Layer 1-10)	0.4	Molecular weight of Methane (CH_4)	$16.043x10^{-3}$ *kg /gmole*
Hydrate saturation (Layer 1-10)	0.3	Molecular weight of Hydrate (CH_4. nH_2O)	119.543×10^{-3} *kg /gmole*
Gas Saturation (Layer 11-20)	0.8	Molar Density (Water)	5501.5*gmole/m*^{3}
Water Saturation (Layer 11-20)	0.2	Molar Density (Hydrate)	919.7*kg/m*^{3}
Hydrate saturation (Layer 11-20)	0	Gas phase viscosity	3.8×10^{-3}*cp*
K (Layer 1-10) (*md)*	25		
k (Layer 11-20) (*md)*	100		

Table 3. 3 Phases and Saturation Properties

Parameter	Value
Reservoir Reference depth	1100m
Reference Pressure	101kPa
Reference Temperature	25^{o}C
Geothermal gradient	1^{o}F/(100ft)
Porosity	0.3
Permeability	20
Molecular weight of Water (H_2O)	18.015×10^{-3}kg/gmole
Molecular weight of Methane (CH_4)	16.043×10^{-3}kg/gmole
Molecular weight of Hydrate (CH_4. nH_2O)	119.543×10^{-3}kg/gmole
Molar Density (Water)	5501.5gmole/m^3
Molar Density (Hydrate)	919.7kg/m^3
Gas phase viscosity	3.8×10^{-3}cp
Thermal Conductivity (Reservoir)	1.5×10^5J/(m.day.C)
Thermal Conductivity (Water)	6×10^4J/(m.day.C)
Thermal Conductivity (Gas)	2.93×10^3J/(m.day.C)
Fluid Enthalpy	1.925×10^{-1}J/gmole
Pore Compressibility	5.0 x 10-10 Pa-1
Capillary Pressure α parameter	0.132 m-1
Capillary Pressure *n* parameter	2.823
Relative Permeability	0.6458
Hydraulic Conductivity	0.1 Darcy

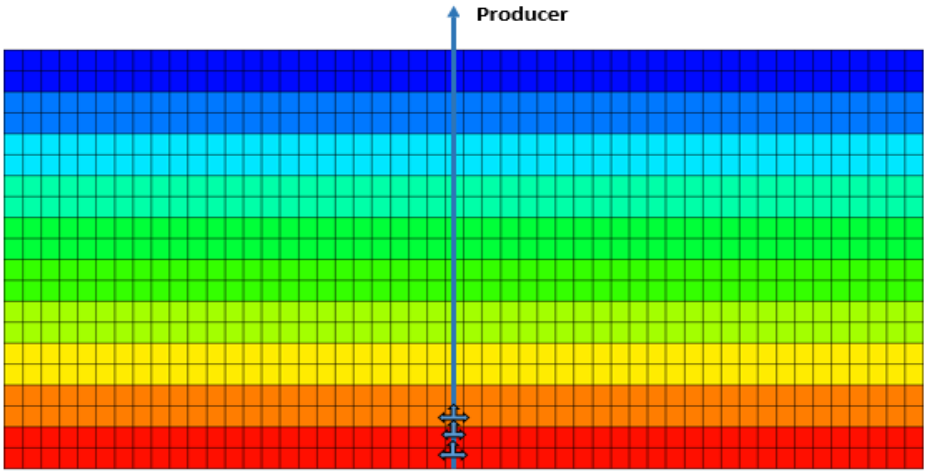

Figure 3. 7 Two-Dimensional Reservoir Model (CMG-STARS')

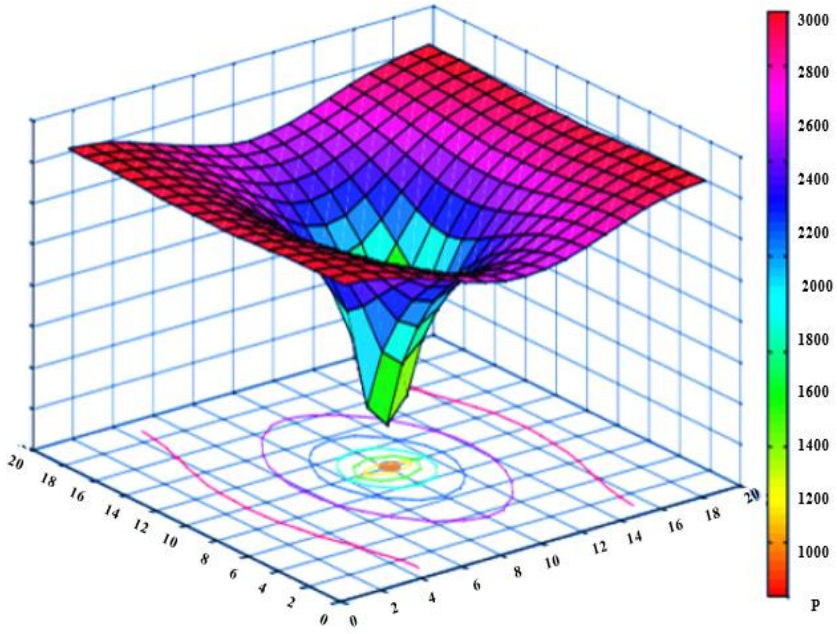

Figure 3. 8 Two-Dimensional Reservoir Model in Space (Thesis')

3.4.2 Verification and Validation of Model

Model verification and validation are used to establish the credibility in numerical models. While verification is used to establish that the model implementation meets the design requirements and base case solution description, validation is used to determine the performance and accuracy the model compared with respect to the physical system and in comparison, with previous work (ASME, 2006). Model verification procedure involves steps

described by Hillston (2003) and includes debugging, structured walk-through, continuity testing, degeneracy testing and consistency testing.

First a synthetic base case model (without accounting for diffusive flux and threshold pressure) was built and verified by comparing with CMG STARS simulation using default values from the CMG STARS manual for hydrate simulation and range of values of hydrate reservoir properties listed in table 3.1 and 3.2. The spatial distributions of Pressure and saturations of gas, water and hydrate over time for gas production at the constant production rate are evaluated in the base case with the CMG STARS and Thesis model. Figures 3.9 to 3.16 showed the results obtained for the distributions of pressure, gas saturation, water saturation and hydrate saturation both in space and time during production.

Results obtained with both models are in good agreement in all cases of the spatial profiles and time evolutions of the pressure, gas, water and hydrate saturations. Figures 3.9 and 3.10 showed that the pressure gradient and the minimum pressure of drive force around the wellbore increased over time and tend to remain steady to the end of the production. It can be inferred that equilibrium conditions started at 1,000 days as the pressure distribution in both cases reached the equilibrium at about 1000 days. It can be observed from figure 3.11 to 16 that the saturations of both gas and aqueous phases reached plateau at around 1,000 days also. The results from both models showed similar trajectories for all the parametric responses measured.

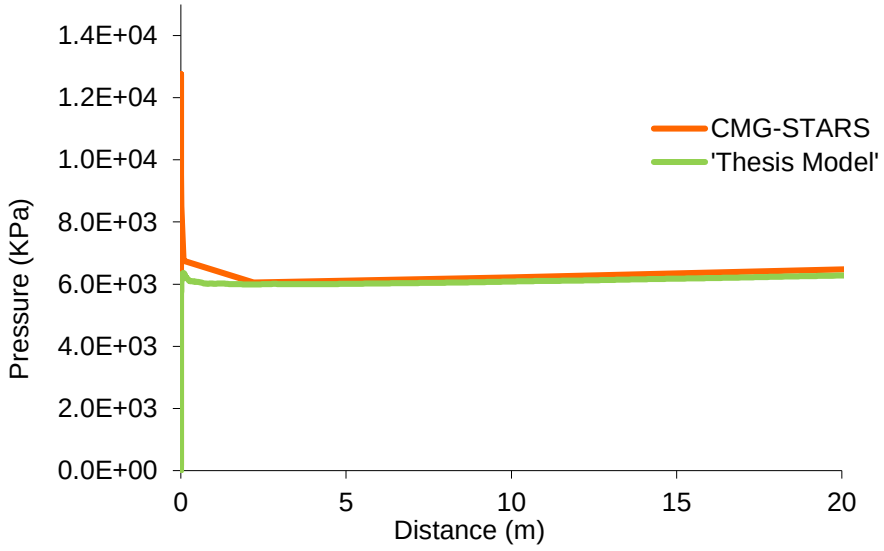

Figure 3. 9 Pressure Profile of Gas Hydrate Production

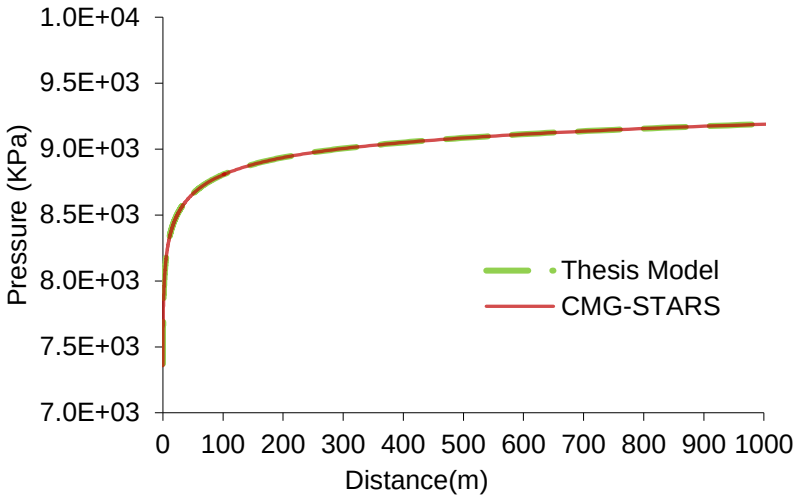

Figure 3. 10 Evolution of the Pressure distribution with Time

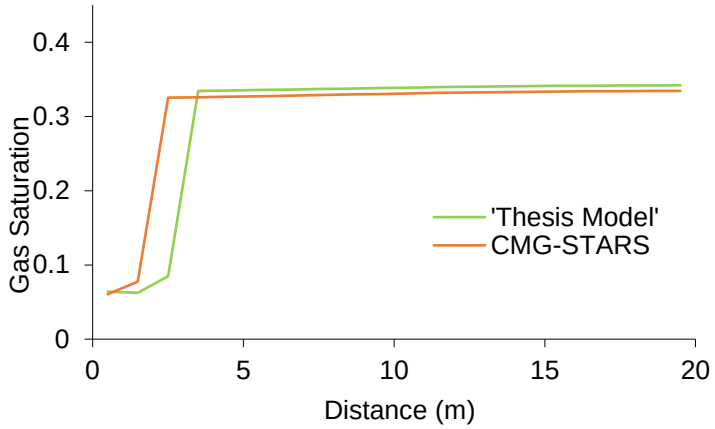

Figure 3. 11 Gas Saturation of Gas Hydrate Production

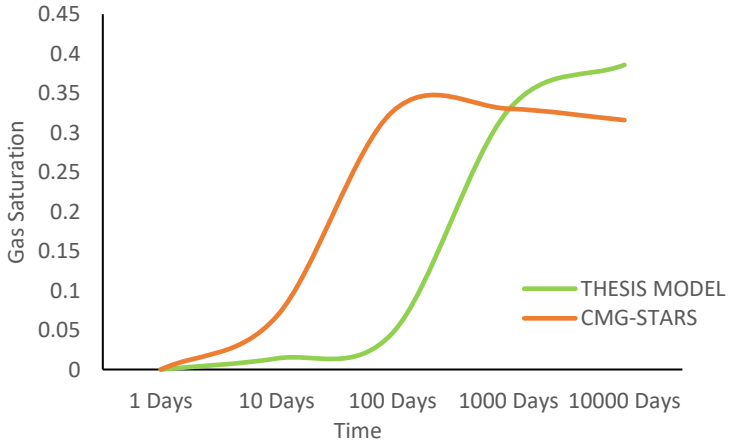

Figure 3. 12 Evolution of the Gas Saturation with time

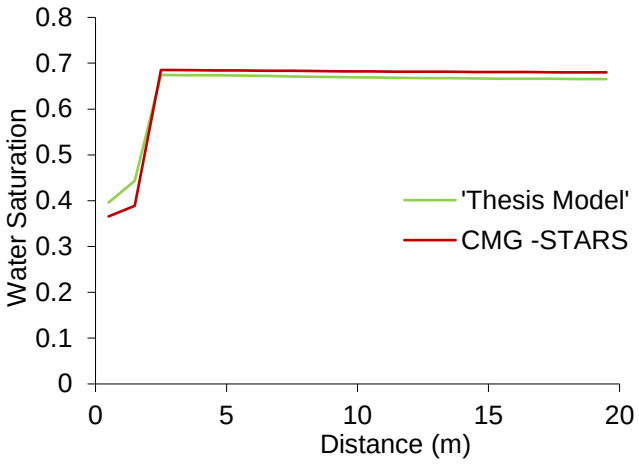

Figure 3. 13 Water Saturation of Gas Hydrate Production

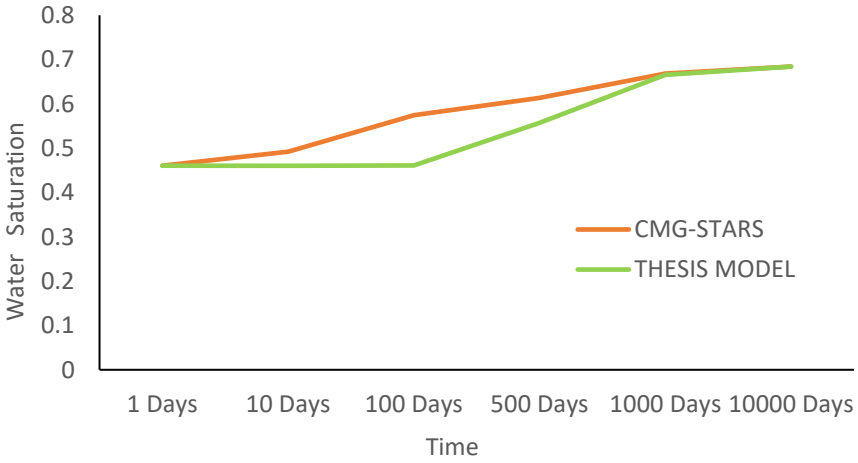

Figure 3. 14 Evolution of the Water Saturation with time

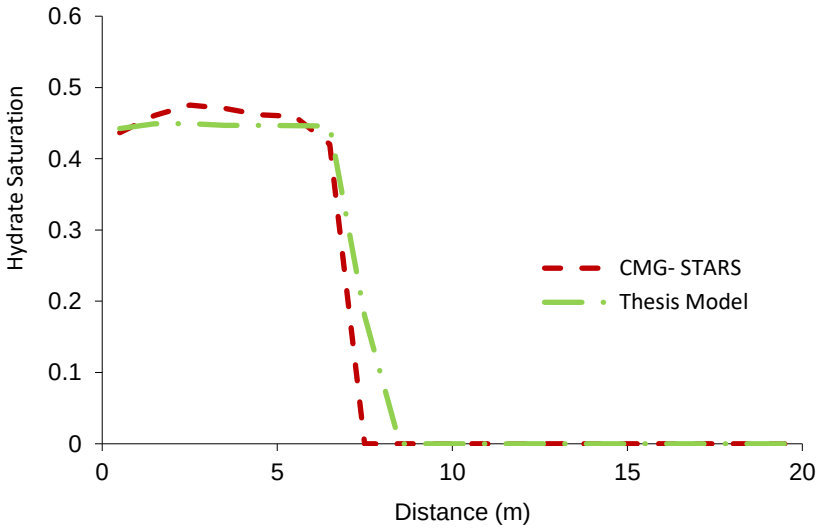

Figure 3. 15 Hydrate Saturation Profile of Gas Hydrate Production

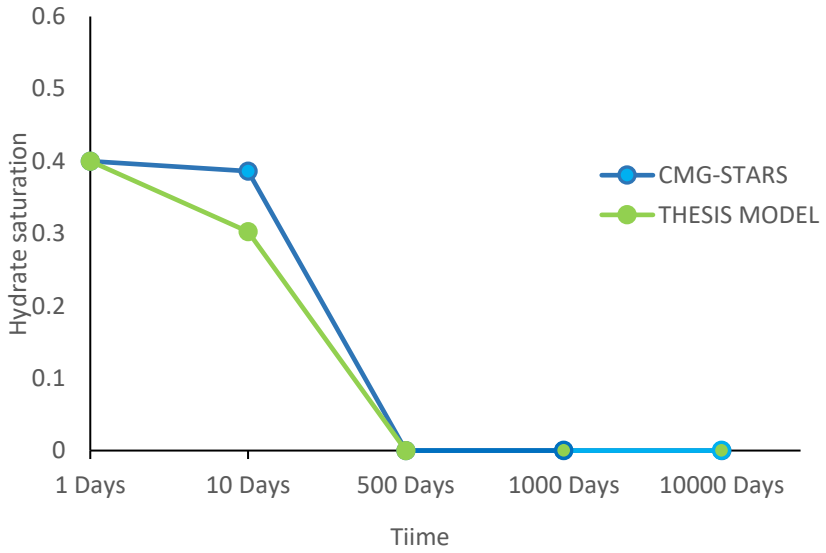

Figure 3. 16 Evolution of the Hydrate Saturation with Time

3.5 Temperature dependent model

To develop a forward model for profiling the temperature dynamics in the reservoir, the internal energy conservation is considered. The energy balance equation would entail combining the mass, momentum, and heat balance equations. The conservation of energy is based on first law of thermodynamics with respect to changes in the internal energy of a closed system. Applying material balance law and appropriate boundary conditions, the energy conservation equation for any phase, *p*, in the porous medium can be written as

$$\sum \frac{\partial}{\partial t}\rho_p \left(U_p + \frac{1}{2}v^2\right) + \sum \frac{\partial}{\partial z}\rho_p v \left(h_p + \frac{1}{2}v^2\right) = \dot{Q}_H + \dot{Q}_s \quad (3.101)$$

Change in internal energy and enthalpy are defined respectively as follows:

$$U_p = h_p - \frac{P}{\rho_p} \quad (3.102)$$

$$h_p = \rho_p c_p \Delta T \quad (3.103)$$

Where,

$$\dot{Q}_{\square} = \dot{Q}_T + \dot{q}_H$$

$$\dot{Q}_{\square} = \dot{Q}_{in} \pm \dot{Q}_{loss/gain(Thermal\ wellbore)}$$

$\dot{Q}_{\square} = \frac{\partial}{\partial x}\left(k_T \frac{\partial T}{\partial x}\right) = \nabla.\left(-K_{Tp}\nabla T\right)$

U_p = specific internal energy of phase, *p*; h_p -= enthalpy of the phase;

$\dot{Q}_H$ = heat exchange in the hydrate zone and interface between the reservoir and wellbore; $\dot{Q}_T$= conductive heat transfer;

$\dot{q}_H = \dot{q}_h + \dot{q}_w + \dot{q}_g$ = internal source/sink term of phase conserved per unit volume of formation;

$\dot{Q}_s$ = External heat source/sink term; $\dot{Q}_{in}$ is reservoir thermal stimulation source term; $\dot{Q}_{loss/gain(Thermal\ wellbore)}$ = heat loss or gain in the wellbore and completion.

$\dot{Q}_{\square} \rightarrow \dot{Q}_{loss/gain(Thermal\ wellbore)}$ when there is no heat added to the reservoir in terms of thermal stimulation

$\dot{Q}_{\square} \rightarrow 0$ for isothermal model consideration

For our hydrate system with three phases (hydrate, water and gas), the energy balance equation is the sum of the energy conservation of individual phases. The energy balance equation can be express as:

$$\frac{\partial}{\partial t}\left[\phi\rho_g S_g h_g + \phi\rho_w S_w h_w + \phi\rho_h S_h h_h + (1-\phi)\rho_r h_r\right]$$
$$+\frac{\partial}{\partial x}\left(k_T \frac{\partial T}{\partial x}\right) - \frac{\partial}{\partial x}\left(\rho_g v_g h_g + \rho_w h_w\right) = \dot{q}_H + \dot{Q}_T + \dot{Q}_s \qquad (3.104)$$

The effective thermal conductivity is

$$k_T = \phi S_g k_g + \phi S_w k_w + \phi S_h k_h + (1-\phi)k_r$$

In this chapter of the thesis, isothermal model is considered. It has been noted that hydrate dissociation is an endothermic process. Thus, a temperature model could be required for the depressurisation controlled production. Decomposition in the depressurization method is enabled by sensible heat of the hydrate sediment surroundings in relation to the hydrate itself; no external heat source. The heat transfer phenomenon would be treated in the next section of this chapter. The implications of the heat conservations on the application of boundary dominated flow regime would be assessed. The transient dominating flow regime model will be treated in the next chapter of this thesis.

3.5.1 Heat Transfer in Porous Media (Hydrate Zone)

By the first law of thermodynamics, the total energy of a system is conserved; that is, the energy stored in a volume is equal to the energy that enters the volume, minus the amount of energy that leaves the volume. The internal energy of a system is therefore conserved and is equal to the sensible component of the thermal energy which incorporate temperature. The conservation law is described by the heat equation which presents the transport of energy or heat flow as summation changes of energy by conduction and convection as follows:

$$\rho_p c_p \frac{\partial T}{\partial t} + \rho_p c_p v_p . \nabla T + \nabla . \left(-K_{Tp} \nabla T\right) = \dot{q}_H \quad (3.105)$$

Where $\dot{q}_{\square}$ can be represented by

$$\dot{q}_{\square} = -m_h \Delta H_D \quad (3.107)$$

ΔH_D is the heat change due to the hydrate decomposition (rate of heat supplied from the surroundings per unit time for hydrate dissociation) and can be obtained by regression (Selim and Sloan, 1989).

$$\Delta H_D = 446.12x103 - 132.638T \quad (3.108)$$

The solid rock energy balance equation is simplified by the assumptions that the thermal expansion for the solid phase is negligible and that solid phase has zero velocity. For most solids, thermal expansion is proportional to the temperature gradient, ∇T . Thus, for the solid phase energy balance equation is expressed as

$$(1-\phi)\rho_h c_h \frac{\partial T}{\partial t} - \nabla . (1-\phi) k_{T,h} \nabla T = 0 \quad (3.106)$$

Combining the energy equations of the individual phases, the general energy equation for the hydrate dissociation kinetics in the reservoir can giving as

$$\left[\rho_p c_p + (1-\phi)\rho_r c_r\right]\frac{\partial T}{\partial t} + \nabla T\left[\rho_g c_g v_g + \rho_w c_w v_w\right] - \nabla\left[\left(K_{Tp}\nabla T + (1-\phi)K_{Tr}\nabla T\right)\right] = -m_h \Delta H_D \quad (3.107)$$

The energy equation above comprises of convective and conduction transport. To account for energy change by molecular mechanisms (e.g. thermal diffusion and expansion) and energy change due to body forces, as had been identified in the literature for our hydrate system, the mechanisms for thermal signals should, Joule-Thomson (JT) effect and adiabatic expansion/compression, are incorporated. Thus, the energy equation for fluid phase (p = gas, water) is expressed as

$$\rho_p c_p \frac{\partial T}{\partial t} + \rho_p c_p v_p . \nabla T + K_T \nabla^2 T - \beta T \frac{\partial P}{\partial t} + \beta T v \nabla P - \tau_T \nabla v = 0 \qquad (3.109)$$

Where τ_T = thermal tortuosity; β = thermal expansion coefficient.

Considering the whole system, the pore space occupied by each phase would be defined by average porosity, ϕ , and the solid rock would occupy the remaining space, $1 - \phi$. Thus, multiply equations 2.33 and 2.34 by the pore space occupied and combining them will result to the volumetric average of the heat equation equations as follows:

$$\left[\phi\rho_p c_p + (1-\phi)\rho_h c_h\right]\frac{\partial T}{\partial t} - \phi\beta_p T\frac{\partial P}{\partial t} = -\phi\rho_p c_p v_p . \nabla T + \left[\phi K_{T,p} + (1-\phi)K_{T,h}\right]\nabla^2 T + \phi\beta_p T v_p \nabla P - \phi\tau_{T_p}\nabla v_p + \dot{q}_H \qquad (3.110)$$

Considering the expression of thermal diffusivity (Eq.3.84), thermal tortuosity, τ (Cooper, et al., 2013; Cooper, et al., 2013) and thermal expansion coefficients, β (Tipler and Gene, 2008),

$$\alpha = \frac{K_{T,p} + (1-\phi)K_{T,r}}{\rho_p c_p + (1-\phi)\rho_r c_r} \qquad (3.111a)$$

$$\beta = \frac{1}{V}\left(\frac{\partial \rho_p}{\partial T}\right)_P \qquad (3.111b)$$

$$\tau_T = V\frac{K_{T,bulk}}{K_{T,eff}} \qquad (3.111c)$$

and equating the actual velocity in the porous medium, v, to the average linear (intrinsic) velocity, u, (i.e. flow rate per unit cross sectional area), and defining the viscous dispersion term as Darcy flow, $\phi v = u$,

The final energy balance equation becomes

$$\left[\phi\rho_p c_{s,p} + (1-\phi)\rho_r c_r\right]\frac{\partial T}{\partial t} - \phi\beta_p T\frac{\partial P}{\partial t} = -\rho_p c_{p,p} u_p . \nabla T + \lambda_t \nabla^2 T + \mu_{JT,p}\rho_p c_p u_p \nabla P + \dot{q}_H \qquad (3.112)$$

By dividing Eq. 2.35 through by c_t (where $c_t = \phi\rho c_p + (1-\phi)\rho_r c_r$), Eq. 2.35 can be reduced to

$$\frac{\partial T}{\partial t} - \beta_p H_c \phi \frac{\partial P}{\partial t} + H_c u \nabla T - \alpha \nabla^2 T - \mu_{JT} H_c u \nabla P = \dot{q}_H / c_t \qquad (3.113)$$

Where:

$\mu_{JT} = \frac{(\beta_p T - 1)}{\rho_p c_p}$ Joule-Thomson effect

$H_{\square} = \frac{\rho_{\square} c_p}{c_t}$

$\alpha = \frac{\lambda_t}{c_t}$ Thermal diffusivity

$\lambda_t = \phi K_{T,p} + (1-\phi) K_{T,h}$

$c_t = \phi \rho_p c_p + (1-\phi)\rho_h c_h$

Since we have resolved the pressure solutions, the energy conservation is resolved and coupled to the pressure model. First the governing energy equation is expressed in terms of phases saturation to match the pressure model. Implicit finite difference discretisation scheme and Newtons method are also used to obtain the numerical solutions of the conservations of energy. The resulting temperature solution is then combined with the pressure model at level of Jacobian matrix implemented in MATLAB.

3.5.2 Governing equation

Applying the concept of control volume, we expand the energy balance equation (Eq. 2.38) for each phase – hydrate, water, and gas phase, and multiply the pore volume with the saturation of each phase to account for volume in place. The combine energy balance equation is:

$$\frac{\partial T}{\partial t} - \alpha_L H_{cp} \frac{\partial P}{\partial t} = -H_{cp} \nabla T + \alpha \nabla^2 T - \mu_{JT} H_{cp} \nabla P + \dot{q}_H / c_t \qquad (3.114)$$

Constitutive equations:

$\alpha_L = \frac{v_p \beta_p T}{\rho_p C_p}$ The thermal linear expansion

$v_{\square} = -\frac{k k_{\square\square}}{\mu_p} \nabla P_p \quad ; v_{\square} = -\left(1 + \frac{b}{P_{\square}}\right) \frac{k k_{rg}}{\mu_g} \nabla P_g$

$H_{\square\square} = \frac{S_{\square}}{c_t} \quad ; \alpha = \frac{\lambda_t}{c_t} \quad ; S_{\square} = \phi \sum_{p=h,w,g} (\rho_p S_p c_p)$

$$\lambda_t = \phi \sum_{p=h,w,g} \left(S_p k_{Tp}\right) + (1-\phi) K_{Tr}$$

$$c_t = \phi \sum_{p=h,w,g} \left(\rho_p S_p c_p\right) + (1-\phi)\rho_r c_r$$

The reservoir is subjected to no-flow boundary conditions so such that heat flow in and out of the boundary cells is zero.

$\dot{q}_{in}^n = 0$

$T_{(t=0)} = T_{i,(r \geq \Delta x)}$

$T_{(t>0)} = T_{i,(r \to \infty)}$

$T = T_{i,(r \geq 0)} = T_{i,(r \to \infty)}$

$\frac{\partial T}{\partial x}\Big|_{x=0}^{x=x,y,0} = 0$

3.5.3 Numerical Solution

The energy conservation equations were discretised in two-dimensional using the finite difference method. The backward difference scheme was used for the space discretisation with spatial upwind for the first order derivative and centred difference for the second order derivative. Time discretisation was by first order forward difference scheme.

The discretise form of the heat equation is as follows:

$$\frac{\partial T}{\partial t} = \frac{T_{i,j}^{n+1} - T_{i,j}^{n}}{\Delta t} \tag{3.115}$$

$$\nabla T = \frac{T_{i+1/2,j}^{n+1} - T_{i-1/2,,j}^{n+1}}{\Delta x} + \frac{T_{i,j+1/2}^{n+1} - T_{i,j-1/2}^{n+1}}{\Delta y} \tag{3.116a}$$

$$\nabla^2 T = \frac{T_{i+1,j}^{n+1} - 2T_{i,j}^{n+1} + T_{i-1,j}^{n+1}}{\Delta x^2} + \frac{T_{i,j+1}^{n+1} - 2T_{i,j}^{n+1} + T_{i,j-1}^{n+1}}{\Delta y^2} \tag{3.116b}$$

Thus, Eq. 2.38, is can be written as:

$$T_{i,j}^{n+1} - T_{i,j}^{n} = \Delta t \left(\frac{T_{i+1,j}^{n+1} - 2T_{i,j}^{n+1} + T_{i-1,j}^{n+1}}{\Delta x^2} + \frac{T_{i,j+1}^{n+1} - 2T_{i,j}^{n+1} + T_{i,j-1}^{n+1}}{\Delta y^2} + \frac{T_{i+1/2,j}^{n+1} - T_{i-1/2,,j}^{n+1}}{\Delta x} + \frac{T_{i,j+1/2}^{n+1} - T_{i,j-1/2}^{n+1}}{\Delta y} \right) (\alpha - H_{cp})^{n+1} + (\alpha_L - \mu_{JT})^{n+1} H_{cp}^{n+1} (P_{i,j}^{n+1} + S_{i,j}^{n+1}) + \left(\dot{q}_h / c_t \right)^{n+1} \tag{3.117}$$

Apply Newton Raphson method, the above equation can be written in Jacobian matrix form as follows:

$$J[f(T^n)]\delta\vec{T} = -R[f(T^n)] \tag{3.118}$$

$$f(T^{n+1}) = \left(\frac{T_{i+1,j}^{n+1} - 2T_{i,j}^{n+1} + T_{i-1,j}^{n+1}}{\Delta x^2} + \frac{T_{i,j+1}^{n+1} - 2T_{i,j}^{n+1} + T_{i,j-1}^{n+1}}{\Delta y^2} + \frac{T_{i+1/2,j}^{n+1} - T_{i-1/2,,j}^{n+1}}{\Delta x} + \frac{T_{i,j+1/2}^{n+1} - T_{i,j-1/2}^{n+1}}{\Delta y}\right)\left[(\alpha - H_{cp})^{n+1} + (\alpha_L - \mu_{JT})^{n+1} H_{cp}^{n+1}(P_{i,j}^{n+1} + S_{i,j}^{n+1}) + \left(\dot{q}_H / c_t\right)^{n+1}\right] - \frac{T_{i,j}^{n+1} + T_{i,j}^{n}}{\Delta t} \quad (3.119)$$

Thus, for the 2 -D system, the solution of the discretised continuity equation for temperature is modified to penta-diagonal system of matrix equations, as residual $R \rightarrow 0$, as follows:

$$b_S^{n+1^v}(\delta T)_{n-\Delta x} + c_W^{n+1^v}(\delta T)_{n-\Delta y} + d_n^{n+1^v}(\delta T)_n + e_E^{n+1^v}(\delta T)_{n+\Delta x} + f_N^{n+1^v}(\delta T)_{n+\Delta y} = R_{nT}^{n+1^{v+1}} \quad (3.120)$$

$b_S, c_W, e_E \; and \; f_N$ are the coefficients whose Jacobian are $f(T^{n+1})^{v+1}$ in the south, west, east and north directions respectively and d_n is the total diagonal element of the matrix.

Going forward, the solution of the discretised energy conservation equation is coupled to the pressure model at the level of the Jacobian matrix for the newton iteration. The process flow chart is as follows:

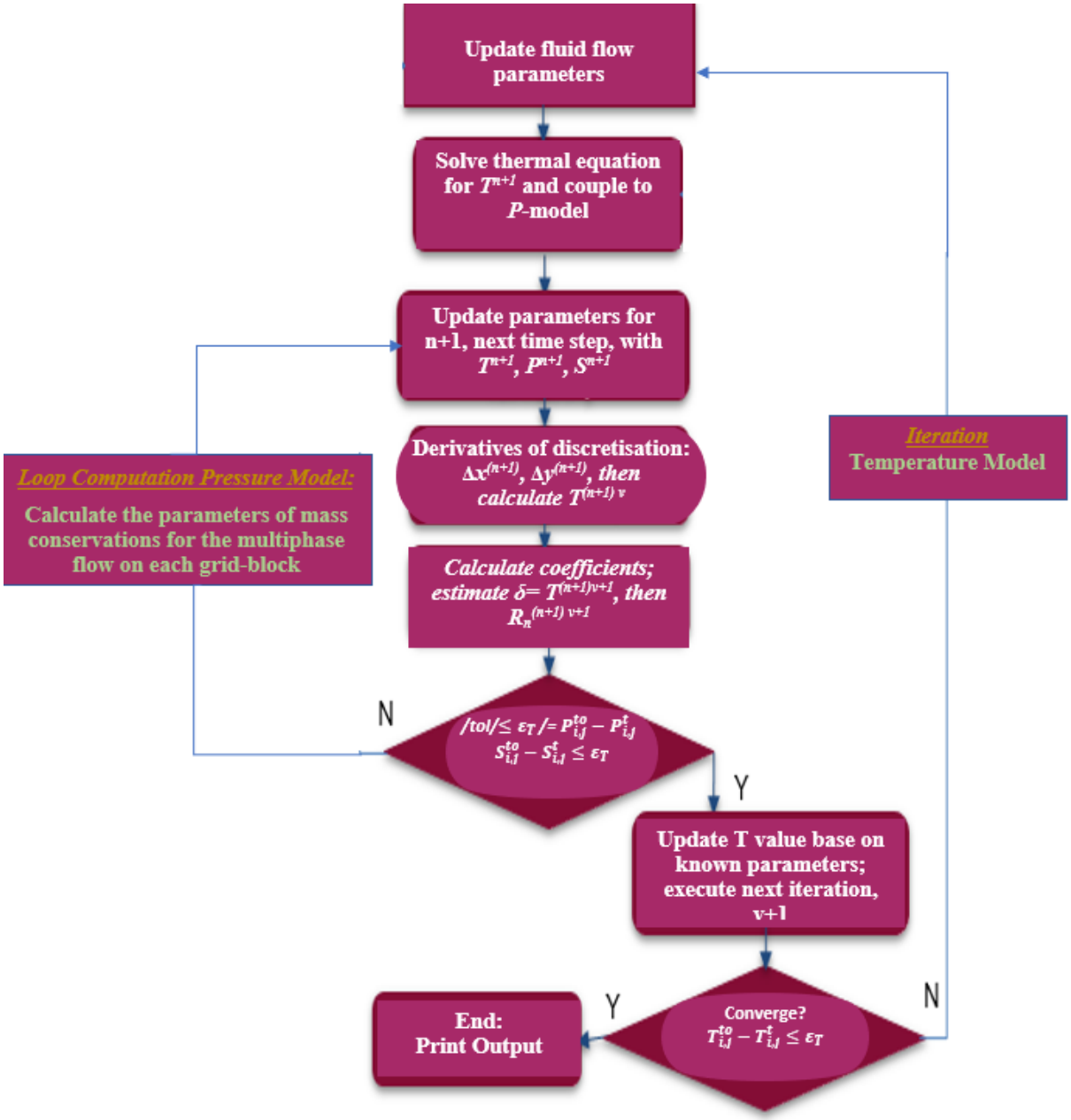

Figure 3. 17 Flow Chart of algorithm for mass and heat flow in the Reservoir

3.6 Validation with Experimental Data

The thesis model was further validated using the experimental data of Li et al, 2010a, to benchmark the simulation of the gas hydrate production. The experimental properties are based on the field data of the hydrate deposit at Site SH7 in Shenhu Area, South China Sea and is presented at table 3.4. An excellent match with Li et al experimental results is seen with both production rates and cumulative productions with gas and water simulation trends matching closely as can

be seen from figures 3.18 to 3.21 respectively. Although, the thesis model did not initially include injection scenario, we introduced a source term to account for the injection cases in the Li et al problem. We specify two injection and production rates respectively from the Li et al., 2010a reference values. The rates are processed from the reference values as follows

Table 3. 4 Experimental Data and Parameters used for Simulation (Li et al., 2010a, 2010b)

Parameters	**Values**	**Parameters**	**Values**
Depth to Seafloor	1108m	Intrinsic Permeability	0.075*mD*
Reservoir Top	1263m	Porosity ϕ	0.4
Reservoir Bottom	1285	Relative Permeability	$k_{rA} = (S_A^*)^n$; $k_{rA} = (S_A^*)n^G$
Overburden thickness	30 m		
Hydrate layer thickness	20m	Capillary pressure model	P_{co}^* Genchten et al., (1980)
Under-burden thickness	30 m		
Initial Pressure	13.8MPa	Irreducible water saturation, S_{irA}	0.30
Initial temperature	287.31(14.15^{o}C)	Irreducible gas saturation, S_{irG}	0.05
Initial hydrate saturation, S_h	0.44	λ	0.45
Initial aqueous saturation, S_A	0.56		
Gas composition	100% CH4		
N_h (Hydration number)	3.572		
Geothermal gradient	0.0433 K/m		
Formation density	2600 kg/m3		
Formation Thermal conductivity, dry	1.0 W·m^{-1}·K^{-1}	Fluid Thermal conductivity	43.35 W·m-1·K-1
Formation Thermal conductivity, wet	3.1 W·m^{-1}·K^{-1}	Wellbore diameter	0.3m

Case 1: Q_{inj} = (4.32 + 0.13) t/d/cycle× 1cycle = 4.45 t/d;

Q_{pro} = (5.18 + 0.17) t/d/cycle × 1 cycle = 5.35 t/d.

Case 2: Q_{inj} = (4.32 + 0.22) t/d/cycle× 1cycle = 4.54 t/d;

Q_{pro} = (5.18 + 0.35) t/d/cycle × 1 cycle = 5.53 t/d.

Figures 3.12 to 3.15 presents the thesis model results and the respective inset results from Li et al, 2010a. The results in each case are in close agreement and showed that the flow processes captured in the thesis model are necessary the flow mechanisms. The gas production behaviours are typical of the unconventional gas hydrate system.

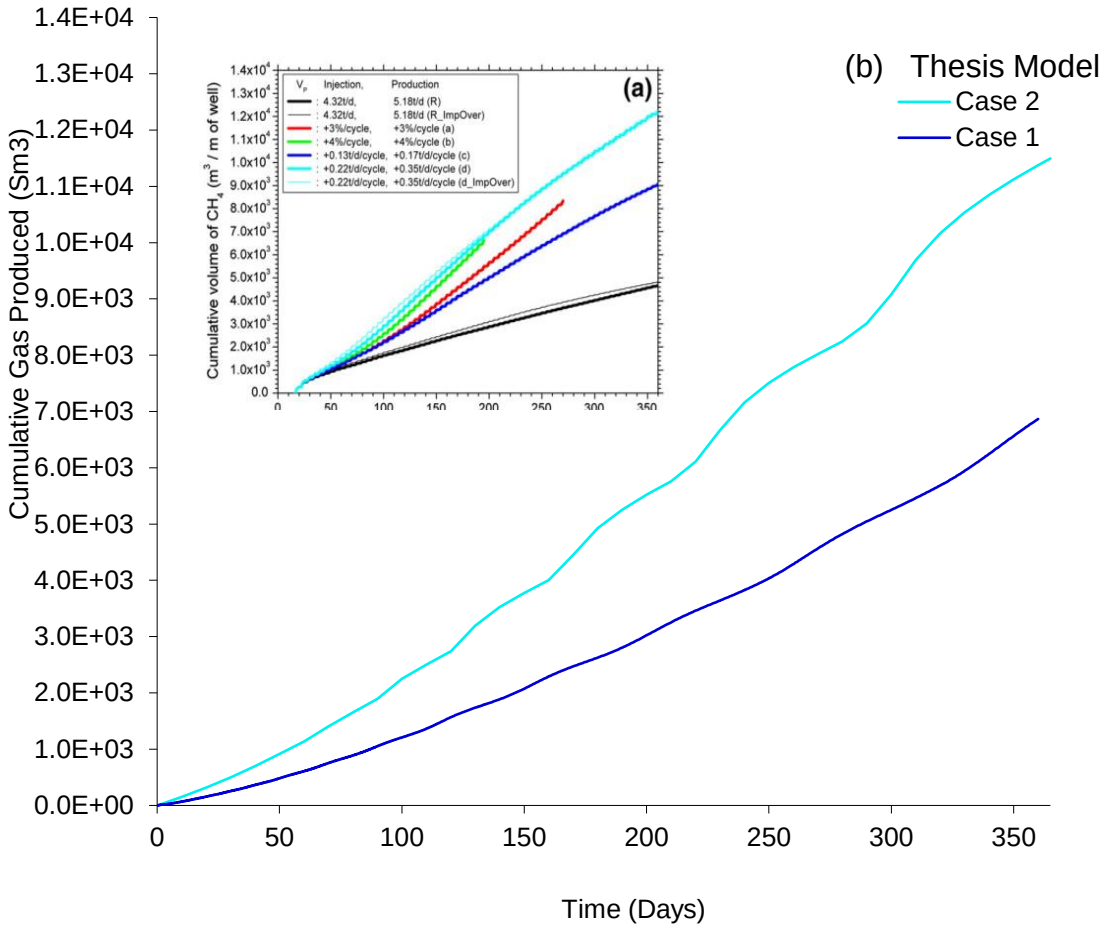

Figure 3. 18 Production Profile – Cumulative volume of gas produced with time

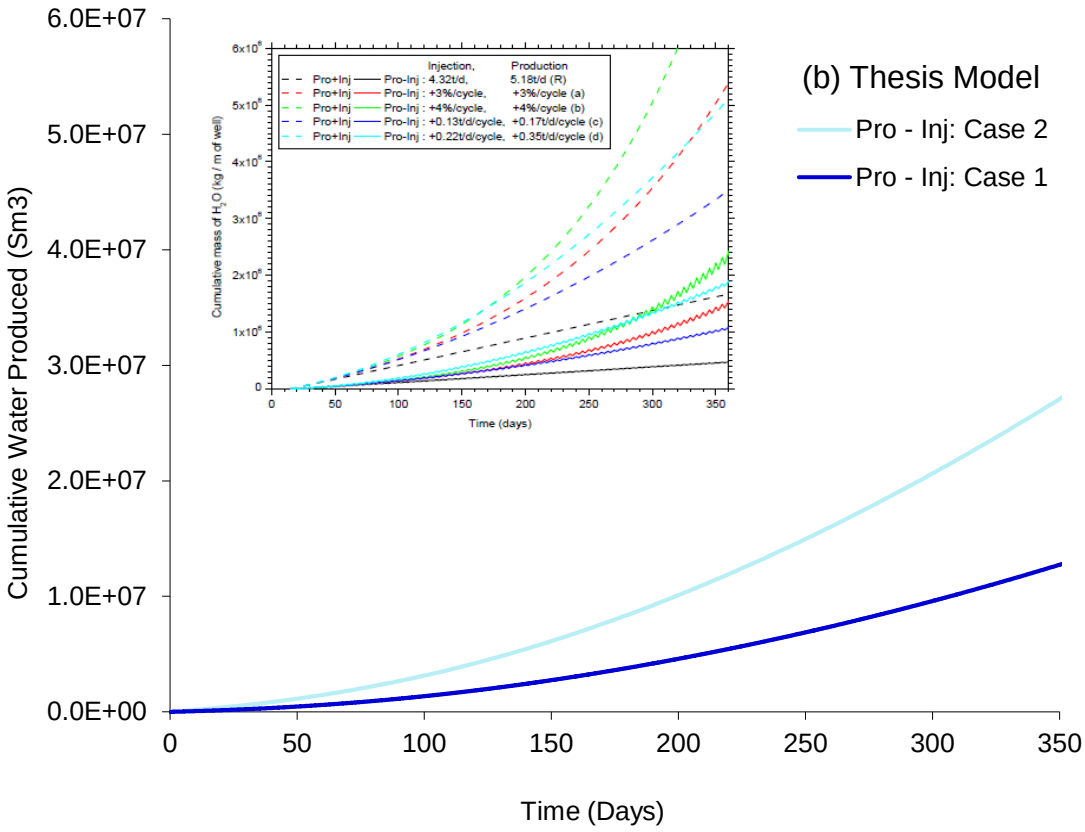

Figure 3. 19 Production Profile – Cumulative volume of water produced with time

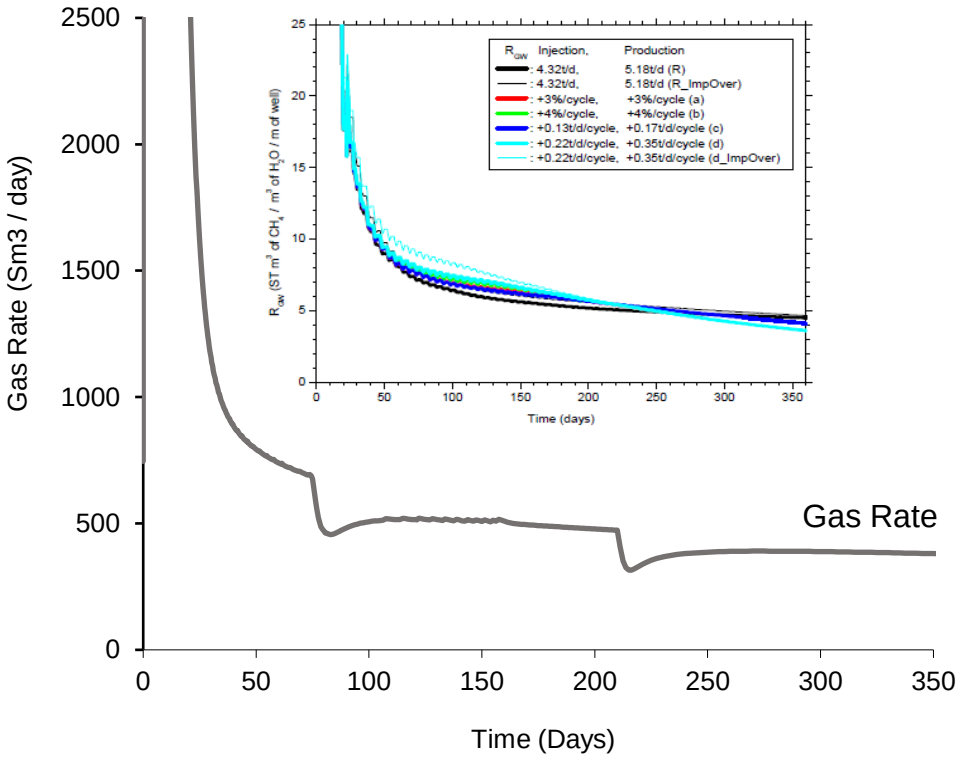

Figure 3. 20 Gas Production Rate Profile Validation

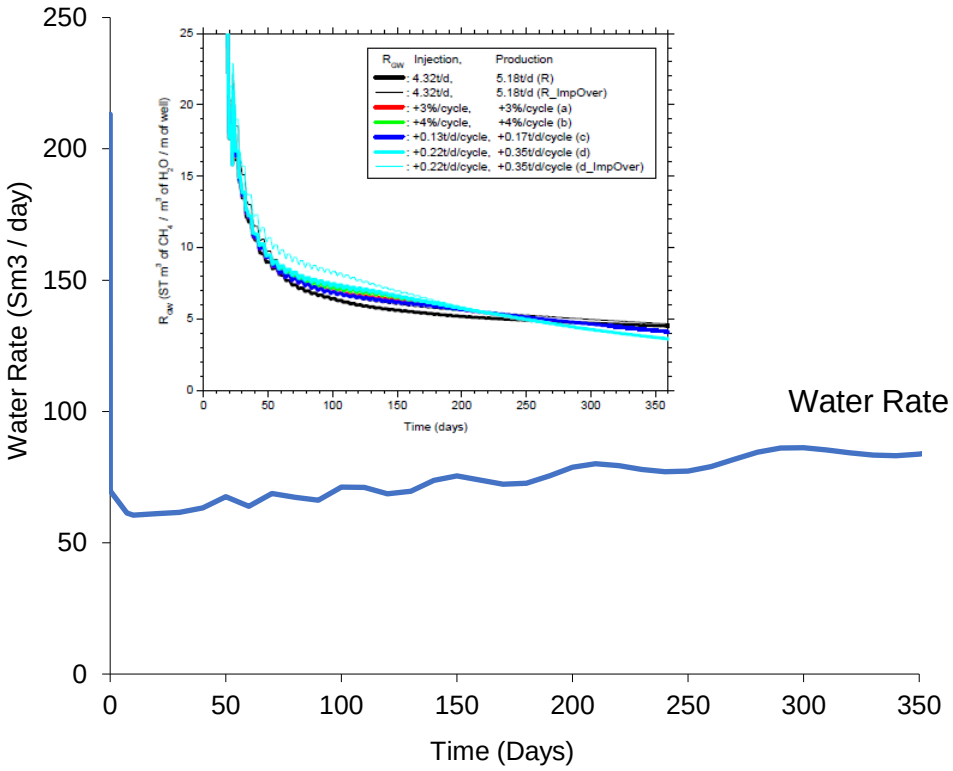

Figure 3. 21 Water Production Rate Profile Validation

3.7 Results and Discussion

Sensitivity analysis is used to investigate the influence of the incorporated variables on the gas recovery from the gas hydrate reservoir.

3.7.1 Effect of Diffusive Flux

Simulation studies to illustrate the effect of gas diffusivity flux was conducted by setting the diffusion coefficient to zero when initialising the model and results compared with original model that incorporated diffusion flux term. Effect on production rate and cumulative production was then studied. Figures 3.22 to 3.25 show the results of simulations with and without diffusion flux consideration. Simulations were run for 350 days and 1200 days to see the effects at later stage. It can be observed that with the inclusion of gas diffusion flux term, there is significant increase in production rate. Thus, not including diffusion flux term in gas hydrate production prediction model means production could be underestimated. From Figures

3.24 and 3.25 showed the effects of diffusion coefficient and tortuosity. Results is indicated that the increase of tortuosity results in decrease in the amount of cumulative gas production rate and at a short breakthrough time. In such instance, the influence of diffusion coefficient would not be felt at later stages of production as can inferred from figures 3.23. It can be observed that the effect is more at the early stage of production. Thus, the sharp decrease of the production rate can be attributed to high diffusion flux affected by low tortuosity.

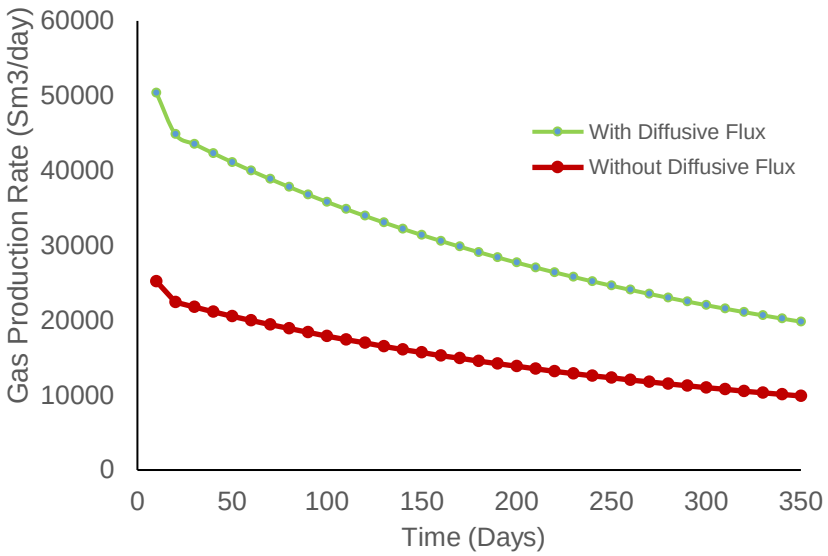

Figure 3. 22 Gas production rates with and without Diffusive Flux at 350 days

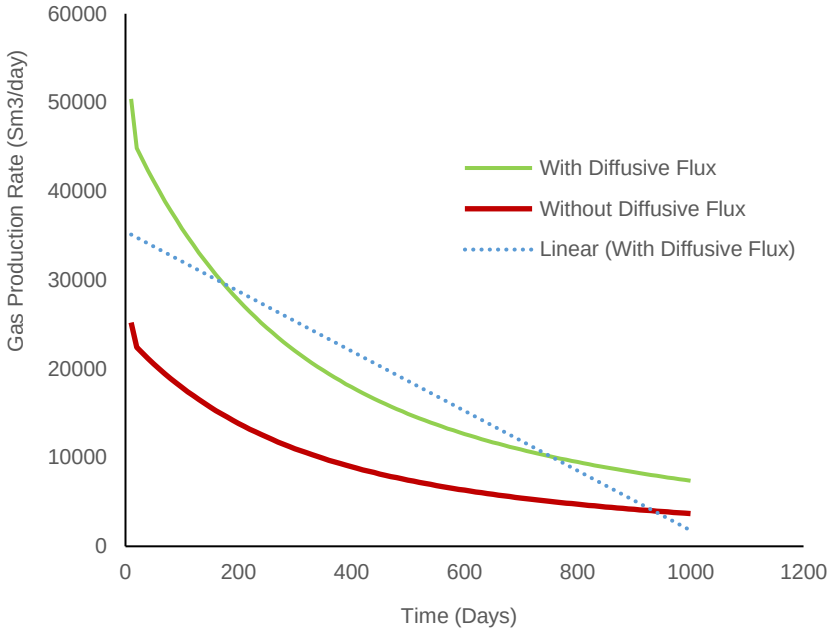

Figure 3. 23 Gas production rates with and without Diffusive Flux at 1200 days

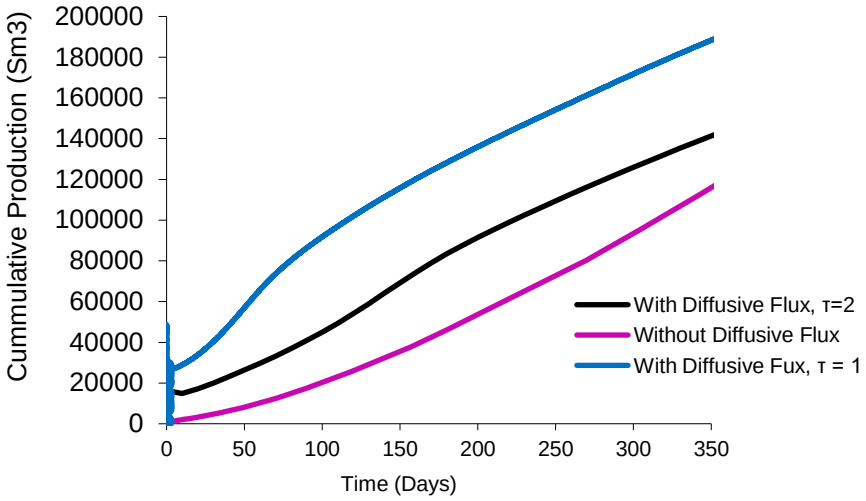

Figure 3. 24 Effect Tortuosity on Diffusive Flux

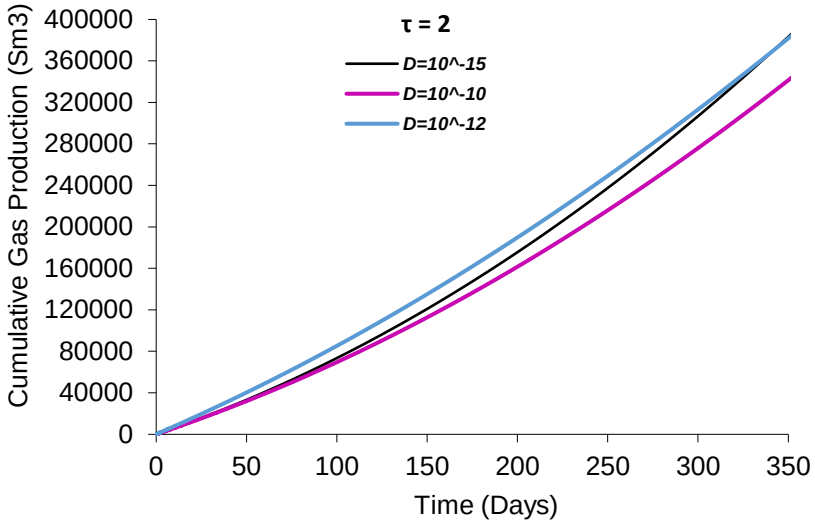

Figure 3. 25 Effect of Diffusion Coefficient on Diffusive Flux

3.7.2 Effect of Hydrate Reservoir Heterogeneity and the dynamic Permeability

In gas hydrate production, Heterogeneity has a great influence on permeability which is very important in determining the reservoir fluid flow and gas production performance. When hydrate dissociates during production, it creates dual continuum of dissociating and dissociated front. This presents the hydrate system with phenomena of dual porosity in addition to the heterogeneity of the depositional environment. These make permeability anisotropy a strong issue to be considered in this thesis. Figs. 3.26 showed that as the permeability anisotropy

increases, the faster the gas production rate reaches its maximum. The results from Figs. 3.27 and 3.28 also showed that as permeability anisotropy increased, the cumulative gas production increased. It can also be observed the figures that main contributing channel towards production is from the horizontal permeability. In figure 3.15, we compared first case: (k_x =50, k_y=10) verses (k_x =30, k_y=10), given anisotropic difference of 50/10 – 30/10 = 2; and in figure 4.15, we compare second case: (k_x =50, k_y=5) verses (k_x =30, k_y=10), given anisotropic difference of 50/5 – 30/10 = 7. Though in the second case the permeability anisotropy is higher, the cumulative production is in closer match. Cumulative

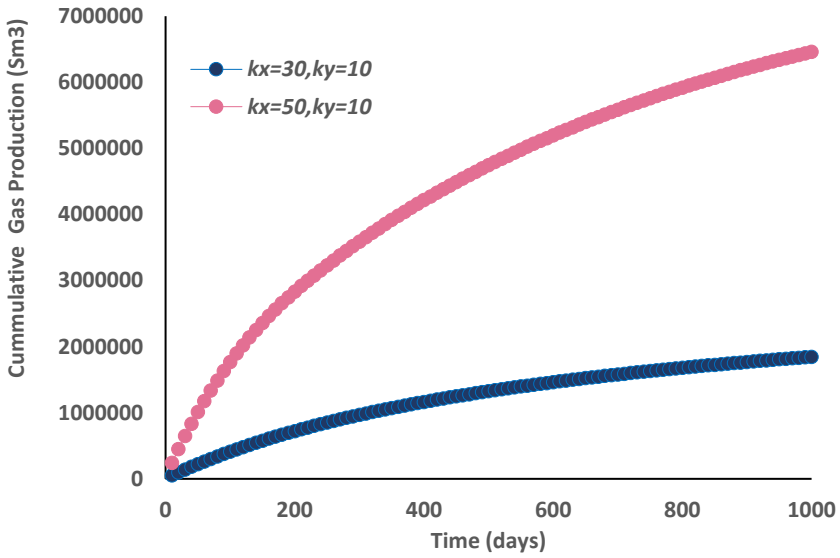

Figure 3. 26 Effect of permeability anisotropy on cumulative production (case 1)

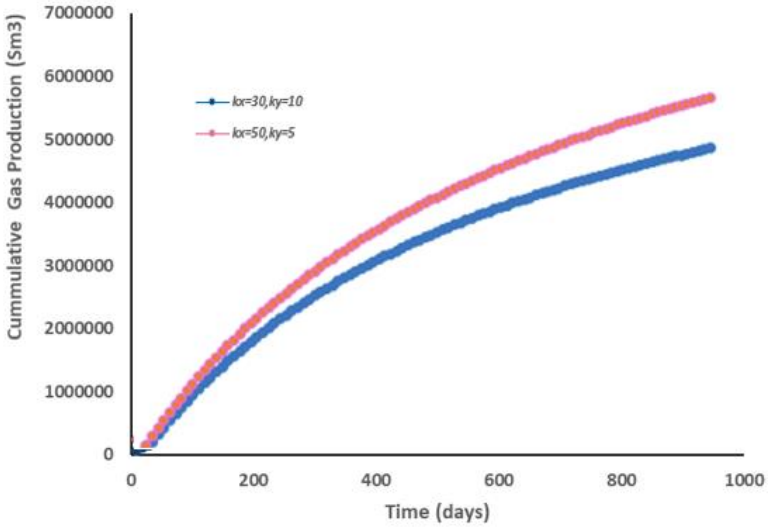

Figure 3. 27 Effect of permeability anisotropy on cumulative production (case 2)

3.7.3 Effect of Gas Slippage Factor

To study the effect of gas slippage on production from gas hydrate reservoirs, different gas slippage factors were considered for sensitivity analysis gas and water, total production rate and bottom-hole pressure. Gas slip effect controls gas flow behaviour in porous media especially tight gas reservoirs. It occurs because gas does not adhere to the pore walls, as liquids do, when flowing through porous medium even the very tight and low permeability reservoirs. Gas tends to find its way out of the porous medium or stay as free gas adsorbed on solid or dissolved in liquid. The slippage of gases causes low differential pore pressures pressure and lead to increase in gas flow rate in porous media. and pressure dependence of permeability. One important problem effecting gas relative permeabilities in porous media is the effect of gas slippage. For gas hydrate reservoirs, the gas permeability has a great influence on gas production and the slippage correction is essential for accurate water permeability calculation. Since this aspect of production from the tight gas hydrate reservoir (a good candidate for slippage effect) remain unknown, this study applied slippage correction factor to develop the thesis model. It was incorporated by non-Darcy flow consideration and with the factor *b* in the Klinkenberg equation. The slippage effect could be expressed as a measure of inertia force and the effect is evaluated by varying the inertia coefficient β in the equation. The equation is:

$$k_{eff} = k\left(1 + \frac{b}{P}\right)$$

$$b = \beta_1 \left(\frac{kk_r(S_g)}{\phi_g}\right)^{-\beta_2}$$

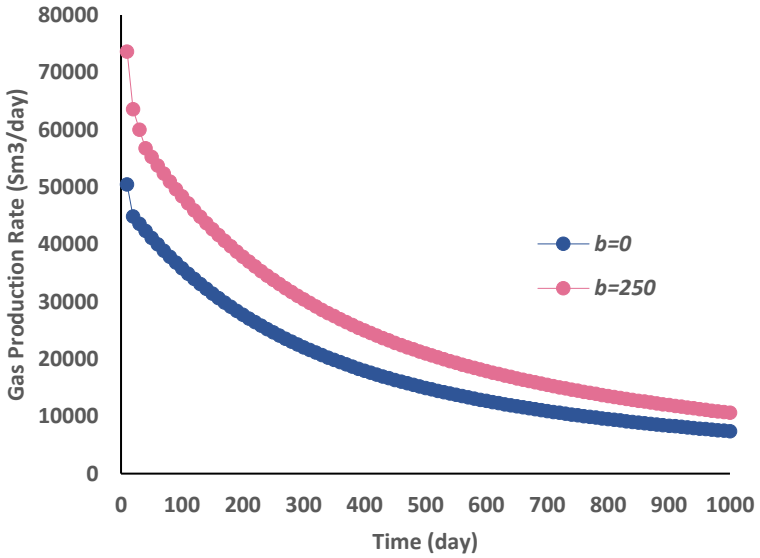

Figure 3. 28 Effect of gas slippage on gas production rate

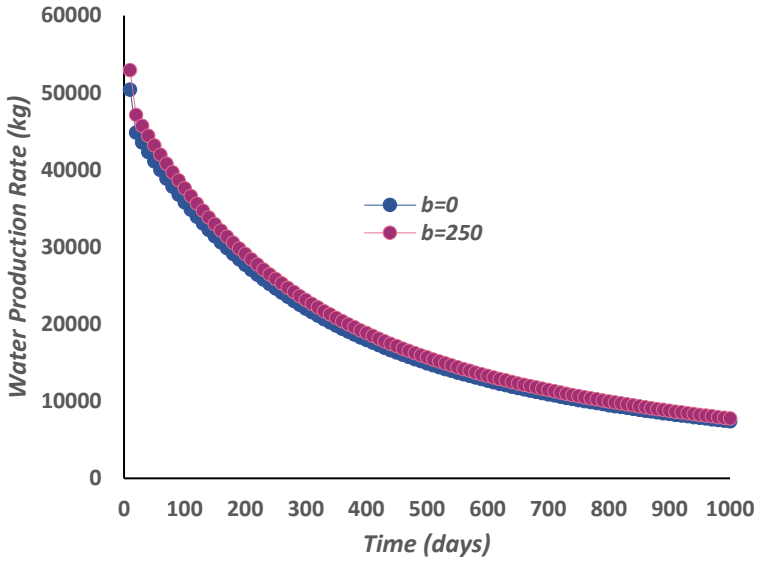

Figure 3. 29 Effect of gas slippage on water production rate

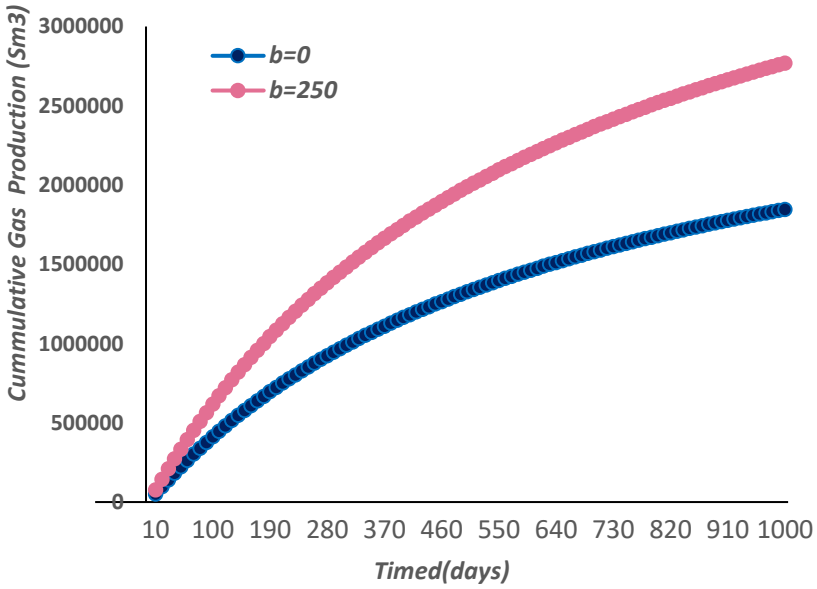

Figure 3. 30 Effect of gas slippage factor on cumulative gas production rate

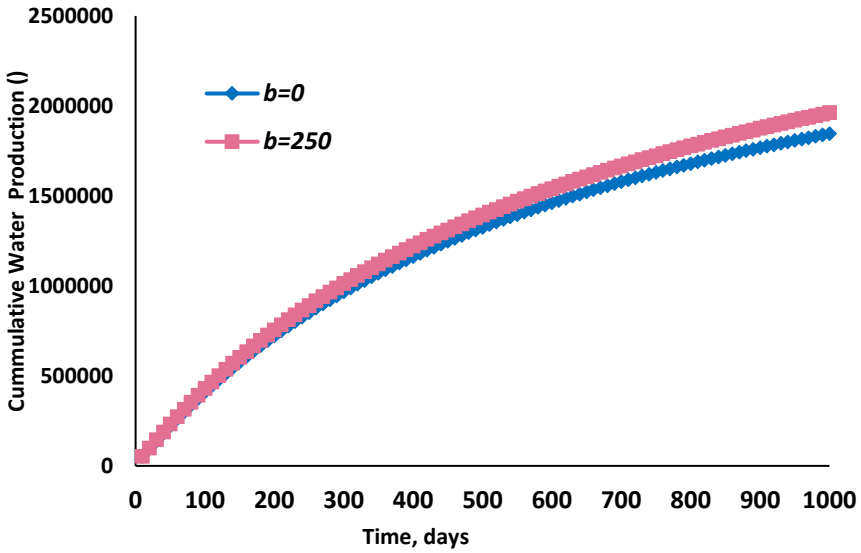

Figure 3. 31 Effect of slippage factor on cumulative water production rate

Figs. 3.28 to 3.31 showed that slippage factor leads affect gas production rate, and it has a significant effect on cumulative gas production from hydrate reservoir which is felt more during the early stage. However, inference can be drawn to the effect that at later stage, the effect gas slippage factor would be lowered with increasing gas production. The early stage's increase in gas production could be attributed to effect of diffusion flux also, initially discussed in the section above. And because permeability was measured as a function of water saturation, the effect of gas slippage weakens with increasing water production. The slippage effect has no or minimal influence on water production rate and cumulative water production. The results obtained are important in crucial consideration of numerical modelling of relative permeabilities and capillary pressure functions correlation to forces of inertia and slippage effect especially in gas hydrate fluid flow where solid phase of hydrate constitute in such an influence.

3.7.4 Effect of Threshold Pressure Gradient (TPG).

Figs. 3.32 presents the effect of threshold pressure on the pressure drive potentials for gas hydrate production. Because the conservative fluxes are gradient forces, the pressure drives are determined as gradient pressure. Examination of the pressure curves portrays that the pressure curve with higher TPG tends to be hyperbolic while very low TPG is more or less of harmonic function. The results are indicative that difficulty in fluid flow would occur in the reservoir with higher TPG. Thus, in a low-permeability reservoir, a more driving potential is required

for the fluid flow. More so, the effect of threshold pressure gradient on the pressure changes are negligible at early stage of production but resulted in sharp pressure drops in later stages. Results indicate that threshold pressure gradient causes a significant increase of the total pressure drop. Thus, production rate would be higher with low threshold pressure gradient. To this end, threshold pressure gradient could be made a limiting pressure in reservoir performance modelling of low permeability reservoirs to eliminate backpressure effects and effects of grain size. Thus, suggest would be to set the backpressure to a higher than the limit pressure. This is can help to stabilise permeability and improve production rate.

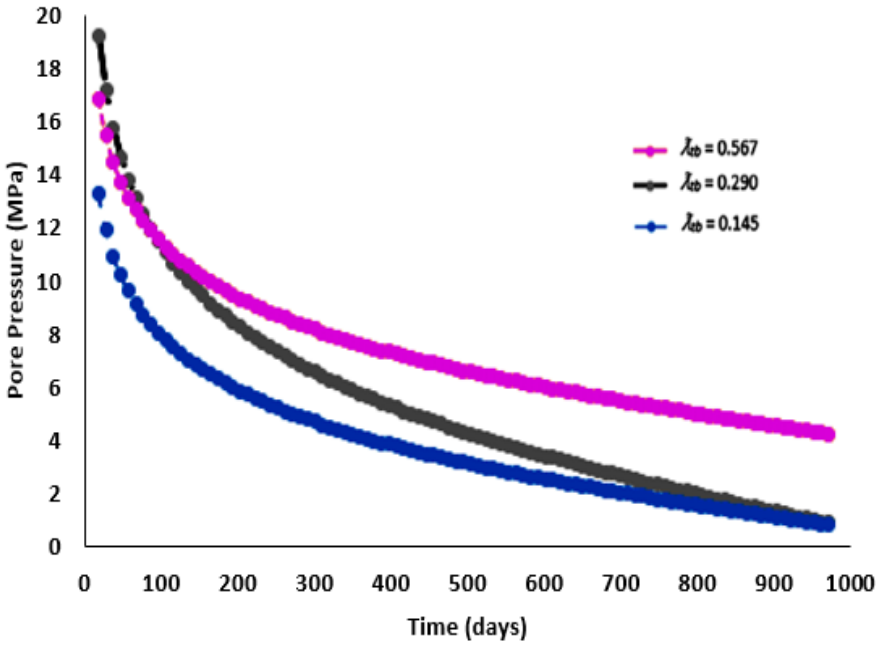

Figure 3. 32 Effect threshold pressure gradients on pressure draw down

3.7.5 Effect of the sensible heat of dissociation.

The sensible heat of dissociation is the latent tendency of hydrate to absorb heat from the surrounding and undergone kinetic decomposition. The thesis investigated the heat transfer and phase transition process in the porous media and found that the sensible heat increases with increase production rate. Thus, hydrate production occurs under isothermal condition because of the sensible heat of the dissociation/reservoir. Production by depressurization therefore leads to only a slight reduction in the temperature of the reservoir, which in turn only minimally changes the internal energy of formation. However, for a low production pressure, the temperature can fall below the hydrate formation temperature during dissociation, resulting in decreased sensible heat of dissociation. Consequently, the production of methane hydrate is

hampered to a point of abrupt cessation and to condition less than the hydrate formation temperature. The heat of dissociation is therefore relatively low at higher pressures. Fig. 3.33 also shows that in the depressurization process, heat transfer from the ambient environment will decrease the contribution of the sensible heat of the reservoir to hydrate dissociation, especially for porous media with high thermal conductivity. Thus, it is indicative that the sensible heat of dissociation is available from Joule-Thomson effect and adiabatic expansion above the gas hydrate formation temperature. Due to the self-reformation tendencies of hydrates, depressurization recovery method because reduced for hydrate dissociation above ice point. Thus, conduction heat from boundary contribute to the dissociation from boundary below ice point. The effect of convective heat can be said to be negligible at this early stage and may be prominent in the fluid flow. By appropriating the contributions, it can be said that feature like Joule-Thomson and adiabatic expansion supplies the sensible heat of hydrate dissociation at the initial stage while heat conduction impacts the hydrate dissociation at later stage.

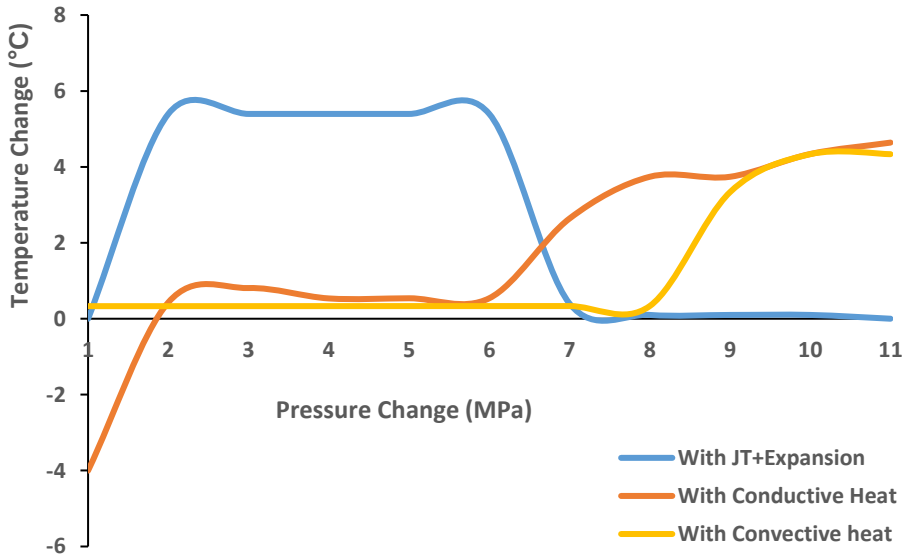

Figure 3. 33 The thermal expansion and Joule Thomson

3.7.6 Effect of thermal expansion and Joule Thomson coefficient

The effects of Joule-Thomson and adiabatic expansion can be clearly identified from the temperature profiles. Through identification of temperature responses induced by Joule-Thomson and adiabatic expansion effects, a substantial temperature changes in the hydrate zone is possible. This thesis identified the four major thermal properties contributing to the

temperature signals, which include conduction heat transfer, convection heat transfer, Joule-Thomson effect, and thermal expansion. Drawing from the inference from preceding section, sensitivity of the temperature response to the fluid properties at the hydrate zone at the reservoir level is temporal. The temperature profile is quasi-linear with typical conduction and convection heat transfer. This points to the thermal expansion and Joule effect, with the harmonic effect, as the prevailing driving potential on the averaging fluid flow along the porous media. Joule-Thomson (JT) effect and thermal expansion provide the energy balance driving the temperature difference and signal between major mechanism of heat transfer and dissociation temperature in the natural gas hydrate reservoir.

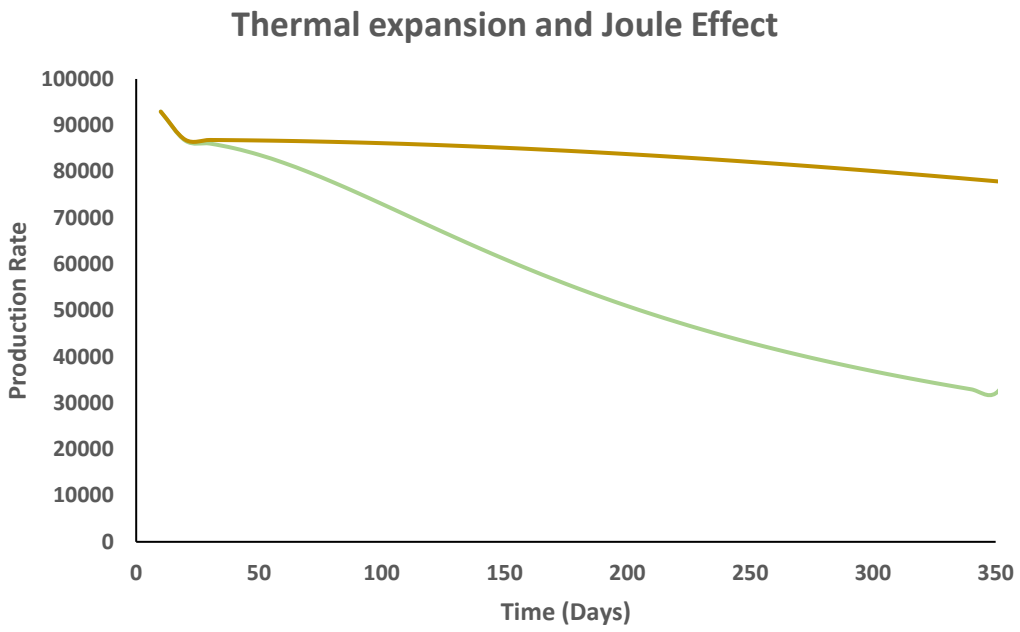

Figure 3. 34 The thermal expansion and Joule Thomson

3.8 Uncertainty Assessment and Conclusion

The comparative effect of various sensitivity parameters on the gas flow is demonstrated based on the Monte Carlo simulation. The Monte Carlo simulation (MCS) is a statistics-based analysis tool which, through generating probability and value relationships for sensitivity parameters, can indicate the range of uncertainties for a situation, necessary for better decision making. The essential elements of Monte Carlo forecasting comprise sampling and assigning distributions to input variables and the output random variable probability distributions scheme such as uniform, normal, triangular and logarithmic distributions. The Monte Carlo simulation

is implemented in MATLAB. To simulate the probability function based on the Monte Carlo method, the range of uncertainties associated with estimated amount of gas production were quantified to low case estimate, P10, best-case estimate, P50, and high case estimate, P90. In each run, the numerical solver executed several Monte Carlo trials, spanning 10 min of computational time to hours. The generated relationship between probability distribution and production rate is shown in figure 3.35. As can be seen from the bell cover indicated by the continuous orange line, the production rate decreased quickly with increased cumulative probability of value about 0.9, indicative of a high probability event. °C from the simulation results of the two distributions. The probability range of the effect of each sensitive parameter on the production rate was calculated, and are shown in Table 3.5. The higher the probability, the lower the production rate.

A sensitivity analysis ascertained those input factors most responsible for output variability. With this, one can identify which input parameter, having a significant influence on the wellbore's thermal behaviour, could be managed by changing the major influential parameter, coupling with the accurate numerical model. In this analysis, the input parameter was the random variables, while other parameters were treated as fixed inputs at the P50 value. To quantify the individual contribution of each parameter to the cumulative output variances, a random variable is chosen as input and other parameters held constant for P50 values. The degree of the effect of each parameter is shown in figure 3.36. The sensible heat of dissociation has the highest influence (22.3%). It can be concluded that fluid properties, permeability, diffusivity flux and slippage factors contribute eminently to the gas production. The complete wellbore thermal capacity, however, is not treated as the essential target during the even though it has a considerable effect on reducing wellbore temperature. Other parameters also showed significant percentage that cannot be neglected in managing and sustaining gas production from the hydrate reservoir.

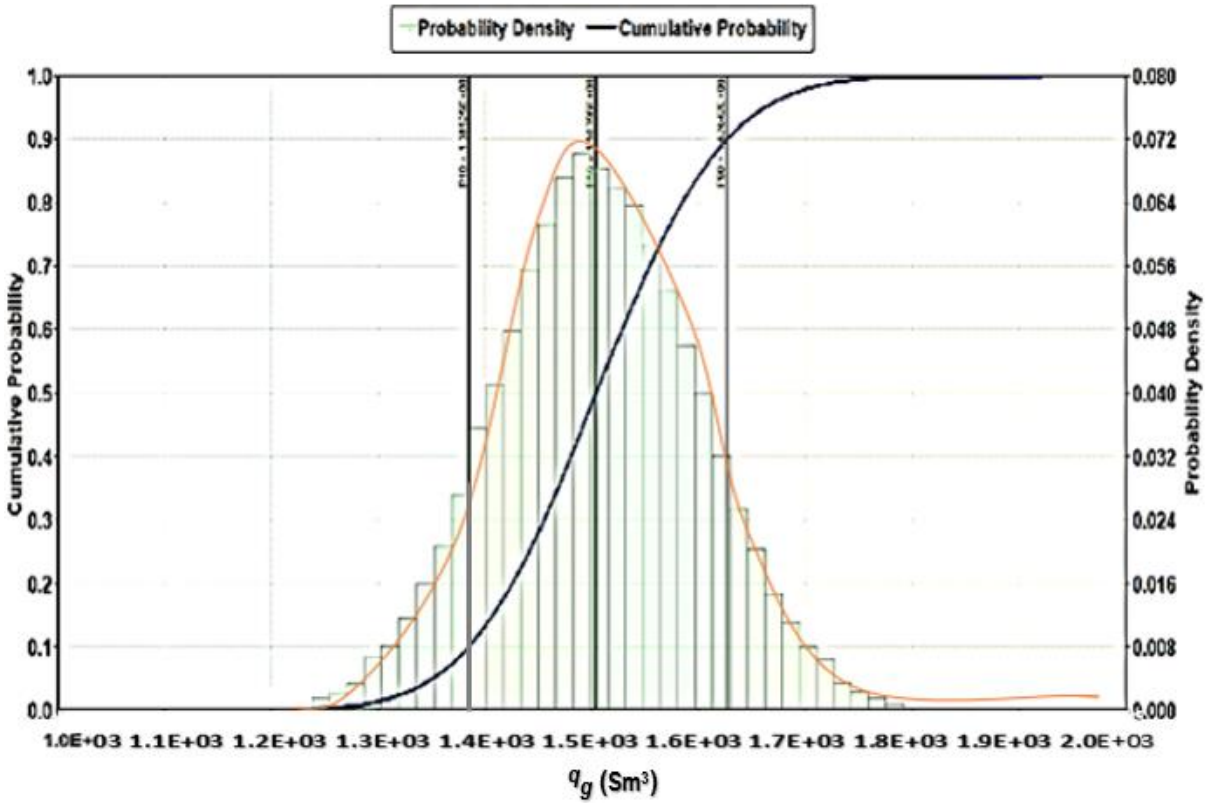

Figure 3. 35 Parameter Effects and Production Rate Probability

Table3.5 Data analysis of the sensitivity parameter (Effects on gas production rate)

Sensitivity Parameter	Probabilistic Simulation (Scf) P90	Probabilistic Simulation (Scf) P50	Probabilistic Simulation (Scf) P10	Deterministic Simulation (Scf)
Threshold Pressure	1.48E+3	1. 45E+3	1. 43E+3	1. 50E+3
Slippage factor	1.58E+3	1. 58E+3	1. 45E+3	1. 50+3
Diffusive flux	1.60E+3	1. 58E+3	1. 50E+3	1. 55E+3
Permeability	1.60E+3	1. 58E+3	1. 53E+3	1. 55E+3
Joule Thomson Effect	1.70E+3	1. 59E+3	1. 57E+3	1. 55E+3
Thermal Expansion	1.80E+3	1. 60E+3	1. 58E+3	1. 56E+3
Thermal Conductivity	1.83E+3	1. 62E+3	1. 58E+3	1. 56E+3
Sensible Heat of Dissociation	1.85E+3	1. 65E+3	1. 60E+3	1. 60E+3

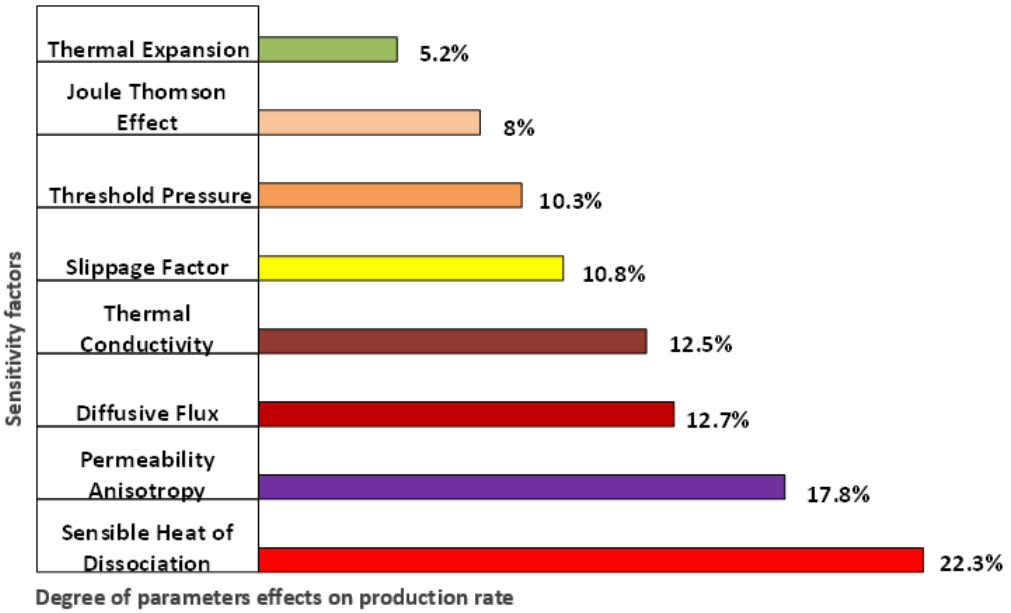

Figure 3. 36 Tornado plot of influence of variable parameters on gas production rate

CHAPTER 4

FULLY IMPLICIT FULLY COUPLED RESERVOIR AND WELLBORE FLUID FLOW FOR NATURAL GAS HYDRATE PRODUCTION

4.1 Fully Coupled Wellbore Model

In this chapter a fully implicit fully coupled reservoir -wellbore flow model is being developed for the more conservative representation of the continuum process in a seamless physical production system of gas hydrate, typical of figure 4.1 below.

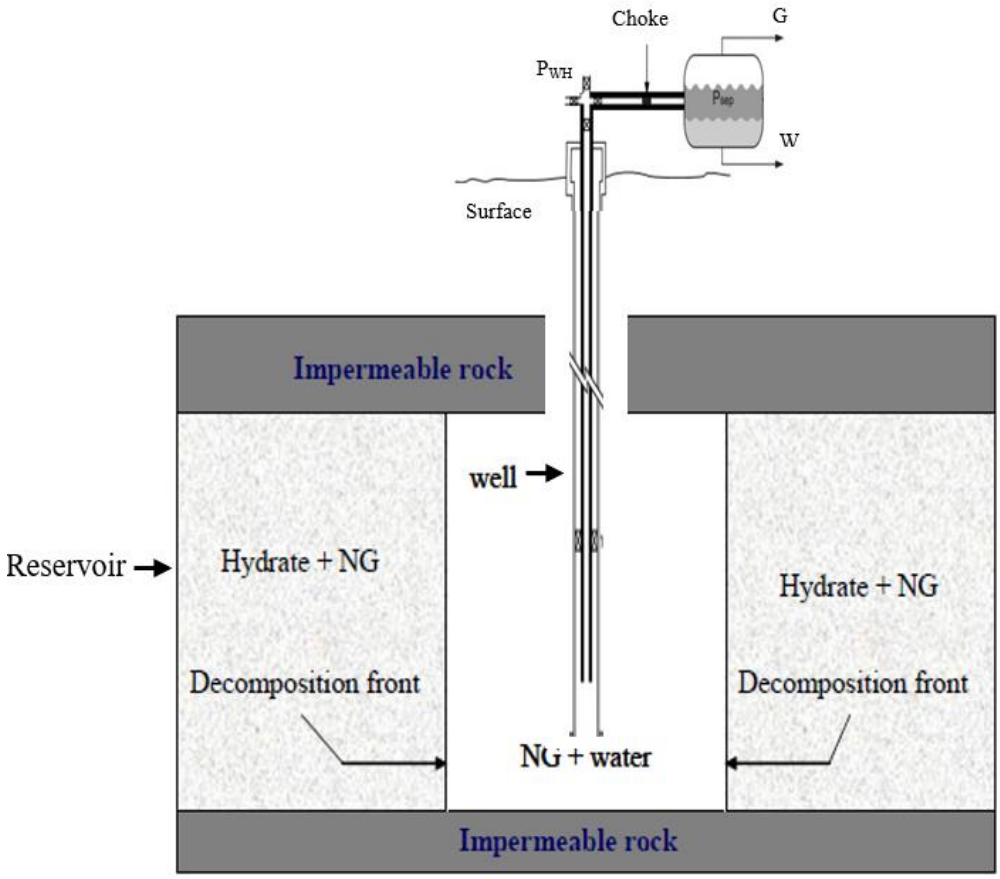

Figure 4. 1 Schematic of Model of Physical Gas Hydrate Production System.

This thesis has underscored that difficulties in gas hydrate production might be attributed, in part, to continued use of the decoupled approach in solving the flow and conservation problems for a system with complex convective mixing processes and near-wellbore complexity. A fully integrated and implicitly coupled reservoir and well continuity equations that capture the hydraulics communication and interface interactions has been advised (Pan, 2014; Ertekin, 2001;

Mazumba, 2016; Halliburton, 2017). In this method the reservoir and well system are treated as a continuum where relevant variables that affect fluid flow in the reservoir and wellbore are coupled implicitly by solving simultaneously the various continuity equations in both the reservoir and the well. The systems of equations would comprise the balance of the mass, momentum and energy conservations in both the reservoir and wellbore. The resulting stiff partial differential equations of the fluid flow in both the gas hydrate reservoir and wellbore in this thesis would be resolved and coupled by implementing an interface mass balance equation which act as a mortar between the two sub-models. The systems of equations would be coupled implicitly through an appropriate interface treatment that capture the reservoir and wellbore interaction and the transient flow problems such as phase segregation and reservoir-wellbore counter-current flow dynamics in the near-wellbore via computational fluid dynamic scheme.

The solutions of the coupled reservoir – wellbore flow model consists of solving the derived governing flow difference equations using fully implicit numerical approach and Newton-Raphson method implemented in MATLAB. The equations are discretised separately and then combined at the level of Jacobian matrix for simultaneous solutions of the objective functions. The corresponding solutions of the reservoir model have been derived in the previous chapter of the thesis. The coupled wellbore model would therefore be developed in this chapter and implicitly coupled to the reservoir model to further create the fully coupled reservoir -wellbore flow model for gas hydrate application. A model of a discretized fully coupled reservoir-wellbore system is illustrated below:

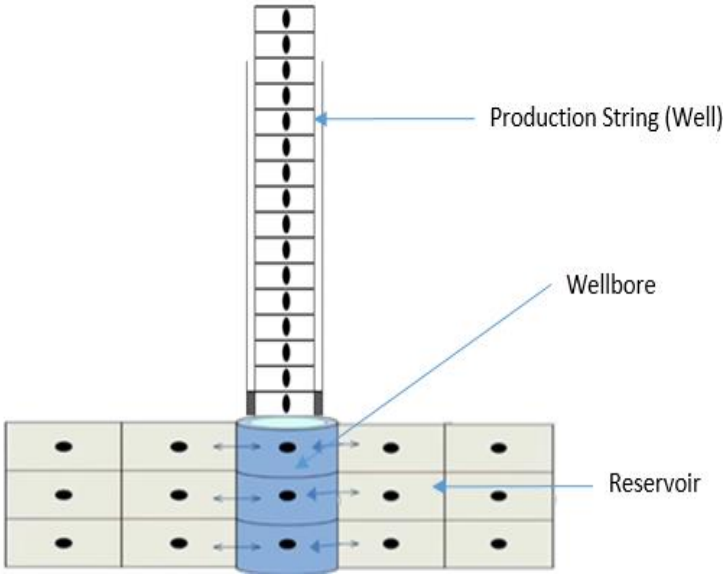

Figure 4. 2 Illustration of Discretised Fully Coupled Reservoir/Wellbore System

.

4.1.1 Mathematica Formulation

Fluid flow in wellbore, tubing or annulus, undergoes physical changes and components material balance by conservations of mass, momentum and energy like those in reservoir. This research seeks to account for the pressure losses – Friction, acceleration and kinetic energy losses associated with the fluid flow dynamics and velocity change along the well trajectory. Thus, the wellbore hydraulics would be incorporated into the reservoir model by considering the transient multiphase flow dynamics across a micro-section, Fig 4.3a, of a vertical well divided into several small *N*-segments (fig4.3b). According to the conservation law, the mass flow rate from the reservoir last grid-block into the first segment/node of the wellbore is equal to the summation of the reservoir mass flow rate, each wellbore/well segment acting as finite conductivity.

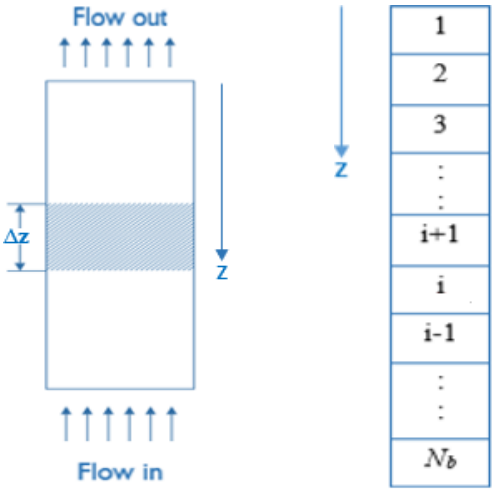

Figure 4. 3 Schematic of delineated and discretised Wellbore.

The mass, momentum and energy balance equations would be presented in the next section of this chapter. The governing equations are tailored to the gas hydrate system based on the following assumption.

4.1.2 Assumptions

The following assumptions are made in addition to the reservoir modeling assumptions in previous chapter:

- Reservoir and well are seamlessly connected.
- No hydrate in the well, only fluid (water and gas flow)
- The phases pressures are equal, there is no suction pressure between the two mobile phases.

- The fluid in the tubing has the same temperature as the tubing.
- The velocity of fluid in the tubing is equal to gas phase velocity that can sustain the liquid (water) phase flow.
- Mixture properties of velocity and density are used for momentum conservation in the tubing and were correlated to reservoirs using correction factors in the wellbore interface.
- Threshold pressure concept is applied to account for fluid flow velocity is equal to gas velocity at which the gas phase could be the waiting phase.

4.1.3 Mass Conservation Equation

Consider multiphase flow dynamics of gas hydrate fluid across a micro-section of the vertical wellbore at depth, *z*, measuring from the surface as shown in Fig 4.3a; the mass conservation through the delineated section, Δz, with cross-sectional area, A, of the wellbore can be expressed as:

Mass inflow – Mass outflow = Accumulation + Sink/Source term.

$$(m_z A)_t - (m_{z+\Delta z} A)_{\Delta t} = (\rho_{t+\Delta t} - \rho_t) A \Delta z + q_{m\Delta t} \quad (4.1)$$

As $\Delta z \rightarrow 0$ and $\Delta t \rightarrow 0$, Eq.4.1 becomes the mass flow rate and can be expressed as:

$$\frac{\partial m}{\partial t} = \frac{\partial (\rho v)}{\partial z} - q_m \quad (4.2)$$

Considering the volumetric flow rate, the mass balance equation can be written as,

$$\frac{\partial}{\partial t}(\rho) + \frac{\partial}{\partial z}(\rho v) = q_m \quad (4.3)$$

For multiphase flow, we multiply by saturation of each phase, p,

$$\sum \frac{\partial}{\partial t}(\rho_p S_p) + \sum \frac{\partial}{\partial x}(\rho_p S_p v_p) = \sum q_{mp} \quad (4.4)$$

4.1.4 Momentum Conservation Equation

Considering the transient flow phenomena in the gas hydrate production and the fact that gas phase is highly compressible and expands with high velocity, the transient momentum equation for unsteady state flow would be used to incorporate the wellbore hydraulics into the model. The rate of change of momentum equals the sum of forces imposed on the fluid which comprise gravitational, frictional and kinetic energy losses. Based on the conservation law, the momentum equation is described as:

$$\frac{d(\rho v)}{dt} + \frac{\rho v dv}{dz} = -\frac{dP}{dz} - \frac{f \rho v^2}{2d} - \rho g sin\theta \quad (4.5)$$

For multiphase flow, the equation becomes

$$\frac{\partial(\rho_m v_m)}{\partial t} + \frac{\partial(\rho_m v_m^2)}{\partial z} = -\frac{\partial P}{\partial z} - \frac{f_m \rho_m v^2 m}{2d} - \rho_m g \sin\theta \quad (4.6)$$

The 2-phase friction factor is calculated from correlations that approximate the data on Moody chart to the Reynolds number for mixture properties or Colebrook expression (Paul et al, 2010).

For laminar flow regimes, where Re < 2100;

$$f_m = \frac{64}{Re} \quad (4.7)$$

For flows beyond the laminar regime, Re > 2100, Colebrook expression can be used.

Colebrook expression for smooth pipe for turbulent regimes is considered for the hydrate system to achieve minimum head loss. The friction factor is expressed as:

$$\frac{1}{\sqrt{f_c}} = \left[1.74 - 2\log\left(\frac{2\varepsilon}{D} + \frac{18.7}{Re\sqrt{f_{est}}}\right)\right]^{-2} \quad (4.8)$$

ε is the pipe roughness.

f_c *and* f_{est} are calculated and estimated values of the friction factor

Initial $f_{est}$to start iteration is obtained from the friction factor expression for smooth pipes in turbulent regimes (Chukwudozie, 2013).

$$f_{est} = 0.0056 + 0.5Re^{-0.32} \quad (4.9)$$

4.1.5 Energy Conservation Equation

A complete account of the flow system would entail descriptions and solutions of the mass and heat transport processes. This becomes very pertinent as gas hydrate production involves endothermic reaction, dissociation, and requires strong thermodynamic flow processes. The heat continuity equation is coupled with mass flow equation by to obtain the whole energy balance equation. In previous chapter, we considered an isothermal case in respect of boundary dominated flow regime, and assumed no external heat source. In this chapter, the non - isothermal transient flow regime model is applied. Consideration is given to the heat flux (heat exchange) between the reservoir and wellbore. Sources and sink are considered and properly treated. An important step is the calculation of the heat loss, evaluation of the temperature at the reservoir/wellbore interface and cement/tubing interface. Formulation for heat loss calculation is given by Willhite (1989) as follows:

$$Q_{\square\square\square\square} = AU_{hc}(T_f - T_s) \quad (4.10)$$

Where,

$U_{hc} = \frac{\dot{q}}{\Delta T}$ = the overall heat transfer coefficient; A= surface area where the heat transfer takes place; T_f = Inside tubing/fluid temperature, T_s = formation temperature or solid surface temperature, $\dot{q}$ = heat flux; ΔT = difference in temperature between the solid surface and surrounding fluid area

From the derived energy balance equation, the transient model of the energy conservation in the hydrate system can be presented by the transient heat continuity equations as follows:

For the hydrate reservoir:

$$\left[\phi\rho_{\square}c_p + (1-\phi)\rho_r c_r\right]\frac{\partial T}{\partial t} - \phi\beta_p T\frac{\partial P}{\partial t} = \rho_p c_p u_p.\nabla T - \lambda_t\nabla^2 T - \mu_{JT,p}\rho_p c_p u_p\nabla P + \dot{q}_p + Q_{\square} - AU_{hc}\left(T_e - T_{sf}\right) \quad (4.11)$$

For the wellbore fluid flow:

The final wellbore fluid continuity equation can be expressed

$$\left[\frac{\square}{\partial t}\left(U + \frac{v_{\square}^2}{2}\right)\rho_m\right] + \frac{\partial}{\partial x}\left[\left(h + \frac{v_g^2}{2}\right)\rho_m v_m\right] = -v\frac{\partial v}{\partial t} - \rho v^2\frac{\partial v}{\partial z} + \rho v_m g sin\theta - 2\pi r_{to}U_{hct}\left(T_f - T_{\square\square}\right) \quad (4.12)$$

The heat source is treated as the viscous thermal flux from mechanical effect and is given as

$$Q_{\square} = \rho v\frac{\partial v}{\partial t} - \rho v^2\frac{\partial v}{\partial z} - \rho v g sin\theta \quad (4.13)$$

Combining Eqs 4.12 and 4.13 and substituting the expression U and h in terms of c , the final heat diffusivity equation can be written as:

$$\rho_{\square}c_g\frac{\partial T}{\partial t} - \beta_g T\frac{\partial P}{\partial t} = \rho_m c_g v_m.\nabla T - k_t\nabla^2 T - \mu_{JT}\rho_m c_g v_m\nabla P - \rho v\frac{\partial v}{\partial t} - \rho v^2\nabla v + \rho v g sin\theta - AU_{hc}\left(T_f - T_{sf}\right) + \dot{q}_g h_{rcg} \quad (4.14)$$

For the fully coupled wellbore:

The wellbore completions (tubing wall, insulation, annulus, casing, cement, perforations) can be treated jointly or severally as heat transfer interface between the wellbore fluid and the formation. This thesis is limited to the tubing resistance, and it is incorporated by coupling the governing equation obtained in line with Bergman et al (2011) as follows.

$$\rho_t c_t\frac{\partial T}{\partial t} = k_t\frac{\partial T^2}{\partial Z^2} + \frac{2h_{rt}(r_{0t}-r_{it})(T-T_{sf})}{r_{ot}^2} \quad (4.15)$$

Where, ,

r_{it} = *inner radius of tube*

r_{oc} = *external radius of tube/wellbore,*

h_r = *radial thermal resistance*

$T_{sf} = T_{wh} - g_T Z$ = *Sandface temperature*

T_{wh} = *wellhead temperature*

g_T = *the geothermal gradient*

Z = the vertical depth(height) of the reservoir

Subscripts t and c indicate tubing and cement.

Thus, we substitute for *U* and *h* functions with temperature and velocity variables and combine the heat transfer equations in reservoir. The final energy conservation equation for the fully coupled wellbore can expressed as follows:

$$\left[\phi\rho_{\square}c_p + (1-\phi)\rho_r c_r\right]\frac{\partial T}{\partial t} + \rho_t c_t \frac{\partial T_{\square}}{\partial t} - \phi\beta_p T\frac{\partial P}{\partial t} = \rho_p c_p u_p.\nabla T - \lambda_t \nabla^2 T - \mu_{JT,p}\rho_p c_p u_p \nabla P + \dot{q}_{\square} + Q_s - AU_{hc}\left(T_e - T_{sf}\right) - k_t\frac{\partial T_{\square}^2}{\partial Z^2} + \frac{2h_{rt}(r_{0t}-r_{it})(T-T_{sf})}{r_{ot}^2} \quad (4.16)$$

4.2 Treatment of Well–Reservoir Interaction and Interface Dynamics

To accounts for interactions between the reservoir and well, it is important to define the pressure drop due to flows in completion and perforations and in the near wellbore. It had been noted that the flow in the vicinity of wells is rather radial than linear. The volume integral over the convection term of the continuity equation is replaced with a surface integral, Eq. (4.17). The surface integral represents fluid flow through the perforations and across the boundary blocks in the near wellbore from the reservoir to the well.

$$\int \nabla\Phi_p.ndS_e = -\int_{Pw}^{Pe}\frac{kk_{rp}}{B_p\mu_p}dP \quad (4.17)$$

Where $\nabla\Phi_p$ is the phase potential across the cross-sectional surface area derivative of the grid block and can be expressed as

$$\nabla\Phi_p = -\frac{q_p}{2\pi h} \quad (4.18)$$

$$\frac{q_p}{2\pi h}\int_{rw}^{re}\frac{dr}{r} = -\frac{kk_{rp}}{B_p\mu_p}\int_{Pw}^{Pe}dP \quad (4.19)$$

$$\frac{q_{p\mathrm{B_p}}}{2\pi rh} = -\frac{kk_{rp}}{B_p\mu_p}\left(\frac{\partial P}{\partial r} - T_{\lambda_{l,n}}{}^{m}\right) \tag{4.20}$$

However, the convectional backpressure correlation could not be applied for wells which approached stabilized producing conditions slowly (Bahonar, 2011). This slow stabilization characteristic has been associated with wells producing from reservoirs of low permeability, typical of natural gas hydrate reservoirs. Therefore, to ensure that the right remedial action is taken to improve the productivity of our gas hydrate well, the divergence theorem is applied to formulate the interface equation that fully implicit coupled the reservoir and the well (Muggeridge et al, 2002). Considering the velocity of fluid in the tubing as equal to gas phase velocity that can sustain the liquid (water) phase flow, the mass conservations is assumed to be equivalent to the volume conservation under the same conditions. Thus, an interface equation which expresses the evolution of the volume fraction is added to the coupled wellbore mass and momentum equations (Saurel and Abgrall,1999).

$$\frac{\partial}{\partial t}\left(\rho_g \acute{q}_g\right) + v_i \frac{\partial}{\partial z}\left(\rho_g \acute{q}_g\right) = T_{\mu g}\left(P_g - P_w\right) \tag{4.21}$$

The gas flow rate derivation requires special consideration. The volume fraction across the reservoir-wellbore interface which propagates with the mean interfacial velocity that might not be equal to the fluid velocity would require incorporating the pressure correction factor that couple the reservoir and wellbore mass and momentum continuity equations. Hence with the adjustment for the two-phase water and gas flow, the modified equation obtained can be expressed as follow:

$$(1-\phi)\frac{\partial}{\partial t}\left(\rho_g \acute{q}_g + \rho_w \acute{q}_w\right) - (v_m + v_i)\frac{\partial}{\partial z}(\rho_m q_{sc}) = 2T_{\mu g}\left(P_g - P_w - P_i\right) \tag{4.22}$$

Where $\dot{q}_g$ = outflow or inflow rate through the perforations/completions; v_i = velocity correction factor; P_i = pressure correction factor to account for the interfacial pressure differential for the two-phase crossflow and wall effect $T_{\mu g}$ = Crossflow/flux term and can be calculated from the formula of Kazemi et al. (1976) in Kast and Hohenthanner (2000).

$$T = \frac{k_m \rho_g \sigma (P_i - P_w)}{\mu} \tag{4.23}$$

$$\sigma = 4\left(\frac{1}{\Delta x^2} + \frac{1}{\Delta y^2} + \frac{1}{\Delta z^2}\right) \text{ = the crossflow coefficient} \tag{4.24}$$

The well-block flowrate for the anisotropic system can be calculated from the Forchheimer analytically model of HU et al (2007).

$$-\left(\nabla\Phi_p\right) = \frac{\mu_p}{kk_{rp}} v_p + \beta_p \rho_p v_p^2 \tag{4.25}$$

$$\beta_p = \frac{1.485\ X\ 10^9}{k^{1.021}} \tag{4.26}$$

The plot of the derivative of the flowrate against the pressure gradient is represented by the finite difference approximation in one spatial dimension as follows.

$$q_P^{n+1} = a_p^n P_p^{n+1} + b_p^n \tag{4.27}$$

The wellbore model provides the boundary pressure which the reservoir model uses to calculate the flow rates of the phase flowing into the well. Whereas "a" and "b" are sensitivity coefficients calculated at the last iteration of the Jacobian matrix as follows (Sagen et al., 2007).

$$a_p^n = \left(\frac{\mu_p}{k_{eq}}\right)^n \tag{4.28}$$

$$b_p^n = q_P^n + a_p^n P_p^n \tag{4.29}$$

4.3 Governing Equations of the Fully Coupled reservoir-wellbore Model

The derived system of equations that described the mass and heat transfers in the gas hydrate reservoir and wellbore fluid flow are combined to obtain the complete description of the systems mass and heat transfer equations for the fully coupled reservoir-wellbore model. Therefore, combining with the appropriate reservoir model in the previous chapter and boundary conditions, and rearranging, the continuity equations are as follows:

Reservoir:

$$\frac{\partial}{\partial t}\left(\frac{\phi S_g}{B_g}\right) = \nabla.\frac{kk_r}{\mu_g B_g}\left(1 + \frac{b}{P_g}\right)\left(\nabla P_{fg} - \lambda_{tpg}\right) + D_F \nabla S_g - \acute{m}_g + \frac{q_{gsc}}{B_g} \tag{4.30}$$

$$\frac{\partial}{\partial t}\left(\frac{\phi S_w}{B_w}\right) = \nabla.\frac{kk_{rw}}{\mu_w B_w}\left(\nabla P_{fg} - \lambda_{tpw}\right) - \acute{m}_w + \frac{q_{wsc}}{B_w} \tag{4.31}$$

$$\frac{\partial(\phi\rho_h S_h)}{\partial t} = -\acute{m}_h \tag{4.32}$$

$$\left[\phi\rho_{\square} c_p + (1-\phi)\rho_r c_r\right]\frac{\partial T}{\partial t} - \phi\beta_p T\frac{\partial P}{\partial t} = \rho_p c_p u_p.\nabla T - \lambda_t \nabla^2 T - \mu_{JT,p}\rho_p c_p u_p \nabla P - \dot{q}_p + Q_{\square} + AU_{hc}(T_e - T_{wb}) \tag{4.33}$$

Interface:

$$(1-\phi)\frac{\partial}{\partial t}\left(\rho_g \acute{q}_g + \rho_w \acute{q}_w\right) - (v_m + v_i)\frac{\partial}{\partial z}(\rho_m q_{sc}) = 2T_{\mu g}\left(P_g - P_w - P_i\right) \tag{4.34}$$

$$\rho_t c_t \frac{\partial T}{\partial t} = -k_t \frac{\partial T^2}{\partial Z^2} + \frac{2h_{rt}(r_{0t}-r_{it})(T-T_{sf})}{(r_{ot})^2} \quad (4.35)$$

Wellbore:

$$\frac{\partial}{\partial t}\left(\rho_g S_g + \rho_w S_w\right) + \frac{\partial}{\partial z}\left(\rho_g v_g + \rho_w v_w\right) = q_g + q_w + m_g + m_w \quad (4.36)$$

$$\frac{\partial}{\partial t}\left(\rho_g v_g + \rho_w v_w\right) + \frac{\partial}{\partial z}\left(\rho_g v_g^2 + \rho_w v_w^2\right) = -\frac{\partial P}{\partial z} - \frac{f_m \rho_m v_m^2}{2d} - \rho_m g sin\theta + P_i \frac{\partial}{\partial z}\left(\rho_g \acute{q}_g\right) \quad (4.37)$$

$$\rho_m c_g \frac{\partial T}{\partial t} - \beta_g T \frac{\partial P}{\partial t} + \rho v \frac{\partial v}{\partial t} = \rho_m c_g v_m \frac{\partial T}{\partial z} - k_t \frac{\partial^2 T}{\partial z^2} - \mu_{JT} \rho_m c_g v_m \frac{\partial P}{\partial z} - \rho v^2 \frac{\partial v}{\partial z} + \rho v g sin\theta - AU_{hc}\left(T - T_{sf}\right) + \dot{q}_{gsc} h_{cg} \quad (4.38)$$

4.4 Boundary condition

- **Initial conditions**

The initial conditions from which the solution of the pressure and saturation equations propagates are conveyed by specifying a single value of pressure and saturation throughout of the grid blocks, such that

$$P_{wf(t=0)} = P_{(z)(t+\Delta t)} \quad (4.39)$$

$$v_{x(t=0)} = 0 \quad (4.40)$$

Also, the formation and wellbore fluid and completions (tubing wall, insulation, annulus, casing, cement) are in thermal equilibrium initially. So, the initial temperature conditions can be written as

$$T_{(r,t=0)} = T_{sf} \quad (4.41)$$

$$T_{sf} = T_{ei} \qquad \text{for } (Z \leq Z_o) \quad (4.42)$$

$$T_{sf} = T_{ei} + g_T Z \qquad \text{for } (Z > Z_o) \quad (4.43)$$

- **Inner Boundary condition**

The wellbore model provides the boundary pressure which the reservoir model uses to calculate the flow rates of the phase flowing into the well. Considering the inertial forces and convective flow processes in the near wellbore, rate constraints are imposed. Flow rate would be set at value that limits transformation of the pressure loss from weak inertia regime to strong inertia regime. As such, Dirichlet boundary conditions was imposed to keep the presence of gas phase

on the wellbore boundary. The whole wellbore domain would therefore be all together of aqueous phases under a given pressure and temperature condition and constant gas flow rate well constraint. The fluid flow velocity is equated to gas velocity at which the gas phase would be able to sustain the liquid (water) phase. The molar flux of the gas through the surface is equated to the absolute value of the rate of change in the moles of the gas at the interface.

$$J_p^k = \left|\dot{m}_g\right|, \;\; t > 0 \tag{4.44}$$

A more realistic inner boundary condition is to consider as infinite conductivity, implying that the pressure along the open portion of the well-bore is uniform and the integral of the resultant flux over the perforated interval is equal to the constant specified rate. Thus, the inner boundary is as such that:

$$\left.\frac{\partial\,(P-\lambda_{bw}r)}{n\partial r}\right|_{r=r_w} = q_{gsc}\frac{\mu_g}{2\pi rhk_g}\frac{zTP_{sc}}{T_{sc}P} + \beta\rho_g q_{gsc}\left(\frac{zTP_{sc}}{T_{sc}P}\right)^2 \tag{4.45}$$

$$q_{sc_{i+\frac{1}{2}}}^{n+1} = \frac{2\pi k_{eq}\Delta z}{\ln(r_{eq}/r_w+S)}\left(\frac{k_{rp}}{B_p\mu_p}\right)_{i+1}^{n+1}\left(P_i^{n+1} - P_{wf}^{n+1} - \lambda_{bw}\right) + 2\beta_{i+1}^{n+1}\left(\frac{k_{rg}}{B_g\mu_g}\right)_{i+1}^{n+1} \tag{4.46}$$

The unconventional flow factor, beta factor β , is obtained by combining and modifying Fick's law and Forchheimer- Drift model law (Takhanov, 2011; Shi et al, 2005).

$$\beta_{i+1}^{n+1} = \beta_{max} = J_D^k\frac{S_g|v_m|}{v_{sfg}} \tag{4.47}$$

$$J_D^k = \left|\dot{m}_g\right|_{(Z>Z_o)} \tag{4.48}$$

$$J_D^k = \left|D_F\nabla S_g\right|_{(Z\leq Z_o)} \tag{4.49}$$

$$\frac{\partial J_D^k}{\partial S_g} = 1 \tag{4.50}$$

$$\frac{\partial J_D^k}{\partial v_m} = 1 \tag{4.51}$$

v_{sfg} = gas wetting phase velocity. That is the velocity at which the gas phase would be able to sustain the liquid (water) phase flow. v_m = mixture velocity.

Outer Boundary condition

The reservoir in this work is subjected to a no – flow boundary condition on all sides so that the flow rate of the gas and water phases into the boundary cells is zero. This is equivalent to

the reservoir system bounded on all sides by impermeable media. Thus for the boundary grid blocks.

$$P_{(r\to\infty,t)} = P_{wf} = P_{ei} - P_{bh} \text{ for } (Z > Z_o) \quad (4.52)$$

$$T_{(r\to\infty,t)} = T_{sf} = T_{ei} + g_T Z \text{ for } (Z > Z_o) \quad (4.53)$$

$$\left.\frac{\partial P_{wf}}{\partial r}\right|_{z=0} = 0 \quad (4.54)$$

$$\left.\frac{\partial T_{sf}}{\partial r}\right|_{z=0} = 0 \quad (4.55)$$

4.5 Numerical Solutions

The numerical solution would involve discretization of the equations in time and space using finite difference scheme. Time discretisation would be by the first-order backward difference and space discretisation by the first and second order centred finite difference scheme. Production from a vertical well in one dimensional transient flow model is considered here in developing the coupled wellbore model. The well is divided spatially into N_b segments and the flow continuity equations are discretised and applied to each block starting from the surface down to the wellbore where it translates to and link up to the reservoir model via the appropriate boundary treatment.

4.5.1 Discretization of the Coupled wellbore

Consider a one-dimensional flow through of a segmented vertical well represented by figure 4.9, with reference depth, z, at a node with centre node, j, the lower and upper adjacent segments would be $j + 1$ and $j - 1$ respectively. The transient wellbore model can be written in reduced form as follows:

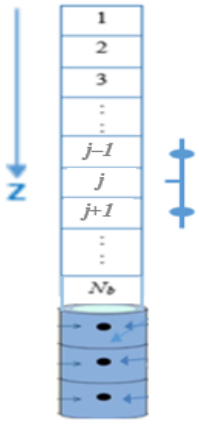

Figure 4. 4 One-dimensional Discretised Wellbore.

$$\frac{\partial U}{\partial t} + \frac{\partial F(U)}{\partial z} = H(U)\frac{\partial U}{\partial z} + S(U) \qquad (4.56)$$

Where

U is the vector of the conservative variables; F is the spatial flux vector; H is interface matrix containing the non-conservative variables; S is a vector of algebraic source terms. The matrices can be expressed in primitive form as below;

$$U = \begin{pmatrix} \rho_g \\ \rho_w \\ \rho_g v_g \\ \rho_w v_w \\ \rho_g \acute{q}_g \end{pmatrix}; \qquad F = \begin{pmatrix} \rho_g v_g \\ \rho_w v_w \\ \rho_g v_m^2 + P_g \\ \rho_w v_m^2 + P_w \\ 0 \end{pmatrix}$$

$$S(U) = \begin{pmatrix} -q_{gsc} \\ q_{gsc} \\ F_{pg} + G_{pg} \\ F_{pw} + G_{pw} \\ -T_{\mu g}P_g + T_{\mu g}P_w \end{pmatrix} \qquad H = \begin{pmatrix} 0 & 0 & 0 & 0 & 0 \\ 0 & 0 & 0 & 0 & 0 \\ 0 & 0 & P_i & 0 & 0 \\ 0 & 0 & 0 & -P_i & 0 \\ 0 & 0 & 0 & 0 & -v_i \end{pmatrix}$$

$$G_{pg} = \rho_m g sin\theta; \; F_{pg} = \frac{f_m \rho_g v_g^2}{2d}$$

Computing the Jacobian Matrix:

We write the finite difference approximations for each phase flow through each grid block/segment in residual form, $R = 0$. The reference wellbore segment is represented with *i* with *i-1* and *i+1* as lower and upper adjacent segments respectively, with segment length = Δz, cross-sectional area = A_s, whereas n and *n+1* represent the current and next time levels; L_N = Full length of well or Length to point being analysed).

$$R_i = \sum\left(\frac{U_i^{n+1} - U_i^n}{\Delta t}\right) + \sum\left(\frac{F_{i+1}^{n+1} - F_{i-1}^{n+1}}{\Delta z}\right) + \sum SU_i^{n+1} + H_i^n \frac{U_{i+1}^n - U_{i-1}^n}{2\Delta z} = 0 \qquad (4.57)$$

The implicit finite difference discretisation of the conservation equations can be written as follows:

- *Mass conservations*

$$R_{M.g} = \frac{A_s \Delta z\left(\rho_{g,j}^{n+1} - \rho_{g,j}^n\right)}{\Delta t} + \frac{A_s\left(\rho_{g,j+1/2}^{n+1} v_{m,j+1/2}^{n+1} - \rho_{g,j-1/2}^{n+1} v_{m,j-1/2}^{n+1}\right)}{\Delta z} - q_{sc_{jg}}^{n+1} \qquad (4.58)$$

$$R_{M,w} = \frac{A_s \Delta z\left(\rho_{w,j}^{n+1} - \rho_{w,j}^{n}\right)}{\Delta t} + \frac{A_s\left(\rho_{w,j+1/2}^{n+1} v_{m,j+1/2}^{n+1} - \rho_{w,j-1/2}^{n+1} v_{m,j-1/2}^{n+1}\right)}{\Delta z} - q_{scjw}^{n+1} \quad (4.59)$$

$$R_{M,h} = 0 \quad (4.60)$$

- *Momentum* conservations

$$R_{F,g} = \frac{A\Delta z\left(\rho_{m,j}^{n+1} v_{m,j}^{n+1} - \rho_{g,j}^{n} v_{w,j}^{n}\right)}{\Delta t} + \frac{\rho_{m,j}^{n+1} A\left(v_{m,j}^{n+1}\right)^2 - \rho_{m,j-1}^{n+1} A\left(v_{m,j-1}^{n+1}\right)^2}{\Delta z} + \frac{P_{j+1}^{n+1} - P_j^{n+1}}{\Delta z} +$$

$$\frac{f_{mi}^{n+1} \rho_{mj}^{n+1}\left(v_{mj}^{n+1}\right)^2}{2d} + \rho_m^{n+1} v_m^{n+1} \mathrm{g}\, \rho_{gi}^{n+1} \mathrm{g} sin\theta + P_i \frac{\Delta t \partial \acute{q}_i^n}{\Delta z} \quad (4.61)$$

$$R_{Fw} = \frac{\left(\rho_{w,i}^{n+1} v_{m,i}^{n+1} - \rho_{w,i}^{n} v_{w,i}^{n}\right)}{\Delta t} + \frac{\rho_{,i}^{n+1}\left(v_{m,i}^{n+1}\right)^2 - \rho_{w,i-1}^{n+1}\left(v_{m,i-1}^{n+1}\right)^2}{\Delta z} + \frac{P_{i+1}^{n+1} - P_i^{n+1}}{\Delta z} + \frac{f_{mi}^{n+1} \rho_{wi}^{n+1}\left(v_{mi}^{n+1}\right)^2}{2d_i} +$$

$$\rho_{wi}^{n+1} \mathrm{g} sin\theta - P_i \frac{\Delta t \partial \acute{q}_i^n}{\Delta z} \quad (4.62)$$

- Interface equation

$$R_i = \frac{A_s \Delta z}{\Delta t} \acute{q}_{sc_{i-\frac{1}{2}}}^{n+1}\left(\rho_{g,i}^{n+1} - \rho_{g,i}^{n}\right) - \frac{\left(\rho_{g,j+1}^{n+1} v_{m,j+1}^{n+1} - \rho_{g,j}^{n+1} v_{m,i}^{n+1}\right)}{\Delta z} - \left(T_{\mu g}\right)_i^{n+1} \frac{\left(P^{n+1} + P_i^{n+1}\right)}{\Delta z} - v_i \frac{\Delta t \partial \acute{q}_i^n}{\Delta z} \quad (4.63)$$

- *Energy* conservations

$$R_{T,p} = 2\rho_{p,j}^{n} c_{p,j}^{n} \frac{T_{i,j}^{n+l} - T_{i,j}^{n}}{\Delta t} - \beta_p^n T^n \rho_{p,j}^{n} c_{p,j}^{n} \frac{P_{i,j}^{n+l} - P_{i,j}^{n}}{\Delta t} + \rho_{p,j}^{n} v_{p,j}^{n} \frac{v_{i,j}^{n+l} - v_{i,j}^{n}}{\Delta t} +$$

$$2k_t \left(\frac{T_{i+j}^{n+l} - 2T_j^{n+l} + T_{i-j}^{n+l}}{\Delta z^2}\right) - \rho_{p,j}^{n} c_{p,j}^{n} v_{p,j}^{n} \left(\frac{T_{j+l/2}^{n+l} - T_{j-l/2}^{n+l}}{2\Delta z}\right) + \mu_{JT}^{n} \rho_{p,j}^{n} c_{p,j}^{n} v_{p,j}^{n} \left(\frac{P_{j+l/2}^{n+l} - P_{j-l/2}^{n+l}}{2\Delta z}\right) +$$

$$\rho_{p,j}^{n} v_{p,j}^{2n} \left(\frac{v_{j+l/2}^{n+l} - v_{j-l/2}^{n+l}}{2\Delta z}\right) - \frac{U_{hc}^{n} \pi r\left(T^{n+1} - T_{sf}^{n+l}\right)}{2} - \rho_{p,j}^{n} v_{p,j}^{n} \mathrm{g} + \left(\dot{q}_{gsc} h_{cg}\right)^{n+1} +$$

$$\frac{h_{rt}(r_{0t} - r_{it})(T_{i+j}^{n+l} - 2T_j^{n+l} + T_{i-j}^{n+l} - T_{sfj}^{n+l})}{2d} \quad (4.64)$$

4.5.2 Newton-Raphson Method

Applying Newton-Raphson method, the above derived finite difference solution of systems of governing equations can be implicitly combined and coupled to the reservoir model at the level of Jacobian matrix.

Computing the Jacobian matrix for the Coupled Wellbore results in

$$\left[R^{n+1^{v+1}}_{f(x),\Delta z,\Delta t+1)}\right] = J\left[f\left[\frac{R^{n+1^{v}}_{(f_x)}}{\partial f(x)}\right]\right]\delta[f(x)] \tag{4.65}$$

The objective function $f(x)$ are the main unknown variables. For our case, they are pressure (P), fluid temperature ($T_f = T$) and flow rate which is a function of the velocity (δq_{sc}).

$J\left[f\left[\frac{R^{n+1^{v}}_{(f_x)}}{\partial f(x)}\right]\right]$ = the Jacobean matrix (i.e. matrix of the derivatives of the coefficients of the unknown variables of the finite difference equations).

$\left[R^{n+1^{v+1}}_{f(x),\Delta z,\Delta t+1)}\right]$ = vector matrix of the residual of the equations

The derivatives of the non-zero conservative primary variable items in the Jacobian matrix are

$$\frac{\partial R^{n+1^{v}}_{i,g}}{\partial v_{m,i}} = A_s(-\rho_{mi});\quad \frac{\partial R^{n+1^{v}}_{i,g}}{\partial v_{m,i\pm1}} = A_s(\rho_{m,i\pm1});$$

$$\frac{\partial R^{n+1^{v}}_{i,g}}{\partial P_i} = A_s\left(-q_{ig}\frac{\partial \rho_g}{\partial P} - -q_{ig}\frac{\partial \rho_w}{\partial P}\right)_i;$$

$$\frac{\partial R^{n+1^{v}}_{i,g}}{\partial P_{i\pm1}} = A_s\left(-q_{ig}\frac{\partial \rho_g}{\partial P} - q_{ig}\frac{\partial \rho_w}{\partial P}\right)_i + A_s\left(-q_{ig}\frac{\rho_g\,\partial \rho_g}{\partial P} - -q_{ig}\frac{\partial \rho_w}{\partial P}\right)_i$$

$$\frac{\partial R^{n+1^{v}}_{i,w}}{\partial T_i} = -1;\quad \frac{\partial R^{n+1^{v}}_{i,w}}{\partial P_{i\pm1}} = 1;$$

$$\frac{\partial R^{n+1^{v}}_{i,w}}{\partial T_{m,}} = \frac{L_N(-2\rho_{mi}v_{m,i})}{\Delta z};\quad \frac{\partial R^{n+1^{v}}_{i,w}}{\partial v_{m,i\pm1}} = L_N\left(\frac{\rho_{m,i\pm1}}{\Delta t} + \frac{2\rho_{m,i\pm1}v_{m,i\pm1}}{d_i}\right) + L_N\left(\frac{f_{m,i}\rho_{m,i\pm1}v_{m,i\pm1}}{d_i}\right);$$

$$\frac{\partial R^{n+1^{v}}_{i,g}}{\partial q_i} = -A_s\left(-\frac{v_{m,i}\,\partial \rho_{mi}}{\partial q_{i,}}\right);$$

$$\frac{\partial R^{n+1^{v}}_{i,w}}{\partial q_{i\pm1}} = \left(\frac{-v^2_{m,i}\,\partial \rho_{mi}}{\Delta z\,\partial q_{i,}}\right);\quad \frac{\partial R^{n+1^{v}}_{i,w}}{\partial q_{i,i\pm1}} = \left(\frac{\partial \rho_{m,,i\pm1}}{\partial q_{i,,i\pm1}}\right)\left(\frac{v_{m,i\pm1}}{\Delta t} + \frac{v^2_{m,i\pm1}}{\Delta z} + \frac{f_{m,i}\rho_{m,i\pm1}v_{m,i\pm1}}{d_i} + g\sin\theta L_N\right)$$

Thus, for the one-dimensional wellbore, the solution of the difference equations can be modified to tridiagonal systems of equations as follows

$$c_i^{n+1^{v}}(\delta P + \delta T + \delta q_{sc}) + d_i^{n+1^{v+1}}(\delta P + \delta T + \delta q_{sc}) + e_i^{n+1^{v}}(\delta P + \delta T + \delta q_{sc}) = R_i^{n+1^{v+1}} \tag{4.66}$$

Where,

$c_i, d_{i,} and\ e_i$ are the derivatives of the coefficient of the primary variables, and d_n is the diagonal element of the sum of the matrixes.

$$\begin{bmatrix} c_{g_{i-1}}^1 & c_{w_{i-1}}^1 & c_{h_{i-1}}^1 \\ c_{g_{i-1}}^2 & c_{w_{i-1}}^2 & c_{h_{i-1}}^2 \\ c_{g_{i-1}}^3 & c_{w_{i-1}}^3 & c_{h_{i-1}}^3 \\ c_{g_{i-1}}^4 & c_{w_{i-1}}^4 & c_{h_{i-1}}^4 \end{bmatrix} \begin{bmatrix} \delta P \\ \delta P_i \\ \delta T \\ \delta q_{sc} \end{bmatrix} + \begin{bmatrix} d_{g_i}^1 & d_{w_i}^1 & d_{h_i}^1 \\ d_{g_i}^2 & d_{w_i}^2 & d_{h_i}^2 \\ d_{g_i}^3 & d_{w_i}^3 & d_{h_i}^3 \\ d_{g_i}^4 & d_{w_i}^4 & d_{h_i}^4 \end{bmatrix} \begin{bmatrix} \delta P \\ \delta P_i \\ \delta T \\ \delta q_{sc} \end{bmatrix} + \begin{bmatrix} e_{g_{i+1}}^1 & e_{w_{i+1}}^1 & e_{h_{i+1}}^1 \\ e_{g_{i+1}}^2 & e_{w_{i+1}}^2 & e_{h_{i+1}}^2 \\ e_{g_{i+1}}^3 & e_{w_{i+1}}^3 & e_{h_{i+1}}^3 \\ e_{g_{i+1}}^4 & e_{w_{i+1}}^4 & e_{h_{i+1}}^4 \end{bmatrix} \begin{bmatrix} \delta P \\ \delta P_i \\ \delta T \\ \delta q_{sc} \end{bmatrix} = \begin{bmatrix} R_P^{n+1^{\nu+1}} \\ R_T^{n+1^{\nu+1}} \\ R_{P_i}^{n+1^{\nu+1}} \\ R_{q_{sc}}^{n+1^{\nu+1}} \end{bmatrix}$$

Superscripts 1, 2, 3 and 4 indicate the discretised conservation equations (mass, momentum, energy difference equations and interface equation respectively) and subscript g, w, and h indicate gas, water, and hydrae phase respectively.

The solution of the coupled wellbore model and interface equations above is combined with the solutions of the reservoir difference equations at the level of the Jacobian matrixes as obtained in previous chapter, chapter 3 and solved together via orthomin-diagonalisation method implemented in MATLAB.

4.6 Implementation

The simulation deck was set up in the MATLAB with entries of necessary parameters. Because measurement is required at the wellhead, well constraints are defined. The well rate is specified to a targeted value and controlled in the simulation by decreasing or increasing the flow rate slowly, at small time steps, to a reasonable value or as desired. The initial production rate was set a minimal guessed value, as the possible mass flow rate of the reservoir that would enter the wellbore from the last reservoir grid block across the perforation up to the wellhead or grid-block being analysed. The reservoir and wellbore are fully implicit coupled via the coupled wellbore interface model. The residual form of the rate constraint would be defined in next time step n+1 as follows

$$\rho_{sc} q_{sc} = A_{n_{sg}} \rho_{n_{sg}}^{n+1} v_{n_{sg}}^{n+1} - R_{Rcgw_{n_{sg}}}^{n+1} \tag{4.67}$$

The iterative relay is offered by the boundary communication equation below

$$q_{sc}^{n+1} = a_p^n P_i^{n+1} + b_p^n \tag{4.68}$$

where $P_i$and q_{sc} are the cross-flow pressure term and flow rate for a specified phase, p, while 'a' and 'b' are coefficients.

Using the pressure calculated, flow rate terms are updated to the current time step and passed as wellbore potential. The sensitivity coefficients of the coupling equations are calculated and

updated. The iteration is then proceeded to the next time step. When the wellhead pressure drops to or below a specified value, a constant wellhead pressure is specified as constraint using the expression below

$$R_{Pseg}^{n+1} = P_{seg}^{n+1} - P_i = 0 \quad (4.69)$$

Once convergence is achieved, the iteration solution is updated to the new time step and proceeds to end. The simulation steps are summarised below; and the flow chart is illustrated in figure 4.5.

i. Initialize all the parameters with data from the file.
ii. Set up the Newton iteration algorithm.
iii. Calculate the residuals and the Jacobian matrix of all the auxiliary equations
iv. The linear equations are iteratively solved, and the residuals are compared with the tolerance. During the iteration step, the coefficients are updated with the parameters calculated for the next time level
v. If the convergence requirement is met, then next time step.
vi. If the iteration cannot converge, you may cut time step and repeat the Newton iteration. If the final time step is not reached, go to step (iii) for simulation at a new time step.
vii. Write an output file at the designated time steps.

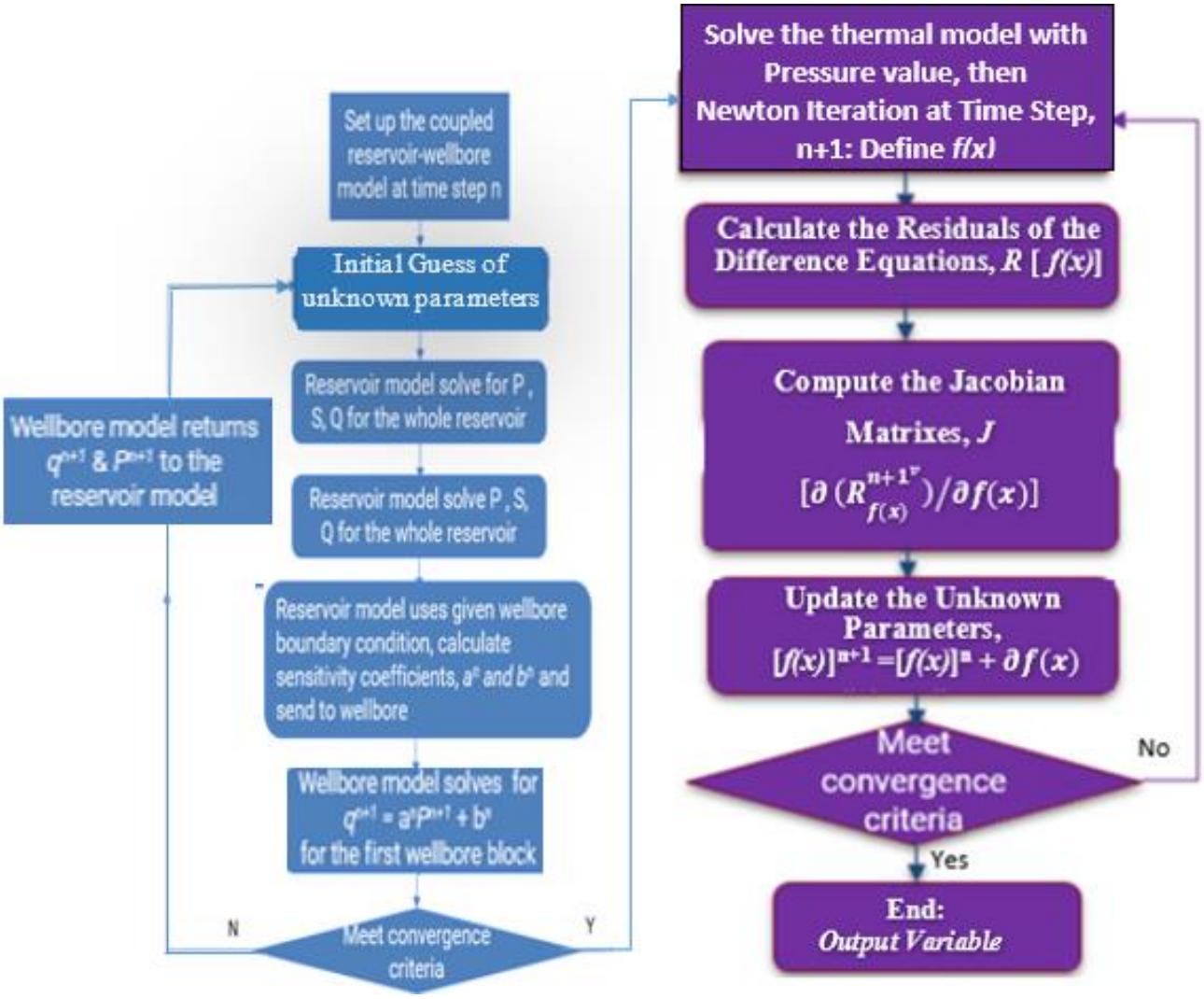

Figure 4. 5 Simulation Flow Chart of the Fully Implicit fully Coupled Model

4.7 Validation

To validate the developed the fully implicit fully coupled gas hydrate reservoir-wellbore model, results are compared with alternative solution schemes with similar subsets of the parameters and processes. This is because there is no directly related analytical or alternative numerical model in the literature. Use of alternative solution schemes that numerically verify the subdomains of the fully implicit fully coupled model can suffice to verify the reliability of the fully coupling processes and validate the simultaneously implicit coupled parts to whole. In this thesis, the reservoir part (decoupled from the wellbore) of the fully coupled model had been validated

in the previous chapter. The coupled wellbore model is hereby being validated using analytical model of non-isothermal transient flow in natural gas well by the approach of Abbaspour and Chapman (2008). It entails solving the transient gas well flow equations of mass, momentum and energy, where the compressibility factor is treated as a function of temperature and pressure, and gas (methane) is considered to behave ideally. Data from the classic Masuda experiment (Masuda et al., 1999) are used in the simulations. The Masuda et al. (1999) is considered classic as a pioneering experiment widely used to verify the accuracy of gas hydrate models (Hardwick and Mathias, 2018; Sun et al., 2019a; Deng et al., 2020). The fully coupled wellbore-reservoir model is solved using the fully implicit method of Sun et al. (2019). It entails coupling the algorithms of the subdomains using both the successive over relaxation and the general minimum residual methods. The derivation of the analytical model solutions is shown in the Appendix B. Base on the conservation laws, Mass, momentum and energy balance equation are as follows:

$$\frac{\partial}{\partial t}\left(\phi\rho_g S_g + \phi\rho_w S_w + \phi\rho_h S_h\right) + \frac{\partial}{\partial x}\left(\rho_g v_g + \rho_w v_w\right) = q_g + q_w + m_g + m_w + m_h \quad (4.70)$$

$$\frac{\partial}{\partial t}\left(\rho_g v_g\right) + \frac{\partial}{\partial x}\left(\rho_g v_g^2\right) = -\frac{\partial P_g}{\partial z} - \frac{f_m \rho_g v_g^2}{2d} - \rho_m g sin\theta \quad (4.71)$$

$$\frac{\partial}{\partial t}\left[\phi\rho_g S_g h_g + \phi\rho_w S_w h_w + \phi\rho_h S_h h_h + (1-\phi)\rho_r h_r\right] + \frac{\partial}{\partial x}\left(k_T \frac{\partial T}{\partial x}\right) - \frac{\partial}{\partial x}\left(\rho_g v_g h_g + \rho_w h_w\right) = q_g h_g + q_w h_w + q_h + q_{in} \quad (4.72)$$

The solutions of the Mass, momentum and energy conservations by the analytical model are given by equations 5.1, 5.2 and 5.3 respectively.

$$\frac{\square\square}{\partial t} = \left[\frac{1}{T} + \frac{1}{Z}\left(\frac{\partial Z}{\partial T}\right)_P\right]\left[\frac{1}{P} - \frac{1}{Z}\left(\frac{\partial Z}{\partial P}\right)_T\right]^{-1}\frac{\partial T}{\partial t} - \frac{\rho_{\square\square\square} zRT}{PA}\left[\frac{1}{P} - \frac{1}{Z}\left(\frac{\partial Z}{\partial P}\right)_T\right]^{-1}\frac{\partial q_{scg}}{\partial x} \quad (4.73)$$

$$\frac{\square\square}{\partial t} = -\left(\frac{\rho_{\square\square\square} q_{scg} zRT}{PA}\right)\frac{\partial T}{\partial x} - \left\{\left[\frac{zRTT}{C}\left(\frac{\rho_{scg} q_{scg} zRT}{PA}\right)\right]\left[\frac{1}{T} + \frac{1}{Z}\left(\frac{\partial Z}{\partial T}\right)_P\right]\frac{dT}{dx}\right\}\left\{\frac{1}{q_{scg}}\frac{\partial q_{scg}}{\partial x} - \left[\frac{1}{P} - \frac{1}{Z}\left(\frac{\partial Z}{\partial P}\right)_T\right]\frac{dP}{dx} + \left[\frac{1}{T} + \frac{1}{Z}\left(\frac{\partial Z}{\partial T}\right)_P\right]\frac{dT}{dx}\right\} + \frac{2f_{\square} zRT q_{scg}^3}{CDAP} - m_h \Delta H_D + \frac{q_{scg}}{C_{scg}} \quad (4.74)$$

$$\frac{\partial q_{scg}}{dt} = -\frac{\rho_{scg} zRT}{PA}\frac{\partial q_{scg}}{\partial x} + q_{scg}\left[\frac{1}{P} - \frac{1}{z}\left(\frac{\partial z}{\partial P}\right)_T\right]\left[\frac{\partial P}{\partial t} + \frac{\rho_{scg} q_{scg} zRT}{PA}\frac{\partial P}{\partial x}\right] - q_{scg}\left[\frac{1}{T} + \frac{1}{z}\left(\frac{\partial z}{\partial T}\right)_P\right]\left[\frac{\partial T}{\partial t} + \frac{\rho_{scg} q_{scg} zRT}{PA}\frac{\partial T}{\partial x}\right] - \frac{A}{\rho_{scg}}\frac{\partial P}{\partial x} - \frac{2f_m \rho_{scg} zRT q_{scg}^2}{DAP} \quad (4.75)$$

Figure 2 and 3 show the comparison of gas production rate and cumulative production between this thesis simulation results and the analytical model, respectively. An excellent match has been obtained for both cases of pressure and temperature rates of change as shown by figures 4.6 and 4.7. There is also a close match with very small variation in the trends of production rates in the results. Thus, the thesis model is verified as cable of representing the flow mechanism in the gas hydrate reservoir under the experiment conditions.

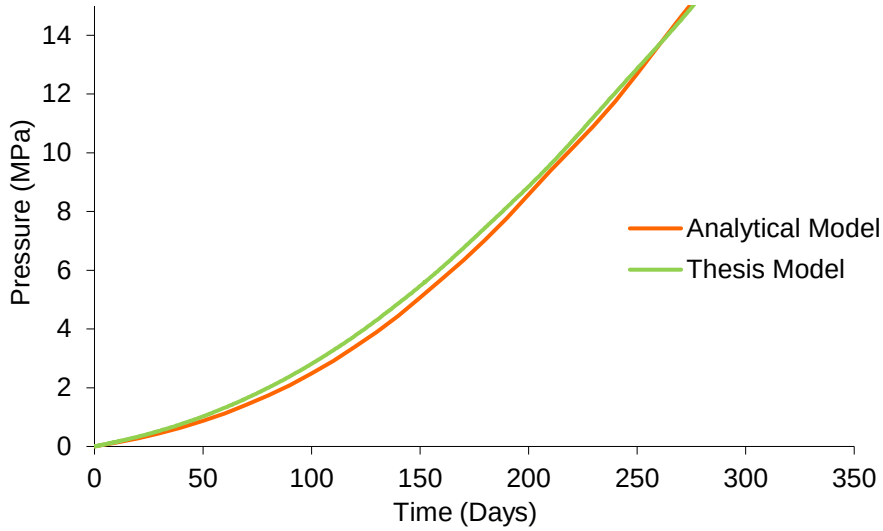

Figure 4. 6 Pressure Change Comparison of numerical and analytical solutions

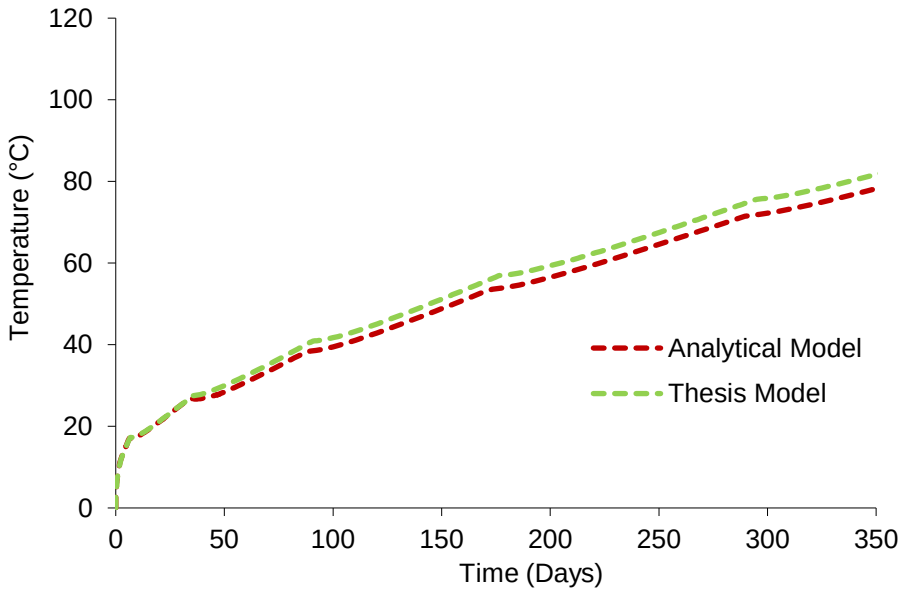

Figure 4. 7 Temperature Comparison of numerical and analytical solutions

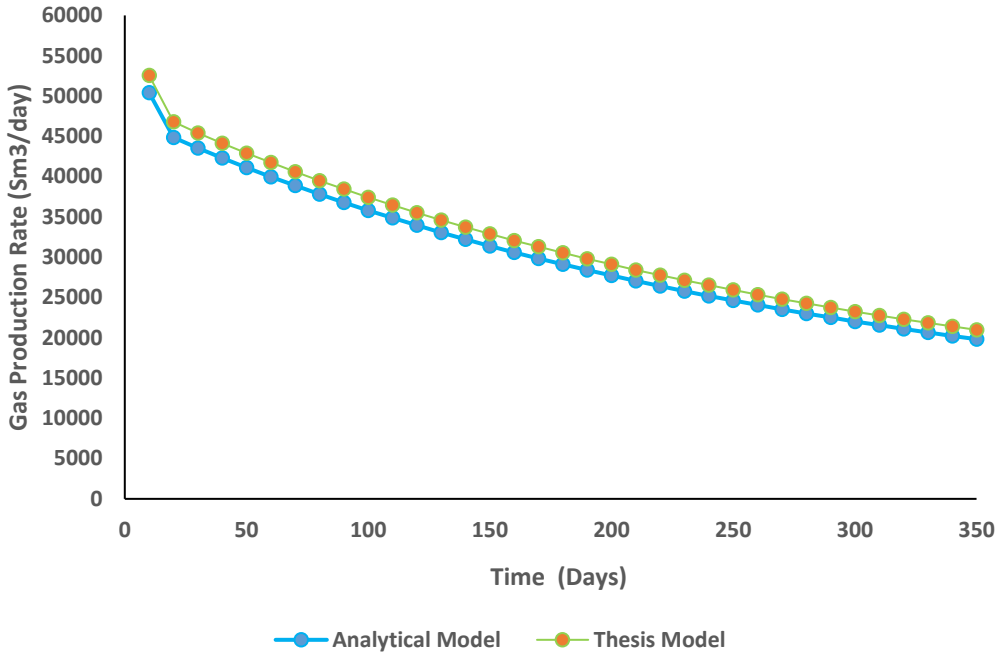

Figure 4. 8 Gas Production Rate Comparison of numerical and analytical solutions

4.8 Comparison with Sequential Coupled Model

To provide confidence in the fully coupled model as a whole continuum, the simulations using the developed fully coupled model are compared with the simulations using the alternative sequential coupled model. The sequential model is developed by coupling the independent solutions of the differences equation of the reservoir model and the wellbore model using the implicit-pressure-explicit-saturation (IMPES) method to obtain quick convergence. According to IMPES method, the pressure of the phases will be solved implicitly and the solution obtained will be used to explicitly solve for the saturation of the phases. To obtain the implicit pressure solution, the gas and water equations are scaled by multiplication with their respective formation volume factors and then combined to eliminate saturation terms. Starting from the initial condition, at each time step, the equations are iterated until the solution obtained converges with a predefined tolerance level (10^{-5}). During the iteration step, the coefficients are updated with the pressures calculated for the previous iteration level. Once convergence is achieved, the solutions obtained for the current and the next time steps were used to update the coefficients of the systems of equations and then the algorithm proceeds to end. The

corresponding average reservoir pressure and bottom-hole pressure are evaluated. The flowing pressure of any grid-block is:

$$P_{wfgi} = P_i - \sum P_{fgi}^{n+1^{v+1}} \tag{4.76}$$

The pressure solution in residual form are computed as follows:

$$R_p^{n+1^v} = b_n^{n+1^v} P_{fg,(S)}^{n+1^{v+1}} + c_n^{n+1^v} P_{fg,(W)}^{n+1^{v+1}} + d_n^{n+1^v} P_{fg,n}^{n+1^{v+1}} + e_n^{n+1^v} P_{fg,(E)}^{n+1^{v+1}} + f_n^{n+1^v} P_{fg,(N)}^{n+1^{v+1}} \tag{4.77}$$

The saturation for individual grid blocks is obtained from the diffusivity equation for water, given by

$$R_s^{n+1^v} = S_{w,n}^{n+1} + \frac{1}{C_{wwn}^{n+1^v}} \{ \sum_{l \epsilon \psi_n} T_{wl,n}^{n+1^v} \left[\left(P_{g,l}^{n+1^{v+1}} - P_{g,n}^{n+1^{v+1}} \right) - \left(P_{cgw,l}^{n+1^{v+1}} - P_{cgw,n}^{n+1^{v+1}} \right) \right] + q_{wsc,n}^{n+1} - C_{wpn}^{n+1^v} \left(P_{g,n}^{n+1^{v+1}} - P_{g,n}^{n} \right) \} - S_{w,n}^{n} + 1 \tag{4.78}$$

The developed wellbore model is coupled to the reservoir by constraining the bottom-hole pressure since measurement is meant to be at the surface for the coupled model. The solutions of the discretised the well model equations are applied to each block starting from the surface and solving till the bottom-hole pressure is obtained.

$$R_w^{n+1^v} = U_i^{n+1} - U_i^n - \frac{\Delta t}{\Delta z} \left(F_{j+1}^n - F_{j-1}^n \right) - \Delta t \acute{q}_i^n \tag{4.79}$$

$$\nabla \left(F_{j+1}^n - F_{i-1}^n \right) = \frac{A \Delta z \left(\rho_{m,j}^{n+1} v_{m,j}^{n+1} - \rho_{g,j}^n v_{m,j}^n \right)}{\Delta t} + \frac{\rho_{m,j}^{n+1} A \left(v_{m,j}^{n+1} \right)^2 - \rho_{m,j-1}^{n+1} A \left(v_{m,j-1}^{n+1} \right)^2}{\Delta z} + \frac{P_{j+1}^{n+1} - P_j^{n+1}}{\Delta z} + \frac{f_{mi}^{n+1} \rho_{mj}^{n+1} \left(v_{mj}^{n+1} \right)^2}{2d} + \rho_m^{n+1} v_m^{n+1} \mathrm{g}\, \rho_{gi}^{n+1} \mathrm{g} sin\theta + P_i \frac{\Delta t \partial \acute{q}_i^n}{\Delta z} \tag{4.80}$$

The mixture in velocity is evaluated using drift-flux wellbore model of one-dimensional gas flow through an open pipe, represented by the empirical constitutive relationship below:

$$V_g = C_0 V_m + V_d \tag{4.81}$$

The variables have been defined in literature review

The energy conservation equations are solved and coupled to the solutions of the systems of equations for non-isothermal model at the level of Jacobian matrix. For the isothermal model, the temperature component is eliminated from both coupled schemes. The discretized energy balance obtained can be expressed as:

$$R_T^{n+1^v} = T_{i,j}^n - S_x T_{i+1,j}^{n+1} - S_x T_{i-1,j}^{n+1} - S_y T_{i,j+1}^{n+1} - S_y T_{i,j-1}^{n+1} + \left(1 + 2S_x + 2S_y\right) T_{i,j}^{n+1} - \frac{Q_{i,j}^n}{\rho_m c_p} \quad (3.81)$$

In coupling the systems of equations, the method of simple iteration of all non-linear coefficients is used. The global matrix of the solutions of the coupled systems of equations can be expressed as Bahonar M. (2011). The norm is diagonolised and implement in MATLAB. Where the convergence is achieved in each subdomain when

$$\lim_{\to 0} \left\| R_i^{n+1^v} \right\| \leq 10^{-6}.$$

The global matrix of the solutions of the coupled systems of equations can be expressed in line with Bahonar (2011) as follows:

$$\|R_i\| = \left[\left(\frac{\|R_p\|}{R_p^{n+1^{v+1}}} \right)^2 + \left(\frac{\|R_s\|}{R_s^{n+1^{v+1}}} \right)^2 + \left(\frac{\|R_w\|}{R_w^{n+1^{v+1}}} \right)^2 + \left(\frac{\|R_T\|}{R_T^{n+1^{v+1}}} \right)^2 \right]^{\frac{1}{2}} \quad (4.82)$$

The production potential of the hydrate deposit at Site SH7 in Shenhu Area, South China Sea and experimental data of Li et al, 2010a are evaluated using the two coupling schemes. The parameters for the simulation are as listed in chapter 3 of this thesis. Production from a single vertical well is considered with the production pressure of the well set as 4MPa. The numerical simulation of the hydrate production features using the two models were compared.

4.9 Results and Discussions

4.9.1 Effect on Production rates

Figures 4.9 and 4.10 present the responses of the fully implicit fully coupled model of this thesis production and the sequential coupled model to varying production rates. The cumulative productions are evaluated consequently. A 350days production of the gas hydrate is simulated. As can be seen from the figures, the gas flow rate and the cumulative production in both models showed similar trends. However, with the thesis model, the flow rate started gradual decrease from the initial drop while with the sequential scheme, it experienced a sharp decrease for some days before it started to gradually decrease. Also, the fully coupled enabled higher flow rate from the beginning. This was followed by almost equal decline rate with the sequential model towards the end of the simulation. Subsequently a staggered decrease and gradually decrease can be extrapolated for long time production with methods applying the thesis model and sequential scheme respectively. It can be implied that, with the thesis model, the hydrate experienced stable dissociation as the saturation and aqueous' equilibrised toward the near-

well, while with the sequential scheme inertia and slippage effect could be prominent leading to the sharp decrease the flow curve. It could be said that the sensible heat of the dissociation is activated and acting out better in the model; initial analysis in previous chapter can be used to encapsulate this inference. The cumulative produced volumes of gas from the thesis model graphs are consistent with the observations made on the relative magnitude and evolution over time in the Shenhu Area of the South China Sea by Li et al (2009a). Moreover, the maximum gas production rate has higher order of magnitude with the thesis model. Thus, gas production from hydrate deposits may be more technical viable with the fully implicit fully coupled reservoir-wellbore simulation model in this thesis.

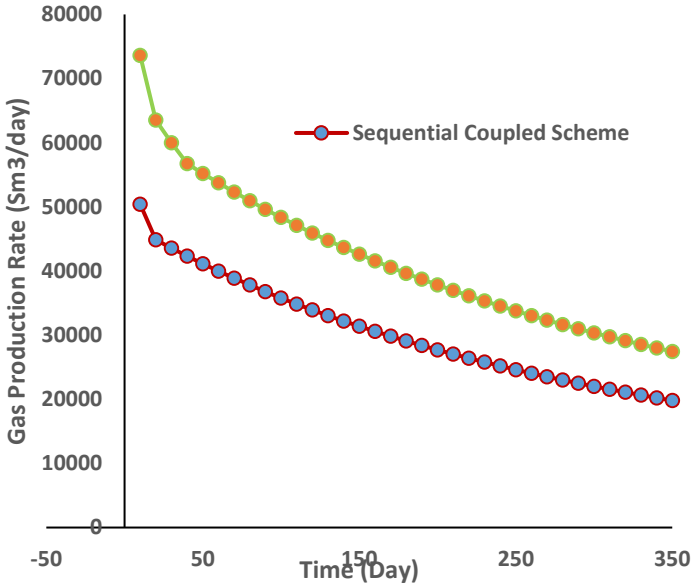

Figure 4. 9 Gas production Rate of the Coupled Models

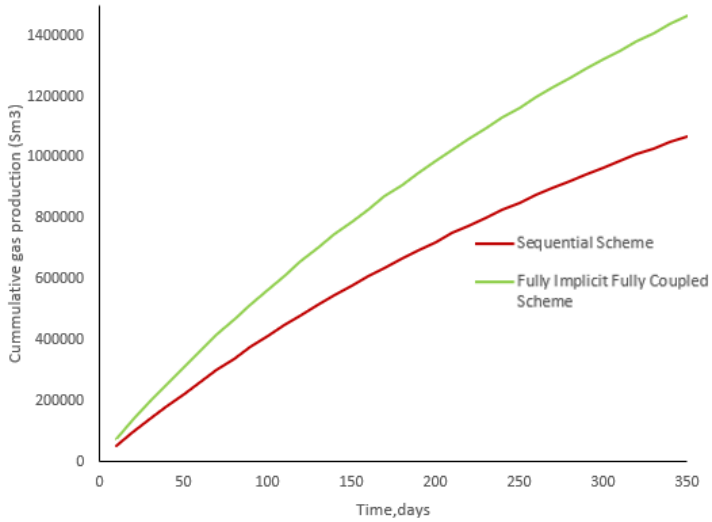

Figure 4. 10 Cumulative Gas Production of the Coupled Models

4.9.2 Gas Recovery Factors

Figure 4.12 presents the evolution of the predicted gas recovery factors. The gas recovery factor is calculated from:

$$RF = \frac{m_{diss}}{m_h}$$

Where, m_{diss}= amount of the dissociated hydrate (mol); m_h = total amount of the hydrate(mol) of hydrate occupying the dissociation area. It is therefore dimensionless and can be expresses as a fraction or percentage.

Figure 4.11 showed the gas recovery factor by the fully and sequential coupled schemes. It depicts that the fully coupled scheme in this thesis enables higher recovery factor. It can be seen that the ultimate recovery for fully and sequential coupled scheme are 48% and 30% respectively. Apparently, the gas recoveries with fully coupled model is 18% higher. This without any difference between the two methods. The recovery with the fully coupled method is therefore higher than that of sequentially coupled method under same production time and conditions.,

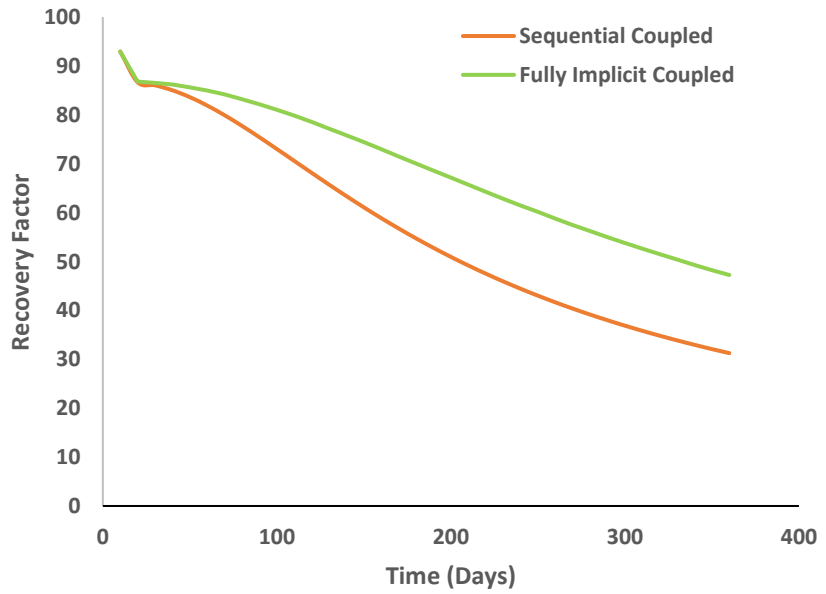

Figure 4. 11 Gas Recovery Factor with the Coupled Models

4.9.3 Measurement at Wellhead

We considered applying the developed fully coupled reservoir-wellbore as a simulation tool that can utilise measurement at the wellhead and the parameters to characterise and control the reservoir. We therefore use the model to measure the responses of the reservoirs to wellhead pressure and production rate. A case of gas production with the wellhead pressure, P_W = 4MPa, 3 MPa and 2MPa is simulated under the modelling parameters using the fully coupled model. The wellhead responses of the production parameters in table 4.1 are used to evaluate the effects of the transient temperature and pressure based on the fully coupled model.

Table 4. 1 Simulation Parameters

PROPERTY	VALUE
Depth	1450m
Water surface	1000 m
Hydrostatic pressure gradient	0.01035 psi/ft
Pore pressure	15 MPa
Initial Reservoir Temperature	287K
k_1	0.5.md
k_2	5 md
Pressure Gradient	0.022633 MPa/m
wellbore radius, r_w	0.13m
Mass flow rate	0.706 kg/m3
Gas production rates	0.03kg/s 0.05kg/s 0.07kg/s

4.9.4 Transient Pressure and Temperature Analysis

Pressure and temperature responses through of a production wellbore are commonly measured downhole parameters, and have been proven to be quite valuable. While the transient pressure analysis has been used for reservoir characterizations and near wellbore analysis, the use of transient temperature data has not been much focused on to demonstrate that it is quite valuable to characterize a formation, provide more detailed near-wellbore analysis and also discriminate between produced fluids. This thesis analysed the gas hydrate thermodynamic based on threshold solution of the Pressure and temperature transient modelling carried out using the

developed model. The methods for modelling gas hydrate thermodynamic have been reviewed and the fully coupled wellbore model have been developed. Considerations were given to various factors affecting multiphase flow scenarios in the gas hydrate system/well, but could not be extended to the thermal wellbore effect.

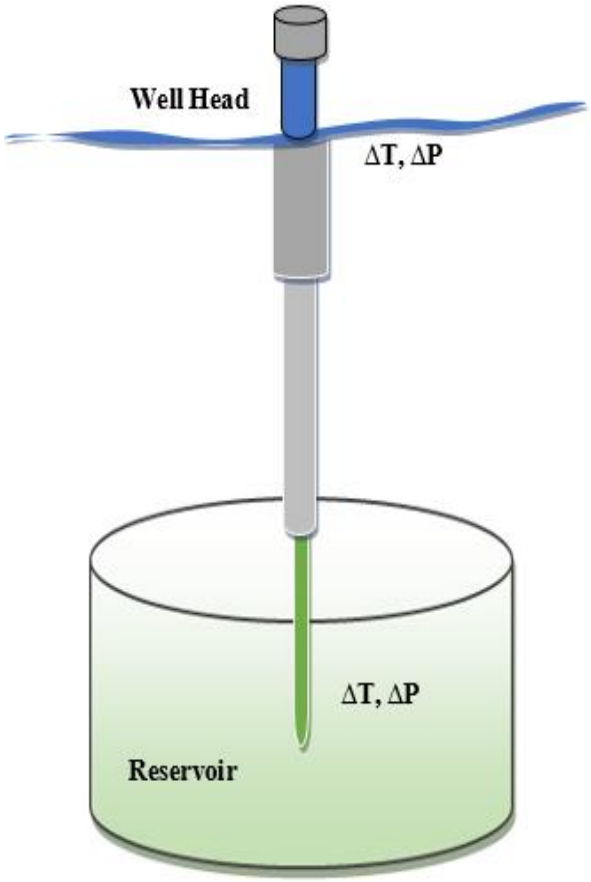

Figure 4. 12 Schematic of Transient Pressure and Temperature Analysis System

Figures 4.13 show the combinations of the fully coupled reservoir-wellbore temperature and pressure gradients measured from the wellhead under different flow rate operating conditions of the hydrate system. Simulations are run at fluid flow rate of 0.03 m^3/s, 0.05 m^3/s and 0.07 m^3/s at a total production constraint 30,000m^3 under the initial conditions of wellhead back pressure of 4MPa and temperature of 60°C. It can be seen that the increase in temperature gradient within the reservoir system would result in decrease in the saturation pressure gradient. It is indicative from the points of meeting and departure of the curves and the exponents that the best operating condition at wellhead for the optimum gas production is at pressure of 3MPa and 40.5C. The meeting of the exponent and linear of the higher flow rate dilated up to point of retard production which is toward towards the base of the hydrate bearing sediment column. With the increase of the flow rate, the fluid velocity in the wellbore would increase under the same production rate, which reflects the bottom-hole pressure would decrease while the reservoir pressure does not change significantly.

For the reservoir system with high bottom-hole pressure, using decoupled wellbore model will underestimate the saturation pressure gradient through of the gas release from the dissociated hydrate and free gas saturation. Hence, pressure transient analysis without the corresponding transient temperature analysis may not sufficiently account for the near wellbore effects. Thus, the application of the combined transient analyses using the fully implicit fully coupled reservoir-wellbore model is advised in the management of gas hydrate production.

Fig. 4.14 shows the relationship between the temperature gradient and pressure gradient on reservoir recovery. It can be inferred that temperature gaps, encompassing difference between the initial reservoir temperature and effects of dissociations under non-Darcy flow as discussed in previous chapter effect the normal depressurization significantly. The recovery factor increases with the increasing temperature gap which in turn is equivalent to the sensible heat of dissociation which increases under adiabatic processes and threshold pressure conditions in the reservoir. On the other hand, the recovery factor decreases with increase pressure which also reduces the effect of sensible heat of hydrate dissociation at certain high value. It can be concluded that right combinations of temperature and pressure are necessary for optimized production of gas hydrate reservoir and these are in turn affected by the defying feature to the flow, including wellbore effects, identified and evaluated in this thesis. The gas hydrate recovery factor under the transient pressure and temperature analysis can be up to 90% under the flow rate condition of 0.05 m^3/s and temperature gradient of about 8°C. At this condition, incremental pressure gradient has no serious effect on the reservoir temperature gradient. The recovery factor of the normal depressurization has shown linear relationship with the temperature gaps. It points to fact that hydrate dissociation is a strongly endothermic phenomenon. Following the dissociation occurrence therefore, hydrate stability may issue due to the self-preserving tendencies except if heat is supplied through natural advection or conduction or thermal stimulation. The dissociation rate in our experiments was reduced by dissociation-induced temperature fluctuations, Increase the boundary temperature has corresponding inverse change in the hydration pressure. Hence normal depressurization alone cannot sufficiently account for the adequate recovery of the hydrate reservoir, corresponding thermal stimulation is needed for improved performance.

Figure 4.15 indicates molar volume fraction of gas release from hydrate dissociation under various combination of wellhead temperature and pressure. It is indicative of the dependence of production rate to the wellhead parameters. Figure 4.16 showed that when the pressure is decreased from 4MPa to 3MPa and to 2MPa, the volume of gas released increased by about 22% and 12% respectively under same operating temperature and the results remained close with changes in the wellhead temperature. Results support the fact that large pressure drawdown enhance dissociation and large

pressure graduate results from reduced wellhead pressure and increase temperature. Considering the importance of this application, the developed fully implicit fully coupled wellbore – reservoir model is an effective simulation model for gas hydrate production performance analyses.

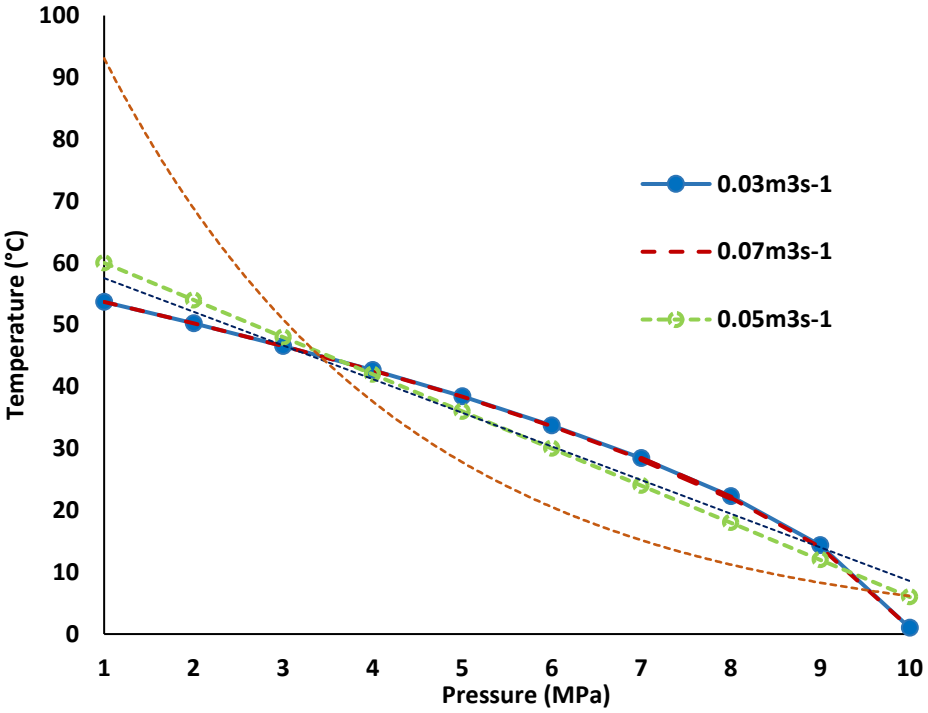

Figure 4. 13 Transient Temperature and Pressure Analysis Curve

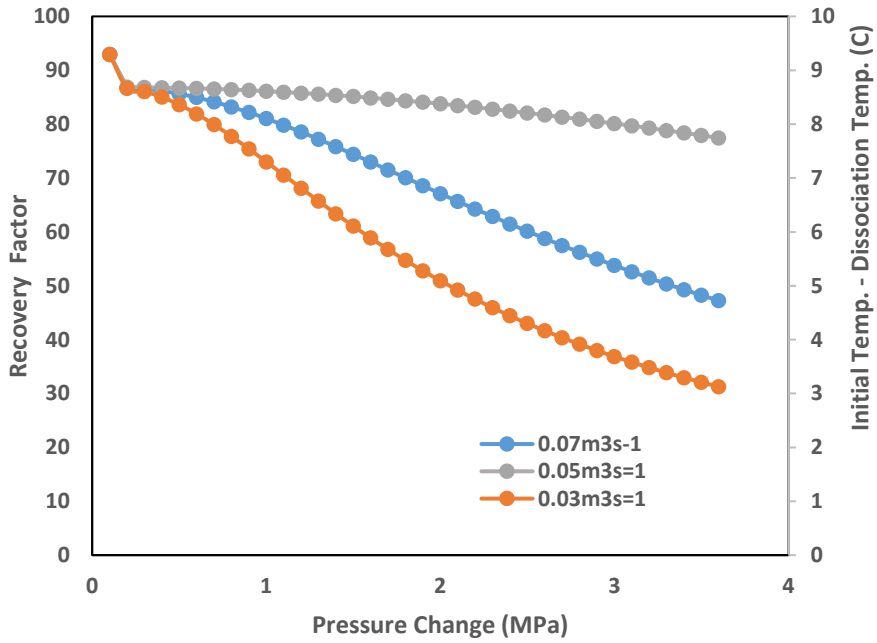

Figure 4. 14 Gas recovery factor from the hydrate dynamic decomposition under different gas flow rates

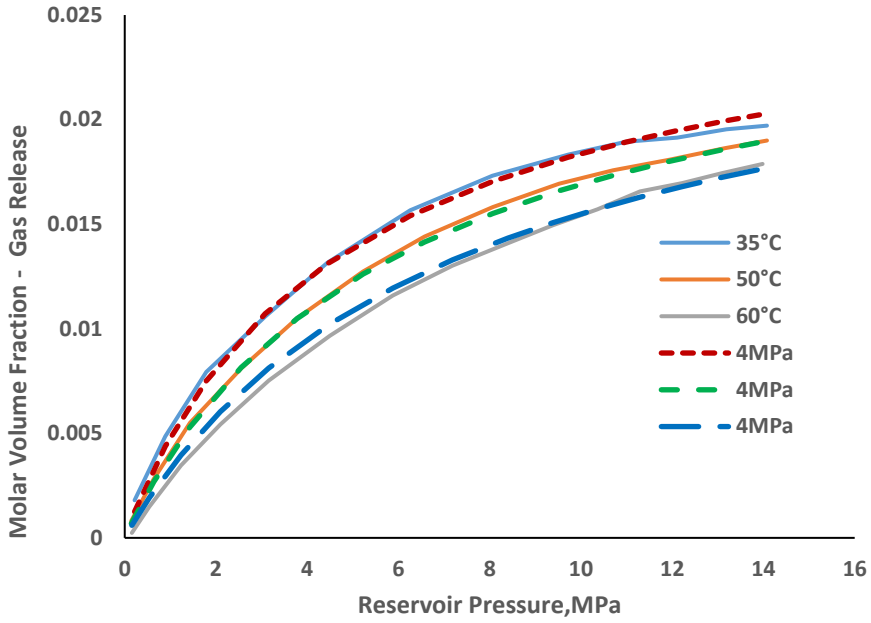

Figure 4. 15 Effect of Wellhead Temperature on Gas Molar Fractional Flow (Aqueous CH_4 Mass Fraction)

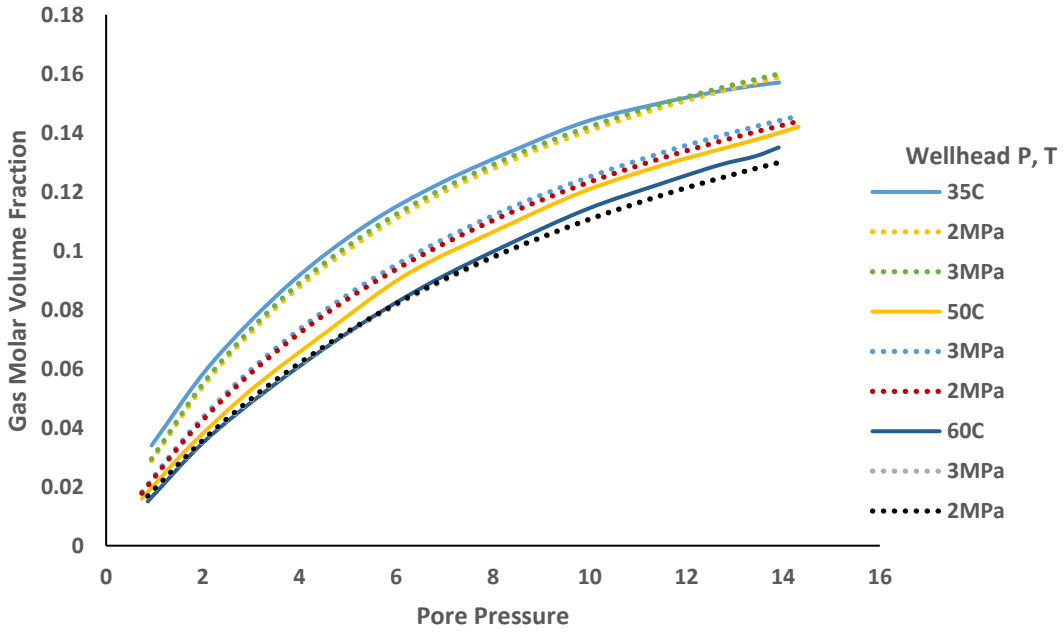

Figure 4. 16 Effect of Wellhead Pressure and Temperature on Gas Molar Fractional Flow (Aqueous CH_4 Mass Fraction)

4.10 Near-Wellbore Upscaling for Capillary Pressure and Relative Permeability Functions on Gas Hydrate Production.

This thesis underscored that the importance of capturing the various multiphase fluid flow factors that can affect the near wellbore characteristics in the integrated reservoir-wellbore for the natural gas hydrate production. Near-wellbore upscaling can be employed to characterised and re-evaluate the key parameters such as relative permeability and capillary pressure functions that affects fluid-particle interaction and preferential fluid flow for a fundamental understanding of the behaviour of the hydrate production systems. Upscaling entails reducing the number of grid cells and averaging the reservoir properties within them to achieve high resolution field-scale simulation. Use of fine multi -grid cells make the running of reservoir simulation difficult and time consuming. Upscaling makes simulations runs more ease. To compensate for scale heterogeneity, vertical effects in the 2D areal model and the numerical dispersion, the coarse grids are created with the pseudo variable (upscaled relative permeability and capillary pressure) (Chierici, 1984; Hearn et al., 1971; Pickup et al. 2000). Thus, coarse grid simulation curves are called pseudo functions to differentiate them from the fine grid curves (the rock/base case).

Near-wellbore Upscaling method is employed to upscale the relative permeability and capillary pressure functions for gas and water flow in gas hydrate production because of the complexity of the pore geometries. The heterogeneity of the porous medium and the macroscopic behaviour may not be easily deduced from the pore level or micro scale analysis. The major objective in flow analyses is to determine the in-situ mass distribution and fluid flow in reservoirs. The physical concepts used to describe the flow are fluid and rock properties. Flow and movement of fluids in porous media is a dynamic process and is driven by energy that is stored within reservoirs or supplied by injection. The challenge is to predict how much fluid that can be produced under given geological and operational conditions. Or, how can the performance of the reservoir be optimized for maintaining long-term productivity or higher recovery rate. To optimise flow, we need to evaluate some fluid flow and rock properties, such fluid viscosity, absolute permeability, wettability, interface tension, relative permeability and capillary pressure concepts, etc. We also need to know the driving forces or flow mechanisms, i.e., the main energy driving fluid to flow from reservoir to well, such as pressure and potential gradient, potential energy, or capillary force. Past investigations of displacement of a more viscous fluid by less viscous fluid, such as a crude oil displaced by gas, and water seepage in thick unsaturated zones of fractured rocks, have indicated that flow and transport processes in

such an environment may occur in non-volume-averaged fashion and proceed, in part, by means of localized preferential pathways (Pruess, 1999).

In a continuum system like the coupled reservoir- wellbore model, conventional modeling approaches may not adequately capture the physics of multiphase flow displacement along those preferential flow pathways if the spatial variability is not properly represented by constraints of the computational requirements. For practical application, almost all theories on flow phenomena occurring in porous media lead to macroscopic laws applicable to a finite volume or a controlled of the subdomain of the system under investigation. The dimensions of the macroscopic model are larger compared with those of pores. The method of generating the pseudo functions involves equations in which the porous medium and flow system are treated as continuous and characterized by local values of the thermodynamic variables, rock and fluid parameters, defined for all points with appropriate averaging or representative elementary volume (Bear, 1972). The main focus of this section is to appropriate and verify the relative permeability and capillary pressure functions that account for the reservoir heterogeneities and analyse the near-well flow challenges associated with the pseudo functions in the gas hydrate reservoir model.

4.10.1 Dynamic Permeability, Capillary Pressure and Characterization

The concept of dynamic permeability and characterization of the permeability of natural gas hydrate can be established by using time-series analysis. The dissociation process and transport in the pore network will produce gas and water under the influence of heterogeneous pressure field and pore permeability characteristics which ultimately affect the efficiency of the reservoir production (Zhang et al. 2015). Generally, the permeability is set as a constant in many practices based on the concept of permeability in conventional oil and gas, which ignores the variation of permeability caused by structural changes of the sediment. Many researches have based on visualization techniques and core analysis of natural gas hydrate deposits under steady-state conditions to construct the pore network models of hydrate deposits. The premise of this study is that core permeability is a constant value, and the existing relevant studies are mainly focused on the steady-state conditions of the two-phase migration characteristics of gas and water. It is relevant therefore to incorporate the hydrate dissociation process with changeable hydrate phase state in the pore structures under pressure and/or temperature fields.

Various relative permeabilities and Capillary Pressure models are analysed and compared as follows

Corey (1954):

$$P_c = P_o \left(\frac{S_w - S_{rw}}{1 - S_{rw}}\right)^{\lambda} \quad (4.83a)$$

$$k_{rw} = \left(\frac{S_w - S_{rw}}{1 - S_{rw} - S_{rg}}\right)^{4} \quad (4.83b)$$

$$k_{rg} = \left(1 - \frac{S_w - S_{rw}}{1 - S_{rw} - S_{rg}}\right)^{2} \left[1 - \left(\frac{S_w - S_{rw}}{1 - S_{rw} - S_{rg}}\right)^{2}\right] \quad (4.83c)$$

van Genuchten (1980):

$$P_c = P_o \left[\left(\frac{S_w - S_{rw}}{1 - S_{rg} - S_{rw}}\right)^{\frac{1}{m}} - 1\right]^{1-m} \quad (4.84a)$$

$$k_{rw} = \left(\frac{S_w - S_{rw}}{1 - S_{rw}}\right)^{0.5} \left[1 - \left(1 - \left(\frac{S_w - S_{rw}}{1 - S_{rw}}\right)^{\frac{1}{m}}\right)^{m}\right]^{2} \quad (4.84b)$$

$$k_{rg} = \sqrt{1 - \left(\frac{S_g - S_{rg}}{1 - S_{rw}}\right)} \left(1 - \left(\frac{S_w - S_{rw}}{1 - S_{rw}}\right)^{\frac{1}{m}}\right)^{2m} \quad (4.84c)$$

Stone (1970) (Modified):

$$k_{rw} = \left(\frac{S_w - S_{rw}}{1 - S_{rw}}\right)^{n_w} \quad (4.85)$$

Linear interpolation method can be used to calculate the capillary pressure and relative permeability as a function of water saturation as follows

$$P_{cgw} = P_{cgw} - \frac{P_{cgw1} - P_{cgwo}}{S_{w1} - S_{wo}} (S_w - S_{wc}) \quad (4.85a)$$

$$k_{rw} = k_{rwo} - \frac{k_{rw1} - k_{rw0}}{S_{w1} - S_{w0}} (S_w - S_{wc}) \quad (4.85b)$$

$$k_{rg} = k_{rgo} - \frac{k_{rg1} - k_{rgo}}{S_{w1} - S_{wo}} (S_w - S_{wc}) \quad (4.85c)$$

Hydrate Evolution Model:

The previous permeability models assumed homogeneous structure and the permeabilities are function of water saturation. Following that natural gas sediments are innately heterogeneous, and inertia to the fluid flow in the pore space arises in the presence of the hydrate phase distribution, the media constitutes in permeability changes. The fluid flow pathways are laced with non-Darcy flow subjected to effects of hydrate saturation and threshold pressure gradient which depends on water saturations:

$$S_w = 1 - S_g - S_h$$

The permeability functions of the hydrate fluid flow have been explicated to be a function of hydrate saturation rather (Jang and Santamarina, 2011, 2014; Liang et al., 2010; Spangenberg, 2001; Holtzman and Juanes, 2011; Dai and Santamarina, 2013; Johnson et al, 2011; Masuda et al 1997, 1999; Kumar et al., 2010; Matyka, et al., 2008; Dai and Santamarina, 2013). The modified Kozeny-Carman equation has been applied for hydrate saturation/ pore network permeability model (Dai and Seol, 2014) as follows:

$$k_r = \frac{k}{k_o} = \frac{(1- S_h)^3}{(1+ 2S_h)^2} \qquad (4.86)$$

I, the relation with equivalent changing porosity, tortuosity and specific surface can be expresses as:

$$1 - S_h = \phi_r = \frac{\phi_h}{\phi_o} \qquad (4.86a)$$

$$1 + 2S_h = (\tau . A_s)_r \qquad (4.86b)$$

Where, subscripts *'o', 'h'* and *'r'* represent hydrate-free porosity, hydrate-bearing porosity, and relative porosity values, respectively.

The apparent permeability of both can therefore be expressed as a function of the hydrate saturation and the porosity as follows:

$$k = k_o exp\left[\eta_1\left(\frac{\phi}{\phi_o} - 1\right)\right]\left\{max\left[\frac{\phi(1- S_h)-\phi_c}{\phi_o-\phi_c}, 0\right]\right\}^{\eta_2} \qquad (4.87)$$

where

ϕ and ϕ_o = absolute porosity and the intrinsic porosity, respectively;

k_o and S_h = intrinsic permeability and hydrate saturation, respectively;

ϕ_c = critical porosity where the intrinsic permeability is decreased to zero;

η_1 and η_2 = exponents or empirical parameters of the permeability equation.

Upscaled relative permeability and capillary pressure curves

Upscaled relative permeability and capillary pressure curves are normally called pseudo functions (i.e Pseudo relative permeability and pseudo capillary pressure). These are the curves or equations used for coarse grid simulation as against the fine grid curves (the rock/basecase). The dynamic pseudo functions, as their name indicates, require dynamic fine grid simulations to be run, and then the results are used to generate pseudos for the coarse models. The flow in the vicinity of wells is rather radial and is affected by high pressure gradient (Ding, 1995; Durlofsky,1999). Therefore, many of the upscaling techniques may not give good results if the heterogeneity in the well nearby is significant, which requires a specific treatment to be upscaled. Using near well upscaling can provide a significant improvement to the upscaling results. There are several methods developed to generate or improve two phase pseudo functions for upscaling. Generally, without regard to the upscaling method used, the upscaling process can be considered successful when the coarse model gives results as close as the fine model results, or in other words, the fine model can be replaced by the coarse model (Durlofsky and Chen, 2008). This is of course assuming that the fine model represents the "correct" answer of the problem investigated. Comparisons between the coarse and fine models are usually done on case by case bases. Modified Stone (1970) model is used to create the base case. Capillary pressure is also scaled by accounting for the hydrate phase in the equation.

$$S_w + S_g + S_H = 1 \;; \qquad P_w(S_w) += P_g - P_w$$

$$\frac{P_c}{P_c^e} = h_c(s_w) = \left(\frac{\frac{s_w}{(s_w+s_g)} - S_{wirr}}{1 - S_{wirr}}\right)^{-n_c}$$

4.10.2 Numerical Solutions

Numerical methods are performed by running reservoir fine-scale simulation to solve pressure

It has been presented in the previous chapter that non-Darcy effects including threshold pressure gradients affects the fluid flow in the low velocity, low permeability gas hydrate reservoir. The effects in the near-wellbore and interface boundaries can be investigated by modelling a radial system of gas production at a given constant rate. The flow rate can be gas production rate, water production rate or cumulative/total production rate. Considering the well as infinite conductivity, it can be assumed that the well-bore pressure and the pressure along the open portion of the reservoir are uniform and the integral of the flux over the perforated interval is equal to the constant specified rate. For the infinite acting reservoir, we have:

$$q_{psc} = -\int_{P_{ref}}^{P_{sc}} \frac{2\pi hkk_{rw\infty}}{\mu_p B_p} r \left.\frac{dP}{dr}\right|_{r=r_w} \quad (4.88)$$

$$\left.\frac{d\,(P-\lambda_{bw}r)}{dr}\right|_{r=r_w} = q_{gsc}\frac{\mu_g}{2\pi rhk_g}\frac{zTP_{sc}}{T_{sc}P} + \beta\rho_g\left(\frac{q_{gsc}}{2\pi rh}\frac{zTP_{sc}}{T_{sc}P}\right)^2 \quad (4.89)$$

$$\frac{\partial}{\partial t}\left(\phi\, S_p\rho_p\right) + \frac{\partial n_H}{\partial t} = -\nabla.(\rho_p v_p + \beta_p\rho_p v_p^2) + Q_p \quad (4.90)$$

$$-\left(\nabla\Phi_p\right) = \rho_p v_p + \beta_p\rho_p v_p^2 = \nabla\left(\frac{k}{\mu}P\nabla P\right) \quad (4.91)$$

Where

$$v_p = -\frac{k}{\mu}v_i\left(\frac{dP}{dr} - \alpha_v\right) \qquad ; \qquad \rho_p = \frac{M}{RT}P = \alpha P$$

In the radial coordinates, Pseudo-pressure method is employed to linearise the diffusivity equation by equating the pressure dependent terms (viscosity and gas compressibility) with the normalised pressure to a pseudo-pressure term as follows (Ji, et al., 2003; Makogon, 1997, Freij-Ayoub, R. et al (2007).

$$\psi(P) = \int_{P_{\mathrm{m}}}^{P} \frac{2P}{\mu Z} dP \quad (4.92)$$

Then, we could get a transient-pressure solution with dissociation kinetics and non-Darcy flow as follows:

$$\frac{1}{r}\frac{\partial}{\partial r}\left(r\frac{\partial P^2}{\partial r}\right) = \frac{1}{\lambda_t}\frac{\partial P^2}{\partial t} - \frac{1}{V}\frac{\partial (N_H)}{\partial t} \quad (4.93)$$

$$\left(\frac{1}{r}\frac{\partial P^2}{\partial r} + \frac{\partial^2 P^2}{\partial r^2}\right) = \left(\frac{1}{\lambda_t}\right)\frac{\partial P^2}{\partial t} - \frac{1}{V}\frac{\partial (N_H)}{\partial t} \quad (4.94)$$

$$\frac{1}{r}\frac{\partial}{\partial r}\left(r\frac{\partial P^2}{\partial r}\right) = \left(\frac{\phi\mu cr}{Pk} + \frac{\phi\mu cr}{P\beta k}\right)\frac{\partial P^2}{\partial t} - \frac{\left(K_{d,0}e^{-\frac{\Delta E_\infty}{RT}}\right)^2 Q_d\phi^3(1-S_h)^3\partial P^2}{2kQ_{sc}\partial t} \quad (4.95)$$

$$P_{ws}^2(\Delta t) = P_i^2(t) - \frac{Q_d Z_0 TP_{sc}}{2\pi rhk_{\mathrm{g}}T_{sc}}\left[ln\left(-\frac{\phi\mu(1-S_w)r^2}{4\lambda_t t}\right) - E_i\left(-\frac{\phi(1-S_h)^3}{4\alpha_v}\right)\right] \quad (4.96)$$

We define coefficient (correction factor) as a function of Knudsen number, *Kn*, as follows

$$\frac{1}{\lambda_t} = \frac{2\phi\mu(1-S_w)}{2P_m.Kn} + \frac{\mu(1-S_h)P^2}{\beta P_m.Kn} \quad (4.97)$$

$$\beta = \frac{1.485\mathrm{x}10^9}{k^{1.021}} \quad (4.98)$$

Threshold pressure gradient threshold pressure gradient can be related to pore pressure and saturation with the general formulation below (Li et al., 2019a; Sakhaee and Bryant, 2014; Tian, et al., 2018).

$$P_{t\lambda} = \alpha_1 \left(P_f\right)^{\alpha_2} \tag{4.99}$$

where α_1 and α_2 are fitting parameters

The well boundary flow condition proposed for the radial wellbore is written as:

$$Q_d = \lim_{x \to 0} \left(\frac{\pi r h k_g \beta}{\mu} . \frac{\partial P^2}{\partial r} \right) \tag{4.100}$$

The velocity constant of the dissociation front

$$\alpha_v = \lim_{K_d \to K_{d,0}} \left(\frac{2k\dot{m}_g^2}{\left(K_{d,0} e^{-\frac{\Delta E_\infty}{RT}}\right)^2 \left(P_{eq} - P_g\right)^2} \right) - P_{t\lambda} \tag{4.101}$$

Therefore,

$$q_{sc} = \frac{\pi h k_a k_{rg} \lambda_t Z_0 T_{sc} P}{\mu T P_{sc}} \frac{1}{ln(r_D)} \left[\left(- \frac{\phi \mu (1 - S_w) r^2}{4t} \right) - \left(- \frac{\phi (1 - S_h)^3}{4 \alpha_v} \right) \right] \tag{4.102}$$

Well pseudo functions are functions that represent the flow from grid blocks to the wellbore and could be used to keep the wells at their original position after upscaling. Azoug and Tiab (2003) studied the effect of using local grid refinement (LGR) instead of well pseudo functions on breakthrough time and length of production rate plateau. They found that results of using LGR are not as good as those obtained when using well pseudo functions. Durlofsky and Chen (2008) indicated that Emanuel and Cook (1974) introduced a method of calculating the well pseudo functions as follows:

$$\left(k_{rp}\right)_A = \frac{\sum_{i=1}^{nc} \left[k_{rp} C_p (P_e - P_w)\right]_i}{\sum_{i=1}^{nc} C_{pl} \left[\frac{\sum_{i=1}^{nl} (P_e \phi V)_i}{\sum_{i=1}^{nl} (\phi V)_i} - P_{wA} \right]} \tag{4.103}$$

$$\overline{k}_{rw}(S_w) = \frac{\sum_{i=l1}^{nc} \sum_{k=k1}^{Kc} (k_{rw} S_w T_x)_k}{\sum_{i=l1}^{nc} \sum_{k=k1}^{Kc} (T_x)_k} \tag{4.104}$$

$$\left(S_p\right)_A = \frac{\sum_{i=1}^{nl} (S_p \phi V)_i}{\sum_{i=1}^{nl} (\phi V)_i} \tag{4.105}$$

$$\overline{S}_w = \frac{\sum_{i=l1}^{lc} \sum_{k=k1}^{Kc} \left(V_p S_w\right)_k}{\sum_{i=l1}^{lc} \sum_{k=k1}^{Kc} \left(V_p\right)_{ik}} \tag{4.106}$$

where,

A = areal area; Cp = flow coefficient analogous to productivity index; krp = phase relative permeability; Pe and Pw = formation and wellbore pressures respectively; V = block volume; Sp = phase saturation; ϕ = porosity

The system of pressure equations was solved to obtain pressures solutions in fine grid blocks of the synthetic two-dimensional hydrate reservoir model. The aim here is to provide coarse scale flux that matches the fine scale model using near well upscaling method. The fine scale the two-dimensional reservoir model having dimensions of 50m x 50m and discretized into grids-blocks with dimensions of 1m x 1m, would have 50 x 50 uniform grid-blocks totalling 2500cells. The mesh coarsened to grids-blocks with dimensions of 10m x 10m would result to 5 x 5 grid-blocks totalling 25 cells for the upscale model. The pressure distribution and solutions are plotted over space and time respectively at the observation points x = 5 m, 10 m, 15 m, 20m and 25m and after a period of 10days, 100days, 500days and 1000days. The mesh of the fine and coarse scales shown in Figure 4.23. The solutions of the rock type pressure diffusivity equations are obtained for the fine grids and the upscaled model (with pseudo functions) using Stone (1970) permeability model as baseline. Finally, the results of the fine model were compared to the results of the upscaled model with the pseudo functions generated from different permeability equations.

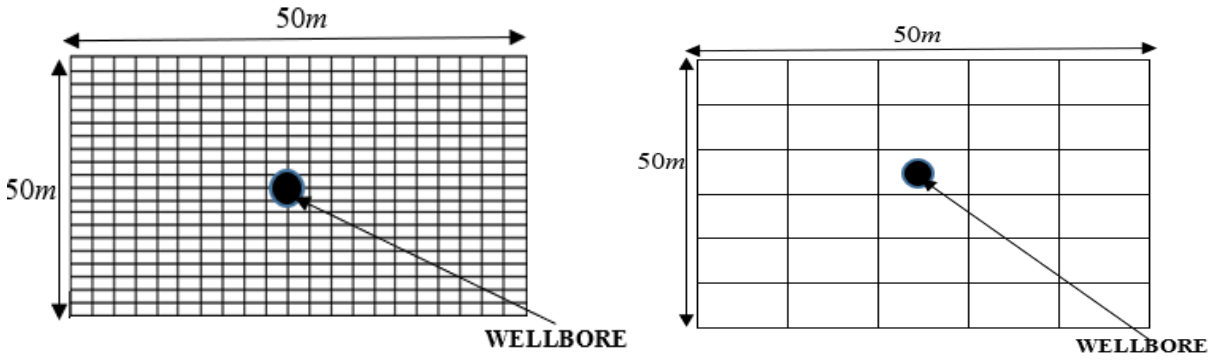

Fine grids scale model 2500 **Coarse grids scale model, 25**

Figure 4. 17 Grid Refinement and coarsened gridding model

4.10.3 Effect of coarsened gridding and flow-convergence into the wellbore.

Figures 4.18 and 4.19 showed the pressure distribution observed across the reservoir to the wellbore place at the centre of the discretised domain during dissociation at different time from the two models. Hydrate dissociation profiles are also shown. The dissociation rates and temperature values in the confining fluid are the same for the two models. It can be found that the with upscaled grids model the emergency of dissociation front around the wellbore is strong as can be seen from well discrete contours starting from early stage at 10days. The diffusion rate of the dissociation front for the upscaled model is obviously much faster than that of fine grids. The dissociation front of the hydrate with the fine grid model is mainly around the

wellbore from about 100 days. It implies that the dissociation front near the boundary are impeded and got to develop gradually and slower. However, hydrate seemed to have dissociated completely at 1000days in both models. With the upscaled (not upscale model is different from coarsened model had be explained) the vertical and horizontal expansion of the dissociation front basically synchronous. It implies that the upscaled model enable both the upper and lower wellbore to dissociate at same time and frequency. With the radius around the wellbore saturated at about the 100days, the upscaled model can be said to promote transmission of wellbore pressure and the decomposition front around the wellbore, which weaken inertial effect. Thus, research attention in advance modelling of the reservoir model and wellbore for gas hydrate simulation would involve accurate analysis of the wellbore flow complexity factors and near-wellbore upscaling and modelling.

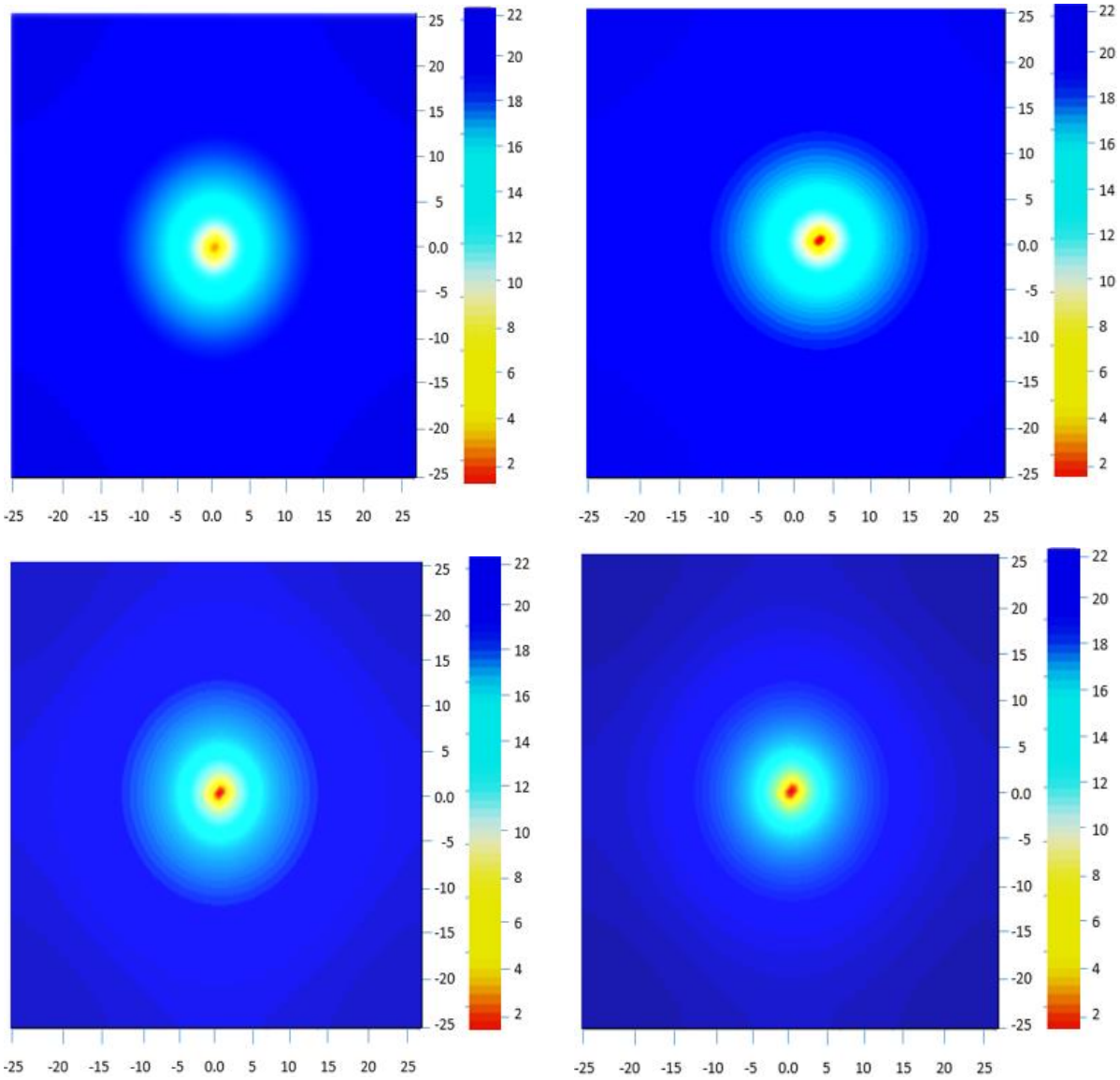

Figure 4. 18 Pressure distribution profile of fine-grids model

after 10, 100, 500 and 1000days.

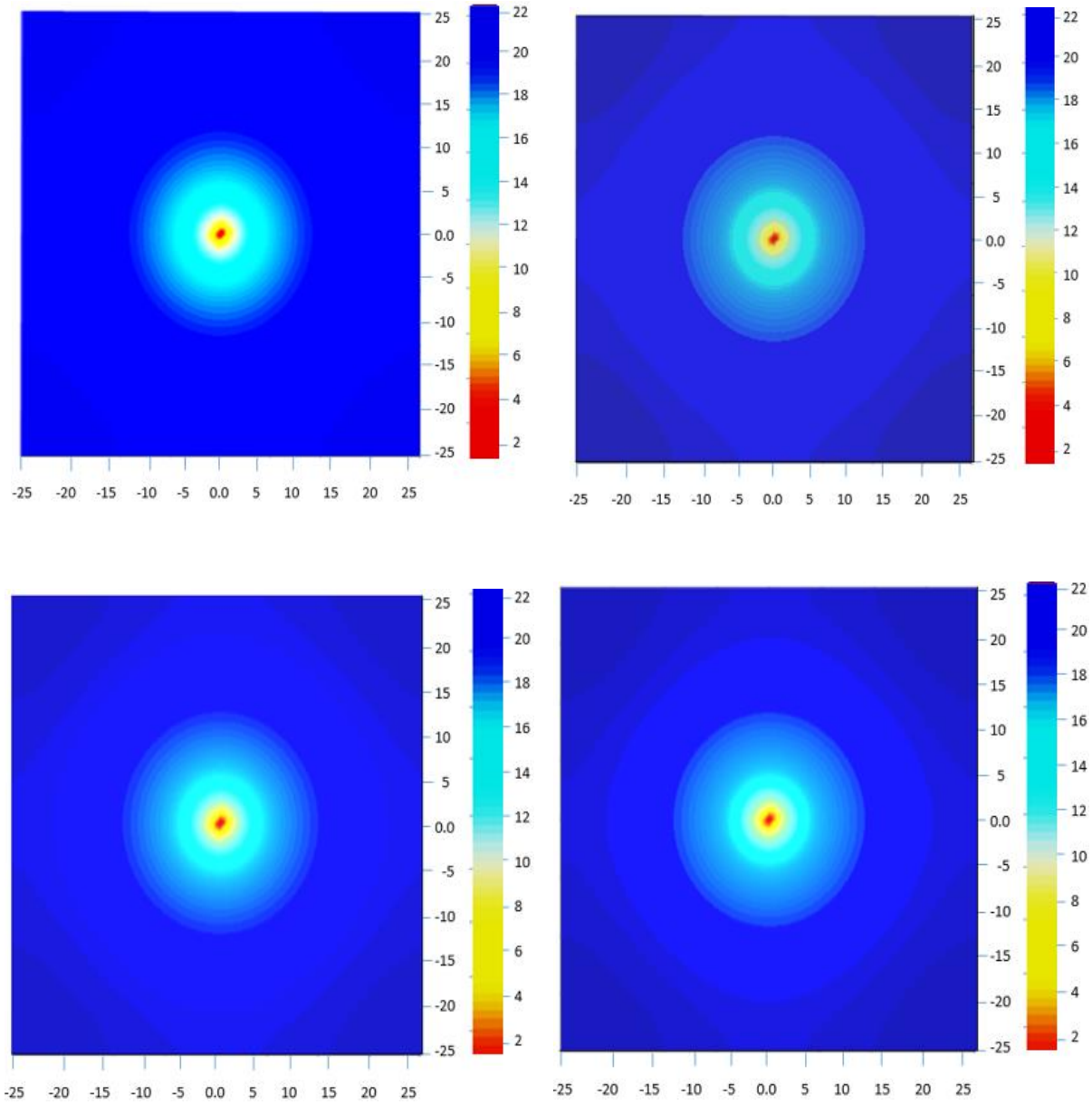

Figure 4. 19 Pressure distribution profile of coarse-grids/upscaled model after 10, 100, 500 and 1000days.

4.10.5 Effect on Various Relative Permeability and Capillary Pressure Equations

Figures 4.20 and 4.21 present the effects of relative permeability and capillary pressure equations respectively on rate of gas release from gas hydrate production. Data from table 4.1 in the previous section and from literature are processed and used in the analysis. Figure 4.39 showed that showed that all the models gave similar trend profile. The modified Stone model

which is also our upscale model showed the highest performance. All models are within matching performance with allowable error functions. However, there is need to evaluate the degree of accuracies; the difference in the highest performing model, Upscaled Stone Model and the hydrate model is wide and require further analyses to measure chances of over estimation or under estimation. The rate of release of aqueous molar gas fraction is also dependent on gas partial pressure and capillary pressure affects relative permeability. More so the exponents of each equation differ and has been shown to affect the performance of the various equations by Jang (2016). The results of the effects of the exponents parameter of relative permeability and capillary pressure equations can be found at the appendix D. In this study, a set of suggested fitting parameters are used. Figures 4.21 showed the effects of capillary pressure on the rates of the gas released from the hydrate. It can be noted that Stone model and Corey's portrayed similar behaviour while the hydrate model and Van Genuchten's appeared to perform closely. It is interesting that note that Stone model and Corey's had depicted higher relative permeability than the hydrate model and Van Genuchten's as seen in figure 4.20. The intrigues could come from the response of the aqueous saturation to pressure gradients leading to advective migration with dissociation front, with hydrate dissociation. Here force of inertia, slippage factor and threshold pressure would be at play. The other reason is need to incorporate the dependency of each equation or model to initial hydrate saturation. More so, the results have shown that the relative permeabilities are dependent on capillary pressure and consequently the effects on the aqueous flowrate and saturation.

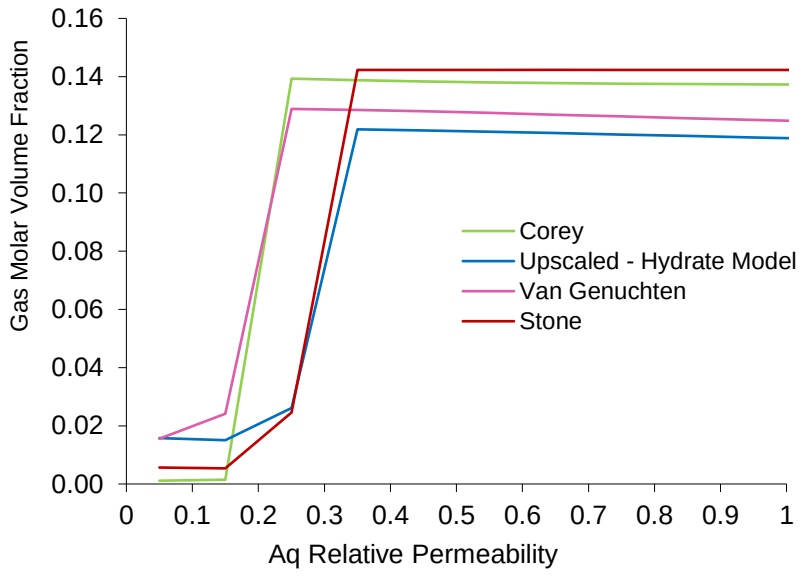

Figure 4. 20 Effects of Various Relative Permeability Equations on Gas Fractional Flow from Natural Gas Hydrate

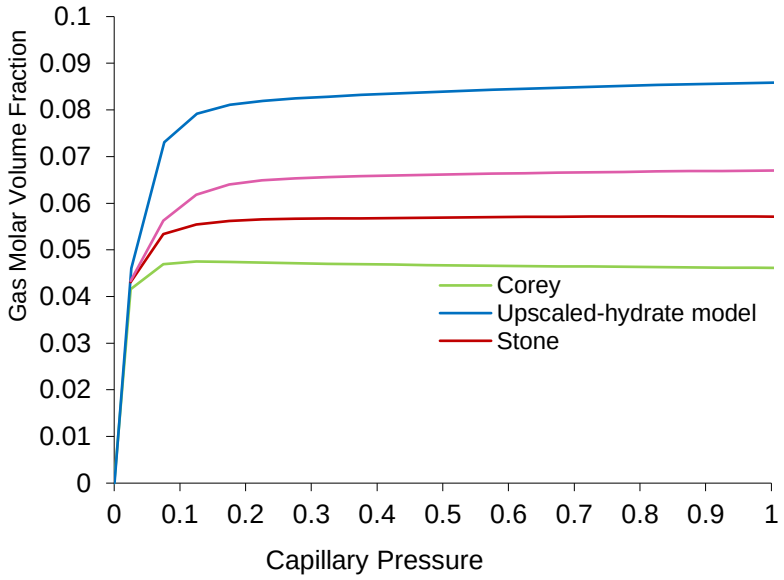

Figure 4. 21 Effects of Various Capillary Pressure Equations on Gas Fractional Flow from Natural Gas Hydrate

Conclusion:

The challenge of economic production of natural gas hydrate reservoirs has nexus to near wellbore complexity and the effect of convective mixing processes related to the fluid flow. Feature defying the flow mechanism has been analysed and conversely incorporated into the integrated approach that coupled the reservoir and wellbore as a continuum. Though the features are not exhaustive but ultimately the characterisation carried dealt with the more significant feature that can be impact the unconventional. In this section attention is given to capillary and relative permeabilities as two parameter that influence the gas recovery from hydrate bearing sediment greatly especially with consideration of the near wellbore flow complexity, and are two parameter that are highly dependent on the fluid flow characteristic including viscosity and saturations. The effect of hydrate saturation is accommodated in the non-Darcy flow assumptions which is related via the various parameter modelled. However, this need to be considered for conservative and accurate predictions. An important conclusion is that near wellbore modelling can be used to always benchmark relative permeability and capillary pressure values and upscaling makes reservoir simulation runs less difficult. Incorporating, therefore, into fully implicit fully coupled modelling should be advanced.

CHAPTER 5

CONCLUSIONS

5.1 Conclusion

A new fully implicit fully coupled reservoir-wellbore fluid flow model for natural gas hydrate application has been developed in this thesis. It allows for a more integrated modelling of gas hydrate flow behaviour by coupling the governing equations for the flows in the reservoir and wellbores for the simultaneous solutions of the systems of equations as a continuum. Though fully coupled modelling approach and solution had been suggested to provide better computational accuracy and a fit-for-purpose optimization platform, it has received limited attention in gas hydrate production studies. The thesis presented two outstanding novelty,

1. The new reservoir model that aggregated and simultaneously incorporated the inherent defying features to the gas hydrate fluid flow including threshold pressure gradient, diffusivity flux and Knudsen diffusion coefficient, gas slippage effects, thermal expansion and Joule-Thomson effects.
2. The fully implicit fully coupled reservoir-wellbore fluid flow model for gas hydrate application.

The descriptions of the procedure and advantages are summarised as follow:

- The thesis identified various microscopic and macroscopic flow feature defying the gas hydrate production, and aggregated them into the modelling approach of the fully implicit coupled reservoir-wellbore model.
- The advantage of the decoupled approach is that the reservoir flow model can be developed independent of the wellbore model. This takes less computational time but lower accuracy.
- The fully implicit fully coupled reservoir-wellbore flow model provided more accurate analysis of the parameters measured.
- In the decoupled method, the bottom-hole pressure which should couple reservoir flow model with the wellbore equations is decoupled from both models and is assumed to have a fixed value. This fixed value is used as the well boundary condition in the reservoir inflow performance analyses. The same fixed pressure is also used in the wellbore flow analysis to predict pressure drop across the well and fluid flow rate at the surface facilities. This allowed, albeit disadvantageous, for the wellbore to be developed without hydraulic communication with the reservoir. However, bottom-hole

pressure in real reservoirs are never constant. Instead, it fluctuates during reservoir production due to fluid depletion, especially in complex heterogeneous reservoirs like gas hydrate sediments. Besides, the common practice to control wellbore behaviour is to constraint the producing pressure or fluid rates at surface facilities and the pressure behaviour is transmitted down to the bottom hole pressure. For the gas flow through the high-pressure reservoir, the variations of pressure around the production well were large and as such would not follow the ideal Newtonian law to justify the use of constant properties. More so, using the decoupled approach lead to inaccurate predictions of surface flow rates and flow pressure which in turn affected the well performance predictions.

- The fully implicit fully coupled model incorporated the convective and diffusive mass fluxes and conversely the wellbore hydraulics, near-wellbore convective mixing processes/crossflow parameters; and offered an optimised production.

5.2. Summary of Results

From the sensitivity analysis of the variables evaluated, it was inferred that the identified parameters have significant influence on the well production performance. The comparative effect of the various sensitivity parameters on the gas production rate is performed using the Monte Carlo simulation. In this analysis,

- The sensible heat of dissociation has the highest influence. It could be concluded that fluid properties such as permeability anisotropy, diffusivity flux, slippage factors and threshold pressure gradient have significant influence on the gas production. The complete wellbore thermal capacity, however, is not treated as the essential target during the study but extrapolating the degree of influence of the sensible heat of dissociation would enable conclusion of important of thermal recovery and stimulation factor as one parameter to stands to have greatest influence o though it has a considerable effect on reducing wellbore temperature. Other parameters also showed significant percentage that cannot be neglected in managing and sustaining gas production from the hydrate reservoir.
- Develop pressure and temperature transients' interpretation workflow (numerical solutions) based on the analytical model.
- Evaluate the parameters for capillary pressure and relative permeability functions and analyse the effects of the different equations on gas hydrate production.

- The threshold pressure gradient (TPG) has significant implication on the non-Darcy flow in the low-permeability porous media. TPG enables pore network boundary that flow when the pressure gradient overcomes the viscous forces. Sensitivity analysis conducted showed the TPG influenced the pore pressure and the pressure derivative with initial declined rate performance and a later stabilised boundary performance effect. This is seen from the plot relationship that the larger the pore pressure, the larger the TPG, and the smaller the diffusion distance and the production rate.
- The thesis model has been developed based on stringent assumptions, inner boundary conditions and strictly derived numerical solutions; with high precision benchmarked validations. It is believed, therefore, that the results evaluated are reasonably accurate. Though it a challenging task solving the integrated model which coupled the reservoir fluid flow and wellbore hydraulics, combining with the potential of complex flow patterns in gas hydrate, the ensuing accuracy obtained using the integrated approach justifies the complexity of the models used.
- This thesis would help to understand the performance of the natural gas hydrate system and guide the reasonable development of the reservoir production. The findings have application in flow system planning and design, enabling optimization of the gas hydrate reservoir performance and the production well itself. Application of the model and/or the modelling approach, therefore, can help operators and researchers to refine their reservoir performance prediction procedures and to better manage the risk of flow assurances problems related to gas hydrates reservoir recovery. It can be leveraged on to improve recovery of other unconventional reservoir, benchmark flow sustainability, maximise production efficiency and streamline the resource management.

5.3 Recommendation for Future Work

Future work with respect to this research should include incorporation of geomechanics in the fully implicit fully coupled model. In this study, crucial elements of the hydrate reservoir geometry, structural consolidation and wellbore mechanical effect are not considered. Future studies can consider the stress and strain factors, poroelasticity and deformation phenomena related to gas hydrate sediment and incorporate the geomechanics in the fully implicit fully coupled reservoir-wellbore model. Also, the mechanical completion of the wellbore could be treated unit per unit (tubing wall and casing wall, cement wall and formation). In the current the system, contribution of each unit in the heat transfer analyses is ignored. The completion

was treated like a single tubing. In a strong temperature dependent process like gas hydrate production, every source of thermal effect should be considered. Thus, further studies related to models that coupled horizontal wellbore and multi branch wellbore are recommended. In summary, future work can consider –

- Incorporation of geomechanics into the fully implicit fully coupled reservoir-wellbore model.
- Incorporation of capillary pressure and permeability as a function of hydrate saturation rather than water saturation.
- Modelling and coupling the unique nature of the thermal wellbore and heat transfer mechanisms that unitised the wellbore completions (including tubing, annulus, insulation, casing, cementing), evaluate and integrate the combining effects of the thermal wellbore.
- Creating specialized statistical templates and automated design of the fully implicit fully coupled reservoir-wellbore modelling approach for industry analyses of gas hydrate performance.

REFERENCES

Abbaspour, M. and Chapman, K. S. (2008). Non-isothermal Transient Flow in Natural Gas Pipeline. *Journal of Applied Mechanics*, *75*(3). https://doi.org/10.1115/1.2840046

Anderson, B. D. O., Boswell, R., Collett, T. S., Farrell, H., Ohtsuki, S., White, M. D., & Zyrianova, M. V. (2014). Review of the findings of the Ignik Sikumi CO2-CH4 gas hydrate exchange field trial. *Energu Fuel*.

Aziz, K. and Settari, A. (1979). *Petroleum Reservoir Simulation*. Applied Sc. Publishers Ltd.

Adesina, F. et al. (2016). An improved model for estimating productivity of horizontal drain hole. *SPE-169386-MS*

Ahmadi, G., Ji, C., and Smith, D. H. (2010), Constant rate natural gas production from a well in a hydrate reservoir, *Energy Conversion & Management 2003; 44:*2403-2423.

Bhagwat, S. M., & Ghajar, A. J. (2014). A flow pattern independent drift flux model based void fraction correlation for a wide range of gas–liquid two phase flow. *International Journal of Multiphase Flow*, *59*, 186–205.

Deng, X., et al. (2020). An improved model for the migration of fluids caused by hydrate dissociation in porous media. *Journal of Petroleum Science and Engineering*, *188*, 106876.

Freij-Ayoub, R. et al (2007). A wellbore stability model for hydrate bearing sediments. *Journal of Petroleum Science and Engineering*, 57, *209–220*

Agarwal, R. K. (1980). A New Method to Account for Producing Time Effects When Draw-down Type Curves are Used to Analyse Pressure Build-up and Other Test Data. *Proceedings of SPE Annual Technical Conference and Exhibition*. https://doi.org/10.2523/9289-ms.

Ahmed, T., (2000) Reservoir Engineering Hand Book. Gulf Pub. Co, Houston, TX.

App, J.F. (2010). Non-isothermal and Productivity Behaviour of High Pressure Reservoirs, *SPE Journal, 15*, 50-63

Aregba, A.G. (2017). Gas Hydrate Properties, Formation and Benefits. *Open Journal of Yangtze Gas and Oil*, 2, 27- 44.

ASME, (2006). Guide for Verification and Validation in Computational Solid Mechanics. *The American Society of Mechanical Engineers,* ASME V, 10 – 2.

Atkinson, P.G. and Ramey, H.J. (1972). Problems of Heat Transfer in Porous Media. *52nd SPE Annual Fall Technical Conference and Exhibition*, Denver, Colorado.

Averbuch, D (2010) IFP Technologies for Flow Assurance: the Current State of the Art. Society for underwater Technology Journal, Rueil Malmaison Cesex, France.

Bahonar M. (2011). Transient Non-isothermal Wellbore Fluid Flow and Heat Transfer Modelling, *Ph.D Thesis*, University of Calgary.

Bai, Y. et al. (2009). The experimental and numerical studies on gas production from hydrate reservoir by depressurization. *Transport in porous media*, *79*(3), 443-468.

Beaudoin, Y. C., Boswell, R., Dallimore, S. R., and Waite, W. (2014a). *Frozen Heat: A UNEP Global Outlook on Methane Gas Hydrates*. United Nations Environment Programme, GRID-Arendal. Accessed 19 February 2018, from netl.doe.gov/sites/ default/files /netl-file/gas-hydrate-global-assessment-executive-summary.pdf.

Beaudoin, Y. C., Dallimore, S. R. and Boswell, R. (2014b). *Frozen Heat: A UNEP Global Outlook on Methane Gas Hydrates, Volume 2*. United Nations Environment Programme, GRID-Arendal. Accesses from https://www.grida.no/resources/6632.

Beggs, H. D. (1991). Production optimisation using NODAL analysis, oil and gas consultants international publications, Tulsa, Oklahoma.

Bellarby, J. (2009). *Well completion design*, Elsevier.

Bendakhlia, H. and Aziz, K. (1989). Inflow performance relationships for solution-gas drive horizontal wells, SPE 19823, Richardson, TX 75083-3836 USA.

Bergman, T. L., Lavine, A. S., Incropera, F. P., and DeWitt, D. P. (2011). *Introduction to heat transfer*. John Wiley & Sons

Besson, J. (1990). Performance of slanted and horizontal wells on an anisotropic medium *SPE-20965-MS, In: European Petroleum Conference*, The Hague, Netherlands.

Bhagwat, S. M., & Ghajar, A. J. (2014). A flow pattern independent drift flux model based void fraction correlation for a wide range of gas–liquid two phase flow. *International Journal of Multiphase Flow, 59*, 186–205.

Blöcher G., et al (2010). Conceptual Model for Coupling Geothermal Power Plants with Deep Reservoirs. In Proceedings of the World Geothermal Congress 2010, Bali, Indonesia.

Borraz-Sanchez, C. and Rios-Mercado, R. Z. (2004), A Non- Sequential Dynamic Programming Approach for Natural Gas Network Optimisation. Wseas transactions on systems, Is 4, Vol.3.

Boswell, R., Schoderbek, D., Collett, T., Ohtsuki, S., White, M., & Anderson, B. (2017). The Iġnik Sikumi Field Experiment, Alaska North Slope: Design, Operations, and Implications for CO2–CH4 Exchange in Gas Hydrate Reservoirs. *Energy & Fuels*, *31*(1), 140-153.

Bourdet, D. P. (2002). Well Test Analysis: The Use of Advanced Interpretation Models. *Handbook of Petroleum Exploration and Production*. https://doi.org/10.1016/s1567-8032(03)x8026-x

Bradley, H. B. et al. (1987). Petroleum engineering handbook, 1987 Ed., Society of Petroleum Engineers, Richardson, Texas.

Brill J. P. and Mukherjee. H. (1999). Multiphase flow in wells, Henry L. Doherty MF of AIME, SPE Inc. Richardson, Texas

Brogioli, D. and Vailati, A. (2001). *Diffusive mass transfer by nonequilibrium fluctuations: Fick's law revisited.* Phys. Rev. E. 63 (1–4): 012105

Bump, P. (2012). There's methane trapped at the bottom of the ocean, so obviously we should get it and burn it. *https://grist.org/climate-energy/theres-methane-trapped-at-the-bottom-of-the-ocean-so-obviously-we-should-get-it-and-burn-it/.*

Camacho, R.G. and Raghavan, R.(1987), Inflow Performance Relationship for Solution Gas Drive Reservoirs. SPE 16204, Richardson, Texas.

Catak, E. (2006). Hydrate dissociation during drilling through in-situ hydrate formations. Istanbul: Louisiana State University, http://etd.lsu.edu/docs/available/etd-01232006 230233/unrestricted/Catak_thesis.pdf.

Chan, E.T.S. and Chung S.H. (2004), Multi Criteria Genetic Optimization for Distribution Network Problems. International Journal of Advanced Manufacturing Technology, 24:517-532

Chen, L. et al. (2018). Construction and simulation of reservoir scale layered model for production and utilization of methane hydrate: The case of Nankai Trough Japan, *Energy 143*, 128 -140.

Chen, Z., Bai, W., Xu, W., and Jin, Z. (2010). An Analysis on Stability and Deposition Zones of Natural Gas Hydrate in Dongsha Region, North of South China Sea. *Journal of Thermodynamics*, *2010*, 1–6. https://doi.org/10.1155/2010/185639

Chong Z. R. (2016) Recoverable gas from hydrate-bearing sediments: pore network model simulation and macroscale analyses. *J. Geophys. Res. 116*, 1.

Chukwudozie, C. (2013). A variational approach to the modelling and numerical simulation of hydraulic fracturing under in-situ stresses. In *Proceedings of the 38th Workshop on Geothermal Reservoir Engineering*. Stanford, Calif.

Civan, F. (2011). *Porous Media Transport Phenomena*. John Wiley & Sons.

Clarke, M. A. and Bishnoi, P. R. (2001). Determination of the activation energy and intrinsic rate constant of methane gas hydrate decomposition. *Can. J. Chem. Eng., 79, 143*–147

Clarke, M.A. and Bishnoi, P.R. (2004). Determination of the intrinsic rate constant and activation energy of CO2 gas hydrate decomposition using in-situ particle size analysis. *Chem. Eng. Sci., 59,* 2983–2993.

Cooper, S. J. et al. (2016). Taufactor: an opensource application for calculating tortuosity factors from tomographic data. *SoftwareX*, 5, 203–210.

Cooper, S. J. et al. (2016). Taufactor: an opensource application for calculating tortuosity factors from tomographic data. *SoftwareX*, 5, 203–210.

Craft, B.C., Hawkins, M.F. and Terry, R.E. (1991). *Applied Petroleum Reservoir Engineering*, Prentice Hall Inc, Old Tappan, NJ, USA.

Cui, Y., et al. (2018). Review of exploration and production technology of natural gas hydrate,

Advances in Geo-Energy Research, 2, 53-62.

Cussler, E.L. (2009) *Diffusion: Mass Transfer in Fluid Systems*; Cambridge University Press: Cambridge, UK.

Dai, S., and Santamarina, J. C. (2013). Water retention curve for hydrate-bearing sediments, *Geophys. Res. Lett., 41*, 4176 – 4184

Dai, S., and Seol, Y (2014). Water permeability in hydrate-bearing sediments: A pore-scale study. *Geophys. Res. Lett., 40*, 5637–5641

Dake, L.P. (2001). The practice of reservoir engineering, Revised Ed., Elsevier Science Amsterdam

da Silva, D.V.A. and Jansen, J.D. (2015). A Review of Coupled Dynamic Well-Reservoir Simulation. *IFAC-Papers Online*, *48*, 6, https://doi.org/10.1016/j.ifacol.2015.08.037

Davie, M. K. & Buffett, B. A. (2003). Sources of methane for marine gas hydrate: Inferences from a comparison of observations and numerical models, *Earth Planet. Sci. Lett., 206, 51– 63.*

Dawe et al (2007), Modelling of decomposition of a synthetic core of methane gas hydrate by coupling intrinsic kinetics with heat transfer rates. Can. J. Chem. Eng. 67, 948–954

De Waele, A. T. A. M. (2017). Basics of Joule–Thomson Liquefaction and JT Cooling. *Journal of Low Temperature Physics*. 186 (5–6): 385–403.

Dikken, B.J. (1990), Pressure drop in horizontal wells and its effect on production performance. J. Pet. Technol. 42 (11), 1426–1433.

Dillon, W. (1992), Gas (Methane) Hydrates – A New Frontier. United States Geological Survey. *http://marine.usgs.gov/fact-sheets/gas-hydrates/title.html*

Donev J.M.K.C. *et al*, (2021). Energy Education - Fossil fuel [Online]. Available: *https://energyeducation.ca/encyclopedia/Fossil_fuel*. [Accessed: July 27, 2021].

Duru, O.O. and Horne, R.N. (2010a). Modelling Reservoir Temperature Transients and Reservoir-Parameter Estimation Constrained to the Model, *SPE Reservoir Evaluation & Engineering*, **13**, 873-883.

Duru, O.O. and Horne, R.N. (2010b). Joint Inversion of Temperature and Pressure Measurements for Estimation of Permeability and Porosity Fields. *SPE Annual Technical Conference and Exhibition*, Florence, USA.

Duru, O.O., and Horne, R.N. (2011). Combined Temperature and Pressure Data Interpretation: Applications to Characterization of Near-Wellbore Reservoir Structures, *SPE Annual Technical Conference and Exhibition*, Denver, Colorado, USA.

Dutch, S. (2009) Natural Gas Hydrates: Structure II. University of Wisconsin - Green Bay.

Edmister, W. C and Lee, B. I. (1984). *Applied Hydrocarbon Thermodynamics*. Vol. 1 (2nd ed.). Gulf Publishing.

Epstein, N. et al (1989). On tortuosity and the tortuosity factor in flow and diffusion through porous media, *Chemical Engineering Science, 44*, 3, 777-779.

Ertekin, T., King, G.R., and Schwerer, F.C. (1986). Dynamic Gas Slippage: A Unique Dual-Mechanism Approach to the Flow of Gas in Tight Formations.*SPE Form Eval 1* (1), 43–52.

Ertekin, T., King, G.R. and Schwerer, F.C. (2001). Dynamic Gas Slippage: A Unique Dual-Mechanism Approach to the Flow of Gas in Tight Formations. *SPE Formation Evaluation* 1 (1): 43–52. http://dx.doi.org/10.2118/ 12045-PA.

Evans, R.D. and Civan, F. (1994). Characterization of Non-Darcy Multiphase Flow in Petroleum Bearing Formation. Final Report for US Department of Energy Assistant Secretary for Fossil Energy.

Fanchi, J. R. (2018). Principles of Applied Reservoir Simulation, Elsevier Gulf Professional Publishing.

Finsterle, S. (2010). iTOUGH2 Universal Optimization Using the PEST Protocol. Berkeley, University of California, USA.

Foroozesh, J., Abdalla, A.I.M. and Zhang, Z. (2018). Pore Network Modelling of Shale Gas Reservoirs: Gas Desorption and Slip Flow Effects. *Transport in Porous Media, 126*, 633–653 https://doi.org/10.1007/s11242-018-1147-6.

Frick, T.P., Economides, M.J., 1993. Horizontal well damage characterization and removal. SPE Prod. Fac. 8 (1), 15–22.

Feng, Y. et al. (2019). Enhancement of gas production from methane hydrate reservoirs by the combination of hydraulic fracturing and depressurization method. *J. Energy conversion and management*, 184: 194-204.

Furui, K., Zhu, D., Hill, A.D., 2002. A rigorous formation damage skin factor and reservoir inflow model for a horizontal well. SPE Prod. Fac. 18 (3), 151–157.

Gabitto, J. F., and Tsouris, C. (2014). Physical properties of gas hydrates: A review. *J. Thermodyn., 7*, 2176

GASTEG, (1999), Pressure and Network Analysis. Module 4, Universiti Technologi Malaysia, 25-50. Johor Bharu, Malaysia.

Ge, L. et al. (2014). Design of Pressure and Temperature Monitoring Device While Drilling in Deepwater Surface. *Transducer Microsystem Tech. 33*, 92–94.

Geffen, T.M., Parrish, D.R., Haynes, G.W., Morse, R.A., 1952. Efficiency of gas displacement from porous media by liquid flooding. J. Pet. Technol. 4 (2), 29–38.

Ghanbarian, B., Hunt, A.G., Ewing, R.P. and Sahimi, M. (2013). Tortuosity in porous media: a critical review. *Soil Sci. Soc. Am. J. 77* ,5, 1461–1477.

Graue, G. E. (2010). Natural gas hydrates. Norway: University of Bergen. Accessed: http://cdn.intechopen.com/pdfs/11475/InTech-Natural_gas_hydrates.pdf.

Gringarten, A. C. (2008). From straight lines to deconvolution: The evolution of the state of

the art in well test analysis. *SPE Reservoir Evaluation & Engineering, 11 (1),* 41- 62. doi.org/10.2118/102079-PA

Gudmundsdottir, H. (2102), A Coupled Wellbore-Reservoir Simulator utilizing Measured Wellhead Conditions, *University of Iceland Reykjavik*, Iceland.

Guo B., Lyons W.C and Ghalambor A. (2007). Petroleum Production Engineering. A Computer-Assisted Approach. Elsevier Science & Technology Books, Oxford, UK

Guo, C., Wei, M. and Liu, H. (2015). Modelling of gas production from shale reservoirs considering multiple transport mechanisms. *PLoS One 10, 0143649,* 1–24.

Gao, Q. et al. (2021). Experimental study on Fluid Production from Methane Hydrate Sediments under the Marine Triaxial Condition. *J. Nat. Gas Sci. Eng. 85*, 103707.

Grover, T., Moridis, G. J., and Holditch, S. A. (2008). Analysis of Reservoir Performance of the Messoyakha Gas Hydrate Reservoir. doi.org/10.2118/114375-ms

Gupta, A.; Lachance, J.; Sloan, E. D.; Koh, C. A. (2008). Measurements of methane hydrate heat of dissociation using high pressure differential scanning calorimetry. *Chem. Eng. Sci., 63* (24), 5848−5853

Hagdu T., Zimmerman R. and Bodvarsson G. (1995). Coupled ReservoirWellbore Simulation of Geothermal Reservoir Behavior. Geothermics, 24(2):145-166

Hågenvik, C. (2013). CO2 Injection in Hydrate Bearing Sandstone with Excess Water. Norway: University of Bergen.

Halliburton (2017), well-completion-selection-optimization - using-coupled-reservoir-well-hydraulics-simulators. *https://halliburtonblog.com/ well-completion-selection-optimization*

Hardwick, J. S. and Mathias, S. A. (2018). Masuda's sandstone core hydrate dissociation experiment revisited. *Chemical Engineering Science, 175,* 98–109.

Hasan, A.R. and Kabir, C.S. (2009). Modelling two-phase fluid and heat flows in geothermal wells. J. Pet. Technol. 71 (1–2), 77–86.

Hasan, A.R. and Kabir, C.S. (2002). Fluid Flow and Heat Transfer in Wellbores. Society of Petroleum Engineers, Richardson, TX. (Chen friction en)

Hassanizadeh, M. (1986). *Derivation of basic equations of mass transport in porous media: generalized Darcy's and Fick's laws, Advances in Water Resources,* Vol.9, Is. 4.

Hawkins, M.F., 1956. A note on the skin effect. J. Trans. AIME 207 (12), 356–357.

He, Y. (2012) Formation of methane and CO2 hydrate in bulk and in porous media. china: wohrmann print service.

Heidemann, R.A.; Jeje, A.A.; Mohtadi, F. 1984. *An Introduction to the Properties of Fluids and Solids*. University of Calgary Press, Calgary, AB

Hillston, J. (2003). Model validation and verification. Edinburgh: University of Edinburgh.

Holder G. D., (1982) Development of Methane Hydrate Production Method, National Institute of Advanced Industrial Science and Technology. Japan.

Hong, H., Pooladi-Darvish, M. and Bishnoi, P.R. (2002). Analytical modelling of gas production from hydrates in porous media. *J. Can. Pet. Technol.*, *42*, 45–56.

Huneker, R. H. (2010). Natural gas production and CO_2 sequestration in a class 2 hydrate accumulation: a numerical simulation study. *Delft University of technology*, Netherlands.

Ikoku, C. U. (1992), Natural Gas Engineering – A Systems Approach. Krieger Publishing Company, Florida.

Itodo, E.J. (2010), Interference of Oil and Gas Flow: Optimization Strategy and Network Analysis. Institute of Petroleum Studies, Heriot-Watt University, Edinburgh, UK.

Jadhawar et al, 2005, Evaluation of Gas production potential from gas deposits in National Petroleum Reserve Alaska using numerical simulations.

Jang, J., and Santamarina, J. C. (2011). Recoverable gas from hydrate-bearing sediments: Pore network model simulation and macroscale analyses. *J. Geophys. Res.*,*116*, B08202,

Jang, J., and Santamarina, J. C. (2014). Evolution of gas saturation and relative permeability during gas production from hydrate-bearing sediments: Gas invasion vs. gas nucleation. *J. Geophys. Res. Solid Earth*, *119*, 116–126.

Jansen J.D. and Currie P.K. (2004), Modelling and Optimization of Oil and Gas Production, Systems. Delft University of Technology, The Netherland.

Javadpour, F. (2009). Nanopores and Apparent Permeability of Gas Flow in Mudrocks (Shales and Siltstone). *Journal of Canadian Petroleum Technology*, *48*(08), 16–21.

Javadpour, F., Fisher, D., & Unsworth, M. (2007). Nanoscale Gas Flow in Shale Gas Sediments. *Journal of Canadian Petroleum Technology*, *46*(10).

Ji, C., Ahmadi, G. and Smith, D. H. (2003), Natural gas production from hydrate decomposition by depressurization, *Chem. Eng. Sci.* 56, 5801–5814.

Jia, B., Tsau, J., and Barati, R. (2018). Experimental and numerical investigations of permeability in heterogeneous fractured tight porous media. *Journal of Natural Gas Science and Engineering*. https://doi.org/10.1016/j.jngse.2018.08.011

Jiang, B. et al, (2016). Multiple fracturing parameters optimization for horizontal gas well using a novel hybrid method. J. Nat. Gas. Sci. Eng. 34, 604–615.

Johansen, T.E., Khoriakov, V. (2007) Iterative techniques in modeling of multi-phase flow in advanced wells and the near well region. J. Pet. Sci. Eng. 58 (1–2), 49–67.

Johnson, A., Patil, S. and Dandekar, A. (2011). Experimental investigation of gas-water relative permeability for gas-hydrate-bearing sediments from the Mount Elbert Gas Hydrate Stratigraphic Test Well, Alaska North Slope, *Mar. Pet. Geol.*,*28*, 2, 419–426.

Jones S. C. and Bird R.B. (1985). Calculation of diffusion coefficient of dilute gases and of

the self-diffusion coefficient of dense gases. *AIChE J., 4,* 2,137–142.

Jones, S.C. (1987). Using the Inertial Coefficient to Characterize Heterogeneity in Reservoir Rock. *SPE Annual Technical Conference and Exhibition*, Dallas, Texas.

Kanno, T. et al (2014). In-situ Temperature Measurement of Gas Hydrate Dissociation during the World-First Offshore Production Test. Paper presented at the Offshore Technology Conference, Houston, Texas.

Kast, W., and Hohenthanner, C. (2000) Mass transfer within the gas-phase of porous media. *Int. J. Heat Mass Transf*er, 43, pp807–823.

Kazeem A. L., (2007). Constructing inflow performance relationship from Surface Measurements: Retreating to the Fundamentals, *Shell Petroleum Development Company*, Nigeria.

Keelan, D.K., Pugh, V.J., (1975) Trapped-gas saturations in carbonate formations. Soc. Pet. Eng. J. 15, 149–160.

Khoriakov, V., Johansen, and A.C., Johansen, T.E. (2012) Transient flow modelling of advanced wells. J. Pet. Sci. Eng. 86–87, 99–110.

Kleinberg, R. L., Flaum, C. and Collett T., (2005). *Magnetic Resonance Log of Mallik 5L-38 Gas Hydrate Production Research Well: Gas Hydrate Saturation, Growth Habit, and Relative Permeability*. Natural Resources Canada, Northwest Territories, Canada.

Kim H., et al (1987). Kinetics of methane hydrate decomposition. *Chemical Engineering Science, 42,* 1645–1653.

Kimoto, S. et al (2010), A chemo–thermo–mechanically coupled analysis of ground deformation induced by gas hydrate dissociation, International Journal of Mechanical Sciences 52 (2010) 365–376.

Konno, Y. et al. (2016). Hydraulic fracturing in methane-hydrate-bearing sand. *J. RSC advances,* 6(77): 73148-73155.

Kumar, A. et al. (2010). Experimental determination of permeability in the presence of hydrates and its effect on the dissociation characteristics of gas hydrates in porous media, *J. Petrol. Sci. Eng.,70,* 1, 114–122.

Kurihara, M., and Ouchi, H. (2011). Gas Production from Methane Hydrate Reservoirs. *In Proceedings of the 7th International Conference on Gas Hydrates*, Edinburgh, UK,

Kurihara, M., et al. (2011). Analysis of formation pressure test results in the Mount Elbert methane hydrate reservoir through numerical simulation. *Marine and Petroleum Geology*, *28*(2), 502–516.

Kvenvolden, A and Lorenson, T. D. (2001). The global occurrence of natural gas hydrate. *J. Natural Gas Hydrates: Occurrence, Distribution, and Detection: Occurrence, Distribution, and Detection,* 124: 3-18.

Lake W. L. (2007), Petroleum Engineering Handbook, University of Texas at Austin, SPE, Richardson, TX, USA.

Landman, M.J., (1994) Analytic modelling of selectively perforated horizontal wells J. Pet. Sci. Eng. 10 (3), 179–188.

Lanfrey, P.Y., Kuzeljevic, Z. and Dudukovic, M. (2010). Tortuosity model for fixed beds randomly packed with identical particles. *Chem. Eng. Sci. 65*, 5, 1891–1896.

Lee et al, (2003) Review on the gas hydrate development and production as a new energy resource. KSCE Journal of Civil Engineering. 15, 689–696.

Lee, J. et al. (2011). Review on the Gas Hydrate Development and Production as a New Energy Resource. *KSCE Journal of Civil Engineering., 15*. 689-696.

Li, J. et al., (2019). Pore-scale study of the pressure-sensitive effect of sandstone and its influence on multiphase flows. *Pet Sci. 20*, 16, 382–95

Li, G.; Moridis, G. J.; Zhang, K. and Li, X. S. (2010a). The Use of Huff and Puff Method in a Single Horizontal Well in Gas Production from Marine Gas Hydrate Deposits in the Shenhu Area of South China Sea. *SPE, Proceedings of International Oil and Gas Conference and Exhibition in China*.

Li, G.; Moridis, G. J.; Zhang, K. and Li, X. S. (2010b). Evaluation of Gas Production Potential from Marine Gas Hydrate Deposits in Shenhu Area of South China Sea. *Energy Fuels, 24*(11), 6018–6033.

Li, G., Li, X.S., Tang, L.G. and Zhang, Y. (2007). Experimental investigation of production behaviour of methane hydrate under ethylene glycol stimulation in unconsolidated sediment. *Energy Fuels 21 (6),* 3388–3393.

Li, H. et al. (2018), A semi-analytical model for predicting inflow profile of horizontal wells in bottom-water gas reservoir, State Key Laboratory of Oil and Gas Reservoir Geology and Exploitation, Southwest Petroleum University, Chengdu, China.

Li, K., and Horne, R. N. (2001). Gas Slippage in Two-Phase Flow and the Effect of Temperature. *SPE Western Regional Meeting*.

Li, K., and Horne, R. N. (2004). Experimental Study of Gas Slippage in Two-Phase Flow. *SPE Reservoir Evaluation & Engineering*, *7*(06), 409–415.

Li, S., Lian, P.Q., Li, X., (2009) Non-steady state model of gas reservoir and horizontal well wellbore coupling. J. Southwest. Pet. Univ. 31 (1), 53–57.

Liang, H. et al (2010). Study of the permeability characteristics of porous media with methane hydrate bypore network model, *J. Nat. Gas Chem.,19,* 3, 255–260.

Linga, G., Mathiesen, J. and Renard, F. (2017). Self-similar distributions of fluid velocity and stress heterogeneity in a dissolving porous limestone, *J. Geophysical Res: Solid Earth,122,* 1726–1743, doi:10.1002/2016JB013536.

Liu, F. et al. (2018). *Managing Information of Gas Hydrate Reservoirs of the South China Sea in an Integrated GIS Database.* Springer, 37-44. Singapore.

Liu, H., Georgi, D. and Chen, J. (2015). Correction of source rock permeability measurements owing to slip flow and Knudsen diffusion: a method and its evaluation. *Pet. Sci. 15(1),* 116–125.

Liu, X., and Flemings, P. B. (2007). Dynamic multiphase flow model of hydrate formation in marine sediments, *J. Geophys. Res.,112,* B03101.

Liu, Y., Strumendo, M. and Arastoopour, H. (2009). Simulation of methane production from hydrates by depressurization and thermal stimulation. *Ind. Eng. Chem. Res.*, 48, 2451–2464

Livescu, S., Durlofsky, L.J. and Aziz, K. (2010). A semi-analytical thermal multiphase wellbore-flow model for use in reservoir simulation. *SPE journal*, *15*(03), pp.794-804.

Lu, S. M. (2015). A theoretical study of the hydration of methane, from the aqueous solution to the SI hydrate-liquid water-gas coexistence. *Int. J. Mol. Sci. 17*, 378.

Luo, E. el at. (2019). Analytical Solutions for Non-Darcy Transient Flow with the Threshold Pressure Gradient in Multiple-Porosity Media. *Mathematical Probs. in Engineering, Volume, Vol. 2019*, 13

Makogon, Y. F. (1997). *Hydrates of hydrocarbons*. Pennwell Books. Tulsa, OK.

Massanori, K. (2011). Gas production from methane hydrate reservoirs. International Conference on Gas Hydrate. *Edinburgh*, Scotland.

Masuda, Y. et al. (1997), Numerical calculation of gas production performance from reservoirs containing natural gas hydrates, *SPE J.,29* (3), 201–210.

Masuda, Y. (1999). Modeling and experimental studies on dissociation of methane gas hydrates in berea sandstone cores. *Proceedings of the Third International Gas Hydrate Conference*.

Matyka, M., A. Khalili, and Z. Koza (2008), Tortuosity-porosity relation in porous media flow, *Phys. Rev. E,78*, (2), 026,306

Maurer Engineering Inc., (1996) Wellbore Hydraulics Model (Hydmod3) Theory and User's Manual, *Maurer Engineering Inc.*, Houston, Texas 7701 8

McCabe, W. L. and Smith, J. C. (1973) Unit Operations of Chemical Engineering. 3rd Ed, New York: McGraw-Hill, 31 - 101.

McCormick and Bellamy, C. J. (1968) A Computer Program for the Analysis of Pipes and Pumps**.** The Journal of the Institution of Engineering Australia, 38, (3): 51 – 58.

Michael V. (2007) Joint Industry Project (JIP) to Quantify Hydrate Management Risks. Research & Technology Development, the University of Tulsa,

Miller, C.W. (1980), Wellbore User's Manual. Berkeley, University of California, Report, no. LBL-10910, USA.

Minagawa, H., R. et al. (2005). Water permeability measurements of gas hydrate-bearing

sediments, paper presented at Fifth International Conference on Gas Hydrate.

Minghao, Y. et al, (2016), Numerical study of gas production from methane hydrate deposits by depressurization at 274K, *Journal of Applied Energy*, 17, 10.013

Mo M, Hossein G, Matthew A. M. (2003), Pipeline Design and Construction: A Practical Approach. 2nd Ed; New York: ASME.

Moridis, G. J. (2014). *TOUGH+HYDRATE v1.5 User's Manual: A Code for the Simulation of System Behaviour in Hydrate-Bearing Geologic Media*. Lawrence Berkeley National laboratory, Berkeley, CA.

Moridis, G. J. et al. (2008). Toward Production from Gas Hydrates: Current Status, Assessment of Resources, and Simulation-based Evaluation of Technology and Potential. Lawrence Berkeley National Laboratory

Moridis, G.J. and Collett T.S. (2003). *Strategies for Gas Production from Hydrate accumulations Under Various Geologic Conditions.* Report LBNL-52568, Lawrence Berkeley Natl. Laboratory, Berkeley, California.

Moridis, G. J., Kowalsky, M. B. and Pruess, K. (2007). Depressurization-Induced Gas Production from Class-1 Hydrate Deposits. *SPE Reservoir Evaluation & Engineering 10.5*: 458-81. Web.

Mousavi, M., & Bryant, S. L. (2012). Connectivity of Pore Space as a Control on Two-Phase Flow Properties of Tight-Gas Sandstones. *Transport in Porous Media*, *94*(2), 537–554.

Myshakin, E.; Gamwo, I. and Warzinski, R .(2009). *Experimental Design Applied to Simulation of Gas Productivity Performance at Reservoir and Laboratory Scales Utilizing Factorial ANOVA Methodology.* In Proceedings of the TOUGH Symposium, Berkeley, CA, USA, 14–16

Naderi, M., Rostami, B., Khosravi, M., (2015) Effect of heterogeneity on the productivity of vertical, deviated and horizontal wells in water drive gas reservoirs. J. Nat. Gas. Sci. Eng. 23, 481–491.

Nagao, J. (2012), Development of methane hydrate production method. National institute of advanced industrial science and technology. Japan: national institute of advanced industrial science and technology.

Narayanan, G. A. (2004). An Assessment of Methane Hydrate Recovery and Processing at Hydrate Ridge. USA: FSc 503 http://www.ems.psu.edu/~elsworth/courses/egee580

Nicholls T. (2009) How the energy industry works – an insider guide. Silverstone Communications Ltd, London, UK

Novy, R.A. (1995) Pressure drops in horizontal wells: when can they be ignored*? SPE Reservoir Eng.* 10 (1), 29–35.

Ohaegbulam, M. C., Izuwa N. C., and Onwukwe S. I. (2017). Analysis of Wellbore Pressure Drop on Horizontal Well Performance. *Oil and Gas Res, 3*: 138.

Osiadacz A.J. and Chaczykowski M. (2001). Comparison of Isothermal and Non-isothermal Pipeline Gas Flow Models. *Chem. Eng. Journal, 81*, 41-51.

Osiadacz A.J. (1987). *Simulation and Analysis of Gas Network*. E&FN Spon., London.

Osunsanya, B. (2013), Domestic Gas Market: Challenges and Opportunities for Expanding Gas Utilization. Oando Gas and Power Limited, Nigeria

Ouyang, L.B., Huang, W.S.B., (2005) A Comprehensive Evaluation of Well-completion Impacts on the Performance of Horizontal and Multilateral Wells[C]//SPE Annual Technical Conference and Exhibition, Dallas, Texas.

Ozkan, E., Sarica, C., Haci, M., (1999) Influence of pressure drop along the wellbore on horizontal-well productivity. J. SPEJ 4 (3), 288–301.

Ozkan, E., Raghavan, R., and Apaydin, O.G. (2010). Modelling of Fluid Transfer from Shale Matrix to Fracture Network. Paper SPE 134830 presented at the SPE ATC&E, Florence, Italy, http://dx.doi.org/10.2118/134830-MS.

Pan, L. and Oldenburg, C. M. (2014), T2Well - An Integrated Wellbore–Reservoir Simulator, *Earth Sciences*, CA 94720, USA

Parsi, M et al. (2014). A comprehensive review of solid particle erosion modeling for oil and gas wells and pipelines applications. *Journal of Natural Gas Science and Engineering*, 21, 850-873, https://doi.org/10.1016/j.jngse.2014.10.001.

Pascal, H., Quillian, R.G., and Kingston, J. (1980). Analysis of Vertical Fracture Length and Non-Darcy Flow Coefficient Using Variable Rate Tests, *SPE 9438*, Dallas, USA.

Peng, L. (2022). Dynamically coupled reservoir and wellbore simulation in two-phase flow Systems: A Critical Review. *Processes 10*, 9: 1778. doi.org/10.3390/pr10091778

Penmatcha, V.R., Aziz, K., (1998) A comprehensive reservoir/wellbore model for horizontal wells. J. SPEJ 4 (3), 224–234.

Perry, R. H. and Green, D. W. (1984). *Perry's Chemical Engineers' Handbook*. McGraw-Hill. ISBN 978-0-07-049479-4

Phale, H. A. (2006) Simulation study on injection of CO_2Micro-emulsion for methane recovery from gas hydrate reservoirs. Alberta, Canada: SPE 100541.

Pooladi-Darvish, M. and Hong H., (2004), "Simulation of Depressurization for Gas Production from Gas Hydrate Reservoir", University of Calgary, Journal of Canadian Petroleum Technology. vol. 44, pp. 39-46,

Pourafshary, P. et al. (2009). A compositional wellbore/reservoir simulator to model multiphase
flow and temperature distribution. *Journal of Pet. Sc. and Engineering*, *69*(1-2), 40-52.

Pruess, K. Oldenburg, C. and Moridis, G. (1999). *TOUGH2 User's Guide*, Version 2.0. Berkeley, University of California, USA

Pruess, K. (2002). Mathematical modelling of fluid flow and heat transfer in geothermal systems - An introduction. Geothermal Training Manual, Orkustofnun, Reykjavík, Iceland.

Ratnakar, R.R. and Dindoruk, B. (2022). The Role of Diffusivity in Oil and Gas Industries: Fundamentals, Measurement, and Correlative Techniques. *Processes*, *10*, 1194 https://doi.org/10.3390/pr10061194

Rivera Ayala, M. A. (2010). Coupled geothermal reservoir-wellbore simulation with case study for the Námafjall eld, N-Iceland. University of Iceland, Reykjavík, Iceland.

Rubin, B. (2010). Accurate Simulation of Non-Darcy Flow in Stimulated Fractured Shale Reservoirs. Paper SPE 132093 presented at the SPE Western Regional Meeting, Anaheim, California, 27–29 May. http:// dx.doi.org/10.2118/132093-MS.

Rui Sun, Z. D. (2006) An accurate model to predict the thermodynamic stability of methane hydrate and methane solubility Bryin marine environments. Beijing, China: State Key Laboratory of Lithospheric Evolution.

Rutqvist, J and Moridis, G.J. (2007), Numerical Studies on the Geomechanical Stability of Hydrate-Bearing Sediments, Lawrence Berkeley National Laboratory, SPE OTC 188, Houston, Texas

Sakhaee-Pour, A. and Bryant, S. L. (2012). Gas Permeability of Shale. *SPE Reservoir Evaluation & Engineering*, *15*(04), 401–409.

Sakhaee-Pour, A. and Bryant, S. L. (2014). Sakhaee PA, Bryant SL. Effect of pore structure on the producibility of tight-gas sandstones. AAPG Bull. 2014;98(4):663–94.

Saurel, R., and Abgrall, R. A (1999) Multiphase godunov method for compressible multifluid and multiphase flows. *Journal of Computational Physics*, Ed.150, pp 425- 467.

Selim, M. S. and Sloan, E. D. (1989). Heat and mass transfer during the dissociation of hydrates in porous media. *AIChE Journal*, *35*, 6.

Selim, M. S. and Sloan, E. D. (1990). Hydrate dissociation in sediment, *SPE Reservoir Eng. 5*, 02, 245–251.

Seo et al, (2012) Inhibition of methane hydrate re-formation in offshore pipelines with a kinetic hydrate inhibitor. *J. Petrol. Sci. Eng. 88*, 61–66

Shahrul, A. (1996) Development Stages of Gas Network Analysis Program. Master Thesis, University Technology of Malaysia.

Shashi E.M. (2005), Gas Pipeline Hydraulics. Florida: Taylor and Francis Group CRC Press.

Shi *et al*. (2003), Drift-Flux Modelling of Multiphase Flow in Wellbores, *SPE-84228-MS*, SPE Annual Technical Conference and Exhibition, Denver, Colorado,

Shi, H. et al (2005). Drift-flux Modeling of Two-Phase Flow in Wellbores. *SPE J. 10*, 1, 84228, 24-33.

Sholihah M, and Sean W-Y. (2021). Numerical Simulation on the Dissociation, Formation, and Recovery of Gas Hydrates on Microscale Approach. *Molecules*, 26(16), 5021.

Shuqiang G. (2008). Investigation of Interactions between Gas Hydrates and Several Other Flow Assurance Elements. *Energy Fuels 22 (5)*, 3150–3153.

Sidney, P. (1990). Transient Analysis – a Must in Pipeline Design. Dos Santos [Internet]. Available from: <www.psig.org/papers/1990/9703>. [Accessed 12 January, 2018].

Silva, J. M. and Dawe, R. (2011). *Towards Commercial Gas Production from Hydrate Deposits*, Petroleum Engineering Unit, Departments of Chemical engineering, The University of the West Indies, Trinidad and Tobago,

Sloan, E.D and Koh, C. (2008) *Clathrate Hydrates of Natural Gases*, 3rd Ed., CRC Press: Boca Raton, FL, USA.

Sloan, E.D. (1998). Gas hydrates: review of physical/chemical properties. Energy Fuels 12, 191–196.

Smith C. A (2011) Natural Gas Hydrates: Structure II; University of Wisconsin - Green Bay.

Song, H., et al (2015) Impact of permeability heterogeneity on production characteristics in water-bearing tight gas reservoirs with threshold pressure gradient. J. Nat. Gas. Sci. Eng. 22, 172–181.

Song, W. et al (2017). Assessing relative contributions of transport mechanisms and real gas properties to gas flow in nanoscale organic pores in shales by pore network modelling. *Int. J. Heat Mass Transf. 113*, 524–537.

Souza, G.D., Pires, A.P., Abreu, E., (2014). Well-reservoir Coupling on the Numerical Simulation of Horizontal Wells in Gas Reservoirs[C]//SPE Latin America and Caribbean Petroleum Engineering Conference, Maracaibo, Venezuela.

Stone, H. L. (1970). Probability model for estimation of three-phase relative permeability. *J. Pet. Technology, 22*, 214 – 218, doi: 10.2118/2116-pa.

Sui, W. et al. (2008). Model for Transient Temperature and Pressure Behaviours in Commingled Vertical Wells. In *SPE Russian Oil and Gas Technical Conference and Exhibition*. Society of Petroleum Engineers.

Sun, B., Sun, X., Wang, Z., & Chen, Y. (2017). Effects of phase transition on gas kick migration in deep-water horizontal drilling. *Journal of Natural Gas Science and Engineering*, *46*, 710–729

Sun, X. et al (2018), A hydrate shell growth model in bubble flow of water dominated system considering intrinsic kinetics, mass and heat transfer mechanisms, International Journal of Heat and Mass Transfer 117 (2018) 940–950.

Sun, X. et al. (2019). Numerical modeling for the mechanical behaviour of marine gas hydrate-bearing sediments during hydrate production by depressurization. *Journal of Petroleum Science and Engineering*, *177*, 971–982. https://doi.org/10.1016/j.petrol.2019.03.012

Sun, Z., Shi, J., Wu, K., Xu, B., Zhang, T., Chang, Y., & Li, X. (2018). Transport capacity of gas confined in nano-porous ultra-tight gas reservoirs with real gas effect and water storage mechanisms coupling. *International Journal of Heat and Mass Transfer*, *126*, 1007–1018. https://doi.org/10.1016/j.ijheatmasstransfer.2018.05.078

Sung et al., 2002. Development and application of gas hydrate reservoir simulator based on depressurizing mechanism. *Korean J. Chem. Eng*. 17, 344–350.

Sung, W., Lee, H. and Lee, C. (2002). Numerical study for production performances of a methane hydrate reservoir stimulated by inhibitor injection. *Energies*, *24*, 499–512.

Hamed-Tabatabaie, S., & Pooladi-Darvish, M. (2010, October 19). Analytical Solution for Gas Production from Tilted Gas Hydrate Reservoir. doi.org/10.2118/137610-ms

Takhanov, D. (2011), Forchheimer Model for Non-Darcy Flow in Porous Media and Fractures, MSc Thesis, Imperial College London, London UK

Tang, et al. (2005). Experimental investigation of production behaviour of gas hydrate under thermal stimulation in unconsolidated sediment. *Energy Fuels 19*, 2402–2407

Tang, et al. (2007). Control mechanisms for gas hydrate production by depressurization in different scale hydrate reservoirs. *Energy Fuels*, 21(1),227–233.

Tatar, A. et al. (2014). Applying a robust solution based on expert systems and GA evolutionary algorithm for prognosticating residual gas saturation in water drive gas reservoirs. *J. Nat. Gas. Sci. Eng. 21*, 79–94.

Tian, W.B; Li, A.F; Ren, X.X. and Josephine, Y. (2018). The threshold pressure gradient effect in the tight sandstone gas reservoirs with high water saturation. *Fuel*, 226, 221–9.

Tipler, P. A. and Mosca, G. (2008). *Physics for Scientists and Engineers – Mechanics/ Oscillations and Waves/Thermodynamics, Volume 1*. Worth Publishers, New York.

Tjaden, B. et al. (2016). The application of 3-D imaging techniques, simulation and diffusion experiments to explore transport properties in porous oxygen transport membrane support materials. *Solid State Ionics 288*, 315–321

The MathWorks, (2011). *The MathWorks Inc Manual*. Natick, Massachusetts, U.S.A.

Uddin, M., Coombe, D., and Wright, F. (2008). Modeling of CO2-hydrate formation in geological reservoirs by injection of CO2 gas. *J. Energy Resour. Technol., 130*, doi:10.1115/1.2956979

Uddin, M. et al. (2010). Numerical Studies of Gas-Hydrates Formation and Decomposition in a Geological Reservoir. *SPE Paper* 100460

Uddin, M., Wright, F., Coombe, D. (2011). Numerical study of gas evolution and transport behaviours in natural gas-hydrate reservoirs. *J. Can. Petrol. Tech.*, 50, 70–89.

Valko, P.P., Amini, S., (2007) The Method of Distributed Volumetric Sources for Calculating the Transient and Pseudo-steady state Productivity of Complex Well- fracture Configurations, SPE, Texas, U.S.A.

Van Genuchten, M. T. (1980). A closed form equation for predicting the hydraulic conductivity of unsaturated soils. *Soil Sci. Soc. Am. J., 44*, 892–898.

Vedachalam (2016), Assessment of methane gas production from India gas hydrate petroleum systems, Journal of Applied Energy, dx.doi.org/10.1016/j.apenergy.2016.01.117

Vlasov, V. A. (2013) Formation and dissociation of gas hydrate in terms of chemical kinetics.

Reaction Kinetics, Mechanisms and Catalysis, 110:5–13.

Waite, W. F. et al. (2009). Physical properties of hydrate-bearing sediments, *Rev. Geophys., 47*, RG4003.

Wang, H. J. et al. (2012). Profile control method for perforated horizontal wells in heterogeneous reservoirs. *J. China Univ. Pet. 36* (3), 135–139.

Wang, X. and Economides, M. (2009). *Advanced Natural Gas Engineering*, Texas: Gulf Publishing Company.

White, C. and Royer, S. (2003). Experimental Design as a Framework for Reservoir Studies. *In Proceedings of the SPE Reservoir Simulation Symposium*, 3-5, Houston, TX, USA.

White M.D. et al. (2008). Numerical Simulation of Methane Hydrate Production from Geologic Formations via Carbon Dioxide Injection. *OTC 19458*, Texas, USA.

Willhite, G. P. (1967). Over-all heat transfer coefficients in steam and hot water injection wells. *Journal of Petroleum technology*, *19*(05), 607-615.

Wolfsteiner, C., Durlofsky, L.J., Khalid, A. (2000) Approximate model for productivity of nonconventional wells in heterogeneous reservoirs. *J. SPEJ 5* (2), 218–226.

Wu, Y. N. et al. (2014). A Generalized Framework Model for the Simulation of Gas Production in Unconventional Gas Reservoirs. *SPE Journal*, 845–857.

Wu, Y. N. et al. (2010). Gas Hydrate System of Shenhu Area, Northern South China Sea: Wire-line Logging, Geochemical Results and Preliminary Re-sources Estimates. *In Offshore Technology Conference, Houston, Texas*

Wusel007, (2002). *Structure of a gas hydrate (methane clathrate) block embedded in the sediment of hydrate ridge, off Oregon, USA*. Retrieved 19 February 2018, from https://en.wikipedia.org/wiki/Methane_clathrate.

Xia, Z., et al. (2017). Production characteristic investigation of the Class I, Class II and Class III hydrate reservoirs developed by the depressurization and thermal stimulation combined method. *Journal of Petroleum Science and Engineering*, *157*, 56–67. https://doi.org/10.1016/j.petrol.2017.07.012

Yang, B. et al (2017). An integrated method of measuring gas permeability and diffusion coefficient simultaneously via pressure decay tests in shale, International Journal of Coal Geology 179 (2017) 1–10

Yao, C., Shao, Y., Yang, J., Huang, F., He, C., Jiang, Q., & Zhou, C. (2020). Effects of non-darcy flow on heat-flow coupling process in complex fractured rock masses. *Journal of Natural Gas Science and Engineering*, *83*, 103536.

Zhang, R et al. (2015). Enhanced CH4 recovery and CO2 storage via thermal stimulation in the CH4/C2 replacement of methane hydrate. *Chem. Engineering Journal, 308*: 40–49.

Zhang, R et al (2018). Numerical Simulation on Gas Production from Hydrate Reservoirs at first Offshore test site in Nankai Tough, Japan; Faculty of Engineering, China University of Dgeoscience, Wuhan 430074, China.

Zhang, Q. et al. (2020). Analysis of gas transport behaviour in organic and inorganic nanopores based on a unified apparent gas permeability model. *Petroleum Science, 17*, 168–181.

Zhang, W. et al. 2020, Experimental study of hydraulic fracture initiation and propagation in highly saturated methane-hydrate-bearing sands. *J. Journal of Natural Gas Science and Engineering*, 79: 103338.

Zhao, J F. (2019). Physical characteristic of unconsolidated sediments containing gas hydrate. *Journal of Petroleum Science and Engineering, 181*: 106173.

Zhou S, Zhao J, Li Q, et al. 2018, Optimal design of the engineering parameters for the first global trial production of marine natural gas hydrates through solid fluidization. *J. Natural Gas Industry B*, 5(2): 118-131.

Zhu, (2007). Using Carbon Dioxide to Enhance Recovery of Methane from Gas Hydrate Reservoirs: Final Summary Report Springfield, VA: the U.S. Department of Energy.http://www.pnl.gov/main/publications/external/technical_reports/pnnl17035.

APPENDIX

A. Discretization and Linearization Procedure

Governing Equations

$$\frac{\partial}{\partial t}(\phi\rho_g S_g) + \frac{\partial}{\partial x}(\rho_g v_g) = \dot{m}_g + q_g$$
$$\frac{\partial}{\partial t}(\phi\rho_w S_w) + \frac{\partial}{\partial x}(\rho_w v_w) = \dot{m}_w + q_w$$
$$\frac{\partial}{\partial t}(\phi\rho_h S_h) = -\dot{m}_h$$

For a two-dimensional system, this would generate a five-point stencil as shown in figure below.

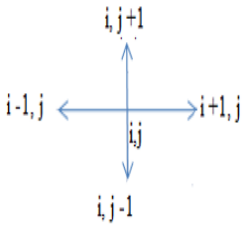

The gas phase diffusivity equation is discretised by the finite difference approximation and applied to the nodes. The flow equation would be upscaled by multiplying by the volume of grid block, V_b. The equation obtained is as follows:

$$\frac{V_b}{\Delta t}\left[\left(\frac{\phi S_g}{B_g}\right)^{n+1}-\left(\frac{\phi S_g}{B_g}\right)^{n}\right]_{i,j}$$

$$=\Delta x\left\{\left[\frac{kk_r}{\mu_g B_g \phi S_g}\left(1+\frac{b}{P_g}\right)\right]_{i+\frac{1}{2},j}\left[\frac{P_{g_{i+1.j}}-P_{gi,j}}{\Delta x_{i+\frac{1}{2}.j}}-\gamma_{gi+\frac{1}{2}.j}\left(\frac{z_{i+1.j}-z_{i,j}}{\Delta x_{i+\frac{1}{2}.j}}\right)-\lambda_{tpg}\right]\right.$$

$$-\left[\frac{kk_r}{\mu_g B_g \phi S_g}\left(1+\frac{b}{P_g}\right)\right]_{i-\frac{1}{2},j}\left[\frac{P_{g_{i.j}}-P_{gi-1,j}}{\Delta x_{i-\frac{1}{2}.j}}-\gamma_{gi-\frac{1}{2}.j}\left(\frac{z_{i.j}-z_{i=1,j}}{\Delta x_{i-\frac{1}{2}.j}}\right)-\lambda_{tpg}\right]$$

$$\left.+\frac{D_{a_{i+\frac{1}{2}.j}}}{\Delta x_{i+\frac{1}{2}.j}}\left[\left(\frac{S_g}{B_g}\right)_{i+1.j}-\left(\frac{S_g}{B_g}\right)_{i.j}\right]-\frac{D_{a_{i-\frac{1}{2}.j}}}{\Delta x_{i-\frac{1}{2}.j}}\left[\left(\frac{S_g}{B_g}\right)_{i.j}-\left(\frac{S_g}{B_g}\right)_{i-1.j}\right]\right\}$$

$$+\Delta y\left\{\left[\frac{kk_r}{\mu_g B_g \phi S_g}\left(1+\frac{b}{P_g}\right)\right]_{i.j+\frac{1}{2}}\left[\frac{P_{g_{i.j+1}}-P_{gi,j}}{\Delta y_{i.j+\frac{1}{2}}}-\gamma_{gi.j+\frac{1}{2}}\left(\frac{z_{i.j+1}-z_{i,j}}{\Delta y_{i.j+\frac{1}{2}}}\right)-\lambda_{tpg}\right]\right.$$

$$-\left[\frac{kk_r}{\mu_g B_g \phi S_g}\left(1+\frac{b}{P_g}\right)\right]_{i.j-\frac{1}{2},}\left[\frac{P_{g_{i.j}}-P_{gi,j-1}}{\Delta y_{i.j-\frac{1}{2}}}-\gamma_{gi.j-\frac{1}{2}}\left(\frac{z_{i.j}-z_{i,j-1}}{\Delta y_{i.j-\frac{1}{2}}}\right)-\lambda_{tpg}\right]$$

$$\left.+\frac{D_{a_{i.j+\frac{1}{2}}}}{\Delta y_{i.j+\frac{1}{2}}}\left[\left(\frac{S_g}{B_g}\right)_{i.j+1}-\left(\frac{S_g}{B_g}\right)_{i.j}\right]-\frac{D_{a_{i.j-\frac{1}{2}}}}{\Delta y_{i.j-\frac{1}{2}}}\left[\left(\frac{S_g}{B_g}\right)_{i.j}-\left(\frac{S_g}{B_g}\right)_{i.j-1}\right]\right\}-\acute{m}_g V_{i,j}$$

$$+q_{gsc}V_{i,j}$$

We defining some terms as follows:

$$T_{gi+\frac{1}{2},j}=\frac{\Delta y}{\Delta x_{i+\frac{1}{2}.j}}\left[\frac{kk_{rg}}{\mu_g B_g \Delta x}\left(1+\frac{b}{P_g}\right)\right]_{i+\frac{1}{2},j};\ T_{gi-\frac{1}{2},j}=\frac{\Delta y}{\Delta x_{i-\frac{1}{2}.j}}\left[\frac{kk_{rg}}{\mu_g B_g \Delta x}\left(1+\frac{b}{P_g}\right)\right]_{i-\frac{1}{2},j};$$

$$T_{gi.j+\frac{1}{2},}=\frac{\Delta x}{\Delta y_{i,j+\frac{1}{2}.}}\left[\frac{kk_{rg}}{\mu_g B_g \Delta y}\left(1+\frac{b}{P_g}\right)\right]_{i.j+\frac{1}{2}};\ T_{gi.j-\frac{1}{2},}=\frac{\Delta x}{\Delta y_{i,j-\frac{1}{2}.}}\left[\frac{kk_{rg}}{\mu_g B_g \Delta y}\left(1+\frac{b}{P_g}\right)\right]_{i.j-\frac{1}{2},}$$

$$;\ T_{D_a i+\frac{1}{2},j}=\frac{\Delta y}{\Delta x_{i+\frac{1}{2}.j}}\left(\frac{D_{a_{i+\frac{1}{2}.j}}}{\Delta x_{i+\frac{1}{2}.j}}\right);\ \ T_{D_a i-\frac{1}{2},j}=\frac{\Delta y}{\Delta x_{i-\frac{1}{2},j}}\left(\frac{D_{a_{i-\frac{1}{2}.j}}}{\Delta x_{i-\frac{1}{2}.j}}\right);\ T_{D_a i.j+\frac{1}{2},}=\frac{\Delta x}{\Delta y_{i,j+\frac{1}{2}.}}\left(\frac{D_{a_{i.j+\frac{1}{2}}}}{\Delta y_{i.j+\frac{1}{2}}}\right);$$

$$T_{D_a i.j-\frac{1}{2},}=\frac{\Delta x}{\Delta y_{i,j-\frac{1}{2}.}}\left(\frac{D_{a_{i.j-\frac{1}{2}}}}{\Delta y_{i.j-\frac{1}{2}}}\right);$$

and substitute in Eq. 3.78. The discretised equation for gas phase is obtained as:

$$\frac{V_b}{\Delta t}\left[\left(\frac{\phi S_g}{B_g}\right)^{n+1} - \left(\frac{\phi S_g}{B_g}\right)^{n}\right]_{i,j} =$$

$$T_{gi+\frac{1}{2},j}\left[\left(P_{g,i+1,j} - P_{g,i,j}\right) - \gamma_{gi+\frac{1}{2},j}\left(z_{i+1,j} - z_{i,j}\right) - \lambda_{tpg}\Delta x_{i+\frac{1}{2},j}\right] + T_{D_a i+\frac{1}{2},j}\left[\left(\frac{S_g}{B_g}\right)_{i+1.j} - \left(\frac{S_g}{B_g}\right)_{i.j}\right]$$

$$- T_{gi-\frac{1}{2},j}\left[\left(P_{g,i,j} - P_{g,i-1,j}\right) - \gamma_{gi-\frac{1}{2},j}\left(z_{i,j} - z_{i-1,j}\right) - \lambda_{tpg}\Delta x_{i-\frac{1}{2}j}\right] + T_{D_a i-\frac{1}{2},j}\left[\left(\frac{S_g}{B_g}\right)_{i.j} - \left(\frac{S_g}{B_g}\right)_{i-1.j}\right]$$

$$+T_{gi.j+\frac{1}{2},}\left[\left(P_{g,i,j+1} - P_{g,i,j}\right) - \gamma_{gi.j+\frac{1}{2},}\left(z_{i,j+1} - z_{i,j}\right) - \lambda_{tpg}\Delta y_{i.j+\frac{1}{2}}\right] + T_{D_a i.j+\frac{1}{2},}\left[\left(\frac{S_g}{B_g}\right)_{i.j+1} - \left(\frac{S_g}{B_g}\right)_{i.j}\right]-$$

$$- T_{gi.j-\frac{1}{2},}\left[\left(P_{g,i,j} - P_{g,i,j-1}\right) - \gamma_{gi.j-\frac{1}{2},}\left(z_{i,j} - z_{i,j-1}\right) - \lambda_{tpg}\Delta y_{i.j-\frac{1}{2}}\right] + T_{D_a i.j-\frac{1}{2},}\left[\left(\frac{S_g}{B_g}\right)_{i.j} -$$

$$\left(\frac{S_g}{B_g}\right)_{i.j-1}\right] - \left(\acute{m}_g V\right)_{i,j}^{n+1} + \left(q_{gsc}V\right)_{i,j}^{n+1}$$

Similarly, the discretisation of the diffusivity equation for water phase continuity equation is obtained as.

$$\frac{V_b}{\Delta t}\left[\left(\frac{\phi S_w}{B_w}\right)^{n+1} - \left(\frac{\phi S_w}{B_w}\right)^{n}\right]_{i,j} =$$

$$T_{wi+\frac{1}{2},j}\left[\left(P_{w,i+1,j} - P_{w,i,j}\right) - \gamma_{wi+\frac{1}{2},j}\left(z_{i+1,j} - z_{i,j}\right) - \lambda_{tpw}\Delta x_{i+\frac{1}{2},j}\right]$$

$$- T_{wi-\frac{1}{2},j}\left[\left(P_{w,i,j} - P_{w,i-1,j}\right) - \gamma_{wi-\frac{1}{2},j}\left(z_{i,j} - z_{i-1,j}\right) - \lambda_{tpw}\Delta x_{i-\frac{1}{2},j}\right]$$

$$+T_{wi.j+\frac{1}{2},}\left[\left(P_{w,i,j+1} - P_{w,i,j}\right) - \gamma_{wi.j+\frac{1}{2},}\left(z_{i,j+1} - z_{i,j}\right) - \lambda_{tpw}\Delta y_{i.j+\frac{1}{2}}\right]$$

$$- T_{wi.j-\frac{1}{2},}\left[\left(P_{w,i,j} - P_{w,i,j-1}\right) - \gamma_{wi.j-\frac{1}{2},}\left(z_{i,j} - z_{i,j-1}\right) - \lambda_{tpw}\Delta y_{i.j-\frac{1}{2}}\right] - \left(\acute{m}_w V\right)_{i,j}^{n+1} + \left(q_{wsc}V\right)_{i,j}^{n+1}$$

The following terms are defined

$$T_{wi+\frac{1}{2},j} = \frac{\Delta y}{\Delta x_{i+\frac{1}{2}.j}}\left(\frac{kk_{rw}}{\mu_w B_w \Delta x}\right)_{i+\frac{1}{2},j}\;;\; T_{wi-\frac{1}{2},j} = \frac{\Delta y}{\Delta x_{i-\frac{1}{2}.j}}\left(\frac{kk_{rw}}{\mu_w B_w \Delta x}\right)_{i-\frac{1}{2},j}\;;$$

$$T_{wi.j+\frac{1}{2},} = \frac{\Delta x}{\Delta y_{i,j+\frac{1}{2}.}}\left(\frac{kk_{rw}}{\mu_w B_w \Delta y}\right)_{i.j+\frac{1}{2}}\;;\; T_{wi.j-\frac{1}{2},} = \frac{\Delta x}{\Delta y_{i,j-\frac{1}{2}.}}\left(\frac{kk_{rw}}{\mu_w B_w \Delta y}\right)_{i.j-\frac{1}{2},}$$

Linearisation of the Flow vector variables

We simplify the right-hand side of equations (3.79a) and (3.79b) by introducing the following linear finite difference operators –

$$\Delta_1 A = \Delta_{1x} A + \Delta_{1y} A$$

$$\Delta_{1x} A = A_{i+\frac{1}{2}.j} \Delta x_{i+\frac{1}{2}.j} - A_{i-\frac{1}{2}.j} \Delta x_{i-\frac{1}{2}.j}$$

$$\Delta_{1y} A = A_{i,j+\frac{1}{2}} \Delta y_{i,j+\frac{1}{2}} - A_{i,j-\frac{1}{2}} \Delta y_{i,j-\frac{1}{2}}$$

$$\Delta_x A \Delta_x B = A_{i+\frac{1}{2},j}\left(B_{i+1,j} - B_{i.j}\right) - A_{i-\frac{1}{2},j}\left(B_{i.j} - B_{i-1,j}\right)$$

$$\Delta_y A \Delta_y B = A_{i,j+\frac{1}{2}}\left(B_{i,j+1} - B_{i.j}\right) - A_{i,j-\frac{1}{2}}\left(B_{i.j} - B_{i,j-1}\right)$$

and rearrange by bringing together variables that share same coefficient and corresponding subscripts

$$\left(i+\tfrac{1}{2},j\right),\quad \left(i-\tfrac{1}{2},j\right),\quad \left(i,j+\tfrac{1}{2}\right),\quad \left(i,j-\tfrac{1}{2},\right)$$

Thus, the fully implicit discretised equations for gas and water phase become-

$$\frac{V_b}{\Delta t}\left[\left(\frac{\phi S_g}{B_g}\right)^{n+1} - \left(\frac{\phi S_g}{B_g}\right)^{n}\right]_n = \sum_{l\in\psi_n} T_{gl,n}^{n+1}\left[\left(P_{g_l}^{n+1} - P_{g_n}^{n+1}\right) - \gamma_{g_{l,n}}^{n+1} H + \Delta_1 \lambda_{tpg}\right] + \sum_{l\in\psi_n} T_{Dgl,_n}^{n+1}\left[\left(\frac{S_g}{B_g}\right)_l^{n+1} - \left(\frac{S_g}{B_g}\right)_n^{n+1}\right] - \sum_{l\in\xi_n} \acute{m}_{g,l,n}^{n+1} + q_{gsc_n}^{n+1}$$

$$\frac{V_b}{\Delta t}\left[\left(\frac{\phi S_w}{B_w}\right)^{n+1} - \left(\frac{\phi S_w}{B_w}\right)^{n}\right]_n = \sum_{l\in\psi_n} T_{wl,n}^{n+1}\left[\left(P_{w_l}^{n+1} - P_{w_n}^{n+1}\right) - \gamma_{w_{l,n}}^{n+1} H + \Delta_1 \lambda_{tpw}\right] - \sum_{l\in\xi_n} \acute{m}_{w,l,n}^{n+1} + q_{wsc_n}^{n+1}$$

B. Derivation of the Analytical Model for validation of the fully coupled model

The transient gas flow equations for gas hydrate well are expressed with the mass, momentum and energy conservations as follows:

Mass conservation

$$\frac{\partial}{\partial t}\left(\phi\rho_g S_g + \phi\rho_w S_w + \phi\rho_h S_h\right) + \frac{\partial}{\partial x}\left(\rho_g v_g + \rho_w v_w\right) = q_g + q_w + m_g + m_w + m_h$$

Momentum conservations

$$\frac{\partial}{\partial t}\left(\rho_g v_g\right) + \frac{\partial}{\partial x}\left(\rho_g v_g^2\right) = -\frac{\partial P_g}{\partial z} - \frac{f_m \rho_g v_g^2}{2d} - \rho_m g sin\theta$$

Energy conservations

$$\frac{\partial}{\partial t}\left[\phi\rho_g S_g h_g + \phi\rho_w S_w h_w + \phi\rho_h S_h h_h + (1-\phi)\rho_r h_r\right] + \frac{\partial}{\partial x}\left(k_T \frac{\partial T}{\partial x}\right) - \frac{\partial}{\partial x}\left(\rho_g v_g h_g + \rho_w h_w\right) = q_g h_g + q_w h_w + q_h + q_{in} \quad (5.1)$$

Where, the effective thermal conductivity is

$$k_T = \phi S_g k_g + \phi S_w k_w + \phi S_h k_h + (1-\phi)k_r$$

$$q_{in} = aA\Delta T$$

$$q_h = m_h \Delta H_D$$

$$\Delta H_D = 446.12 \times 10^3 - 132.638T$$

$$h = c_p T$$

Base on equation of state for ideal gas, the density, velocity and thermodynamic identities can be expressed in terms pressure and temperature at standard conditions as follows

$$\rho_g = \frac{P}{zRT}$$

$$v = \frac{\rho_{scg} q_{scg} zRT}{PA}$$

And

$$dz = \left(\frac{\partial z}{\partial P}\right)_T dP + \left(\frac{\partial z}{\partial T}\right)_P dT$$

$$\frac{dv}{dt} = \frac{1}{q_{scg}}\frac{v dq_{scg}}{dt} - \left[\frac{1}{P} - \frac{1}{Z}\left(\frac{\partial Z}{\partial P}\right)_T\right]\frac{vdP}{dt} + \left[\frac{1}{T} + \frac{1}{Z}\left(\frac{\partial Z}{\partial T}\right)_P\right]\frac{vdT}{dt}$$

The pressure and temperature of the flow system can be described using equation of state formulation for density and velocity to is describe the mass, momentum and energy conservations at standard conditions as follows

$$\frac{\partial}{\partial t}(\rho_g) + \frac{\partial}{\partial x}(\rho_g v_g) = 0$$

$$\frac{\partial}{\partial t}(\rho_w) + \frac{\partial}{\partial x}(\rho_w v_w) = 0$$

$$\frac{\partial}{\partial t}(\rho_g v_g) + \frac{\partial}{\partial x}\left(\rho_g v_g^2\right) = -\frac{\partial P_g}{\partial z} - \frac{f_m \rho_g v_g^2}{2d} - \rho_m g sin\theta$$

$$\frac{\partial}{\partial t}(\rho_w v_w) + \frac{\partial}{\partial x}(\rho_w v_w^2) = -\frac{\partial P_g}{\partial x} - \frac{f_m \rho_g v_g^2}{2d} - \rho_m g sin\theta$$

$$\left[\frac{\partial}{\partial t}\left(u + \frac{v_g^2}{2}\right)\rho_m\right] + \frac{\partial}{\partial x}\left[\left(h + \frac{v_g^2}{2}\right)\rho_m v g\right] = \rho_{scg} q - \rho_{scg} v g sin\theta$$

$$\frac{\partial}{\partial t}(\rho_g) + \frac{\partial}{\partial x}(\rho_g v_g) = 0$$

$$\frac{\partial}{\partial t}(\rho_w) + \frac{\partial}{\partial x}(\rho_w v_w) = 0$$

$$\frac{\partial}{\partial t}(\rho_g v_g) + \frac{\partial}{\partial x}\left(\rho_g v_g^2\right) = -\frac{\partial P_g}{\partial z} - \frac{f_m \rho_g v_g^2}{2d} - \rho_m g sin\theta$$

$$\frac{\partial}{\partial t}(\rho_w v_w) + \frac{\partial}{\partial x}(\rho_w v_w^2) = -\frac{\partial P_g}{\partial x} - \frac{f_m \rho_g v_g^2}{2d} - \rho_m g sin\theta$$

$$\left[\frac{\partial}{\partial t}\left(u + \frac{v_g^2}{2}\right)\rho_m\right] + \frac{\partial}{\partial x}\left[\left(h + \frac{v_g^2}{2}\right)\rho_m v g\right] = \rho_{scg} q - \rho_{scg} v g sin\theta$$

we account for the effect of velocity difference between the phases by calculating an average value for the mixture density at standard conditions

$$\rho_g = \frac{P}{zRT}$$

$$v = \frac{\rho_{□□□} q_{scg} zRT}{PA}$$

From Eq 5.1, the mass conservation equation can be rewritten as

$$\frac{1}{\rho}\frac{d\rho}{\partial t} + \frac{dv}{dx} = 0$$

Substituting Eq 5.6 in 5.8 and differentiating implicitly with time, the accumulation term is expanded as follows

$$\frac{1}{\rho}\frac{d\rho}{\partial t} = \frac{1}{P}\frac{dP}{\partial t} - \frac{1}{T}\frac{dT}{\partial t} - \frac{1}{z}\frac{dz}{\partial t}$$

Where z is the compressibility factor, given as a function of pressure and temperature, as follows

z = z (P, T)

$$dz = \left(\frac{\square\square}{\partial P}\right)_T dP + \left(\frac{\partial z}{\partial T}\right)_P dT$$

Therefore, substituting eq.5.10 in eq. 5.9 and rearranging we have

$$\frac{1}{\rho}\frac{d\rho}{dt} = \left[\frac{1}{P} - \frac{1}{Z}\left(\frac{\partial Z}{\partial P}\right)_T\right]\frac{dP}{dt} - \left[\frac{1}{T} + \frac{1}{Z}\left(\frac{\partial Z}{\partial T}\right)_P\right]\frac{dT}{dt}$$

Substituting equations 5.11 and 5.7 into equation 5.8 we have

$$\left[\frac{1}{P} - \frac{1}{Z}\left(\frac{\partial Z}{\partial P}\right)_T\right]\frac{\partial P}{\partial t} - \left[\frac{1}{T} + \frac{1}{Z}\left(\frac{\partial Z}{\partial T}\right)_P\right]\frac{\partial T}{\partial t} + \frac{\rho_{\square\square\square} zRT}{PA}\frac{\partial q_{scg}}{\partial x} = 0$$

$$\frac{\square\square}{\partial t} = \left[\frac{1}{T} + \frac{1}{Z}\left(\frac{\partial Z}{\partial T}\right)_P\right]\left[\frac{1}{P} - \frac{1}{Z}\left(\frac{\partial Z}{\partial P}\right)_T\right]^{-1}\frac{\partial T}{\partial t} - \frac{\rho_{\square\square\square} zRT}{PA}\left[\frac{1}{P} - \frac{1}{Z}\left(\frac{\partial Z}{\partial P}\right)_T\right]^{-1}\frac{\partial q_{scg}}{\partial x}$$

Also, the momentum conservation equation can be rewritten as

$$\frac{1}{\rho}\frac{d\rho}{dt}.\frac{1}{v}\frac{dv}{dt} + \frac{1}{v}\frac{\partial v^2}{\partial x} + \frac{1}{v}\frac{1}{\rho_m}\frac{\partial P}{\partial x} + \frac{1}{v}\frac{\partial v^2}{\partial x}\frac{2f_m}{d} + \frac{1}{v}gsin\theta = 0$$

From Eq.5.11 the time derivative of the momentum change can be expressed as

$$\frac{1}{v}\frac{dv}{dt} = \frac{1}{q_{\square\square\square}}\frac{dq_{scg}}{dt} - \frac{1}{\rho_{scg}}\frac{d\rho_{scg}}{dt}$$

Substituting equations 5.10 into 5.15 we have

$$\frac{1}{v}\frac{dv}{dt} = \frac{1}{q_{\square\square\square}}\frac{dq_{scg}}{dt} - \left[\frac{1}{P} - \frac{1}{Z}\left(\frac{\partial Z}{\partial P}\right)_T\right]\frac{dP}{dt} + \left[\frac{1}{T} + \frac{1}{Z}\left(\frac{\partial Z}{\partial T}\right)_P\right]\frac{dT}{dt}$$

Similarly, substituting Eq 5.6 in 5.7 and differentiating implicitly with space, the Flux term is expanded

$$\frac{\partial v}{\partial x} = \frac{1}{\rho}\frac{\partial \rho_{\square\square\square}}{\partial x}\frac{\partial q_{scg}}{\partial x} = 0$$

$$\frac{1}{v}\frac{dv}{dx} = \frac{1}{q_{\square\square\square}}\frac{dq_{scg}}{dx} + \left[\frac{1}{P} - \frac{1}{Z}\left(\frac{\partial Z}{\partial P}\right)_T\right]\frac{dP}{dx} + \left[\frac{1}{T} + \frac{1}{Z}\left(\frac{\partial Z}{\partial T}\right)_P\right]\frac{dT}{dx}$$

Substituting equations 5.16 and 5.11 into 5.15 we have

$$\frac{\partial q_{\square\square\square}}{dt} + \frac{\rho_{scg} zRT}{PA}\frac{\partial q_{scg}}{\partial x} - q_{scg}\left[\frac{1}{P} - \frac{1}{Z}\left(\frac{\partial Z}{\partial P}\right)_T\right]\left[\frac{\partial P}{\partial t} + \frac{\rho_{scg} q_{scg} zRT}{PA}\frac{\partial P}{\partial x}\right] + q_{scg}\left[\frac{1}{T} + \frac{1}{Z}\left(\frac{\partial Z}{\partial T}\right)_P\right]\left[\frac{\partial T}{\partial t} + \frac{\rho_{\square\square\square} q_{scg} zRT}{PA}\frac{\partial T}{\partial x}\right] + \frac{A}{\rho_{scg}}\frac{\partial P}{\partial x} + \frac{2f_m \rho_{scg} zRT q_{scg}^2}{DAP} = 0$$

$$\frac{\partial q_{\square\square\square}}{dt} = -\frac{\rho_{scg} zRT}{PA}\frac{\partial q_{scg}}{\partial x} + q_{scg}\left[\frac{1}{P} - \frac{1}{z}\left(\frac{\partial z}{\partial P}\right)_T\right]\left[\frac{\partial P}{\partial t} + \frac{\rho_{scg} q_{scg} zRT}{PA}\frac{\partial P}{\partial x}\right]$$
$$- q_{\square\square\square}\left[\frac{1}{T} + \frac{1}{z}\left(\frac{\partial z}{\partial T}\right)_P\right]\left[\frac{\partial T}{\partial t} + \frac{\rho_{scg} q_{scg} zRT}{PA}\frac{\partial T}{\partial x}\right] - \frac{A}{\rho_{scg}}\frac{\partial P}{\partial x} - \frac{2f_m \rho_{scg} zRT q_{scg}^2}{DAP}$$

For the transient flow in the pipe, the elevation or hydrostatic component conserved for both momentum and energy equations. Thus, the following energy equation is obtained by combining momentum and energy conservations:

$\rho_{\square\square\square}\frac{dh}{dt} - \frac{dP}{dt} - \frac{2f_{\square}\rho_{scg}v^3}{D} = \rho_{scg} q$

Where *h*, the specific enthalpy, and *u*, internal energy can be expressed in the thermodynamic identities as below:

$h_p = u_p + \frac{P^w}{\rho_p}$
$\Delta u = \rho_m c_p \Delta T$

Thus,

$\partial h_p = \partial u_p + \partial\left(\frac{P^w}{\rho_p}\right)$
$\partial u = c_p \partial T + T\left(\frac{\partial P}{\partial T}\right)\partial v - P\partial v$

Thus, the energy equation can be expressed as

$$\rho_{\square\square\square}\frac{1}{\partial t}\left(c_p \partial T + \frac{\partial P}{\partial T} T\partial v - P\partial v + \frac{zRT}{P}\partial P\right)$$
$$= \left\{\left[\frac{1}{T} + \frac{1}{Z}\left(\frac{\partial Z}{\partial T}\right)_{\square}\right]\left[\frac{1}{P} - \frac{1}{Z}\left(\frac{\partial Z}{\partial P}\right)_T\right]^{-1}\frac{\partial T}{\partial t}\right.$$
$$- \frac{\rho_{\square\square\square} zRT}{PA}\left[\frac{1}{P} - \frac{1}{Z}\left(\frac{\partial Z}{\partial P}\right)_T\right]^{-1}\frac{\partial q_{scg}}{\partial x}\Bigg\}\left\{\frac{1}{q_{scg}}\frac{dq_{scg}}{dx} - \left[\frac{1}{P} - \frac{1}{Z}\left(\frac{\partial Z}{\partial P}\right)_T\right]\frac{dP}{dx}\right.$$
$$\left. + \left[\frac{1}{T} + \frac{1}{Z}\left(\frac{\partial Z}{\partial T}\right)_{\square}\right]\frac{dT}{dx}\right\} + \frac{2f_m zRT q_{scg}^2}{CDAP} + \frac{q}{C_{scg}}$$

$$\frac{\partial T}{\partial t}+\left(\frac{\rho_{\square\square\square}q_{scg}zRT}{PA}\right)\frac{\partial T}{\partial x}+\left\{\left[\frac{zRTT}{C}\left(\frac{\rho_{\square\square\square}q_{scg}zRT}{PA}\right)\right]\left[\frac{1}{T}+\frac{1}{Z}\left(\frac{\partial Z}{\partial T}\right)_{P}\right]\frac{dT}{dx}\right\}\left\{\frac{1}{q_{scg}}\frac{\partial q_{scg}}{\partial x}-\left[\frac{1}{P}-\frac{1}{Z}\left(\frac{\partial Z}{\partial P}\right)_{\square}\right]\frac{dP}{dx}+\left[\frac{1}{T}+\frac{1}{Z}\left(\frac{\partial Z}{\partial T}\right)_{P}\right]\frac{dT}{dx}\right\}-\frac{2f_{m}zRTq_{scg}^{2}}{CDAP}-\frac{q}{C_{scg}}=0$$

$$\frac{\partial T}{\partial t}=-\left(\frac{\rho_{\square\square\square}q_{scg}zRT}{PA}\right)\frac{\partial T}{\partial x}-\left\{\left[\frac{zRTT}{C}\left(\frac{\rho_{\square\square\square}q_{scg}zRT}{PA}\right)\right]\left[\frac{1}{T}+\frac{1}{Z}\left(\frac{\partial Z}{\partial T}\right)_{P}\right]\frac{dT}{dx}\right\}\left\{\frac{1}{q_{scg}}\frac{\partial q_{scg}}{\partial x}+\left[\frac{1}{P}-\frac{1}{Z}\left(\frac{\partial Z}{\partial P}\right)_{\square}\right]\frac{dP}{dx}+\left[\frac{1}{T}+\frac{1}{Z}\left(\frac{\partial Z}{\partial T}\right)_{P}\right]\frac{dT}{dx}\right\}+\frac{2f_{m}zRTq_{scg}^{3}}{CDAP}+\frac{q}{C_{scg}}$$

Thus, the solutions of the transient well flow can be written as:

$$\frac{\square\square}{\partial t}=\left[\frac{1}{T}+\frac{1}{Z}\left(\frac{\partial Z}{\partial T}\right)_{P}\right]\left[\frac{1}{P}-\frac{1}{Z}\left(\frac{\partial Z}{\partial P}\right)_{T}\right]^{-1}\frac{\partial T}{\partial t}-\frac{\rho_{\square\square\square}zRT}{PA}\left[\frac{1}{P}-\frac{1}{Z}\left(\frac{\partial Z}{\partial P}\right)_{T}\right]^{-1}\frac{\partial q_{scg}}{\partial x}$$

$$\frac{\square\square}{\partial t}=-\left(\frac{\rho_{\square\square\square}q_{scg}zRT}{PA}\right)\frac{\partial T}{\partial x}-\left\{\left[\frac{zRTT}{C}\left(\frac{\rho_{scg}q_{scg}zRT}{PA}\right)\right]\left[\frac{1}{T}+\frac{1}{Z}\left(\frac{\partial Z}{\partial T}\right)_{P}\right]\frac{dT}{dx}\right\}\left\{\frac{1}{q_{scg}}\frac{\partial q_{scg}}{\partial x}-\left[\frac{1}{P}-\frac{1}{Z}\left(\frac{\partial Z}{\partial P}\right)_{T}\right]\frac{dP}{dx}+\left[\frac{1}{T}+\frac{1}{Z}\left(\frac{\partial Z}{\partial T}\right)_{P}\right]\frac{dT}{dx}\right\}+\frac{2f_{\square}zRTq_{scg}^{3}}{CDAP}+\frac{q}{C_{scg}}$$

$$\frac{\partial q_{\square\square\square}}{dt}=-\frac{\rho_{scg}zRT}{PA}\frac{\partial q_{scg}}{\partial x}+q_{scg}\left[\frac{1}{P}-\frac{1}{z}\left(\frac{\partial z}{\partial P}\right)_{T}\right]\left[\frac{\partial P}{\partial t}+\frac{\rho_{scg}q_{scg}zRT}{PA}\frac{\partial P}{\partial x}\right]-q_{scg}\left[\frac{1}{T}+\frac{1}{z}\left(\frac{\partial z}{\partial T}\right)_{P}\right]\left[\frac{\partial T}{\partial t}+\frac{\rho_{\square\square\square}q_{scg}zRT}{PA}\frac{\partial T}{\partial x}\right]-\frac{A}{\rho_{scg}}\frac{\partial P}{\partial x}-\frac{2f_{m}\rho_{scg}zRTq_{scg}^{2}}{DAP}$$

D. Relative Permeability and Capillary Pressure Exponents Parameters

(Jang, 2016)

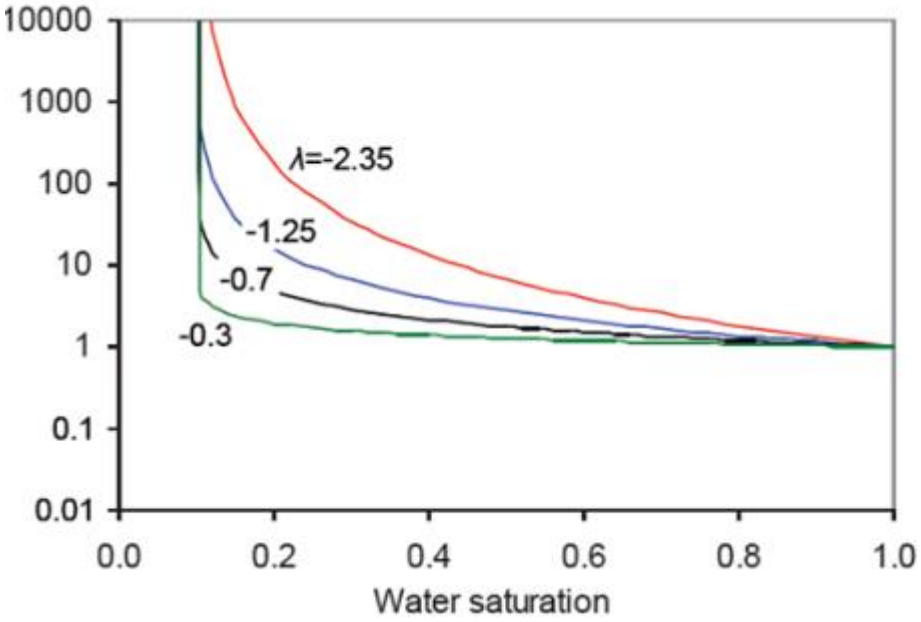

D1: Effects of Capillary Pressure Parameters (Corey's model)

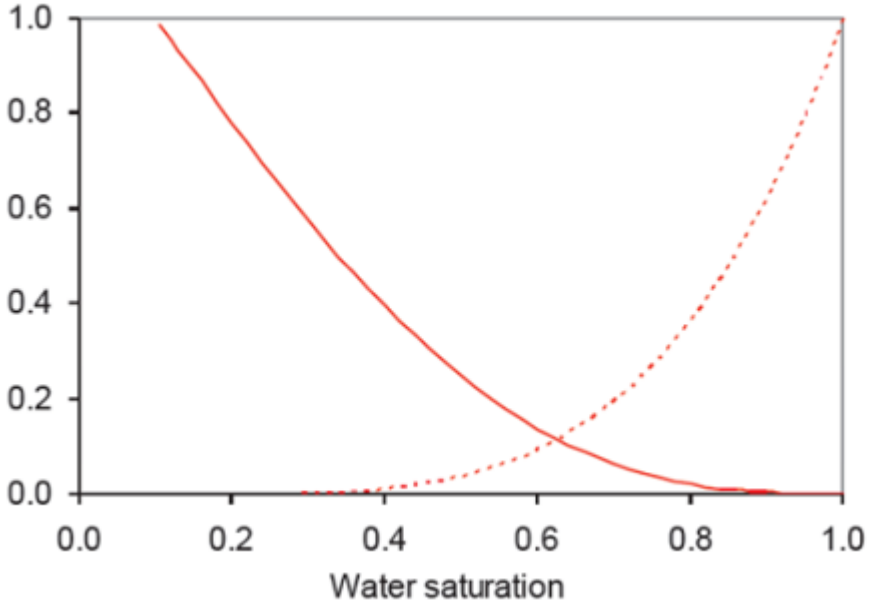

D2: Effects of Relative Permeability Parameters (Corey's model)

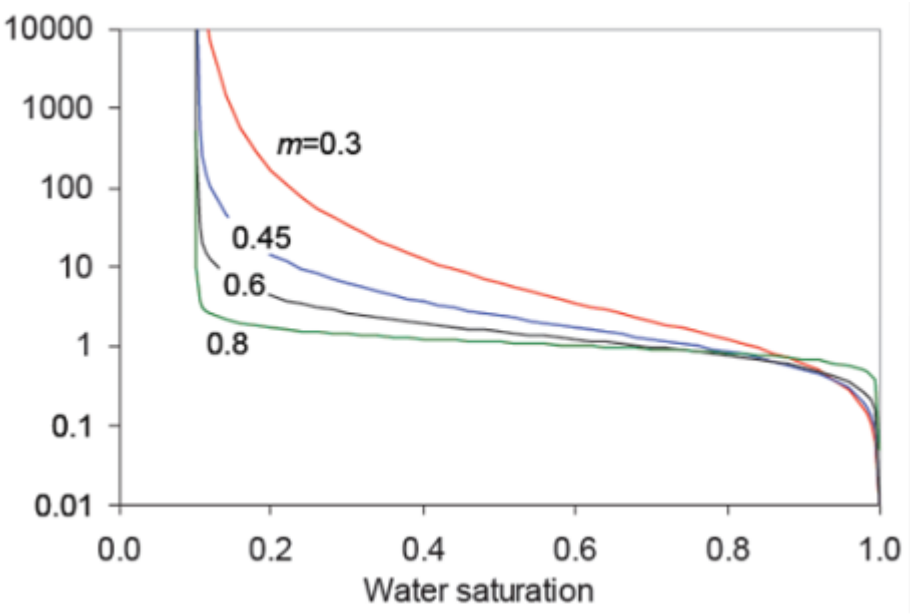

D3: Effects of Capillary Pressure Parameters (van Genuchten's model)

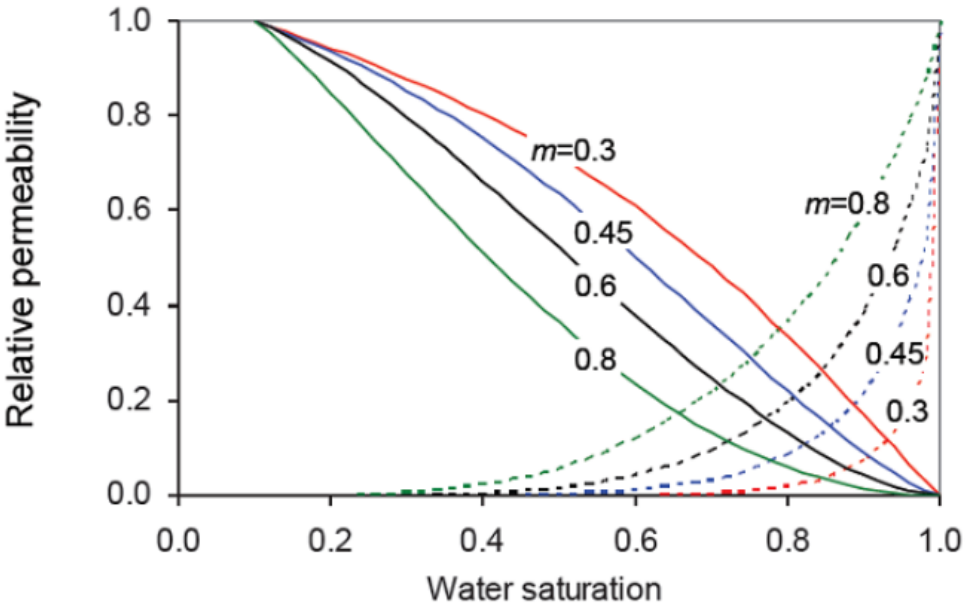

D4: Effects of Relative Permeability Parameters (van Genuchten's model)

D. Reservoir Initialisation Code

```
clc; clear; close all;

%Input paramters

time = 1000;                        %Total simulation time
delta_t = 10;                       %Time step size
Steps = time/delta_t;               %Total steps to reach time
mu = 2;                             %Fluid viscosity
B_w = 1.250;                        %Formation volume factor
phi = 0.2;                          %Porosity
kx = 10;                            %Permeability
ky = 5;                             %Permeability
k_eq = (kx*ky)^0.5;
c_o = 1.5e-5;                       %Rock compressibility
c_f = 1.25e-5;                      %Fluid compressibility
c_t = c_o+c_f;                      %Total compressibility
Lx = 5500;                          %Length in X-direction
Ly = 4500;                          %Length in Y-direction
Lz = 100;                           %Length in Z-direction
Nx = 11;                            %Number of cells in X-direction
Ny = 9;                             %Number of cells in Y-direction
Nz = 1;                             %Number of cells in Z-direction
delta_x = Lx/Nx;                    %Delta_x
delta_y = Ly/Ny;                    %Delta_y
delta_z = Lz/Ny;                    %Delta_z
beta = 158.029*phi*c_t*delta_x^2/delta_t;
d_w = 887.33*B_w*delta_x^2/(delta_x*delta_y*delta_z);
r_w = 0.25;
r_eq = 0.14 * (delta_x*delta_x+delta_y*delta_y)^0.5;
N = Nx*Ny*Nz;

kx_array=kx*ones(N,1);                  %Finite difference matrix
ky_array=ky*ones(N,1);                  %Finite difference matrix
P_n=3200*ones(N,1);                 %Initial time pressure
Qw = 0.;                        %Well rates
Pw = 0.;                        %Well flowing pressures
Swc = 0;
cells = delta_x*[1:1:Nx]';
tolerance = 1e-6;
%Peaceman model for productivity index
no_wells = 1
well_constraints =["Rate","Pressure","Pressure"];
well_type =["Producer","Producer","Producer"];
Qw = 10*ones(no_wells,1);               %Well rates
Pw = 1000*ones(no_wells,1);             %Well flowing pressures
well_indeces = [50 11 20];          %Cell indices for wells
Jw = zeros(no_wells,1);             %Productivity index for wells

for w = 1:no_wells;
```

```
   Jw(w) = 2*pi*0.001127*k_eq*delta_z/(mu*B_w*log(r_eq/r_w));
end


P_2d = reshape(P_n,Nx,Ny)';
iPlot3d=surf(P_2d);
axis([0 Nx 0 Ny 2500 3300])
title('Reservoir Pressure Distribution, t = 0 days','fontsize',20,'fontweight','bold')
xlabel('x-direction','fontsize',20,'fontweight','bold')
ylabel('y-direction','fontsize',20,'fontweight','bold')
zlabel('Pressure (psia)','fontsize',20,'fontweight','bold')
pause()



P = P_n;

for k = 1:Steps;
count = 0;
error = 1e+7;
while(error > tolerance)
Jacobian=zeros(N);                          %Finite difference matrix
Residual=zeros(N,1);                         %Finite difference vector
count = count +1;
   for j = 2:Ny-1;
      for i = 2:Nx-1;
         m = i + Nx*(j-1);
         lambda_E = kx_array(m)*kx_array(m+1)/(kx_array(m)+kx_array(m+1))/mu;
         lambda_W = kx_array(m)*kx_array(m-1)/(kx_array(m)+kx_array(m-1))/mu;
         lambda_N = ky_array(m)*ky_array(m+Nx)/(ky_array(m)+kx_array(m+Nx))/mu;
         lambda_S = ky_array(m)*ky_array(m-Nx)/(ky_array(m)+kx_array(m-Nx))/mu;
         Em = lambda_E;
         Wm = lambda_W;
         Nm = (delta_x^2/delta_y^2)*lambda_N;
         Sm = (delta_x^2/delta_y^2)*lambda_S;
         Cm = Em+Wm+Sm+Nm+beta;
         Jacobian(m,m+1) = -1*Em;
         Jacobian(m,m-1) = -1*Wm;
         Jacobian(m,m+Nx) = -1*Nm;
         Jacobian(m,m-Nx) = -1*Sm;
         Jacobian(m,m)= Cm;
         Residual(m)= -1*beta*P_n(m)-Wm*P(m-1)-Em*P(m+1)-Nm*P(m+Nx)-Sm*P(m-Nx)+Cm*P(m);
 %         fprintf("(Here count %d m = %d %g %g %g %g \n",count,m,Wm,Em,Sm,Nm,-Wm-Em-Sm-
Nm+Cm,Cm,-Wm*P(m-1)-Em*P(m+1)-Nm*P(m+Nx)-Sm*P(m-Nx)+Cm*P(m))

 %         fprintf("(Here count %d m = %d %g %g %g %g %g %g\n",count,m,Jacobian(m,m-
1),Jacobian(m,m+1),Jacobian(m,m+Nx),Jacobian(m,m-Nx),Jacobian(m,m),Residual(m))
      end
   end

%Bottom Boundary condition
   j = 1;
   for i = 2:Nx-1;
      m = i + Nx*(j-1);
      lambda_E = kx_array(m)*kx_array(m+1)/(kx_array(m)+kx_array(m+1))/mu;
```

```
      lambda_W = kx_array(m)*kx_array(m-1)/(kx_array(m)+kx_array(m-1))/mu;
      lambda_N = ky_array(m)*ky_array(m+Nx)/(ky_array(m)+kx_array(m+Nx))/mu;
      lambda_S = 0.;
      Em = lambda_E;
      Wm = lambda_W;
      Nm = (delta_x^2/delta_y^2)*lambda_N;
      Sm = 0.;
      Cm = Em+Wm+Sm+Nm+beta;
      Jacobian(m,m+1) = -1*Em;
      Jacobian(m,m-1) = -1*Wm;
      Jacobian(m,m+Nx) = -1*Nm;
      Jacobian(m,m)= Cm;
      Residual(m)= -1*beta*P_n(m)-Wm*P(m-1)-Em*P(m+1)-Nm*P(m+Nx)+Cm*P(m);
%fprintf("(Here count %d m = %d %g %g %g %g %g %g %g\n",count,m,Wm,Em,Sm,Nm,-Wm-Em-Sm-
Nm+Cm,Cm,-Wm*P(m-1)-Em*P(m+1)-Nm*P(m+Nx)+Cm*P(m))
%fprintf("(Here count %d m = %d %g %g %g %g %g\n",count,m,Jacobian(m,m-
1),Jacobian(m,m+1),Jacobian(m,m+Nx),Jacobian(m,m),Residual(m))


   end

%Top Boundary condition
   j = Ny;
   for i = 2:Nx-1;
      m = i + Nx*(j-1);
      lambda_E = kx_array(m)*kx_array(m+1)/(kx_array(m)+kx_array(m+1))/mu;
      lambda_W = kx_array(m)*kx_array(m-1)/(kx_array(m)+kx_array(m-1))/mu;
      lambda_N = 0.;
      lambda_S = ky_array(m)*ky_array(m-Nx)/(ky_array(m)+kx_array(m-Nx))/mu;
      Em = lambda_E;
      Wm = lambda_W;
      Nm = 0;
      Sm = (delta_x^2/delta_y^2)*lambda_S;
      Cm = Em+Wm+Sm+Nm+beta;
      Jacobian(m,m+1) = -1*Em;
      Jacobian(m,m-1) = -1*Wm;
      Jacobian(m,m-Nx) = -1*Sm;
      Jacobian(m,m)= Cm;
      Residual(m)= -1*beta*P_n(m)-Wm*P(m-1)-Em*P(m+1)-Sm*P(m-Nx)+Cm*P(m);
 %        fprintf("(Here count %d m = %d %g %g %g %g %g %g %g\n",count,m,Wm,Em,Sm,Nm,-Wm-Em-
Sm-Nm+Cm,Cm,-Wm*P(m-1)-Em*P(m+1)-Sm*P(m-Nx)+Cm*P(m))

%fprintf("(Here count %d m = %d %g %g %g %g %g\n",count,m,Jacobian(m,m-
1),Jacobian(m,m+1),Jacobian(m,m-Nx),Jacobian(m,m),Residual(m))

   end


%Left Boundary condition
   i = 1;
   for j = 2:Ny-1;
      m = i + Nx*(j-1);
      lambda_E = kx_array(m)*kx_array(m+1)/(kx_array(m)+kx_array(m+1))/mu;
      lambda_W = 0.;
      lambda_N = ky_array(m)*ky_array(m+Nx)/(ky_array(m)+kx_array(m+Nx))/mu;
      lambda_S = ky_array(m)*ky_array(m-Nx)/(ky_array(m)+kx_array(m-Nx))/mu;
```

```
      Em = lambda_E;
      Wm = 0;
      Nm = (delta_x^2/delta_y^2)*lambda_N;
      Sm = (delta_x^2/delta_y^2)*lambda_S;
      Cm = Em+Wm+Sm+Nm+beta;
      Jacobian(m,m+1) = -1*Em;
      Jacobian(m,m+Nx) = -1*Nm;
      Jacobian(m,m-Nx) = -1*Sm;
      Jacobian(m,m)= Cm;
      Residual(m)= -1*beta*P_n(m)-Em*P(m+1)-Nm*P(m+Nx)-Sm*P(m-Nx)+Cm*P(m);
 %        fprintf("(Here count %d m = %d %g %g %g %g %g %g %g\n",count,m,Wm,Em,Sm,Nm,-Wm-Em-
Sm-Nm+Cm,Cm,-Em*P(m+1)-Nm*P(m+Nx)-Sm*P(m-Nx)+Cm*P(m))

%fprintf("(Here count %d m = %d %g %g %g %g
%g\n",count,m,Jacobian(m,m+1),Jacobian(m,m+Nx),Jacobian(m,m-Nx),Jacobian(m,m),Residual(m))


   end

%Right Boundary condition
   i = Nx;
   for j = 2:Ny-1;
      m = i + Nx*(j-1);
      lambda_E = 0.;
      lambda_W = kx_array(m)*kx_array(m-1)/(kx_array(m)+kx_array(m-1))/mu;
      lambda_N = ky_array(m)*ky_array(m+Nx)/(ky_array(m)+kx_array(m+Nx))/mu;
      lambda_S = ky_array(m)*ky_array(m-Nx)/(ky_array(m)+kx_array(m-Nx))/mu;
      Em = 0.;
      Wm = lambda_W;
      Nm = (delta_x^2/delta_y^2)*lambda_N;
      Sm = (delta_x^2/delta_y^2)*lambda_S;
      Cm = Em+Wm+Sm+Nm+beta;
      Jacobian(m,m-1) = -1*Wm;
      Jacobian(m,m+Nx) = -1*Nm;
      Jacobian(m,m-Nx) = -1*Sm;
      Jacobian(m,m)= Cm;
      Residual(m)= -1*beta*P_n(m)-Wm*P(m-1)-Nm*P(m+Nx)-Sm*P(m-Nx)+Cm*P(m);
 %        fprintf("(Here count %d m = %d %g %g %g %g %g %g %g\n",count,m,Wm,Em,Sm,Nm,-Wm-Em-
Sm-Nm+Cm,Cm,-Wm*P(m-1)-Nm*P(m+Nx)-Sm*P(m-Nx)+Cm*P(m))

%fprintf("(Here count %d m = %d %g %g %g %g %g\n",count,m,Jacobian(m,m-
1),Jacobian(m,m+Nx),Jacobian(m,m-Nx),Jacobian(m,m),Residual(m))


   end

%Bottom-Left Corner Boundary condition
j = 1;
i = 1;
m = i + Nx*(j-1);
lambda_E = kx_array(m)*kx_array(m+1)/(kx_array(m)+kx_array(m+1))/mu;
lambda_W = 0.;
lambda_N = ky_array(m)*ky_array(m+Nx)/(ky_array(m)+kx_array(m+Nx))/mu;
lambda_S = 0.;
Em = lambda_E;
Wm = 0.;
```

```
Nm = (delta_x^2/delta_y^2)*lambda_N;
Sm = 0.;
Cm = Em+Wm+Sm+Nm+beta;
Jacobian(m,m+1) = -1*Em;
Jacobian(m,m+Nx) = -1*Nm;
Jacobian(m,m)= Cm;
Residual(m)= -1*beta*P_n(m)-Em*P(m+1)-Nm*P(m+Nx)+Cm*P(m);
%fprintf("(Here count %d m = %d %g %g %g %g %g %g %g\n",count,m,Wm,Em,Sm,Nm,-Wm-Em-Sm-
Nm+Cm,Cm,-Em*P(m+1)-Nm*P(m+Nx)+Cm*P(m))
%fprintf("(Here count %d m = %d %g %g %g
%g\n",count,m,Jacobian(m,m+1),Jacobian(m,m+Nx),Jacobian(m,m),Residual(m))



%Bottom-Right Corner Boundary condition
j = 1;
i = Nx;
m = i + Nx*(j-1);
lambda_E = 0;
lambda_W = kx_array(m)*kx_array(m-1)/(kx_array(m)+kx_array(m-1))/mu;
lambda_N = ky_array(m)*ky_array(m+Nx)/(ky_array(m)+kx_array(m+Nx))/mu;
lambda_S = 0.;
Em = 0.;
Wm = lambda_W;
Nm = (delta_x^2/delta_y^2)*lambda_N;
Sm = 0;
Cm = Em+Wm+Sm+Nm+beta;
Jacobian(m,m-1) = -1*Wm;
Jacobian(m,m+Nx) = -1*Nm;
Jacobian(m,m)= Cm;
Residual(m)= -1*beta*P_n(m)-Wm*P(m-1)-Nm*P(m+Nx)+Cm*P(m);
%fprintf("(Here count %d m = %d %g %g %g %g %g %g %g\n",count,m,Wm,Em,Sm,Nm,-Wm-Em-Sm-
Nm+Cm,Cm,-Wm*P(m-1)-Nm*P(m+Nx)+Cm*P(m))

%fprintf("(Here count %d m = %d %g %g %g %g\n",count,m,Jacobian(m,m-
1),Jacobian(m,m+Nx),Jacobian(m,m),Residual(m))



%Top-Left Corner Boundary condition
j = Ny;
i = 1;
m = i + Nx*(j-1);
lambda_E = kx_array(m)*kx_array(m+1)/(kx_array(m)+kx_array(m+1))/mu;
lambda_W = 0.;
lambda_N = 0;
lambda_S = ky_array(m)*ky_array(m-Nx)/(ky_array(m)+kx_array(m-Nx))/mu;
Em = lambda_E;
Wm = lambda_W;
Nm = (delta_x^2/delta_y^2)*lambda_N;
Sm = (delta_x^2/delta_y^2)*lambda_S;
Cm = Em+Wm+Sm+Nm+beta;
Jacobian(m,m+1) = -1*Em;
Jacobian(m,m-Nx) = -1*Sm;
Jacobian(m,m)= Cm;
Residual(m)= -1*beta*P_n(m)-Em*P(m+1)-Sm*P(m-Nx)+Cm*P(m);
```

```
%fprintf("(Here count %d m = %d %g %g %g %g %g %g %g\n",count,m,Wm,Em,Sm,Nm,-Wm-Em-Sm-
Nm+Cm,Cm,-Em*P(m+1)-Sm*P(m-Nx)+Cm*P(m))

%fprintf("(Here count %d m = %d %g %g %g %g\n",count,m,Jacobian(m,m+1),Jacobian(m,m-
Nx),Jacobian(m,m),Residual(m))


%Top-Left Corner Boundary condition
j = Ny;
i = Nx;
m = i + Nx*(j-1);
lambda_E = 0.;
lambda_W = kx_array(m)*kx_array(m-1)/(kx_array(m)+kx_array(m-1))/mu;
lambda_N = 0;
lambda_S = ky_array(m)*ky_array(m-Nx)/(ky_array(m)+kx_array(m-Nx))/mu;
Em = lambda_E;
Wm = lambda_W;
Nm = (delta_x^2/delta_y^2)*lambda_N;
Sm = (delta_x^2/delta_y^2)*lambda_S;
Cm = Em+Wm+Sm+Nm+beta;
Jacobian(m,m-1) = -1*Wm;
Jacobian(m,m-Nx) = -1*Sm;
Jacobian(m,m)= Cm;
Residual(m)= -1*beta*P_n(m)-Wm*P(m-1)-Sm*P(m-Nx)+Cm*P(m);
%fprintf("(Here count %d m = %d %g %g %g %g %g %g %g\n",count,m,Wm,Em,Sm,Nm,-Wm-Em-Sm-
Nm+Cm,Cm,-Wm*P(m-1)-Sm*P(m-Nx)+Cm*P(m))
%fprintf("(Here count %d m = %d %g %g %g %g\n",count,m,Jacobian(m,m-1),Jacobian(m,m-
Nx),Jacobian(m,m),Residual(m))

%well condition

for w = 1:no_wells;
   i = well_indeces(w);
   if well_constraints(w) == "Rate";
      if well_type == "Producer";
         Residual(i) = Residual(i)+d_w * Qw(w);
      end
      if well_type == "Injector";
         Residual(i) = Residual(i)-d_w * Qw(w);
      end
   end
   if well_constraints(w) == "Pressure";
      if well_type == "Producer";
         Residual(i) = Residual(i)-d_w * Jw(w)*Pw(w);
         Jacobian(i,i) = Jacobian(i,i) + d_w * Jw(w);
      end
      if well_type == "Injector";
         Residual(i) = Residual(i)+d_w * Jw(w)*Pw(w);
         Jacobian(i,i) = Jacobian(i,i) - d_w * Jw(w);
      end
   end
end
```

```
P = P-Jacobian\Residual;
error = norm(Residual);
end
P_n = P;

P_2d = reshape(P_n,Nx,Ny)';

surf(P_2d);
axis([0 Nx 0 Ny 2500 3300])
szTitle=sprintf('Reservoir Pressure Distribution, t = %.0f days',k*delta_t);
title(szTitle,'fontsize',20,'fontweight','bold')
xlabel('x-direction','fontsize',20,'fontweight','bold')
ylabel('y-direction','fontsize',20,'fontweight','bold')
zlabel('Pressure (psia)','fontsize',20,'fontweight','bold')
pause()


end

Jacobian;
```

E. Coupled Wellbore Initialisation Code

```
% definition of constant parameters

A=(Ggas*Kmi)/Visgas;
B=0;%((1-PoroM)*Mw*PL*VL*denSH)/Vstd;
C=Ggas*PoroM;
D=(Kmi*Ggas*crossflow)/Visgas;
E=A*bm;
G=(Kfi*denG*2*pi)/(Visgas*log((Re/Rw)));% coefficient of production term
A1=(Ggas*Kfi)/Visgas;
% for fractures
K=Ggas*PoroF;
F=A1*bf;

%%-------------------------------------------------------------------------------------------------------------------

dt=10;  % change in time, timestep

maxm=50;
eps=0.00011;
eps1=0.1;

% initial condition
U_init=ones(M,N)*Pi;
V_init=ones(M,N)*Pi;

% Initial guess for Newton raphson
U1=ones(M,N)*500;
U=U1;
```

```
U_1=ones(M,N)*500;

V1=ones(M,N)*500;
V=V1;
V_1=ones(M,N)*500;


% initialise Guess for Jacobi iteration
u_delta=zeros(M,N)*Pi;
v_delta=zeros(M,N);



% define tolerance for convergence
w=0.05;   % relaxation factor
w_1=0.09;


PA=[];PA2=[];PA3=[];
% --------------------------------------------------------------------------
for n=1:15 % change time (100 for 3 years)
   nunkno11=M*M;
   mm1=1;
   numi11=0;

   while (numi11<nunkno11)*(mm1<maxm)

      % Execute Newton Method
      nunkno1=M*M;
      mm=1;
      numi1=0;
      while (numi1<nunkno1)*(mm<maxm)

         % Execute Gauss-Seidel algorithm

         nunkno=M*M;
         m=1;
         numi=0;
         while (numi<nunkno)*(m<maxm)
            numi=0;
            % interior nodes
            for i=2:M-1
               for j=2:N-1
                  if i==(M+1)/2 && j==(N+1)/2
                     f(i,j)=(C+(B/(PL+U(i,j))^2))*((U(i,j)-U_init(i,j))/dt)-(A*((U(i+1,j)-U(i-1,j))/2*dx)^2)-
(A*((U(i,j+1)-U(i,j-1))/2*dy)^2)-((A*U(i,j))*((U(i+1,j)+U(i-1,j)-2*U(i,j))/dx^2))...
                        -((A*U(i,j))*((U(i,j+1)+U(i,j-1)-2*U(i,j))/dy^2))-(E*((U(i+1,j)+U(i-1,j)-2*U(i,j))/dx^2))-
(E*((U(i,j+1)+U(i,j-1)-2*U(i,j))/dy^2))...
                        +(D*(U(i,j)-V(i,j)))+G*(V(i)-pwf);
                     aE=(-1/2*A*((U(i+1,j)-U(i-1,j))/dx^2))-(A*U(i,j)/dx^2)-(E/dx^2);    % left nodes (upper
diagonal)
                     aW=(1/2*A*((U(i+1,j)-U(i-1,j))/dx^2))-(A*U(i,j)/dx^2)-(E/dx^2);    %right nodes  (lower
diagonal)
                     aN=(-1/2*A*((U(i,j+1)-U(i,j-1))/dx^2))-(A*U(i,j)/dx^2)-(E/dx^2);
                     aS=(1/2*A*((U(i,j+1)-U(i,j-1))/dx^2))-(A*U(i,j)/dx^2)-(E/dx^2);
```

```
                a0=(2*B*(U(i,j)-U_init(i,j)))/(dt*(PL+U(i,j))^3)+((C+(B/(PL+U(i,j))^2))/dt)-
(A*((U(i+1,j)+U(i-1,j)-2*U(i,j))/dx^2))-(A*((U(i,j+1)+U(i,j-1)-2*U(i,j)))/dy^2))...

+(((2*A)/dx^2)*U(i,j))+(((2*A)/dy^2)*U(i,j))+(2*E/dx^2)+D*U(i,j)+(2*E/dy^2)+D*U(i,j)+D*(U(i,j)-
V(i,j))+G; % diagonal (middle nodes)
                u_delta0(i,j)=((-f(i,j)-aE*u_delta(i+1,j)-aW*u_delta(i-1,j)-aN*u_delta(i,j+1)-aS*u_delta(i,j-
1))/a0)
                error= abs((u_delta0(i,j)-u_delta(i,j))/u_delta(i,j));
                u_delta(i,j)=u_delta0(i,j);
                if (error<eps)
                   numi=numi+1;
                end

%                    q=G*(U(i,j)-pwf);
             else
                f(i,j)=(C+(B/(PL+U(i,j))^2))*((U(i,j)-U_init(i,j))/dt)-(A*((U(i+1,j)-U(i-1,j))/2*dx)^2)-
(A*((U(i,j+1)-U(i,j-1))/2*dy)^2)-((A*U(i,j))*((U(i+1,j)+U(i-1,j)-2*U(i,j)))/dx^2))...
                   -((A*U(i,j))*((U(i,j+1)+U(i,j-1)-2*U(i,j)))/dy^2))-(E*((U(i+1,j)+U(i-1,j)-2*U(i,j)))/dx^2))-
(E*((U(i,j+1)+U(i,j-1)-2*U(i,j)))/dy^2))...
                   +(D*(U(i,j)-V(i,j)));
                aE=(-1/2*A*((U(i+1,j)-U(i-1,j)))/dx^2))-(A*U(i,j)/dx^2)-(E/dx^2);    % left nodes (upper
diagonal)
                aW=(1/2*A*((U(i+1,j)-U(i-1,j)))/dx^2))-(A*U(i,j)/dx^2)-(E/dx^2);    %right nodes  (lower
diagonal)
                aN=(-1/2*A*((U(i,j+1)-U(i,j-1))/dx^2))-(A*U(i,j)/dx^2)-(E/dx^2);
                aS=(1/2*A*((U(i,j+1)-U(i,j-1))/dx^2))-(A*U(i,j)/dx^2)-(E/dx^2);
                a0=(2*B*(U(i,j)-U_init(i,j)))/(dt*(PL+U(i,j))^3)+((C+(B/(PL+U(i,j))^2))/dt)-
(A*((U(i+1,j)+U(i-1,j)-2*U(i,j)))/dx^2))-(A*((U(i,j+1)+U(i,j-1)-2*U(i,j)))/dy^2))...

+(((2*A)/dx^2)*U(i,j))+(((2*A)/dy^2)*U(i,j))+(2*E/dx^2)+D*U(i,j)+(2*E/dy^2)+D*U(i,j)+D*(U(i,j)-V(i,j)); %
diagonal (middle nodes)
                u_delta0(i,j)=((-f(i,j)-aE*u_delta(i+1,j)-aW*u_delta(i-1,j)-aN*u_delta(i,j+1)-aS*u_delta(i,j-
1))/a0)
                error= abs((u_delta0(i,j)-u_delta(i,j))/u_delta(i,j));
                u_delta(i,j)=u_delta0(i,j);
                if (error<eps)
                   numi=numi+1;
                end
             end
          end
       end
       % left nodes
       % Boundary condition for left node (Neumann BC)
       for i=1
          for j=2:N-1
             f(i,j)=(C+(B/(PL+U(i,j))^2))*((U(i,j)-U_init(i,j))/dt)-(A*((U(i+1,j)-U(i+1,j))/2*dx)^2)-
(A*((U(i,j+1)-U(i,j-1))/2*dy)^2)-((A*U(i,j))*((U(i+1,j)+U(i+1,j)-2*U(i,j)))/dx^2))...
                -((A*U(i,j))*((U(i,j+1)+U(i,j-1)-2*U(i,j)))/dy^2))-(E*((U(i+1,j)+U(i+1,j)-2*U(i,j)))/dx^2))-
(E*((U(i,j+1)+U(i,j-1)-2*U(i,j)))/dy^2))...
                +(D*(U(i,j)-V(i,j)));
             aE=(-1/2*A*((U(i+1,j)-U(i+1,j)))/dx^2))-(A*U(i,j)/dx^2)-(E/dx^2);    % left nodes (upper
diagonal)
             aW=(1/2*A*((U(i+1,j)-U(i+1,j)))/dx^2))-(A*U(i,j)/dx^2)-(E/dx^2);    %right nodes  (lower
diagonal)
             aN=(-1/2*A*((U(i,j+1)-U(i,j-1))/dx^2))-(A*U(i,j)/dx^2)-(E/dx^2);
             aS=(1/2*A*((U(i,j+1)-U(i,j-1))/dx^2))-(A*U(i,j)/dx^2)-(E/dx^2);
```

```
                a0=(2*B*(U(i,j)-U_init(i,j)))/(dt*(PL+U(i,j))^3)+((C+(B/(PL+U(i,j))^2))/dt)-
(A*((U(i+1,j)+U(i+1,j)-2*U(i,j))/dx^2))-(A*((U(i,j+1)+U(i,j-1)-2*U(i,j))/dy^2))...

+(((2*A)/dx^2)*U(i,j))+(((2*A)/dy^2)*U(i,j))+(2*E/dx^2)+D*U(i,j)+(2*E/dy^2)+D*U(i,j)+D*(U(i,j)-V(i,j)); %
diagonal (middle nodes)
                u_delta0(i,j)=((-f(i,j)-aE*u_delta(i+1,j)-aW*u_delta(i+1,j)-aN*u_delta(i,j+1)-aS*u_delta(i,j-
1))/a0)
                error= abs((u_delta0(i,j)-u_delta(i,j))/u_delta(i,j));
                u_delta(i,j)=u_delta0(i,j);
                if (error<eps)
                   numi=numi+1;
                end
             end
          end
          % right nodes
          % Boundary condition for right node (Neumann BC)
          for i=M
             for j=2:N-1
                f(i,j)=(C+(B/(PL+U(i,j))^2))*((U(i,j)-U_init(i,j))/dt)-(A*((U(i-1,j)-U(i-1,j))/2*dx)^2)-
(A*((U(i,j+1)-U(i,j-1))/2*dy)^2)-((A*U(i,j))*((U(i-1,j)+U(i-1,j)-2*U(i,j))/dx^2))...
                   -((A*U(i,j))*((U(i,j+1)+U(i,j-1)-2*U(i,j))/dy^2))-(E*((U(i-1,j)+U(i-1,j)-2*U(i,j))/dx^2))-
(E*((U(i,j+1)+U(i,j-1)-2*U(i,j))/dy^2))...
                   +(D*(U(i,j)-V(i,j)));
                aE=(-1/2*A*((U(i-1,j)-U(i-1,j))/dx^2))-(A*U(i,j)/dx^2)-(E/dx^2);    % left nodes (upper
diagonal)
                aW=(1/2*A*((U(i-1,j)-U(i-1,j))/dx^2))-(A*U(i,j)/dx^2)-(E/dx^2);    %right nodes  (lower
diagonal)
                aN=(-1/2*A*((U(i,j+1)-U(i,j-1))/dx^2))-(A*U(i,j)/dx^2)-(E/dx^2);
                aS=(1/2*A*((U(i,j+1)-U(i,j-1))/dx^2))-(A*U(i,j)/dx^2)-(E/dx^2);
                a0=(2*B*(U(i,j)-U_init(i,j)))/(dt*(PL+U(i,j))^3)+((C+(B/(PL+U(i,j))^2))/dt)-(A*((U(i-1,j)+U(i-
1,j)-2*U(i,j))/dx^2))-(A*((U(i,j+1)+U(i,j-1)-2*U(i,j))/dy^2))...

+(((2*A)/dx^2)*U(i,j))+(((2*A)/dy^2)*U(i,j))+(2*E/dx^2)+D*U(i,j)+(2*E/dy^2)+D*U(i,j)+D*(U(i,j)-V(i,j)); %
diagonal (middle nodes)
                u_delta0(i,j)=((-f(i,j)-aE*u_delta(i-1,j)-aW*u_delta(i-1,j)-aN*u_delta(i,j+1)-aS*u_delta(i,j-
1))/a0)
                error= abs((u_delta0(i,j)-u_delta(i,j))/u_delta(i,j));
                u_delta(i,j)=u_delta0(i,j);
                if (error<eps)
                   numi=numi+1;
                end
             end
          end
          % Top node
          for j=N
             for i=2:M-1
                f(i,j)=(C+(B/(PL+U(i,j))^2))*((U(i,j)-U_init(i,j))/dt)-(A*((U(i+1,j)-U(i-1,j))/2*dx)^2)-(A*((U(i,j-
1)-U(i,j-1))/2*dy)^2)-((A*U(i,j))*((U(i+1,j)+U(i-1,j)-2*U(i,j))/dx^2))...
                   -((A*U(i,j))*((U(i,j-1)+U(i,j-1)-2*U(i,j))/dy^2))-(E*((U(i+1,j)+U(i-1,j)-2*U(i,j))/dx^2))-
(E*((U(i,j-1)+U(i,j-1)-2*U(i,j))/dy^2))...
                   +(D*(U(i,j)-V(i,j)));
                aE=(-1/2*A*((U(i+1,j)-U(i-1,j))/dx^2))-(A*U(i,j)/dx^2)-(E/dx^2);    % left nodes (upper
diagonal)
                aW=(1/2*A*((U(i+1,j)-U(i-1,j))/dx^2))-(A*U(i,j)/dx^2)-(E/dx^2);    %right nodes  (lower
diagonal)
                aN=(-1/2*A*((U(i,j-1)-U(i,j-1))/dx^2))-(A*U(i,j)/dx^2)-(E/dx^2);
```

```
                aS=(1/2*A*((U(i,j-1)-U(i,j-1))/dx^2))-(A*U(i,j)/dx^2)-(E/dx^2);
                a0=(2*B*(U(i,j)-U_init(i,j)))/(dt*(PL+U(i,j))^3)+((C+(B/(PL+U(i,j))^2))/dt)-(A*((U(i+1,j)+U(i-
1,j)-2*U(i,j))/dx^2))-(A*((U(i,j-1)+U(i,j-1)-2*U(i,j))/dy^2))...

+(((2*A)/dx^2)*U(i,j))+(((2*A)/dy^2)*U(i,j))+(2*E/dx^2)+D*U(i,j)+(2*E/dy^2)+D*U(i,j)+D*(U(i,j)-V(i,j)); %
diagonal (middle nodes)
                u_delta0(i,j)=((-f(i,j)-aE*u_delta(i+1,j)-aW*u_delta(i-1,j)-aN*u_delta(i,j-1)-aS*u_delta(i,j-
1))/a0)
                error= abs((u_delta0(i,j)-u_delta(i,j))/u_delta(i,j));
                u_delta(i,j)=u_delta0(i,j);
                if (error<eps)
                   numi=numi+1;
                end
             end
          end
          % Bottom node
          for j=1
             for i=2:M-1
                f(i,j)=(C+(B/(PL+U(i,j))^2))*((U(i,j)-U_init(i,j))/dt)-(A*((U(i+1,j)-U(i-1,j))/2*dx)^2)-
(A*((U(i,j+1)-U(i,j+1))/2*dy)^2)-((A*U(i,j))*((U(i+1,j)+U(i-1,j)-2*U(i,j))/dx^2))...
                   -((A*U(i,j))*((U(i,j+1)+U(i,j+1)-2*U(i,j))/dy^2))-(E*((U(i+1,j)+U(i-1,j)-2*U(i,j))/dx^2))-
(E*((U(i,j+1)+U(i,j+1)-2*U(i,j))/dy^2))...
                   +(D*(U(i,j)-V(i,j)));
                aE=(-1/2*A*((U(i+1,j)-U(i-1,j))/dx^2))-(A*U(i,j)/dx^2)-(E/dx^2);    % left nodes (upper
diagonal)
                aW=(1/2*A*((U(i+1,j)-U(i-1,j))/dx^2))-(A*U(i,j)/dx^2)-(E/dx^2);    %right nodes  (lower
diagonal)
                aN=(-1/2*A*((U(i,j+1)-U(i,j+1))/dx^2))-(A*U(i,j)/dx^2)-(E/dx^2);
                aS=(1/2*A*((U(i,j+1)-U(i,j+1))/dx^2))-(A*U(i,j)/dx^2)-(E/dx^2);
                a0=(2*B*(U(i,j)-U_init(i,j)))/(dt*(PL+U(i,j))^3)+((C+(B/(PL+U(i,j))^2))/dt)-(A*((U(i+1,j)+U(i-
1,j)-2*U(i,j))/dx^2))-(A*((U(i,j+1)+U(i,j+1)-2*U(i,j))/dy^2))...

+(((2*A)/dx^2)*U(i,j))+(((2*A)/dy^2)*U(i,j))+(2*E/dx^2)+D*U(i,j)+(2*E/dy^2)+D*U(i,j)+D*(U(i,j)-V(i,j)); %
diagonal (middle nodes)
                u_delta0(i,j)=((-f(i,j)-aE*u_delta(i+1,j)-aW*u_delta(i-1,j)-aN*u_delta(i,j+1)-
aS*u_delta(i,j+1))/a0)
                error= abs((u_delta0(i,j)-u_delta(i,j))/u_delta(i,j));
                u_delta(i,j)=u_delta0(i,j);
                if (error<eps)
                   numi=numi+1;
                end
             end
          end
          m=m+1;
       end
       for i=1:M
          for j=1:M
             U_1(i,j)=U(i,j)+w*u_delta(i,j);
             error=abs((U_1(i,j)-U(i,j))/U(i,j));
             if (error<eps)
                numi1=numi1+1;
             end
          end
       end
       U=U_1;
       %     plot(x,U_1,'rp--')
```

```
    %     mm=mm+1;
  end

  U(1,1)=1/2*(U(1,2)+U(2,1));
  U(M,1)=1/2*(U(M-1,1)+U(M,2));
  U(1,N)=1/2*(U(1,N-1)+U(2,N));
  U(M,N)=1/2*(U(M,N-1)+U(M-1,N));



  % Boundary condition for Wellbore Interface (Direchlet BC)

  V(1,:)=Pw;
  V(M,:)=Pw;
  V(:,N)=Pw;
  V(:,1)=Pw;

  V_1(1,:)=Tws;
  V_1(M,:)=Tws;
  V_1(:,N)=Tws;
  V_1(:,1)=Tws;

  % Execute Newton Method for Fracture
  nunknoFF=M*M;
  ff=1;
  numiFF=0;
  while (numiFF<nunknoFF)*(ff<maxm)

    % Execute Gauss-Seidel algorithm

    nunknoF=M*M;
    f=1;
    numiF=0;
    while (numiF<nunknoF)*(f<maxm)
      numiF=0;
      for i=2:M-1
        for j=2:N-1
          if i==(M+1)/2 && j==(N+1)/2
            f_f(i,j)=(K*(V(i,j)-V_init(i,j))/dt)-(A1*((V(i+1,j)-V(i-1,j))/2*dx)^2)-
(A1*V(i,j)*(V(i+1,j)+V(i-1,j)-2*V(i,j))/dx^2)-(F*(V(i+1,j)+V(i-1,j)-2*V(i,j))/dx^2)-(D*V(i,j)*(U(i,j)-V(i,j)))...
              -(A1*((V(i,j+1)-V(i,j-1))/2*dx)^2)-(A1*V(i,j)*(V(i,j+1)+V(i,j-1)-2*V(i,j))/dx^2)-
(F*(V(i,j+1)+V(i,j-1)-2*V(i,j))/dx^2)+G*(V(i)-pwf);
            aE_f=((-1/2*(A1/dx^2))*(V(i+1,j)-V(i-1,j)))-((A1/dx^2)*V(i,j))-((F/dx^2));
            aN_f=((-1/2*(A1/dx^2))*(V(i,j+1)-V(i,j-1)))-((A1/dx^2)*V(i,j))-((F/dx^2));
            aW_f=((1/2*(A1/dx^2))*(V(i+1,j)-V(i-1,j)))-((A1/dx^2)*V(i,j))-((F/dx^2));    %right nodes
(lower diagonal)
            aS_f=((1/2*(A1/dx^2))*(V(i,j+1)-V(i,j-1)))-((A1/dx^2)*V(i,j))-((F/dx^2));
            a0_f=(K/dt)-(A1*((V(i+1,j)+V(i-1,j)-2*V(i,j))/dx^2))+((2*(A1/dx^2))*V(i,j))+(2*(F/dx^2))-
(D*(U(i,j)-V(i,j)))+D*V(i,j)...
              -(A1*((V(i,j+1)+V(i,j-1)-2*V(i,j))/dx^2))+((2*(A1/dx^2))*V(i,j))+(2*(F/dx^2))+G; %
diagonal (middle nodes)
            v_delta0(i,j)=((-f_f(i,j)-aE_f*v_delta(i+1,j)-aW_f*v_delta(i-1,j)-aN_f*v_delta(i,j+1)-
aS_f*v_delta(i,j-1))/a0_f);
            error3=abs((v_delta0-v_delta(i,j))/v_delta(i,j));
            v_delta(i,j)=v_delta0(i,j);
            if (error<eps)
```

```
                    numiF=numiF+1;
                end
%                     q=G*(U(i)-pwf);
                 q=-0.333*-((K*(V(i,j)-V_init(i,j))/dt)-(A1*((V(i+1,j)-V(i+1,j))/2*dx)^2)-
(A1*V(i,j)*(V(i+1,j)+V(i+1,j)-2*V(i,j))/dx^2)-(F*(V(i+1,j)+V(i+1,j)-2*V(i,j))/dx^2)-(D*V(i,j)*(U(i,j)-
V(i,j)))...
                    -(A1*((V(i+1,j)-V(i+1,j))/2*dx)^2)-(A1*V(i,j)*(V(i+1,j)+V(i+1,j)-2*V(i,j))/dx^2)-
(F*(V(i+1,j)+V(i+1,j)-2*V(i,j))/dx^2));

            else
                f_f(i,j)=(K*(V(i,j)-V_init(i,j))/dt)-(A1*((V(i+1,j)-V(i-1,j))/2*dx)^2)-
(A1*V(i,j)*(V(i+1,j)+V(i-1,j)-2*V(i,j))/dx^2)-(F*(V(i+1,j)+V(i-1,j)-2*V(i,j))/dx^2)-(D*V(i,j)*(U(i,j)-V(i,j)))...
                    -(A1*((V(i,j+1)-V(i,j-1))/2*dx)^2)-(A1*V(i,j)*(V(i,j+1)+V(i-1)-2*V(i,j))/dx^2)-
(F*(V(i,j+1)+V(i,j-1)-2*V(i,j))/dx^2);
                aE_f=((-1/2*(A1/dx^2))*(V(i+1,j)-V(i-1,j)))-((A1/dx^2)*V(i,j))-((F/dx^2));
                aN_f=((-1/2*(A1/dx^2))*(V(i,j+1)-V(i,j-1)))-((A1/dx^2)*V(i,j))-((F/dx^2));
                aW_f=((1/2*(A1/dx^2))*(V(i+1,j)-V(i-1,j)))-((A1/dx^2)*V(i,j))-((F/dx^2));    %right nodes
(lower diagonal)
                aS_f=((1/2*(A1/dx^2))*(V(i,j+1)-V(i,j-1)))-((A1/dx^2)*V(i,j))-((F/dx^2));
                a0_f=(K/dt)-(A1*((V(i+1,j)+V(i-1,j)-2*V(i,j))/dx^2))+((2*(A1/dx^2))*V(i,j))+(2*(F/dx^2))-
(D*(U(i,j)-V(i,j)))+D*V(i,j)...
                    -(A1*((V(i,j+1)+V(i,j-1)-2*V(i,j))/dx^2))+((2*(A1/dx^2))*V(i,j))+(2*(F/dx^2)); %
diagonal (middle nodes)
                v_delta0(i,j)=((-f_f(i,j)-aE_f*v_delta(i+1,j)-aW_f*v_delta(i-1,j)-aN_f*v_delta(i,j+1)-
aS_f*v_delta(i,j-1))/a0_f);
                error3=abs((v_delta0-v_delta(i,j))/v_delta(i,j));
                v_delta(i,j)=v_delta0(i,j);
                if (error<eps)
                    numiF=numiF+1;
                end
            end
        end
    end

    f=f+1;

end

for i=2:M-1
    for j=2:N-1
        V_1(i,j)=V(i)+w_1*v_delta(i,j);
        error=abs((V_1(i,j)-V(i,j))/V(i,j));
        if (error<eps)
            numiFF=numiFF+1;
        end
    end
end
V=V_1;

end


% ---------------------------------------------------------------------
% %    Checking for convergence before looping back again
% ---------------------------------------------------------------------
% final update solution
```

```
        for i=1:M
            for j=1:N
                error5(i,j)=abs((U_1(i,j)-U1(i,j))/U1(i,j));
                if error5(i,j)< eps1
                    numi11=numi11+1;
                end
            end
        end
        for i=2:N-1
            for j=2:N-1
                error6(i,j)=abs((V_1(i,j)-V1(i,j))/V1(i,j))
                if  error6(i,j)< eps1
                    numi11=numi11+1;
                end
            end
        end
    end
    U_init=U1;
    V_init=V1;
    PA2=[PA2;V_1];
    PA3=[PA3;q]
    figure(1)
    surf(x,y,V_1)
    figure(2)
    surf(x,y,U_1)
    xlabel('distance (m)')
    ylabel('P'; 'T';'Q';)
    pause(0.90)
end


figure(1)
surf(x,y,V)
colorbar
shading interp
jet
colormap(jet)

figure(2)
surf(x,y,U)
colorbar
shading interp
jet
colormap(jet)
```

FORM UPR16

Research Ethics Review Checklist

Please include this completed form as an appendix to your thesis (see the Research Degrees Operational Handbook for more information

Postgraduate Research Student (PGRS) Information				**Student ID:**	UP800333
PGRS Name:	SABASTINE ANIBUEZE				
Department:	SENE	**First Supervisor:**	DR AMJAD SHAH		
Start Date: (or progression date for Prof Doc students)	**01/02/2017**				
Study Mode and Route:	Part-time ☐ Full-time ☒	MPhil ☐ PhD ☒	MD ☐ Professional Doctorate ☐		

Title of Thesis:	Numerical Modelling and Simulation of Fully Coupled Gas Hydrate Reservoir and Wellbore Fluid Flow
Thesis Word Count: (excluding ancillary data)	40103

If you are unsure about any of the following, please contact the local representative on your Faculty Ethics Committee for advice. Please note that it is your responsibility to follow the University's Ethics Policy and any relevant University, academic or professional guidelines in the conduct of your study

Although the Ethics Committee may have given your study a favourable opinion, the final responsibility for the ethical conduct of this work lies with the researcher(s).

UKRIO Finished Research Checklist:
(If you would like to know more about the checklist, please see your Faculty or Departmental Ethics Committee rep or see the online version of the full checklist at: http://www.ukrio.org/what-we-do/code-of-practice-for-research/)

a) Have all of your research and findings been reported accurately, honestly and within a reasonable time frame?	YES ☒ NO ☐
b) Have all contributions to knowledge been acknowledged?	YES ☒ NO ☐
c) Have you complied with all agreements relating to intellectual property, publication and authorship?	YES ☒ NO ☐
d) Has your research data been retained in a secure and accessible form and will it remain so for the required duration?	YES ☒ NO ☐
e) Does your research comply with all legal, ethical, and contractual requirements?	YES ☒ NO ☐

Candidate Statement:

I have considered the ethical dimensions of the above named research project, and have successfully obtained the necessary ethical approval(s)

Ethical review number(s) from Faculty Ethics Committee (or from NRES/SCREC):	ETHICS-10646

If you have *not* submitted your work for ethical review, and/or you have answered 'No' to one or more of questions a) to e), please explain below why this is so:

Signed *(PGRS)*:	**Date:** 16/03/2023

UNIVERSITY OF PORTSMOUTH

EThOS DEPOSIT AGREEMENT FOR UNIVERSITY OF PORTSMOUTH THESES

COVERED WORK
I, **[SABASTINE ANIBUEZE]** "the Depositor", would like to deposit **[Numerical Modelling and Simulation of Fully Coupled Gas Hydrate Reservoirs and Wellbore Fluid Flow]** hereafter referred to as the "Work", in the University of Portsmouth Library and agree to the following:

NON-EXCLUSIVE RIGHTS
Rights granted to the University of Portsmouth through this agreement are entirely non-exclusive and royalty free. I am free to publish the Work in its present version or future versions elsewhere. I agree that the University of Portsmouth or any third party with whom the University of Portsmouth has an agreement to do so may, without changing content, translate the Work to any medium or format for the purpose of future preservation and accessibility.

DEPOSIT IN THE UNIVERSITY OF PORTSMOUTH LIBRARY
I understand that work deposited in the University of Portsmouth Library will be accessible to a wide variety of people and institutions - including automated agents - via the University's Institutional Repository. In addition, an electronic copy of my thesis may also be included in the British Library Electronic Theses Online System (EThOS). I understand that once the Work is deposited, a citation to the Work will always remain visible. Removal of the Work can be made after discussion with the University of Portsmouth Library, who shall make reasonable efforts to ensure removal of the Work from any third party with whom the University of Portsmouth has an agreement.

I AGREE THAT:
- I am the author or co-author of the Work and have the authority on behalf of the author or authors to make this agreement and to hereby give the University of Portsmouth the right to make available the Work in the way described above.

- I have exercised reasonable care to ensure that the Work is original, and does not to the best of my knowledge break any applicable law or infringe any third party's copyright or other intellectual property right.

- The University of Portsmouth does not hold any obligation to take legal action on my behalf, or other rights holders, in the event of breach of intellectual property rights, or any other right, in the Work.

- **I DO/DO NOT [delete as applicable]** wish my thesis to be deposited in EThOS but am aware that EThOS may, at some future date, harvest thesis details automatically (including the full text) from the University's Institutional Repository available at https://researchportal.port.ac.uk/

Signature: .....
Date: 16th March 2023.....

Please return this form to: Faculty Advisor (Research), Research Degree Team, Student Life, Department of Student & Academic Administration, University of Portsmouth, Floor 5, Mercantile House, Hampshire Terrace, Portsmouth, PO1 2EG